Optimization of the Measurement of the Linear Viscoelastic Properties of Complex Fluids

David Banaszek

Institute of Mathematics and Physics
Aberystwyth University
Wales

Supervised by: Dr. D.M. Binding and Prof. A.R. Davies

A Thesis presented for the degree of
Doctor of Philosophy

DECLARATION

This work has not previously been accepted in substance for any degree and is not being concurrently submitted in candidature for any degree.

Signed ..... (D. Banaszek)

Date .....

STATEMENT 1

This thesis is the result of my own investigations, except where otherwise stated. Other sources are acknowledged by footnotes giving explicit references. A bibliography is appended.

Signed ..... (D. Banaszek)

Date .....

STATEMENT 2

I hereby give consent for my thesis, if accepted, to be available for photocopying and for inter-library loan, and for the title and summary to be made available to outside organizations.

Signed ..... (D. Banaszek)

Date .....

ABSTRACT

The linear viscoelastic material functions of complex fluids relate stress and strain when these assume sufficiently small values and are used to simulate fluid flow using more sophisticated constitutive equations in complex flow regimes. The standard method of determination is to apply a sinusoidal torque at discrete frequencies to obtain the complex modulus at those frequency values. In this thesis, the implications of using a completely arbitrary applied torque are investigated. Recent research has concentrated on Fourier transform methods, but here the problem is analyzed in the time-domain in terms of the relaxation modulus, which allows questions of well-posedness to be more easily addressed.

The work falls into two main parts. The first part is concerned with the analysis of the relationship between the applied torque and observed strain response. A variety of candidate torque functions are considered and analytical expressions are obtained for the simulated response using Laplace transform techniques, assuming known material properties. The second part addresses questions concerning stability of the solution of the Volterra integro-differential equation and methods of numerical solution. It is demonstrated that the process of obtaining a solution for the relaxation modulus is equivalent to solving a Volterra integral equation of the first kind, which is known to be an ill-posed problem. Considering the governing equations in such a form allows existing methods involving perturbed solutions to be adapted to provide estimates of bounds on the error level in the data such that a stable solution can exist. It is shown that the applied torque function which minimizes the ill-posedness of the problem is one that corresponds to a kernel with one-smoothing characteristics. Finally, discretization and regularization schemes for numerical solution of the problem are discussed and an existing predictor-corrector regularization scheme is implemented which preserves the Volterra (causal) nature of the problem and allows near real-time solution.

ACKNOWLEDGEMENTS

I would like to thank my supervisors, Dr. Dave Binding and Prof. Russell Davies for many countless hours of invaluable help and discussion. I am also grateful to the staff of the erstwhile Mathematics department at Aberystwyth who were involved in the teaching for the M.Sc. in Complex Fluids, which provided useful background knowledge and a decent grounding in the research area.

The research was funded by an Aberystwyth Postgraduate Research Studentship (ARPS) provided by Aberystwyth University.

Contents

List of Figures

List of Tables

CHAPTER 1

Introduction

Rheology, Linear Viscoelasticity and Rheometry

Rheology is concerned with the deformation and flow of materials. The relevance of this discipline is readily apparent when the importance of modern industry involving the manufacture of materials for which the flow properties are critical to the efficacy of the product are considered. Examples of such industries are the manufacture of plastics, non-drip paints, adhesives, printing inks and multi-grade oils. The motto of the Society of Rheology: "παντα ρει" is due to the Greek philosopher Heraclitus, translated as "everything flows" and highlights the motivation behind this area of study. From the slow erosion of mountain chains over millions of years, to the swirling of coffee in a cup, the phenomenon of flow is all around us, albeit occurring on widely varying timescales. The desire of the rheologist is to obtain constitutive relations linking the stresses to the deformation of a material, which coupled with the kinetics of the flow and conservation laws, provide a complete description of the flow of that material and may then be applied to the solution of engineering problems such as those involved in the manufacturing of products mentioned above.

In this introductory chapter, a review of the literature pertaining to the problem of determining the optimal form for the applied torque in controlled-stress rheometry is first presented, along with a discussion concerning the motivation for the work in this thesis. This is followed by a summary of the background to rheology and linear viscoelasticity which forms a basis to the work in subsequent chapters.

I. LITERATURE REVIEW - RHEOMETRY

The field of rheometry is the aspect of rheology concerned with measurement of the characteristic functions of viscoelastic materials, which relate the stress and strain within the material sample, by experimental methods. The behaviour of viscoelastic materials in simple (rheometrical) flow geometries, such as steady shear flow or small amplitude oscillatory shear is obtained with the intention of utilizing this information to predict the flow in more complex situations. Even the simplest of geometries may prove surprisingly difficult to elucidate the rheological parameters from. The underlying theory of measurement, the microstructure of the fluid and the interaction of the fluid sample and instrument are some of the considerations encountered. Often it is necessary to ensure the deformations are sufficiently small that a linear approximation can be employed; the linear viscoelastic functions being thus determined can be used in non-linear constitutive equations combined with the stress equations of motion and continuity conditions to model industrial processes involving viscoelastic materi-

als by computational methods. The question of whether the parameters determined from these simple flow geometries are applicable to geometries more complex in character is a fundamental question in rheological modelling, but in this thesis only the steps involving acquisition of the rheometrical data are studied. Another motivation of rheometry is to relate the molecular structure to the material behaviour, interpreting the motion of the polymer chains in terms of the relaxation spectrum.

The earliest instruments utilized to characterize fluid materials were known as *viscometers*, which as the name suggests were intended to measure the viscosity of Newtonian fluids. However, in a more general sense these proved inadequate to characterize Non-Newtonian materials, since the viscosity of such fluids is not necessarily independent of the shear-rate. Thus, the need for an instrument termed a "rheometer" was recognized, which may be defined as an "instrument for measuring rheological properties".

A profusion of designs exist for rheometrical instruments, concerned with measurements in steady shear, extensional, rotational, linear or non-linear frameworks. References such as [99] give an idea of the wide variety of instruments which have been available over the years, however in this discourse only measurements involving rotational motion as a result of a prescribed applied torque in the linear viscoelastic regime will be considered. The concept of linear viscoelasticity will be explored fully in the following section, but suffice it to say at this point that for suitably small deformations of a viscoelastic material, the assumption that the stress-strain relationship within the material is linear in nature provides a good approximation.

One of the best known of the first generation of rheometers was the Weissenberg Rheogoniometer [96, 20], which enabled experiments to be carried out in a strain-controlled regime. The material sample was contained between two boundary surfaces, the lower of which was rotated with a prescribed angular motion. The upper platen was constrained by a torsion bar possessing a calibrated elastic constant, allowing the resulting motion of the upper platen to be used to determine the stress exerted upon the platen surface. In steady shear mode the lower platen would be rotated at a steady angular velocity and the torque on the upper platen measured, whereas in oscillatory shear mode the lower platen would be oscillated at a specified angular frequency, resulting in both of the plates oscillating with the same frequency once a quasi-steady state was achieved, albeit with a measurable phase difference.

Several novel experimental geometries [96] such as the eccentric rotating disk (ERD) and tilted sphere (balance rheometer) were tried in the 1970s which offered

steady rotation of the sample whilst subjecting fluid elements to small harmonic strains. The advantage of these experiments was that the real and imaginary parts of the complex modulus $G^*(\omega)$ were measured separately as two forces or torques in two orthogonal directions, whereby eliminating the need to measure the phase difference, which may be problematical under certain conditions. The limiting cases $\phi = 0$ and $\phi = \frac{\pi}{2}$ were formerly difficult to measure and usually contaminated with experimental artefacts such as phase displacements introduced by the electronic system and instrument compliance effects. The new geometries should have resulted in increased accuracy over the standard methods, but have been discarded in preference for the simpler experimental setups combined with the improved design of accurate modern rheometers.

Historically, the preference for strain-controlled instruments has been dominant, mainly as a consequence of the simplicity of design and experimental setup of this type of rheometer. Stress controlled experiments are becoming more popular as instrument sensors become more sophisticated and capable of resolving torque and strain more accurately, although most modern instruments are capable of performing both strain-controlled and stress-controlled experiments. In terms of the mathematical theory, strain-controlled and stress-controlled experiments are equivalent, however experimentally, stress-controlled measurements enjoy some advantages [20]. Operating in controlled-stress mode generally results in higher sensitivity and in the case of oscillatory tests, better measurements of the complex modulus at low frequencies is achievable. Step changes in stress are more easily applied than corresponding variations in strain, the latter being severely limited by the effect of the inertia of the rotating assembly of the rheometer. Certain materials may actually require stress-controlled measurements, such as those which possess a yield-stress or highly elastic gels.

The standard techniques for determining the material functions in the linear regime can be categorized into two groups: *static* and *dynamic* tests. Static tests involve the application of a constant stress (or strain) to the material under investigation and measurement of the resulting strain (or stress) in the time domain.

If the strain is specified as a step function, the behaviour observed is *stress relaxation*, allowing the relaxation modulus to be determined directly. The typical response for a viscoelastic fluid being that illustrated in Figure 1.12, where the measured stress jumps instantaneously to a value $\gamma_0 G_0$ then decreases exponentially to zero as t tends to infinity. For viscoelastic solid materials, the stress decreases towards a constant lim-

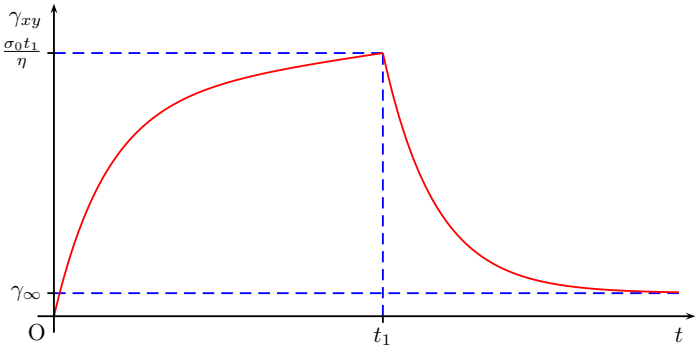

Figure 1.1: Creep response for a viscoelastic liquid.

iting value G_∞, representing a residual finite amount of stored energy. The initial jump in strain can be difficult to reproduce accurately due to inertial effects, since the inertia of the rotating assembly is in general significant in relation to the inertia of the material sample. This technique is limited to relaxation times of at least a few seconds, since the time to reach steady state must be short in comparison with the time over which the response is measured to ensure suitable accuracy. Additionally, the range and resolution of torque measurements limit the reliability of long time-scale data [62].

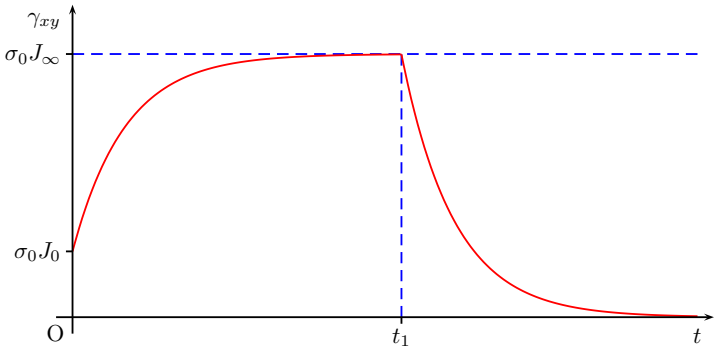

Figure 1.2: Creep response for a viscoelastic solid.

Creep experiments involve the application of a constant stress σ_0, allowing the direct measurement of the creep compliance. A common extension is to consider creep and recovery, where the applied stress is now constant for $0 < t < t_1$, then zero thereafter. The typical strain response observed for a viscoelastic solid is shown in Figure 1.2. The strain jumps instantaneously to an initial value $\sigma_0 J_0$, then increases as an exponential function towards an asymptotic value $\sigma_0 J_\infty$, provided that t_0 is sufficient to allow the displacement to reach a quasi-equilibrium state. For $t > t_0$, the strain then relaxes exponentially to zero, representing the complete recovery of all the stored elastic energy. For viscoelastic fluids, as shown in Figure 1.1, the strain initially grows exponentially, then increases as an approximately linear function in time. When the stress is removed, the strain relaxes exponentially towards a constant value $\frac{\sigma_0 t_0}{\eta}$, repre-

senting the energy dissipated by the viscous component of the material behaviour. The problems concerning inertia combined with the relative ease of measurement of strain in comparison with stress, has resulted in creep tests being preferred over relaxation tests.

The standard method for determining frequency-dependent linear viscoelastic functions, such as the complex modulus, complex compliance or complex viscosity is to apply a sinusoidal waveform of a fixed frequency, whereby upon attaining a quasi-steady state the relevant function can be obtained at that particular frequency. As shown in Figure 1.3, an oscillatory stress (or strain) is applied to the material under investigation at a specific, fixed frequency ω_k and the resulting strain (or stress) is measured, which is also of the same frequency, from which the phase angle δ and amplitude ratio can be used to calculate $G'(\omega_k)$ and $G''(\omega_k)$ at that particular frequency. The experiment is then repeated at the next frequency, and so on until the desired range of frequencies has been covered.

The first reference to oscillatory tests appears in [67], where an oscillatory shear experiment using concentric cylinders was considered. The outer cylinder was oscillated at a prescribed angular frequency and the inner cylinder, which was connected to a torsion balance was used to determine the resulting strain on that cylinder. A similar analysis can be carried out for the cone-plate and parallel plate geometries, the equations for the parallel plate geometry first appearing in [97].

Modern rheometers such as the TA Instruments AR2000 handle this process automatically by performing a "frequency sweep" over the desired frequency range at a specified number of points, usually distributed evenly over a logarithmic scale. For stress-controlled measurements, the linear range would usually be determined by performing a "stress sweep" at certain frequencies; in the linear regime the measurement of $G^*(\omega)$ is independent of the magnitude of the applied stress. Such experiments are termed dynamic since the excitation is a continually varying function of time. Note that the equation for determining $G^*(\omega)$ from oscillatory shear tests is strictly speaking only valid in the limit as t tends to infinity, although it can be reasonably assumed that a quasi-steady state is reached after several cycles. The first few cycles contain a superimposed transient function which necessarily limits the minimum duration of the experiment.

A variation of the oscillatory shear experiment considered relatively early on was the determination of the oscillatory linear material functions using free, rather than

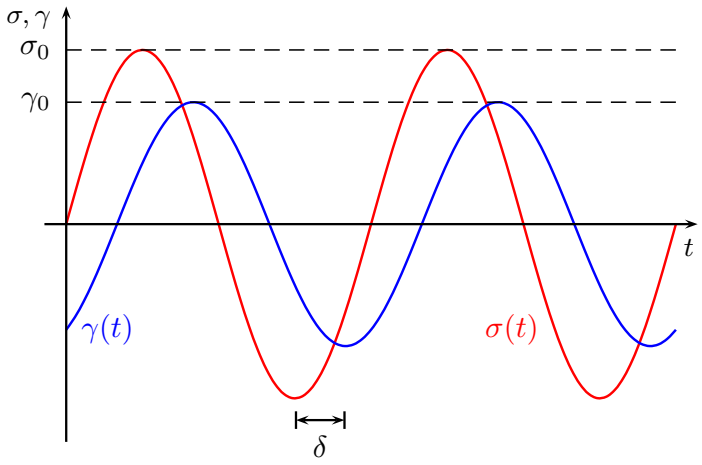

Figure 1.3: Small amplitude oscillatory shear.

forced, oscillations. The technique involves the application of an arbitrary strain profile up until a finite cut-off time, after which the damped oscillations are used to calculate the complex modulus. Experimental investigations in [97] and [90] indicated that the quality of data achievable was decidedly inferior to that produced by the standard method of forced oscillations, due to the rapid diminution of the measured stress to levels which could not be measured with sufficient accuracy and hence resulting in noisy data for higher frequencies.

A number of problems become manifest with experiments made within the frequency domain using fixed frequency waveforms. At low frequencies the instrument transponder is unable to respond to the very small forces or displacements produced, so noise is a potential problem in data collected at those frequencies. At the other end of the scale, the response is dominated by the inertia of the rotating assembly of the rheometer at high frequencies. The frequency data is ultimately used to determine the relaxation spectrum, which reveals problems in the nature of the data. Only a limited range of discrete frequencies are available, and contrary to rheological folklore that this yields relaxation spectrum data over the interval $\left[\omega_{\text{max}}^{-1}, \omega_{\text{min}}^{-1}\right]$, the interval has been conjectured [21] to be shortened to $\left[\mathrm{e}^{\frac{\pi}{2}}\omega_{\text{max}}^{-1}, \mathrm{e}^{-\frac{\pi}{2}}\omega_{\text{min}}^{-1}\right]$. This is known as *sampling localization*.

The standard techniques for determining the material functions of linear viscoelastic materials have maintained their popularity mainly by virtue of the simplicity of the mathematical process for converting the experimental data for output stress or strain into the relevant characteristic function. The primary limitation in a practical sense of these techniques is the timescale involved to collect sufficient data to determine the required characteristic function. Each experiment performed at a fixed frequency only

yields a single datum for the complex modulus, at that particular frequency. For a material sample with stable temporal properties, the only inconvenience is the time expenditure required to characterize the material; the accuracy of the data is independent of the experimental time. However, for so-called "rheokinetic" materials which have unstable and evolving structures, only a short experimental time is available in order to determine the properties of the material before the material changes to another state and hence a change occurs in the properties. Examples of such materials and processes are

1. **Chemical reactions**: Gelation involves a chemical reaction resulting in a transition from a relatively low viscosity fluid to a highly elastic solid. Of particular interest is the *gel-point* at which the material ceases to be fluid and becomes solid. Other examples of chemical reactions include curing processes and polymerization.

2. **Physical aging**: The structure of certain materials may change over time. Examples are crystallization, phase transition, solvent evaporation for polymer solutions and slow structural rearrangements.

Thus, experiments concerning these materials and processes have two competing mechanisms to deal with: stress relaxation which is the approach to an equilibrium state at rest and structural change in the material which results in a change of that equilibrium state, assuming that each transient structure can be characterized by an equilibrium state. Some materials, such as dispersions suffer structural changes as a result of even the smallest deformations [58]. Therefore, it is often desirable to perform experiments which provide the greatest range of data over the shortest possible time period. The progression of certain processes and reactions can be followed given a sufficiently rapid experiment; of particular interest is the gelling-point at which point a material makes the transition from liquid to solid form. In [35] the limitation of experimental data for rheokinetic materials was defined by stating that the experimental time must be short compared with the characteristic time of material change. However, measurement of a relaxation process requires that the experimental time must be of the order of the relaxation time of the process, therefore for a material with high rate of change properties, only the short end of the relaxation spectrum can be investigated. This can be expressed mathematically by requiring the inequality

$$\frac{\lambda}{A}\frac{\partial A}{\partial t} \ll 1 \tag{1-1}$$

to be satisfied, where A symbolizes the rate of change of the relevant property, for the longest relaxation time λ to be determined.

This leads to the first part of the motivation for the problem considered here - to attempt to define the optimal form for an experiment which acquires as much information as possible in the shortest possible time-frame, preferably from a single test. Thus, celerity is of primary importance where acquisition of data is concerned. Much research in the past 25 years has been directed at this particular subject, of which the main achievements are now summarized below.

Two main avenues of investigation have evolved, approaching the problem from subtly different angles, namely

1. **Time domain mechanical spectroscopy (TDMS)**: The determination of the complex modulus $G^*(\omega)$ from measurements in the time-domain was first investigated in [60] by considering an experiment involving the application of a constant strain rate $\dot{\gamma}$ over a finite interval $[0, T_2]$. The response can be divided into two parts. Firstly, starting from a stress-free state the measured stress $\sigma_1(t)$ increases to a constant value $\sigma_0 = \eta_0\dot{\gamma}$ at constant strain rate, allowing the relaxation modulus to be calculated from

$$G(t) = \frac{1}{\dot{\gamma}}\frac{\mathrm{d}\sigma_1}{\mathrm{d}t} \tag{1-2}$$

and the required frequency dependent function can then be obtained from the Fourier transform

$$\eta^*(\omega) = \frac{i\omega}{\dot{\gamma}}\int_0^{T_2}\sigma_1(t)\,\mathrm{e}^{-i\omega t}\,\mathrm{d}t. \tag{1-3}$$

For times subsequent to T_2, stress relaxation is observed after the cessation of steady-state Newtonian flow and the relaxation modulus for this portion of the curve is given by

$$G(t) = -\frac{1}{\dot{\gamma}}\frac{\mathrm{d}\sigma_2}{\mathrm{d}t} \tag{1-4}$$

and correspondingly

$$\eta^*(\omega) = \eta_0 - \frac{i\omega}{\dot{\gamma}}\int_{T_2}^{\infty}\sigma_2(t)\,\mathrm{e}^{-i\omega t}\,\mathrm{d}t. \tag{1-5}$$

The numerical Fourier transform was initially carried out using the FFT, but the Carson-Laplace transform proved to generate better accuracy. Agreement with data obtained from a standard oscillatory test in the "terminal region" (largest relaxation

times) was considered to be reasonable, however a departure from dynamic data at intermediate frequencies was observed. The conclusion was that frequency domain methods provide more accurate data, but the time-saving experienced as a result of using the TDMS method was significant, typically reducing experimental times by a factor of 4 to 8.

2. **Fourier transform mechanical spectroscopy (FTMS)**: Instead of applying a single, fixed-frequency sinusoidal waveform, the idea behind FTMS is to simultaneously apply several harmonic frequencies and thus determine more than one data point on the complex modulus curve from a single experiment using a frequency based analysis. Two approaches have been considered, using periodic and non-periodic waveforms. The first mention of the method concerning periodic waveforms in the literature appears in [35], where a small number of frequencies were simultaneously applied to the sample. Thus, the applied signal has the form of a Fourier series

$$\gamma(t) = \sum_{i=1}^{n} \gamma(\omega_i) = \sum_{i=1}^{n} \gamma_i \sin \omega_i t, \quad \omega_i = m_i \omega_f : \ m_i \in \mathbb{Z}^{\geq 0} \tag{1-6}$$

where ω_f is the fundamental (lowest) frequency applied and the $\{\gamma_i\}$ must satisfy $\sum_{i=1}^{n} \gamma_i \leq \gamma_c$ for some $\gamma_c > 0$ so that the equations of linear viscoelasticity are valid. Linearity implies that the output will also be a periodic signal of the same frequency composition, although with a constant phase shift, provided that sufficient time has elapsed to attain a quasi-steady state. Thus, the output signal takes the form of the Fourier series

$$\sigma(t) = \sum_{i=1}^{m} \sigma(\omega_i) = \sum_{i=1}^{m} [A_i \sin(\omega_i t) + B_i \cos(\omega_i t)] \tag{1-7}$$

where the coefficients of the series can be obtained by applying a discrete Fourier transform to the measured stress data. Thus, the storage modulus $G'(\omega)$ and loss modulus $G''(\omega)$ can be determined for each frequency ω_i using the same equations for the single frequency test,

$$G'(\omega_i) = kl \left[\frac{\sigma(\omega_i)}{\gamma(\omega_i)} \cos \delta(\omega_i) + I\omega_i^2 \right] \tag{1-8}$$

$$G''(\omega_i) = k \frac{\sigma(\omega_i)}{\gamma(\omega_i)} \sin \delta(\omega_i), \tag{1-9}$$

where $\delta(\omega_i)$ is the loss tangent associated with the i-th frequency component and k is a geometric parameter depending upon the specific experimental configuration.

The advantage of this method is that several data can be accumulated from a single experiment, however the experimental time still has to be augmented to allow the transient portion of the response to decline to a negligible magnitude. Additionally, the choice of the amplitudes of each frequency component requires careful choice. If the sum of the magnitudes is too great the linear viscoelastic limit will be exceeded and the governing equations are no longer valid, alternatively the amplitudes of the higher frequency components of the output may be too small to measure with acceptable accuracy if the number of frequencies is increased.

A selection of more sophisticated waveforms was considered in [22] using a moderate number (at least 20) of frequency components in a stress-controlled experimental framework. Two waveforms were considered, based upon a fundamental frequency ω_f:

(**i**) Square waveform:

$$C(t) = C_0 \sum_{j=1,\text{odd}}^{n} \frac{(-1)^{\frac{j-1}{2}} \cos j\omega_f t}{j} \tag{1-10}$$

(**ii**) Equal amplitude cosine waveform:

$$C(t) = C_0 \sum_{k=1,\text{odd}}^{n} \cos k\omega_f t \tag{1-11}$$

In each case the discrete Fourier transform of the data yields the Fourier series coefficients whereby the storage and loss moduli can be obtained using the standard oscillatory equations (1-8)-(1-9). Experimentally, problems encountered with the square wave, taking $n = \infty$ which corresponds to a perfect square wave, were small output strain amplitudes for the higher frequency components, which consequently approached the minimum strain specification for the instrument used in the experimental investigation. This is due to the fact that the torque amplitude of the k-th harmonic is proportional to $1/k$. The highest fundamental frequency is limited by the mechanical inertia of the rotating instrument assembly, which results in very small angular displacements and consequently experimental scatter. The equal amplitude cosine waveform, constructed using $n = 39$, produced generally better agreement with standard data, but the amplitude of higher frequency harmonics in the output strain were still limited by instrument inertia. An increasing amplitude torque waveform was also considered, which gave good agreement at higher frequencies, but conversely a slight discrepancy was observed at lower frequencies due to the low torque amplitudes being applied at low frequencies.

The fundamental question pertaining to the choice of applied torque profile with reference to the FTMS technique is how the applied waveform should be chosen such that the amplitudes of the frequency components of the measured signal are sufficiently large to be measured with acceptable accuracy, whilst conforming to the constraint imposed by the linear viscoelastic limit. The simplest periodic waveforms, such as the square and triangular wave, suffer from very small amplitudes signals at higher frequencies as the number of modes is increased, which leads to inaccurate data at those frequencies [22]. The main constraint upon the amplitudes of the input frequency components is that the sum of the strains should be small enough to lie in the linear viscoelastic regime. The choice of the amplitudes is otherwise arbitrary, but influences the accuracy with which the moduli can be determined. One approach [12] involves minimization of the 'spread' of the amplitudes of both the applied and measured parameters. Assuming the stress is specified as N superimposed frequencies ω_i with phase differences ϕ_i and amplitudes σ_i, for $i = 1, \ldots, N$, then the resultant strain amplitudes will be given by

$$\gamma_i^2 = \frac{\sigma_i^2}{\left[G'(\omega_i) - kI\omega_i^2\right]^2 + \left[G''(\omega_i) - kd\omega_i\right]^2}, \quad i = 1, \cdots, N \tag{1-12}$$

where k, I and d are instrumental parameters. The quantity to be minimized is the parameter S, defined by

$$S = \frac{1}{2}\left[\frac{\sigma_{\max}}{\sigma_{\min}} + \frac{\gamma_{\max}}{\gamma_{\min}}\right]. \tag{1-13}$$

The value $\sigma_{\min}$ can be set arbitrarily due to the linearity of the stress-strain relationship. Rewriting (1-12) in the form

$$\sigma_i = F(\omega_i)\gamma_i \tag{1-14}$$

where $F(\omega_i)$ is a known and strictly non-negative function of ω which has maximum and minimum in the interval $[\omega_{\min}, \omega_{\max}]$ occurring at $\omega = \omega_a$ and $\omega = \omega_b$, respectively. Then, the minimum value of S is satisfied by

$$\frac{\sigma_{\max}}{\sigma_{\min}} = \frac{\gamma_{\max}}{\gamma_{\min}} = \left(\frac{F(\omega_b)}{F(\omega_a)}\right)^{\frac{1}{2}}. \tag{1-15}$$

The extension of the FTMS technique to encompass arbitrary, non-periodic waveforms was first proposed in [59]. However, a potentially significant problem concerning the use of non-periodic functions as an input in controlled stress or strain

rheometry arises from the use of the equations (1-8)-(1-9), which assume that a quasi-steady-state has been achieved. Where periodic waveforms are concerned, this criterion can be satisfied by allowing several cycles to occur before measurement takes place, whereby allowing the transient to decay to negligible values. However, when the property of periodicity is no longer possessed by the applied stress or strain signal, it is no longer obvious whether a steady-state can ever exist and consequently if the equations for $G'(t)$ and $G''(t)$ can be used with any degree of accuracy. If the input profile has significant low frequency components, this may cause more significant problems than a profile consisting mainly of higher frequency components, since the transient constituent of the signal usually decays more rapidly for higher frequencies.

The problem concerning low output amplitudes for higher frequencies can be addressed in an analogous manner to the periodic case. An increasing frequency waveform [29] was tried for which the applied torque was given by

$$C(t) = C_0 \sin\left(\frac{n\pi t^2}{t_1^2}\right), \quad 0 \leq t \leq t_1 \tag{1-16}$$

and is essentially a frequency sweep performed within a single experiment. Although no longer considered to be a candidate for an optimal applied torque, the absolute value of the Fourier transform exhibits a relatively constant value over a finite range of frequencies with a slow decline into the higher frequency region. In [58], the optimal choice of torque input was defined to be that which contains equal amplitudes for all harmonics in a specified range. This implies that in Fourier space the required function is the box function, which assumes a constant value over a defined domain and is zero elsewhere. In the time domain, this is equivalent to applying a strain in the form of the sinc function

$$\gamma(t) = \gamma_0 \frac{\sin \omega_0 t}{t}. \tag{1-17}$$

Favourable results were presented in comparison with standard results in [58], however it is not clear to what extent the method is influenced by the effect of the transient component of the torque which is assumed to be negligible in the subsequent analysis to obtain the storage and loss moduli. In [20] it is noted that from a purely theoretical perspective, the optimal form for an applied strain in terms of frequency content would be the delta function, since the Fourier transform is a Heaviside step function and thus contains equal information about all frequencies.

Another approach taken in [104] was to reduce the experimental time by allowing the use of the transient data to calculate the complex modulus recursively, in comparison to a standard experiment where at least a single oscillation is applied before any measurement takes place, whereby reducing the relative experimental time by at least a factor of two. The advantage is only slight for higher frequencies, but for extremely low frequencies, such as those required by materials composed of fibrin networks or to investigate gelation processes where frequencies as low as 10^{-4} rad s^{-1} might be necessary, the improvement is readily apparent. It was noted in the discourse that data from the first cycle of oscillation can produce errors as great as 16% when the steady state equations are indiscriminately applied, however the error commonly diminishes to around 1% for the second cycle and also that for multi-frequency waveforms the error can be larger, since the sum of the transient responses from all component frequencies is measured, suggesting that the FTMS method can only be reliably applied to periodic waveforms. Another advantage stated for this method is that fluid inertial effects are less significant during the first cycle than are experienced thereafter.

A recent development concerning measurements in the time domain allows $G(t)$ and $J(t)$ to be determined from a single experiment [66], rather than by performing separate creep and relaxation experiments, or performing one experiment and interconverting which requires the solution of an ill-posed problem. The experimental setup is based around "spring loading", as illustrated in Figure 1.4. A viscoelastic bar of the material under investigation of cross-sectional area A_B is connected in series with a Hookean "load spring" with spring constant k_s. At $t = 0$, the lower end of the spring is subjected to a step function displacement of Δl, exerting a tension on the bar which causes a time dependent deformation. As the spring extends, the tensile force decreases, but that in the bar increases. If the material under investigation is a viscoelastic liquid, the length of the bar will increase by the original length of the spring, the spring reverting to its initial length. However, if the material is a viscoelastic solid, an equilibrium will be reached as the force in the spring becomes equal to the elastic forces in the bar.

Applying the linear viscoelastic constitutive equations from (1-34) and (1-37), combined with the relations $\Delta l_b(t) + \Delta l_s(t) = \Delta l$ and $f_{bf}(t) = F_s(t) = k_s\left[\Delta l - \Delta l_b(t)\right]$, the following Volterra integral equations of the second kind are obtained,

$$\Delta l = \Delta l_b(t) + \frac{A_b}{k_s l_b}\left[\int_0^t G(t-t')\,\frac{\mathrm{d}}{\mathrm{d}t'}\left[\Delta l_b(t')\right]\,\mathrm{d}t' + \Delta l_b(0)G(t)\right] \tag{1-18}$$

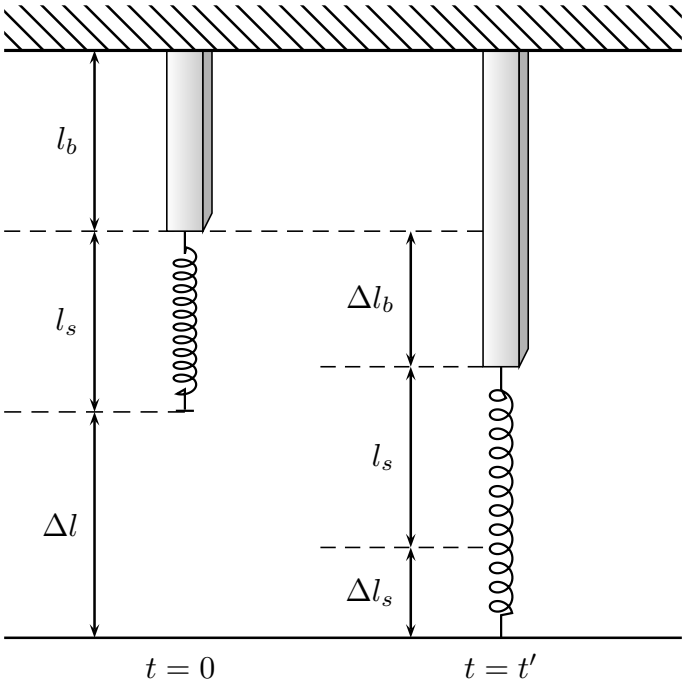

Figure 1.4: Spring-loading experiment to determine creep and relaxation functions simultaneously.

$$k_s \Delta l = \frac{k_s l_b}{A_b} \left[\int_0^t J(t-t') \frac{\mathrm{d}}{\mathrm{d}t'} \left[f_{bf}(t') \right] \mathrm{d}t' + f_{bf}(0) J(t) \right] \tag{1-19}$$

the solutions of which are well-posed problems. Use of the interconversion condition (1-52) provides equations relating the relaxation modulus and creep compliance in terms of either $f_{bf}(t)$ or $\Delta l_b(t)$, indicating that the two equations can be solved simultaneously or sequentially. Although it appears that an ill-posed problem has been replaced by two well-posed problems, in fact the instability is transferred to the data through the presence of the derivatives of the measured variables $f_{bf}(t)$ and $\Delta l_b(t)$. The degree of ill-posedness of the differentiation process is equivalent to the degree of ill-posedness of the interconversion condition. The advantage of being able to obtain both functions from a single experiment is clear however, in terms of experimental time and stable solution techniques are more readily found for the pair of equations of the form in (1-18) and (1-19). This method seems to be the best choice where viscoelastic solids are concerned, however it is not obvious how the setup can be adapted to accommodate viscoelastic liquid materials which cannot easily be constrained in bar form when subjected to extensional stresses.

The approach taken in this thesis differs from previous methods of tackling the problem of defining an optimal form for the applied torque in a stress-controlled experiment by considering the intrinsic properties of the governing equations, which are of Volterra form when the solution is taken to be the relaxation modulus. The optimal

applied torque is defined to be that which minimizes the ill-posedness of the problem, whereby resulting in the most stable solution for the relaxation modulus. Using the definition of the ν-smoothing problem in [50] for Volterra integral equations of the first kind, which are well-known to be ill-posed, the degree of ill-posedness is demonstrated to be dependent upon the behaviour of the platen angular velocity near $t = 0$. The optimal form for the applied torque in a theoretical sense is the delta function, but since it is debatable whether this torque can be reproduced experimentally, the next best form for the applied torque is a box function, which produces a step increase in the platen angular acceleration at $t = 0$. It is concluded that applied torque functions which exhibit slow growth near $t = 0$ produce the least stable problem and should be avoided if possible. This result is compatible with the conclusions in [58], since the sinc function also belongs to the nearly optimal class of 2-smoothing problems - the additional assumption concerning the equal amplitudes for higher frequencies is an experimental consideration, which complements the theoretical conclusions reached here.

Additionally, a numerical scheme for obtaining the relaxation modulus directly in near real-time from a controlled stress experiment is presented here. The basic discretization of the Volterra integral equation is shown to be inadequate for accurate solution for the relaxation modulus due to the ill-posedness of the problem in the presence of noisy data. This is probably the main reason why little interest has been shown in solving the governing integral equations for the controlled-stress rheometry experiment directly. Thus, regularization is required to obtain a reasonable solution and it is here demonstrated that the future-constant [47] and future-polynomial [18] regularization methods of Volterra type are effective at obtaining a stable and accurate solution even in the presence of noisy data, for appropriate choices of the regularization parameter(s).

Despite the abundance of new techniques proposed in recent times, the simple small-amplitude oscillatory shear experiment still remains the standard technique for determining the linear viscoelastic functions, perhaps only superseded by FTMS in its most elementary form using a small number of discrete frequencies to represent the interval of interest. The main rationale is perhaps the mathematical and experimental simplicity involved in obtaining the relaxation modulus from a sinusoidal input once a steady-state has been achieved. Although the experimental time involved in constructing a complete complex modulus curve can be seemingly interminable, particularly if low-frequency data is required, the data acquired by this method for temporally stable

materials is of the best quality attainable, since only a single datum or perhaps several data points are obtained from each experiment and several cycles can be averaged to improve the data further. The method is robust in the sense that accurate data can be reliably obtained for any material, provided the linear viscoelastic limit is adhered to. A further drawback of using the FTMS method with large numbers of frequency components is that the quality of the data is dependent upon the choice of the relative amplitudes in the input signal - if the overall sum is too large, the linear viscoelastic will be exceeded and the governing equations no longer valid and if certain frequency components in the output are small in magnitude, the instrument sensor will be unable to resolve that component with sufficient accuracy.

The main advantage of the technique proposed here is that the relaxation modulus can be obtained directly almost in real-time using the measured values of the applied torque and output platen angular displacement. The relaxation modulus can be determined over the interval defined by the experiment, less the length of the future interval used in the regularization method, whereby circumventing the problem of sampling localization inherent in the frequency-domain experiments. However, there are some disadvantages to take note of. Firstly, in common with multi-frequency waveforms it may be difficult to choose the amplitude of the applied torque such that the output displacement is sufficiently small to lie within the linear viscoelastic region, whilst being sufficiently large that the instrument sensors can measure the displacement with reasonable accuracy. The choice of the value of the regularization parameter for a particular experiment may also be problematic, since there is no automatic means for choosing the optimal value. If the value is chosen to be too high, over-smoothing results and the solution diverges from the actual solution, whereas if the value chosen is too small, the data will still contain spurious oscillations as a result of the data noise and inherent ill-posedness of the problem.

The underlying theory for linear viscoelasticity is now explored in more detail as a basis for the development of the governing equations for stress-controlled rheometry in Chapter 2.

II. LINEAR VISCOELASTICITY

The study of the deformation of materials has long provided an area of interest for philosophers and scientists. The documented history begins in the 17th century with the pioneers in the fields of solid and fluid mechanics: Hooke and Newton, who set

down relations between force and deformation for the first time for solid and liquid materials, respectively. At that time, materials were assumed to belong to one of two distinct classes - which were later to become known as the Hookean elastic solid or Newtonian viscous fluid. A solid or *arrheodictic* material may be defined [94] as one which does not continuously change its shape when subjected to a stress, while a liquid or *rheodictic* material will continuously change its shape (i.e. flow) when subjected to a given stress, irrespective of the size of that stress. A solid possesses a reference state in which the material is free of the effects of any stress or strain history it may have experienced prior to deformation, but for liquids there is no preferred configuration and it makes no sense to talk about an undeformed state.

1.2.1 Hookean Elastic Solid

In 1678, Robert Hooke introduced his theory of elastic materials [37]. Experiments with springs led him to deduce that the tension in the spring was related to the extension by a simple linear equation.

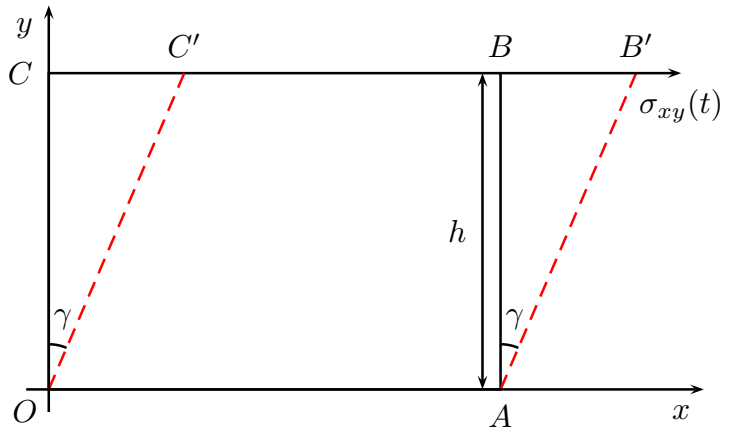

Figure 1.5: Deformation of a Hookean elastic solid material.

By considering a small shear deformation of an elastic solid material, here taken to occupy the rectangular block $OABC$ initially at $t = 0$, which under deformation becomes the parallelogram $OAB'C'$ at $t = t' \geq 0$ with angle $\widehat{COC'}$ denoted by $\gamma(t)$ as shown in Figure 1.5, the relationship between shear stress $\sigma_{xy}(t)$ and strain $\gamma(t)$ at time $t \geq 0$ is given by

$$\sigma_{xy}(t) = g\gamma(t), \tag{1-20}$$

where the constant g is referred to as the *rigidity modulus*.

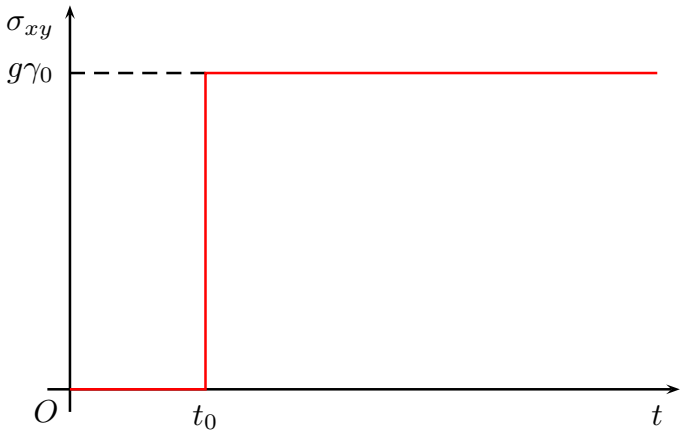

Figure 1.6: Response of a Hookean solid to a step strain function.

Note that if a step strain, $\gamma_{xy}(t) = \gamma_0 H(t - t_0)$ is applied at $t = t_0$, then $\sigma_{xy}(t) = \gamma_0 g H(t - t_0)$. From this it can be deduced that the strain response is instantaneous, reaching an equilibrium value $g\gamma_0$ as shown in Figure 1.6. Conversely, if a step strain is imposed, the stress will also be described by a step function. In a perfectly elastic material, the energy required to deform the material is stored and can be completely recovered when the applied stress is removed.

1.2.2 Newtonian Fluid

The corresponding model for viscous fluids was proposed by Isaac Newton in part of his great mathematical treatise [65]. Consider a liquid contained between two large parallel plates, the upper of which is moved with a constant velocity in a fixed direction until a steady state is obtained as illustrated in Figure 1.7. The velocity at any point is $v_1 = v_1(y), \quad v_2 = v_3 = 0$. Assuming the flow is laminar, if f is the frictional force resisting the motion of two adjacent parallel laminae past each other and a is the area of the plates, then the shear stress (f/a) is given by

$$\sigma_{xy}(t) = \eta\dot{\gamma}(t), \tag{1-21}$$

where η is the *coefficient of shear viscosity* and the *strain-rate* is defined $\dot{\gamma} = \frac{\mathrm{d}v_1}{\mathrm{d}y}$. If a step stress $\sigma_{xy}(t) = \sigma_0 H(t)$ is applied in this case, it can be seen that the strain rate will increase instantaneously to an equilibrium value σ_0/η, but the strain γ will increase linearly as a function of time with gradient σ_0/η as shown in Figure 1.8. The energy required to deform the material, in contrast with the elastic solid, is entirely dissipated as heat due to the friction as the laminae flow over each other.

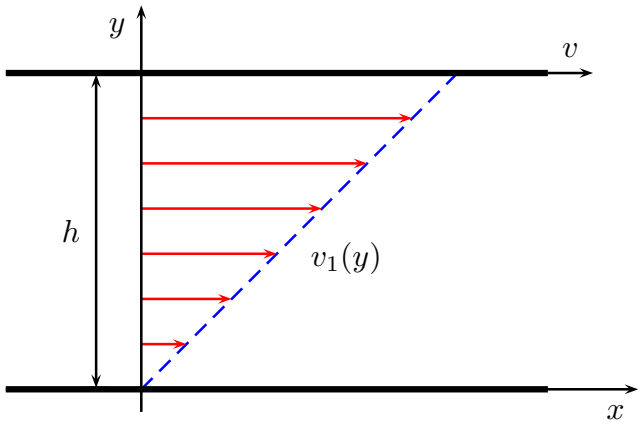

Figure 1.7: Laminar flow for a Newtonian fluid.

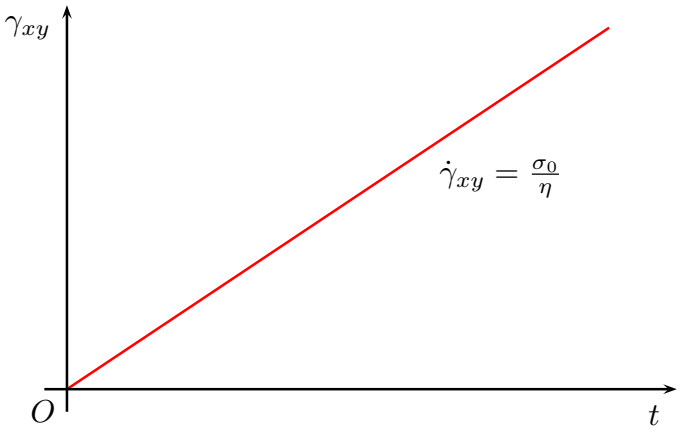

Figure 1.8: Strain-rate response of a Newtonian fluid to a step stress function.

1.2.3 Viscoelasticity

The classification of materials into the extremes of Hookean elastic solid and Newtonian viscous fluid was accepted for over a century, until experiments with certain materials revealed behaviour that could not be described by either of the classical theories of elasticity and viscous fluid flow alone. The permanent deformation of metals when the stress increases beyond a certain limit is one such example. In 1835, the German physicist Wilhelm Weber [98] noted that the elasticity of silk threads in tension is not perfect - an immediate elastic tension is followed by continued slow extension as a function of time. When the force is removed from the thread, it returns to its original length; an process known as creep and recovery today. This was the first description of the concept of a *viscoelastic* material, i.e. one that displays both elastic and viscous tendencies.

It is reasonable to assume that all materials are viscoelastic, since under deformation some energy is always stored and some dissipated. Over large timescales, a material that appears to be solid in nature over short timescales may flow like a fluid. This

leads to the definition of a dimensionless parameter which relates the characteristic time of the deformation process to a characteristic time associated with the material, known as the *Deborah number* [76],

$$D_e = \frac{\lambda_{\text{mat}}}{\lambda_{\text{exp}}}, \tag{1-22}$$

where $\lambda_{\text{mat}}, \lambda_{\text{exp}}$ are the characteristic material and experimental times, respectively. A limiting value of zero corresponds to viscous fluid behaviour while infinity corresponds to that of an elastic solid. For intermediate values, viscoelastic behaviour is observed.

Viscoelastic materials such as polymers, soils, bitumen, concrete, cartilage and many bodily fluids are familiar in modern everyday life. A considerable proportion of rheological study has been directed towards polymeric materials, encouraged by the significant use of these materials in engineering and manufacturing. The viscoelastic behaviour of polymers arises from the movement of thread-like, flexible long-chain *macromolecules* [102] which occupy a volume considerably greater than atomic dimensions. As the material undergoes deformation, internal forces develop as a result of molecular changes in configuration, involving rearrangements on three scales:

1. Long-range contour rearrangements, e.g. convolutions (slow)
2. Local level rearrangements, e.g. kinks (more rapid)
3. Reorientation of bonds on the chain backbone on the atomic scale

Hence, the stresses are influenced on several timescales, giving rise to complex behaviour as the internal stresses adjust varying rates. The distinction between solid-like and fluid-like behaviour is related to the presence of cross-linking in the structure. If present, as illustrated in Figure 1.9 the resulting network limits the maximum possible deformation and intermolecular forces cause the original configuration to be regained. However, if the polymer is not cross-linked (Figure 1.10), under constant stress the macromolecules continue to slide over each other and flow. When the stress is removed, there are no intermolecular forces to return the molecules to their original configuration.

1.2.4 Maxwell Model

The first constitutive equation specifically suited to modelling a viscoelastic material was proposed in 1867 by James Clerk Maxwell [61], although the original purpose of

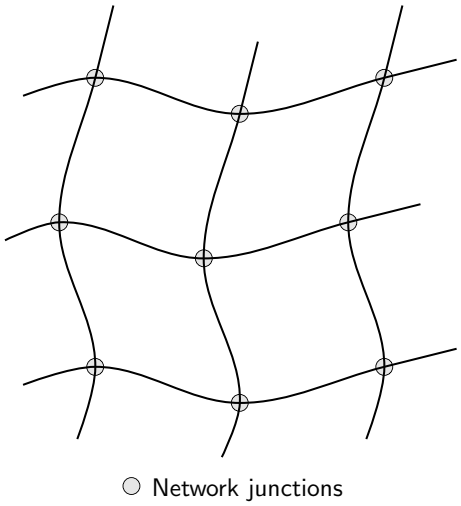

Figure 1.9: Viscoelastic material with cross-linked structure.

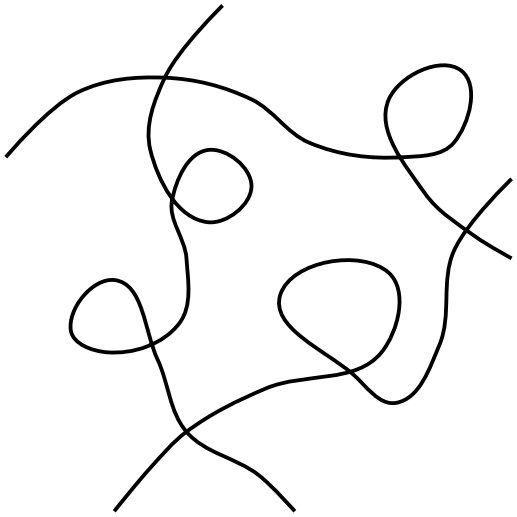

Figure 1.10: Viscoelastic material without cross-linked structure.

the experiment was to determine the viscosity of a gaseous material. In the case of simple shear, the form for the Maxwell constitutive equation is

$$\sigma_{xy}(t) + \lambda\dot{\sigma}_{xy} = \eta\dot{\gamma}_{xy}, \tag{1-23}$$

where λ is a constant termed the *relaxation time*. Linear viscoelastic models such as this are often represented by mechanical analogues, composed of various configurations of springs, which represent the Hookean elastic component, and *dashpots*, which represent the Newtonian fluid component of the material behaviour. In this form, the Maxwell model corresponds to a dashpot and spring in series as shown in Figure 1.11.

The constitutive equation can be derived by assuming that the total strain rate is equal to the sum of the strain rates of the spring and dashpot, i.e.

$$\dot{\gamma}(t) = \dot{\gamma}_e(t) + \dot{\gamma}_v(t) = \frac{\dot{\sigma}(t)}{g} + \frac{\sigma(t)}{\eta} \tag{1-24}$$

Note that taking the limits $\eta = 0$ and $g = \infty$ corresponds to the Hookean and Newtonian cases, respectively.

Solving the differential equation in (1-23) leads to

$$\sigma_{xy}(t) = \int_{-\infty}^{t} \frac{\eta}{\lambda} \mathrm{e}^{-\frac{(t-t')}{\lambda}} \dot{\gamma}_{xy}(t)\,\mathrm{d}t' + c\,\mathrm{e}^{-\frac{t}{\lambda}} \tag{1-25}$$

where $c = 0$, since $\lim_{t\to-\infty} \sigma_{xy}(t)$ must be finite. Under step-strain conditions, $\gamma_{xy}(t) = \gamma_0 H(t)$,

$$\sigma_{xy}(t) = \frac{\eta\gamma_0}{\lambda} \mathrm{e}^{-\frac{t}{\lambda}}, \tag{1-26}$$

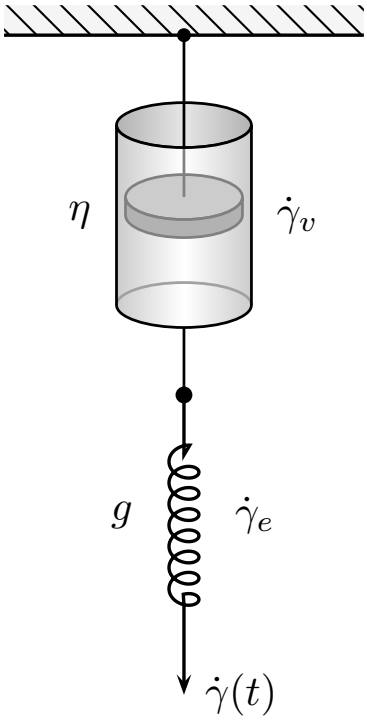

Figure 1.11: Spring-dashpot representation of the Maxwell model. The spring represents the elastic contribution and the dashpot represents the viscous contribution to the behaviour of the material.

it can be seen that the stress jumps to an initial value $\frac{\eta\gamma_0}{\lambda}$, then relaxes exponentially to zero as shown in Figure 1.12. The relaxation time $\lambda = \frac{\eta}{g}$ is the time for the stress to relax to e^{-1} of its initial value. The physical explanation for this behaviour is that while the material body is constrained in a fixed shape, the molecules readjust to more favourable internal configurations which gradually produce lower stresses. For a Newtonian fluid, $\lambda = 0$ and for a Hookean solid $\lambda = \infty$. It has been estimated that for water $\lambda \approx 10^{-12}\, s$. Note that the Maxwell model can only model viscoelastic fluid behaviour, since under step stress conditions the strain does not reach an equilibrium value, corresponding to the indefinite extension of the dashpot element in the mechanical model.

1.2.5 Kelvin-Voigt Model

The second model proposed for viscoelastic materials is often referred to as the Kelvin-Voigt (K-V) model, although the first occurrence of the constitutive equation is attributed to Meyer [63]. Kelvin applied the concept of Meyer's model to the damping of metals, and Voigt later generalized to anisotropic media. The constitutive equation for this model takes the form

$$\sigma_{xy}(t) = g\gamma_{xy}(t) + \eta\dot{\gamma}_{xy}(t), \tag{1-27}$$

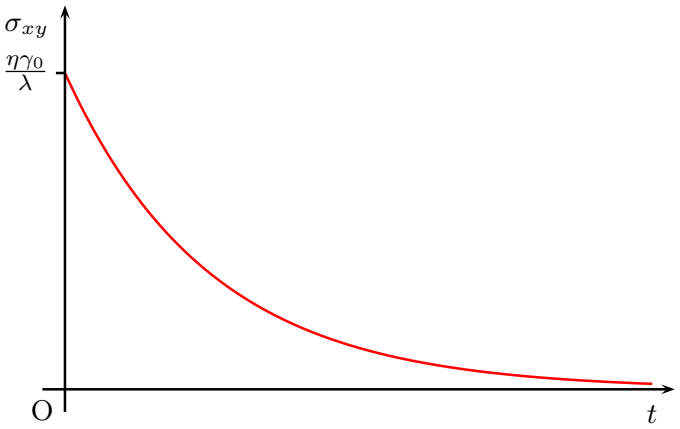

Figure 1.12: Response of a Maxwell fluid to a step-strain function.

which is equivalent to a spring and dashpot in parallel in terms of a mechanical model as shown in Figure 1.13. Occasionally, the parameter used to characterize the spring is the *compliance*, $J = 1/g$. The result in (1-27) is obtained by assuming that the total stress is the sum of the stresses in each component, so that

$$\sigma(t) = \sigma_e(t) + \sigma_v(t) = g\gamma(t) + \eta\dot{\gamma}(t). \tag{1-28}$$

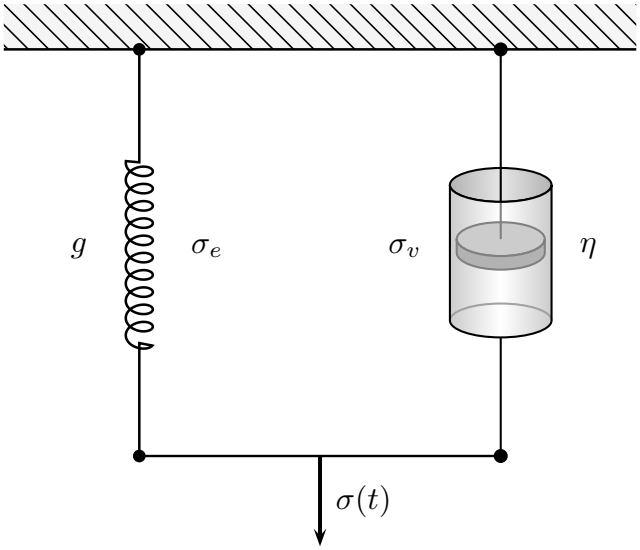

Figure 1.13: Spring-dashpot representation of the Kelvin-Voigt model.

The K-V model does not show stress relaxation under constant strain as for the Maxwell model, since the stress remains constant. Hence, the K-V model is not capable of describing viscoelastic fluid behaviour. However, under step-stress $\sigma_{xy}(t) = \sigma_0 H(t)$,

$$\gamma_{xy}(t) = \sigma_0 J \left(1 - \mathrm{e}^{-\frac{t}{\tau}}\right) \tag{1-29}$$

the strain reaches the same equilibrium value as for the Hookean model, $\frac{\sigma_0}{g}$, but the strain growth is retarded as illustrated in Figure 1.14. The *retardation time*, τ, is defined as the time taken to reach $(1 - \mathrm{e}^{-1})$ of its final equilibrium value, or alternatively the time taken to fall to e^{-1} when the shear stress is removed.

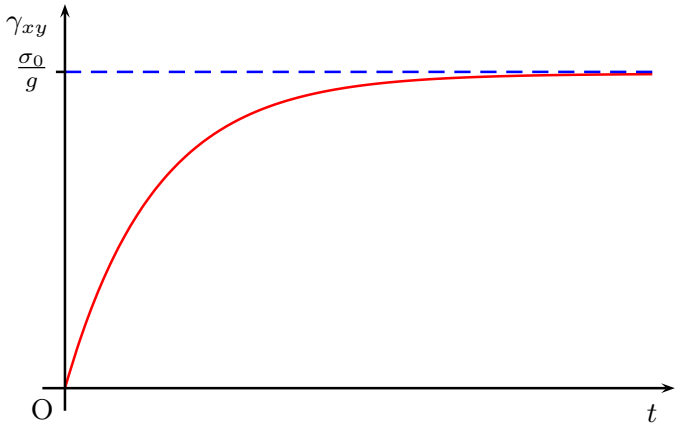

Figure 1.14: Response of the Kelvin-Voigt model to step stress.

1.2.6 General Linear Models

Both of the Maxwell and Kelvin-Voigt models are examples of linear viscoelastic constitutive models, in the sense that the constitutive equations are represented by linear, first-order differential equations. However, it has been noted that neither model is completely general in the sense that the Maxwell model cannot describe strain retardation and the Kelvin-Voigt model cannot describe stress relaxation, hence the two models describe different behaviour for the same prescribed stimulus. To model linear viscoelastic solid-like behaviour, a minimum of three elements are required [94] - namely two springs and one dashpot, while liquid-like behaviour requires at least four elements - two springs and two dashpots. By adding a lone spring in parallel to the Maxwell element, a model which describes solid-like behaviour can be obtained. When these requirements are satisfied and with certain choices of parameters, the qualitative behaviour predicted by any of these models is of the same nature under a given prescribed stimulus.

More complicated models be created by taking various combinations of springs and dashpots in parallel or serial configuration (see [9],[94] for examples), but it has

been shown that all models, irrespective of complexity, can be reduced to one of two canonical forms [82]. These are the generalized Maxwell and Kelvin-Voigt models, respectively.

The generalized Maxwell model consists of a finite number, N, or an enumerably infinite number of Maxwell elements in parallel as illustrated in Figure 1.15, each with a different combination of spring and dashpot constants, g_i and η_i, for $i = 1, \ldots, N$. The stress then has the form

$$\sigma(t) = \sum_{i=1}^{N} g_i \int_{-\infty}^{t} \mathrm{e}^{-\frac{t-t'}{\lambda_i}} \dot{\gamma}(t')\, \mathrm{d}t', \tag{1-30}$$

where $\{g_i\}$ are the spring constants and $\{\lambda_i\}$ are constants with the dimensions of time, known as the relaxation times and are defined by $\lambda_i = \eta_i / g_i$.

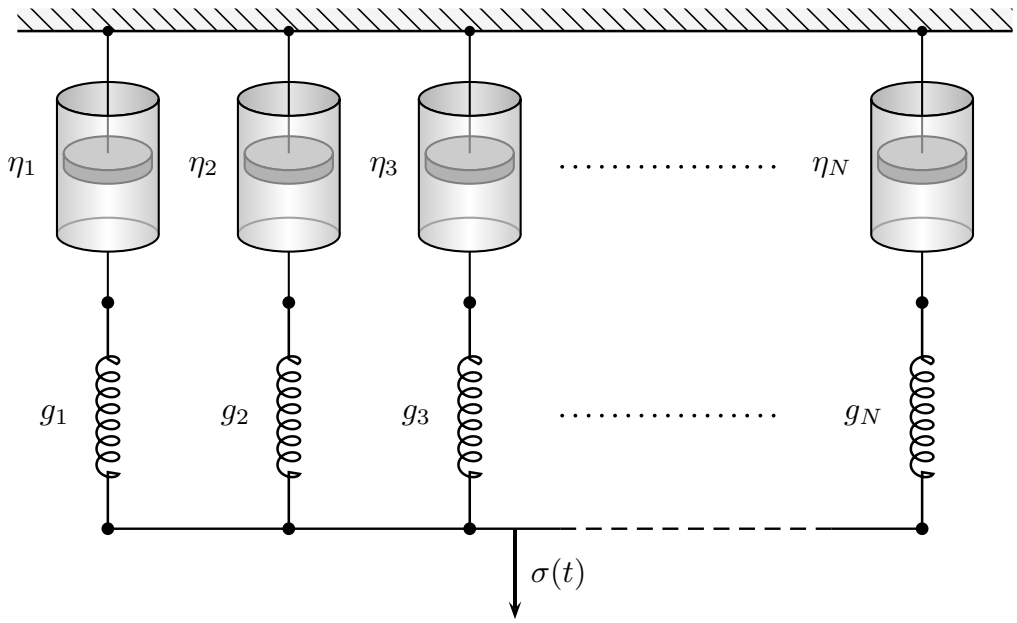

Figure 1.15: Spring-dashpot representation of the N-mode Maxwell model.

The generalized Kelvin-Voigt model is obtained in a similar fashion, but by combining K-V elements in series. This leads to the definition of the *creep compliance* as stress/strain ratio under step-stress conditions.

1.2.7 The Boltzmann Equation

The theory of linear viscoelasticity as it is known today is largely as a result of the work of Ludwig Boltzmann [15]. The concept now known as the principle of fading memory was developed by Boltzmann, and states that the stress at time t depends not only on

the current strain at that time, but also on those for all previous times. The contribution decreases as the interval from the current time increases.

This was followed by the principle of superposition, which implies that if either one of the single-step response functions $G(t)$ or $J(t)$ is known, then the output resulting from any input can be predicted [27, 102]. The relaxation modulus is defined to be the stress/strain ratio under step-strain conditions, thus the stress will be

$$\sigma(t) = \gamma_0 G(t) \tag{1-31}$$

and if a higher strain $\gamma_0 + \gamma_1$ is applied, then $\sigma(t) = (\gamma_0 + \gamma_1)G(t)$ by linearity. However, if a strain γ_0 is applied at time $t = 0$ and an additional strain γ_1 is subsequently applied at $t = t_1$, then according to Boltzmann's superposition principle the total stress will now be the linear superposition of the two resultant stresses at their respective times,

$$\sigma(t) = \gamma_0 G(t - t_0) + \gamma_1 G(t - t_1). \tag{1-32}$$

The generalization to an arbitrary number of step strain functions is then easily deduced to be

$$\sigma(t) = \sum_{t_i=-\infty}^{t_i=t} \gamma_i G(t - t_i) \tag{1-33}$$

Hence, the stress resulting from an arbitrary strain history can be estimated by approximating the function representing the strain by a series of step functions. Taking the limit as the number of step functions increases to infinity and the discrete $\{t_i\}$ approach a continuum, the Stieltjes integral

$$\sigma(t) = \gamma_0 G(t) + \int_{0+}^{t} G(t - t') \, \mathrm{d}\gamma(t') \tag{1-34}$$

is obtained. This is the constitutive equation for linear viscoelasticity, more commonly expressed in the form

$$\sigma(t) = \gamma(0) G(t) + \int_{0+}^{t} G(t - t') \dot{\gamma}(t') \, \mathrm{d}t'. \tag{1-35}$$

By the definition of the convolution integral an equivalent form of (1-35) can be found relating the stress and strain through the *memory function*, $M(t) = -\frac{\mathrm{d}G}{\mathrm{d}t}$.

$$\sigma(t) = G(0)\gamma(t) - \int_{0+}^{t} M(t - t')\gamma(t') \, \mathrm{d}t' \tag{1-36}$$

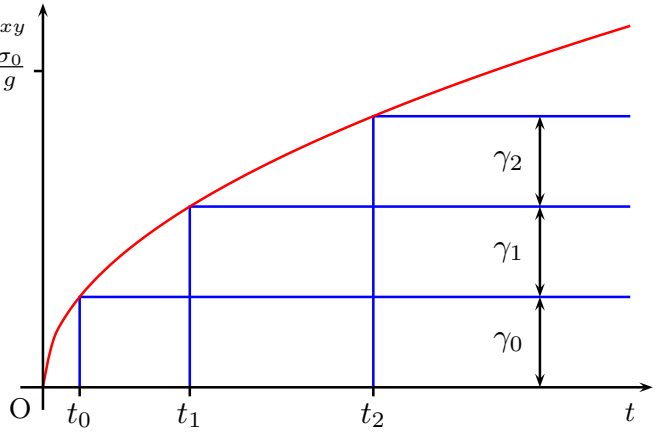

Figure 1.16: The Boltzmann superposition principle, whereby an arbitrary strain history can be approximated by a series of step functions.

Alternatively, by considering the application of step stresses and using the definition of the creep compliance, $J(t)$, as the stress/strain ratio under step-stress conditions, a corresponding equation can be derived relating the strain and stress through the creep compliance.

$$\gamma(t) = \sigma(0)J(t) + \int_{0+}^{t} J(t-t')\,\mathrm{d}\sigma(t') \tag{1-37}$$

The above results are subject to the assumption which underlies the theory of linear viscoelasticity, namely that the deformations considered are sufficiently small, or the rate of deformations sufficiently slow that the linear approximation is valid. Under such conditions, the statistical distribution function characterizing the microstructure of the fluid is only slightly perturbed from equilibrium [62]. Therefore, the theory of linear viscoelasticity can not model viscoelastic behaviour observed in a completely general sense, but provided the deformation constraint is adhered to the agreement between predicted and experimentally observed is considered sufficiently accurate.

Rheological phenomena which are described as *non-linear* are observed in certain fluids with complex structure such as polymer melts and solutions when the deformations are greater than the linear viscoelastic limit. Two examples are:

1. **Shear-rate dependent viscosity**: The viscosity for certain materials either increases for increasing shear-rate (rheopexy), or more commonly decreases (thixotropy). The change in viscosity is time-dependent and the original properties are gradually recovered after cessation of shear.

2. **Normal stress-effects**: In steady flows, the normal stresses defined in terms of the stress tensor, $N_1(\dot{\gamma}) = \sigma_{xx} - \sigma_{yy}$ and $N_2(\dot{\gamma}) = \sigma_{yy} - \sigma_{zz}$, can take non-zero values. These can result in phenomena [9] such as the Weissenberg effect, observed

when a rotating rod is placed in a shallow dish of viscoelastic fluid. A Newtonian fluid would move towards the edge of the vessel by inertia causing a higher surface near the boundary, but the viscoelastic fluid produces a surface higher near the rod and the material appears to climb the rod due to a non-zero $N_1(\dot{\gamma})$ which draws the fluid inwards around the boundary of the rod. Another effect is 'die swell", observed when certain viscoelastic fluids flow from the exit of a tube, whence it swells to a much great diameter than that of the tube which increases with an increase in flow rate.

To model such behaviour requires constitutive equations non-linear in nature and hence of greater complexity than the linear viscoelastic constitutive equation. However, solving problems using such equations is considerably more difficult and determining the material parameters from these equations even for simple geometrical flows can be an intractable problem. Here, the simplicity of the linear model becomes a distinct advantage, allowing the material parameters such as the relaxation modulus to be determined in simple experiments where the deformations are sufficiently small and thence substituted in more complex constitutive models to solve real world problems. Now we proceed to look at how the linear viscoelastic model fits in within the framework of general constitutive models through the simple fluid model.

1.2.8 Simple fluid of Coleman and Noll

Early work on developing constitutive models for non-Newtonian fluids was based upon the assumption that the stress is uniquely determined by the instantaneous rate of deformation, such as the Reiner-Rivlin model [77, 79], which has constitutive equation

$$T_{ik} = 2\eta(I_2, I_3)d_{ik} + 4\zeta(I_2, I_3)d_i^j d_{jk}, \tag{1-38}$$

where I_2, I_3 are the two non-zero invariants of the strain-rate tensor D_{ik}, $T_{ik} = p\delta_{ik} + \sigma_{ik}$ is the extra stress tensor and ζ is a constant. Such a model could account for shear-rate dependent viscosity, but not normal-stress differences and hence was not completely general. This was the motivation for the development of the "simple fluid" model by Coleman and Noll [19]. Here a summary is given of the main features [6] of the constitutive model and demonstrate how the linear model is a special case.

Four axioms form the basic assumptions which underlie the simple fluid theory:

1. **Determinism of stress**: The stress is determined by the entire history of deformation and is independent of future deformations. This introduces the concept of

'memory'.

2. **Local action**: The stress at a given point is uniquely determined by the history of deformation of an arbitrarily small neighbourhood of that material point.

3. **Non-existence of a natural state**: A fluid material has no preferred configuration or 'natural state'. Any difference in stress is due therefore only to a difference in the deformation history experienced. Every simple fluid is isotropic.

4. **Fading memory**: The influence of past deformations on the stress at the present time diminishes the further into the past is considered. The entire history to $t' = -\infty$ can never be known, so fading memory allows experiments of finite duration, since contributions of deformations prior to the experiment give a negligible contribution to the stress. This gives rise to the concept of a 'natural time' for a fluid, which is a measure of the memory span and dictates the minimum acceptable duration of an experiment.

The constitutive equation is based upon a functional to incorporate the concept of memory, the general form for which is

$$\boldsymbol{T}(\boldsymbol{x},t) = \overset{\infty}{\underset{s=0}{\mathcal{H}}}\left[\boldsymbol{G}(\boldsymbol{x},t,s)\right] \tag{1-39}$$

where $s = t - t'$ is the time lag. The *relative finite strain tensor* is defined

$$\boldsymbol{G}(\boldsymbol{x},t,s) \equiv \boldsymbol{C}(\boldsymbol{x},t,t-s) - \boldsymbol{I} \tag{1-40}$$

where $\boldsymbol{C}$ is the Cauchy-Green strain tensor defined in terms of the deformation gradient tensor $\boldsymbol{F}$ by $\boldsymbol{C}(\boldsymbol{x},t,t') = \boldsymbol{F}^T(\boldsymbol{x},t,t')\boldsymbol{F}(\boldsymbol{x},t,t')$, and $\boldsymbol{I}$ is the identity tensor.

The general form for the constitutive equation is of little practical use, but insights can be gained by considering the limiting values of slow flow and small deformations. Coleman and Noll first considered "retarded" strain histories described by

$$\boldsymbol{G}_\alpha(\boldsymbol{x},t,s) = \boldsymbol{G}(\boldsymbol{x},t,\alpha s). \tag{1-41}$$

Taking the limit as $\alpha \to 0$ causes any history $\boldsymbol{G}$ to approach the zero history. By taking N-th order approximations, it can shown that

1. **Zeroth-order**: For $N = 0$, the stress is simply hydrostatic

$$\boldsymbol{T} = -p\boldsymbol{I} \tag{1-42}$$

2. **First-order**: For $N = 1$, the stress is given by the equation for Newtonian flow:

$$\boldsymbol{T} = -p\boldsymbol{I} + \eta \boldsymbol{A}^{(1)} \tag{1-43}$$

where $\boldsymbol{A}^{(1)}$ is the first Rivlin-Ericksen tensor. Hence, Newtonian fluids may be regarded as simple fluids whose natural time is so small that any practical flow of interest may be considered slow.

3. **Second-order**: For $N = 2$, the first contribution of 'memory' appears in the final term

$$\boldsymbol{T} = -p\boldsymbol{I} + \eta \boldsymbol{A}^{(1)} + \alpha_1 \left[\boldsymbol{A}^{(1)}\right]^2 + \alpha_2 \boldsymbol{A}^{(2)}, \tag{1-44}$$

where $A^{(2)}$ is the second Rivlin-Ericksen tensor. Define the norm $\|\boldsymbol{G}\|$ by

$$\|\boldsymbol{G}(s)\|_h = \int_0^\infty |\boldsymbol{G}(s)|^2 h^2(s)\, \mathrm{d}s, \tag{1-45}$$

where the scalar-valued function $h(s)$ is an *influence function* satisfying $h(s) > 0$ for $s \in [0, \infty)$ and $\lim_{s\to\infty} s^N h(s) = 0$. It can then can be shown that provided the deformation is small, the norm $\|\boldsymbol{G}\|$ will be sufficiently small and a first order approximation to the constitutive equation of a simple fluid with fading memory can be shown to be

$$\boldsymbol{T} = -p\boldsymbol{I} + \int_0^\infty G(s)\boldsymbol{A}^{(1)}(\boldsymbol{x}, t, s)\, \mathrm{d}s, \tag{1-46}$$

which should be recognized as the constitutive equation of linear viscoelasticity. Thus, the simple fluid model provides a theoretical justification for the conditions of validity for the model proposed by Boltzmann nearly a century earlier.

III. LINEAR VISCOELASTIC FUNCTIONS

To describe the deformation of a material under a given stress, or vice versa, a constitutive relation is required which links the excitation and response functions through another material dependent function which is unique to the material under consideration. Several such functions exist and all are mathematically equivalent and hence contain the same information about the properties of the relevant material under consideration [27]. Provided the strain or strain gradients are sufficiently small so that the behaviour is linear, the viscoelastic functions are independent of the magnitude of the stress or strain excitation. The material functions are subdivided into two groups:

those associated with stress relaxation experiments and those associated with creep experiments, although any of those functions listed can be determined in principle from either type of experiment. We now proceed to describe each function in turn and see how they are related to each other.

The mathematical equivalence [86] of all the linear viscoelastic material functions described in this section implies that the choice of which function to measure is entirely down to preference, since in principal any of the other material functions can be obtained through exact analytical solution of the interconversion equations. This approach is based on the assumption that the function which is measured is determined with perfect accuracy over the entire domain upon which it is defined, however this is never the case experimentally. Practical considerations dictate that the data obtained from experiments will only cover a subinterval $[0, T]$ of the interval over which the material functions are defined, $[0, \infty]$, where $0 < T < \infty$. Additionally, the data will contain errors of a certain level, which cause problems with inversion of the integral interconversion formulae which are often ill-posed. A graphical summary of the relationships between the various functions is shown in Figure 1.17, while Figure 1.18 shows some of the approximate methods which are required in practice.

1.3.1 Relaxation Modulus

The relaxation modulus is defined through the application of a step strain to the material under consideration. Assuming the strain amplitude is γ_0, then the stress is determined by $\sigma_{xy}(t) = \gamma_0 G(t)$, hence if the strain is measured then the relaxation modulus can easily be determined. More generally, the relaxation modulus is the kernel function relating the stress response to an arbitrary strain in the integral equation in (1-35). In (1-30), the relaxation modulus for the N-mode Maxwell takes the form of a *Dirichlet series*, also known as a *Prony series*:

$$G(t) = G_\infty + \sum_{i=1}^{N} g_i \, \mathrm{e}^{-\frac{t}{\lambda_i}} \tag{1-47}$$

where the $\{g_i\}_{i=1}^N$ are the elastic moduli and the $\{\lambda_i\}_{i=1}^N$ are the relaxation times. The term G_∞ is included to include viscoelastic solid behaviour, representing the fact that under constant strain the stress will never relax to zero. This corresponds to a separate spring in parallel with the N Maxwell elements in the mechanical model.

The mechanical model approach suggests that the relaxation modulus must be of exponential series form as in (1-47), but this is misleading. Several other forms have

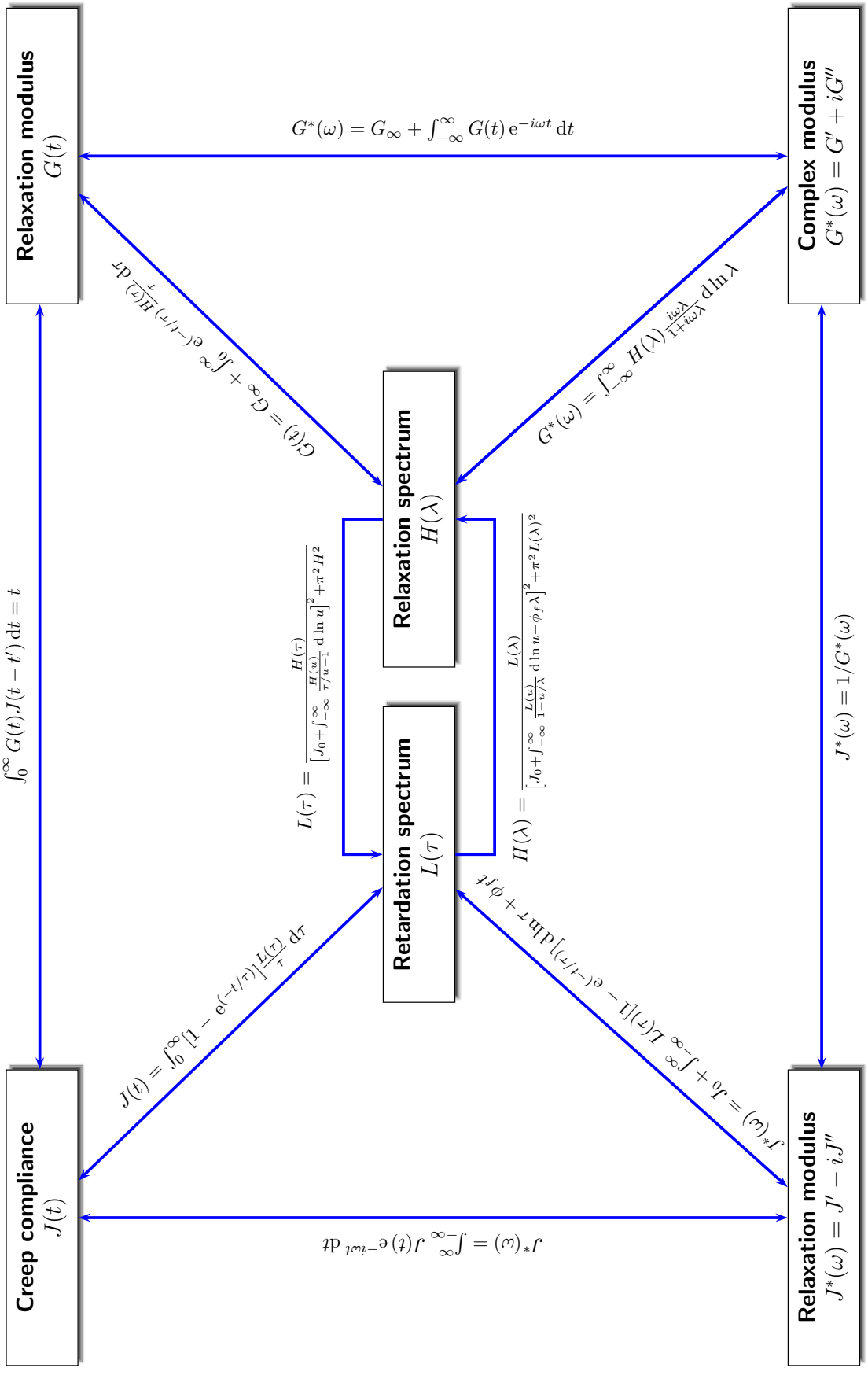

Figure 1.17: Interconversion of linear viscoelastic functions.

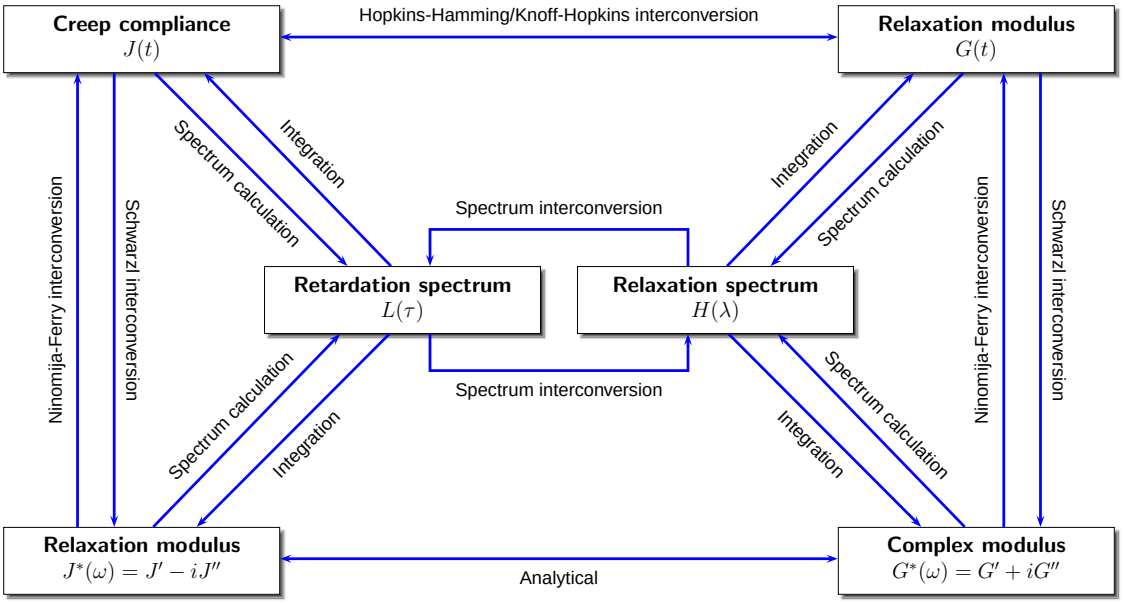

Figure 1.18: Approximate interrelations between the linear viscoelastic functions.

been suggested, such as a rational polynomial form [102]:

$$G(t) = G_\infty + \frac{G_0 - G_\infty}{\left(1 + \frac{t}{\lambda}\right)^n}. \tag{1-48}$$

The relaxation modulus must be a monotonically decreasing function in order to satisfy the principle of fading memory. The Dirichlet series representation satisfies this under certain choices of the parameters and the relaxation modulus can be approximated to arbitrary accuracy by increasing the number of modes, hence the form for the relaxation modulus in (1-47) is the most commonly encountered form for representing the relaxation modulus in discrete form. The constant $G_0 = \lim_{t\to 0} G(t)$ is known as the *glassy modulus*, since amorphous polymers exhibit glass-like behaviour at very short loading times.

The relaxation modulus can be incorporated directly into general constitutive equations for modelling non-linear behaviour, for example of polymer melts and solutions. The KBKZ group of integral constitutive models [42, 11] is one such example, which for the incompressible case has the general form

$$\boldsymbol{T} = \int_{-\infty}^{t} M(t - t')\boldsymbol{H}(t')\,\mathrm{d}t', \tag{1-49}$$

where $M(t) = -\frac{\mathrm{d}G}{\mathrm{d}t}$ is the memory function. The function $\boldsymbol{H}(t')$ is a strain measure defined in terms of the strain tensor $\boldsymbol{C}$ and its first invariant $I_C = \mathrm{tr}\,(\boldsymbol{C})$ by

$$\boldsymbol{H} = h_1\left(I_C, I_{C^{-1}}\right)\boldsymbol{C} + h_{-1}\left(I_C, I_{C^{-1}}\right)\boldsymbol{C}^{-1} \tag{1-50}$$

with constants h_1 and h_{-1}.

1.3.2 Creep Compliance

The creep compliance $J(t)$ is defined by the application of a step stress in a simple shear regime. If the magnitude of the stress is σ_0, then the resulting displacement will be $\gamma_{xy}(t) = \sigma_0 J(t)$, implying that the creep compliance is the ratio strain/stress under such conditions. More generally, the creep compliance is the kernel function in the integral equation relating the strain to an arbitrary stress in (1-37). In terms of a discrete retardation spectrum corresponding to an N-mode Kelvin-Voigt model, the creep compliance takes the form

$$J(t) = \sum_{i=1}^{M} J_i \left(1 - \mathrm{e}^{-\frac{t}{\tau_i}}\right) + \left\{\frac{t}{\eta}\right\} \tag{1-51}$$

where η is the viscosity corresponding to an extra viscous element in series with the K-V model, included for the sake of generality to allow for viscoelastic fluid materials and the $J_i = g_i^{-1}$, $i = 1, \ldots, M$ are the compliances associated with each spring.

The relationship between the relaxation modulus and creep compliance can be obtained by elimination from (1-34) and (1-37), using Laplace transforms to obtain

$$\int_0^t J(t')G(t-t')\,\mathrm{d}t' = t \quad \Leftrightarrow \quad \bar{G}(s)\bar{J}(s) = \frac{1}{s^2}. \tag{1-52}$$

The difficulty in evaluating (1-52) arises due to the ill-posedness of the inversion of the Laplace transform. Examples of approximate methods of inverting (1-52) can be found in [43] and [38]. It has been established empirically that $G(t)$ is more sensitive to short-scale relaxation processes, while $J(t)$ is more sensitive to long-scale relaxation processes, thus for some materials it is advantageous to supplement the data for $G(t)$ with that converted from $J(t)$ over certain intervals.

1.3.3 Complex Functions

Consider the response of a viscoelastic material to small amplitude oscillatory shear, where the strain is prescribed and is assumed to take the form $\gamma(t') = \gamma_0 \mathrm{e}^{i\omega t'}$, so that $\dot{\gamma}(t') = i\omega\gamma_0 \mathrm{e}^{i\omega t'}$. From (1-35), the stress is

$$\begin{aligned}\sigma(t) &= \int_0^t i\omega\gamma_0 G(t-t')\,\mathrm{e}^{-(t-t')}\,\mathrm{d}t' \\ &= i\omega\gamma_0\,\mathrm{e}^{i\omega t}\int_0^\infty G(s)\,\mathrm{e}^{-i\omega s}\,\mathrm{d}s\end{aligned} \tag{1-53}$$

where $s = t - t'$ and $i = \sqrt{-1}$. This is an equation of the form $\sigma(t) = G^*(\omega)\gamma(t)$, where

$$G^*(\omega) = i\omega\hat{G}(\omega) = i\omega \int_0^\infty G(s)\, \mathrm{e}^{-i\omega s}\, \mathrm{d}s \tag{1-54}$$

is the so-called *complex modulus*. Furthermore, $G'(\omega) = \mathrm{Re}\{G^*\}$ and $G''(\omega) = \mathrm{Im}\{G^*\}$ are known as the *storage modulus* and *loss modulus*, respectively. The storage modulus is often thought of characterizing the elastic component of the response and hence the amount of energy stored per cycle of deformation, and the loss modulus as describing the amount energy dissipated per cycle by the viscous component. However, it can be shown that the same information is contained mathematically in either function and that interconversion between the two can be performed [39]. For the N-mode Maxwell model,

$$G^*(\omega) = \sum_{j=1}^{N} \frac{i\omega\lambda_j g_j}{1 + i\omega\lambda_j}. \tag{1-55}$$

Similarly, by considering an applied stress of oscillatory form, it can be shown that $\gamma(t) = J^*(\omega)\sigma(t)$, where $J^*(\omega) = i\omega\hat{J}(\omega)$ is the *complex compliance*, $J^*(\omega) = J' - iJ''$. $J'(\omega)$ is known as the *storage compliance* and $J''(\omega)$ the *loss compliance*. The complex moduli $G^*(\omega)$ and $J^*(\omega)$ are inter-related by a simple reciprocal relationship, so the real and imaginary components are related by

$$J'(\omega) = \frac{G'(\omega)}{[G'(\omega)^2 + G''(\omega)^2]^2} \tag{1-56}$$

$$J''(\omega) = \frac{G''(\omega)}{[G'(\omega)^2 + G''(\omega)^2]^2}. \tag{1-57}$$

By assuming that the resultant stress is of the form $\sigma(t) = \sigma_0\, \mathrm{e}^{i(\omega t + \delta)}$, the *loss tangent* can be defined

$$\tan\delta = \frac{G''}{G'} = \frac{J''}{J'} \tag{1-58}$$

which measures the phase difference between the input strain and resultant stress. At high frequencies, the response is essentially that of an elastic solid with $\delta \sim 0$, while at low frequencies the response is mainly viscous and $\delta \sim 90^\circ$.

Another variation on the theme defines the *complex viscosity*, $\eta^*(\omega) = \eta' - i\eta''$, which relates the stress and shear rate through the equation $\sigma = \eta^*(\omega)\dot{\gamma}(t)$ and characterizes the dissipative effects of an alternating stress. The complex viscosity is therefore simply the Fourier transform of the relaxation modulus, $\eta^*(\omega) = \hat{G}(\omega)$, and related to the complex modulus by $G^*(\omega) = i\omega\eta^*(\omega)$.

1.3.4 Relaxation and Retardation Spectra

The N-mode Maxwell model defines a discrete spectrum of relaxation times, each value of λ_i being associated with a weight g_i. Whether such a discrete spectrum reflects the physical processes occurring during stress relaxation for real materials is debatable. Certain molecular theories, such as the Rouse model do predict discrete spectral lines, but in practice these are too closely spaced to resolve. To model a real material accurately, a very large number of modes are required. If $N \to \infty$, then the result is a continuous spectrum [27] or distribution function of relaxation times, $H(\lambda)$, which is defined such that $H(\lambda)\,\mathrm{d}\lambda$ represents the contribution to the total viscosity of all the Maxwell elements with relaxation times lying in the interval $[\lambda, \lambda + \mathrm{d}\lambda]$. Then, the stress is

$$\begin{aligned}\sigma(t) &= \int_0^\infty \frac{H(\lambda)}{\lambda} \int_{-\infty}^{t} \mathrm{e}^{-\left(\frac{t-t'}{\lambda}\right)} \dot{\gamma}(t')\,\mathrm{d}t'\,\mathrm{d}\lambda \\ &= \int_0^\infty G(t-t')\dot{\gamma}(t')\,\mathrm{d}t' \end{aligned} \tag{1-59}$$

which leads to a general definition of the relaxation modulus, $G(t)$, in terms of an arbitrary relaxation spectrum, $H(\lambda)$ in the form of a Stieltjes integral:

$$G(t) = G_\infty + \int_{\lambda=0}^{\infty} \mathrm{e}^{-\frac{t}{\lambda}} H(\lambda)\,\mathrm{d}\ln\lambda. \tag{1-60}$$

The relaxation modulus for the N-mode Maxwell model in (1-47) is obtained by multiplying the relaxation function $H(\lambda)$ by a sampling function, resulting in a discrete relaxation spectrum of the form

$$H(\lambda) = \sum_{i=1}^{N} \eta_i \delta(\lambda - \lambda_i) \tag{1-61}$$

where the $\{\eta_i\}$ are the partial viscosities defined $\eta_i = \lambda_i g_i$ for $i = 1, \ldots, N$. In this context, $H(\lambda)$ can be thought of as the density (on a log basis) of the elements of the form $\mathrm{e}^{-t/\lambda_i}$ making up $G(t)$.

Various theoretical distributions have been proposed for the relaxation spectrum [94], for example the box distribution, wedge distribution, Wiechert's log-normal distribution [101] and the bimodal log-normal distribution of Honerkamp and Weese [36].

In an entirely analogous fashion to the relaxation spectrum, the retardation spectrum can be defined such that $L(\tau)\,\mathrm{d}\tau$ represents the contribution to the elasticity modulus of the processes with retardation times in the interval $[\tau, \tau + \mathrm{d}\tau]$. This leads to a definition of the creep compliance as

$$J(t) = J_0 + \int_{\tau=0}^{\infty} L(\tau)\left[1 - \mathrm{e}^{-\frac{t}{\tau}}\right] \mathrm{d}\ln\tau + \frac{t}{\eta} \tag{1-62}$$

where J_0 allows for 'instantaneous' elastic deformation for viscoelastic solid materials which would otherwise require infinite stress. Note that for solid materials $\eta = \infty$ and for liquids $J_0 = 0$. The discrete case corresponding to an N-mode retardation spectrum

$$L(\tau) = \sum_{i=1}^{N} J_i \tau_i \delta(\tau - \tau_i) \tag{1-63}$$

has creep compliance of the form

$$J(t) = J_0 + \sum_{i=1}^{N} J_i \left(1 - \mathrm{e}^{-\frac{t}{\tau_i}}\right) + \frac{t}{\eta}. \tag{1-64}$$

The relaxation and retardation spectra occupy a pivotal rôle in the process of interconversion between linear viscoelastic functions, since the relaxation function and complex modulus can be calculated without difficulty from a known discrete relaxation spectrum, and the creep compliance and complex compliance from the retardation spectrum. Hence, much attention has been given to determination of the spectral functions from experimentally measured data. The two spectra are related by the two formulae

$$L = \frac{H}{\left[G_\infty - \int_{-\infty}^{\infty} \frac{H(u)}{\tau/u - 2} \, \mathrm{d} \ln u\right]^2 + \pi^2 H^2} \tag{1-65}$$

$$H = \frac{L}{\left[J_0 + \int_{-\infty}^{\infty} \frac{L(u)}{1 - u/\tau} \, \mathrm{d} \ln u - \frac{\tau}{\eta}\right]^2} \tag{1-66}$$

for which approximate methods of evaluation can be found in [94] and [27].

The question concerning which is the best characteristic function to measure has long been considered. In the time domain, empirical results have suggested [62] that it is better to measure the relaxation modulus and calculate the creep function through the interconversion formulae. The stress-explicit constitutive equations have been derived from molecular or continuum models, so in general there is a bias towards use of the relaxation modulus theoretically. By considering the relative ill-posedness of the process of converting from relaxation modulus to creep function in comparison with that of the reverse process, it can be shown that the former process is more stable with respect to perturbations in the data [2, 3].

CHAPTER 2

Stress Controlled Rheometry

In this chapter, the foundations of stress-controlled rheometry are set out which provide the basis for analysis in subsequent chapters. Firstly, the governing equations for an experimental setup utilizing the parallel plate geometry are derived which relate the applied stress to the resultant displacement through the relaxation modulus. Next a selection of possible functions for the applied torque are considered and response of the system simulated by means of solving the governing equations analytically using Laplace transform analysis. In each case, it is assumed that the material sample has a known relaxation modulus corresponding to a generalized Maxwell model. The first function considered is the delta function, which although strictly speaking a distribution or measure, can indicate the response of the system to an instantaneous impulsive force. Secondly, the response to a constant stress (i.e. a Heaviside step function) is considered, leading on to the box function and also a stress which increases linearly in time. Finally, periodic functions are considered.

I. GOVERNING EQUATIONS

Consider the parallel plate geometry on a controlled stress rheometer as shown in Figure 2.1. Several geometries are available for use with modern rheometers, including the cone and plate and concentric cylinder configurations, however the parallel plate geometry has some advantages. Firstly, the gap between the plates can be altered easily without changing the instrument components and secondly, should it be required, inertial effects can be incorporated more easily than, for example, the cone and plate geometry.

The viscoelastic material under test is contained between two circular plates, of radius a and separated by a distance h. In practice, the lower fixed platen is usually much larger, but since the sample only occupies a cylindrical space of the radius equal to that of the upper platen the actual radius is irrelevant. A torque $C(t)$ is applied to the upper platen of the rheometer and the resulting displacement $\chi(t)$ of the same plate is the measured variable. At this stage in the derivation of the governing equations, no assumptions are made about the form of the applied torque, other than that it is amenable to experimental use. Ignoring edge effects by assuming that the edges of the material sample are orthogonal to the platen surface and in the case of fluids the absence of loss by evaporation at this free surface, with reference to cylindrical polar coordinates (r, θ, z), the velocity field can be assumed to take the form

$$\boldsymbol{v} = (0, rf(z,t), 0) \tag{2-1}$$

subject to the boundary conditions

$$v_\theta|_{z=0} = 0, \quad v_\theta|_{z=h} = r\dot{\chi} \tag{2-2}$$

2.1.1 Equations of Motion

Firstly, note that

$$\nabla\cdot\boldsymbol{v} = \frac{1}{r}\frac{\partial}{\partial r}\left[rv_r\right] + \frac{1}{r}\frac{\partial v_\theta}{\partial\theta} + \frac{\partial v_z}{\partial z} = 0, \tag{2-3}$$

so that the velocity field automatically satisfies the conservation of mass condition for incompressible fluids.

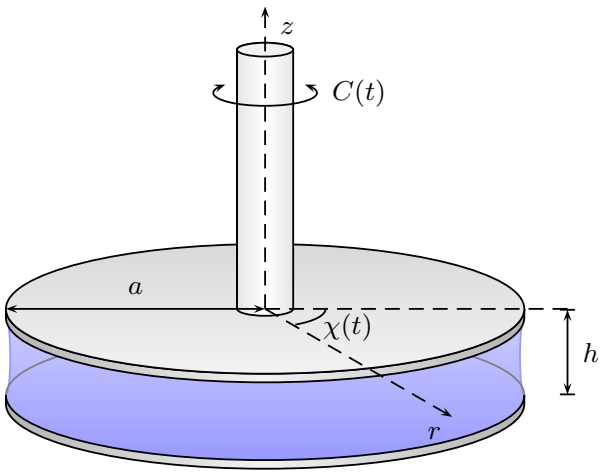

Figure 2.1: Parallel plate geometry. The two plates of radius a are separated by a distance h and a torque $C(t)$ is applied to the top platen.

For infinitesimal displacement gradients, the linear viscoelastic constitutive equation for the stress can be expressed in the form

$$\boldsymbol{\sigma} = -p\boldsymbol{I} + \boldsymbol{T} \tag{2-4}$$

where the extra stress, T, is given by Boltzmann's equation,

$$\boldsymbol{T} = 2\int_{-\infty}^{t} G(t-t')\boldsymbol{D}(t')\,\mathrm{d}t' \tag{2-5}$$

where t is the current time and t' the running time variable. Additionally, the rate of strain tensor, $\boldsymbol{D}$, and velocity gradient, $\boldsymbol{L}$, are defined:

$$\boldsymbol{D} = \tfrac{1}{2}\left[\boldsymbol{L} + \boldsymbol{L}^T\right] \tag{2-6}$$

$$\boldsymbol{L} = \nabla\boldsymbol{v} \tag{2-7}$$

In cylindrical polar coordinates, the velocity gradient tensor can be expressed in the form

$$\boldsymbol{L} = \begin{bmatrix} \frac{\partial v_r}{\partial r} & \frac{\partial v_\theta}{\partial r} & \frac{\partial v_z}{\partial r} \\ \frac{1}{r}\left(\frac{\partial v_r}{\partial \theta} - v_\theta\right) & \frac{1}{r}\left(\frac{\partial v_\theta}{\partial \theta} + v_r\right) & \frac{1}{r}\frac{\partial v_z}{\partial \theta} \\ \frac{\partial v_r}{\partial z} & \frac{\partial v_\theta}{\partial z} & \frac{\partial v_z}{\partial z} \end{bmatrix} \tag{2-8}$$

and for the velocity distribution in (2-1), $\boldsymbol{L}$ can be shown to be

$$\boldsymbol{L} = \begin{bmatrix} 0 & f(z,t) & 0 \\ -f(z,t) & 0 & 0 \\ 0 & r\frac{\partial f}{\partial z} & 0 \end{bmatrix} \tag{2-9}$$

and the rate of strain tensor now becomes

$$\boldsymbol{D} = \begin{bmatrix} 0 & 0 & 0 \\ 0 & 0 & \frac{1}{2}r\frac{\partial f}{\partial z} \\ 0 & \frac{1}{2}r\frac{\partial f}{\partial z} & 0 \end{bmatrix} = \begin{bmatrix} 0 & 0 & 0 \\ 0 & 0 & \frac{1}{2}\frac{\partial v_\theta}{\partial z} \\ 0 & \frac{1}{2}\frac{\partial v_\theta}{\partial z} & 0 \end{bmatrix}. \tag{2-10}$$

Wherefore, the linear viscoelastic constitutive equation for this problem becomes

$$T_{\theta z} = \int_{-\infty}^{t} G(t-t')\frac{\partial v_\theta}{\partial z}\,\mathrm{d}t' \tag{2-11}$$

The stress equations of motion in their most general form are given by

$$\rho\frac{\mathrm{D}\boldsymbol{v}}{\mathrm{D}t} = \nabla\cdot\boldsymbol{\sigma} + \rho\boldsymbol{F} = \nabla\cdot\boldsymbol{T} - \nabla p + \rho\boldsymbol{F} \tag{2-12}$$

where

$$\frac{\mathrm{D}\boldsymbol{v}}{\mathrm{D}t} = \frac{\partial \boldsymbol{v}}{\partial t} + \boldsymbol{v}\cdot\nabla\boldsymbol{v} \tag{2-13}$$

is the *material derivative*, ρ is the density, p is the pressure and $\boldsymbol{F}$ represents the external body forces acting upon the system. In the foregoing analysis, it is assumed that $\boldsymbol{F} = 0$. Ignoring fluid inertia, or equivalently setting $\rho = 0$, results in the set of equations

$$\frac{\partial p}{\partial r} = 0 \tag{2-14}$$

$$\frac{\partial T_{z\theta}}{\partial z} = \frac{1}{r}\frac{\partial p}{\partial \theta} \tag{2-15}$$

$$\frac{\partial p}{\partial z} = 0. \tag{2-16}$$

From (2-14) and (2-16), it is clear that $p = p(\theta, t)$. Since $T_{\theta z}$ is a function of r,z and t, then p must satisfy

$$\frac{\partial p}{\partial \theta} = 0, \tag{2-17}$$

and also the boundary conditions for continuity of the pressure distribution

$$p(0) = p(2\pi) = p_0, \quad p_0 \in \mathbb{R}^+. \tag{2-18}$$

Hence $p = p_0$ is a constant, and (2-15) becomes

$$\frac{\partial^2}{\partial z^2} \int_{-\infty}^{t} G(t-t')v_\theta(t')\,\mathrm{d}t' = 0 \tag{2-19}$$

The relaxation modulus, $G(t)$, is independent of the geometry, so (2-19) can be written in the form

$$\int_{-\infty}^{t} G(t-t')\frac{\partial^2 v_\theta}{\partial z^2}(t')\,\mathrm{d}t' = 0 \tag{2-20}$$

and since $G(t) > 0$, this implies that

$$\frac{\partial^2 v_\theta}{\partial z^2} = 0 \tag{2-21}$$

which has a linear solution in z

$$v_\theta = c_1 z + c_2 \tag{2-22}$$

with constants $c_1, c_2 \in \mathbb{C}$. Utilizing the boundary conditions in (2-2) it is readily apparent that

$$v_\theta = \frac{r\dot{\chi}}{h} z. \tag{2-23}$$

2.1.2 Equation of Motion of the Platen

The equation of motion of the upper (rotating) platen can be written in the form

$$C(t) - C_f(t) = d\dot{\chi} + I\ddot{\chi}(t) \tag{2-24}$$

where $C(t)$ is the applied torque, $C_f(t)$ is the torque exerted on the platen by the fluid, I is the moment of inertia of the rotating assembly and d is a damping coefficient. The latter parameter is a measure of the frictional forces in the bearing assembly, however the air bearings which are found in most modern rheometers are of sufficient quality to justify ignoring the coefficient in the analysis. The torque exerted on the plate by the

material sample is calculated as follows.

$$\begin{aligned}
C_f &= \iint_A r\tau_{\theta z}|_{z=h}\,\mathrm{d}A \\
&= \int_{\theta=0}^{2\pi}\int_{r=0}^{a} r\tau_{\theta z}|_{z=h} r\,\mathrm{d}r\,\mathrm{d}\theta \\
&= \int_0^{2\pi}\int_0^a r^2\left[\int_{-\infty}^{t} G(t-t')\frac{\partial v_\theta}{\partial z}(t')\,\mathrm{d}t'\right]_{z=h}\mathrm{d}r\,\mathrm{d}\theta \\
&= \int_0^{2\pi}\int_0^a r^2\int_{-\infty}^{t} G(t-t')\left[\frac{\partial v_\theta}{\partial z}(t')\right]_{z=h}\mathrm{d}t'\,\mathrm{d}r\,\mathrm{d}\theta \\
&= \int_0^{2\pi}\int_0^a r^2\int_{-\infty}^{t} G(t-t')\frac{r\dot{\chi}(t')}{h}\,\mathrm{d}t'\,\mathrm{d}r\,\mathrm{d}\theta \\
&= \frac{2\pi}{h}\int_0^a r^3\int_{-\infty}^{t} G(t-t')\dot{\chi}(t')\,\mathrm{d}t'\,\mathrm{d}r \\
&= \frac{\pi a^4}{2h}\int_{-\infty}^{t} G(t-t')\dot{\chi}(t')\,\mathrm{d}t' \qquad (2\text{-}25)
\end{aligned}$$

So now have a first order Volterra integro-differential equation (see Section 4.1) is obtained in $\dot{\chi}(t)$ relating the displacement of the plate to a completely arbitrary applied torque,

$$I\ddot{\chi}(t) + k^{-1}\int_{-\infty}^{t} G(t-t')\dot{\chi}(t)\,\mathrm{d}t' = C(t) \qquad (2\text{-}26)$$

where $k = \frac{2h}{\pi a^4}$. Since we are only concerned with $t \geq 0$, (2-26) can be rewritten as

$$I\ddot{\chi}(t) + k^{-1}\left[\chi(0+)G(t) + \int_0^t G(t-t')\dot{\chi}(t)\,\mathrm{d}t'\right] = C(t) \qquad (2\text{-}27)$$

using the notation $\chi(0+) = \lim_{t\to 0}\chi(t)$ to allow the use of functions with step discontinuities at $t = 0$.

A corresponding equation can be obtained from (2-27) relating the displacement to the applied torque in terms of the creep compliance, $J(t)$. Writing $C_f(t) = C(t) - I\ddot{\chi}(t)$ and using the interrelation condition between $G(s)$ and $J(s)$ in (1-52) using the Laplace transform, it is straightforward to obtain the following pair of Volterra equations.

$$C_f(t) = k^{-1}\left[\chi(0+)G(t) + \int_0^t G(t-t')\dot{\chi}(t')\,\mathrm{d}t'\right] \qquad (2\text{-}28)$$

$$\chi(t) = k\left[C_f(0+)J(t) + \int_0^t J(t-t')\dot{C}_f(t')\,\mathrm{d}t'\right] \qquad (2\text{-}29)$$

Now we continue to consider the use of integral transforms to obtain a solution for $\chi(t)$ as given by (2-26) in terms of an arbitrary applied torque $C(t)$.

2.1.3 Fourier Transform Formulation

The Fourier transform of a function, $f \in L^1(\mathbb{R})$ is defined

$$\hat{f}(\omega) = \mathscr{F}\{f(t)\}(\omega) := \int_{-\infty}^{\infty} \mathrm{e}^{-i\omega t} f(t)\,\mathrm{d}t \tag{2-30}$$

This definition can be extended to $f \in L^2(\mathbb{R})$ (see [83]). Taking the Fourier transform of both sides of (2-26), we obtain

$$I\hat{\chi}(\omega) + k^{-1}\mathscr{F}\{G * \dot{\chi}\}(\omega) = \hat{C}(\omega) \tag{2-31}$$

The only assumptions which must be made initially are that the functions $C(t)$, $\dot{\chi}(t)$, $\ddot{\chi}(t)$ possess Fourier transforms. This suggests that any solution to (2-31) must be piecewise continuous and integrable over the whole real line, hence it is reasonable to assume that $\dot{\chi}, \ddot{\chi} \in L^2(\mathbb{R})$. This restriction may be relaxed to $\chi \in L^2[0,\infty)$, since only functions which take the value zero for $t < 0$ need to be considered.

The Fourier transform of the convolution of functions f, g is simply

$$\mathscr{F}\{f * g\} = \mathscr{F}\{f\} \cdot \mathscr{F}\{g\} \tag{2-32}$$

and the Fourier transform of the derivatives of a function f satisfy the following relation.

$$\mathscr{F}\left\{f^{(n)}(t)\right\}(\omega) = (i\omega)^n \hat{f}(\omega) \tag{2-33}$$

Applying (2-32) and (2-33) to (2-31), we obtain

$$I(i\omega)^2\hat{\chi}(\omega) + k^{-1}i\omega\hat{\chi}(\omega)\hat{G}(\omega) = \hat{C}(\omega) \tag{2-34}$$

and using the definition of $G^*(\omega)$ from (1-54), the governing equations in terms of Fourier transforms is given by

$$\hat{\chi}(\omega) = \frac{k\hat{C}(\omega)}{G^*(\omega) - kI\omega^2}, \tag{2-35}$$

which facilitates the determination of the complex modulus, $G^*(\omega)$, experimentally from the known functions $C(t)$ and $\chi(t)$.

2.1.4 Laplace Transform Formulation

Alternatively, the governing equations may be expressed in terms of the Laplace transforms of the constituent functions. The Laplace transform of a piecewise continuous function $f(t)$, $t \in [0,\infty)$, is defined by

$$\bar{f}(s) = \mathscr{L}\{f(t)\}(s) := \int_0^{\infty} \mathrm{e}^{-st} f(t)\,\mathrm{d}t, \quad s > 0. \tag{2-36}$$

Taking the Laplace transform of both sides of (2-26),

$$I\bar{\dot{\chi}}(s) + k^{-1}\mathscr{L}\{G * \dot{\chi}\}(s) + k^{-1}\chi(0)\overline{G}(s) = \bar{C}(s) \tag{2-37}$$

The only assumptions which are made about the functions $\chi(t)$ and $C(t)$ are that the Laplace transform integrals exist. The requirements may be extended to allow the use of certain generalized functions which have experimental usefulness, such as the delta function.

The Laplace transform of the convolution of functions f and g satisfies the following relation,

$$\mathscr{L}\{f * g\} = \mathscr{L}\{f\}\mathscr{L}\{g\}. \tag{2-38}$$

Additionally, for a function $f \in C^{(n-1)}(a,b)$, where $(a,b) \subseteq [0,\infty)$ and $n \in \mathbb{N}$, then provided $\|f(t)\|_\infty \leq M\,\mathrm{e}^{ct}$ for some $c, M \in \mathbb{R}$, the following identity relates the Laplace transform of a derivative of the function to the transform of the function itself.

$$\mathscr{L}\left\{f^{(n)}(t)\right\}(s) = s^n\mathscr{L}\{f(t)\} - \sum_{k=0}^{n} s^{k-1}f^{(n-k)}(0) \tag{2-39}$$

Applying (2-38) and the first and second order versions of (2-39) to (2-37), we obtain

$$I\left[s^2\bar{\chi}(s) - s\chi(0) - \dot{\chi}(0)\right] + k^{-1}s\bar{G}(s)\bar{\chi}(s) + k^{-1}\chi(0)\bar{G}(s) = \bar{C}(s), \tag{2-40}$$

or in terms of $\bar{\chi}(s)$,

$$\bar{\chi}(s) = \frac{k\bar{C}(s) + k[sI\chi(0) + I\dot{\chi}(0)] + \chi(0)\bar{G}(s)}{s\bar{G}(s) + kIs^2}. \tag{2-41}$$

If the assumption is made that the plate starts from rest and that the position of the plate is measured from a zero reference point, i.e. $\chi(0) = \dot{\chi}(0) = 0$, then (2-41) assumes a simpler form. To summarize, the foregoing experimental setup described is represented by a system of three equations in Laplace space; the two equations relating the displacement to the relaxation modulus and creep compliance coupled with the interconversion condition relating the two material functions.

$$\bar{\chi}(s) = \frac{k\bar{C}(s)}{s\bar{G}(s) + kIs^2} \tag{2-42}$$

$$\bar{\chi}(s) = \frac{ks\bar{C}(s)\bar{J}(s)}{1 + kIs^3\bar{J}(s)} \tag{2-43}$$

$$\bar{G}(s)\bar{J}(s) = \frac{1}{s^2}. \tag{2-44}$$

For each applied torque function in turn, the discrete relaxation spectrum $\{g_i, \lambda_i\}_{i=1}^N$ is made use of to provide an expression for the relaxation modulus of the fluid under the assumption that the fluid is described by an N-mode Maxwell model. The relaxation modulus, $G(t)$, thus takes the form of a Dirichlet or Prony series

$$G(t) = \sum_{i=1}^{N} g_i \, \mathrm{e}^{-t/\lambda_i}. \tag{2-45}$$

The Laplace transform of (2-45) is consequently

$$\bar{G}(s) = \sum_{i=1}^{N} \frac{g_i}{s + \frac{1}{\lambda_i}} \tag{2-46}$$

which can be expressed as the rational function

$$\bar{G}(s) = \frac{\sum\limits_{i=1}^{N} g_i \prod\limits_{\substack{i=1 \\ j \neq i}}^{N} \left(s + \frac{1}{\lambda_j}\right)}{\prod\limits_{i=1}^{N} \left(s + \frac{1}{\lambda_j}\right)}. \tag{2-47}$$

Henceforth, the notation for the lower limit $j = 1, i$ shall be used to denote $j = 1, j \neq i$. In the case of a single-mode Maxwell, the expression for the Laplace transform of the relaxation modulus reduces to

$$\bar{G}(s) = \frac{g}{s + \frac{1}{\lambda}} \tag{2-48}$$

II. DELTA FUNCTION

The first form for the applied torque considered is the delta function,

$$C(t) = C_\delta \delta(t - t_0), \qquad t \in [0, T],\ T > t_0 \geq 0. \tag{2-49}$$

The *delta function* is not a true function, but rather a measure or distribution [41]. However, it is often used in an applied mathematical setting to model an impulsive force resembling an infinite spike at $t = t_0$ with zero width and constant unit area. The most important identity in this context is

$$\int_{\alpha-\epsilon}^{\alpha+\epsilon} \delta(t - \alpha) f(t) \, \mathrm{d}t = f(\alpha) \tag{2-50}$$

for $\epsilon > 0$ and is most commonly used with $\lim_{\epsilon \to \infty}$. The delta function can be defined as the limit of a class of delta sequences. A sequence of functions δ_n is called a *delta sequence* if

$$\lim_{n \to \infty} \int_{-\infty}^{\infty} \delta_n(x) f(t) \, \mathrm{d}t = f(0) = \int_{-\infty}^{\infty} \delta(t) f(t) \, \mathrm{d}t \tag{2-51}$$

for any continuous function f (with compact support). In the language of measure theory, this is weak* convergence of δ_n to δ.

One example of a delta sequence is the Gaussian function, normalized so that $\int_{-\infty}^{\infty} \delta_n(t)\,\mathrm{d}t = 1$,

$$\delta_n(t) = \frac{n}{\sqrt{\pi}}\,\mathrm{e}^{-n^2t^2}. \tag{2-52}$$

Alternatively, the delta function may be thought of as the limit of a sequence of box functions as shown in Figure 2.2. Convergence to be understood in the sense of (2-51).

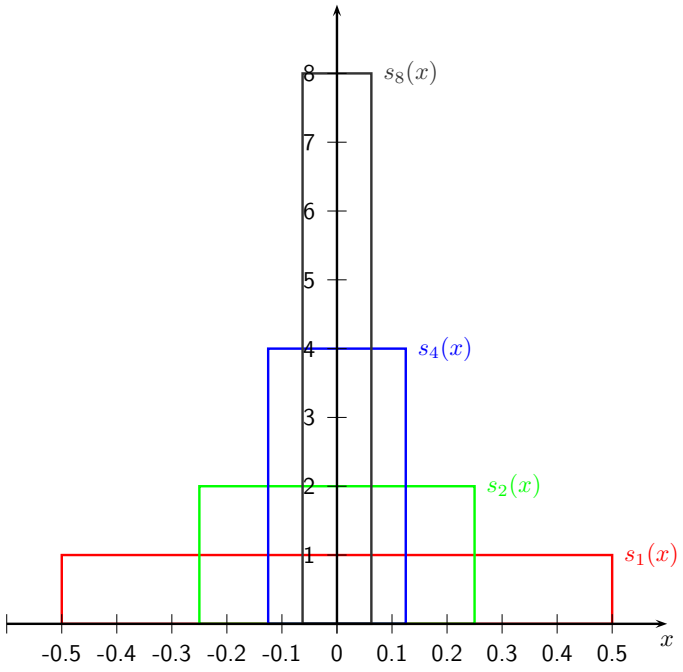

Figure 2.2: Delta function as the limit of a sequence of box function delta sequences

The Laplace transform of the resulting displacement $\chi(t)$ when subjected to a torque $C(t)$ is given by (2-42) and the Laplace transform of the applied torque is

$$\bar{C}(s) = C_\delta \int_0^\infty \mathrm{e}^{-st}\delta(t-t_0) = C_\delta\,\mathrm{e}^{-st_0}, \qquad \mathrm{Re}\,\{s\}, t_0 > 0, \tag{2-53}$$

so the platen displacement for an applied torque in the form of a Delta function has Laplace transform

$$\bar{\chi}(s) = \frac{C_\delta\,\mathrm{e}^{-st_0}}{Is\left[s + (kI)^{-1}\bar{G}(s)\right]}. \tag{2-54}$$

Noting that

$$\begin{aligned} \mathrm{e}^{-t's}\bar{f}(s) &= \int_0^\infty \mathrm{e}^{-(t+t')s} f(t)\,\mathrm{d}t \\ &= \int_{t'}^\infty \mathrm{e}^{-us} f(u-t')\,\mathrm{d}u \\ &= \int_0^\infty \mathrm{e}^{-us} f(u-t')H(u-t')\,\mathrm{d}u \end{aligned} \tag{2-55}$$

where $H(t-a)$ is the *Heaviside step function* defined

$$H(t-a) = \begin{cases} 0 & \text{if } t < a \\ 1 & \text{if } t > a \end{cases} \tag{2-56}$$

the following identity is attained, known as the shift theorem for the Laplace transform,

$$\mathscr{L}\left\{f(t-t')H(t-t')\right\} = \mathrm{e}^{-t's}\bar{f}(s). \tag{2-57}$$

This indicates that the problem can be expressed in terms of a rational function, $\chi_0(t)$, where

$$\chi(t) = \frac{C_\delta}{I}\left\{\chi_0(t-t_0)H(t-t_0)\right\} \tag{2-58}$$

and

$$\bar{\chi}_0(s) = \frac{1}{s\left[s + (kI)^{-1}\bar{G}(s)\right]}. \tag{2-59}$$

provided that the Laplace transform of the relaxation modulus $\bar{G}(s)$ is algebraic. This is equivalent to the problem of calculating the solution for a Delta function located at $t = 0$ and a translation along the t-axis in a positive direction to $t = t_0$, which is to be expected of a linear time-invariant system. We now proceed to consider some specific forms for the relaxation modulus $G(t)$ and look at the form of the response $\chi(t)$ for an applied torque in the form of a delta function.

2.2.1 Newtonian Fluid Model

The simplest form for the relaxation modulus is that of the Newtonian fluid model. The relaxation modulus is $G(t) = \eta\delta(t)$, in which case the Laplace transform of the relaxation modulus is simply $\bar{G}(s) = \eta$. Thus, (2-41) in this case becomes

$$\bar{\chi}(s) = \frac{C_\delta}{Is\left[s + \frac{\eta}{kI}\right]} \tag{2-60}$$

and it is straightforward to invert the Laplace transform using partial fractions and comparing with standard results to obtain

$$\chi(t) = \frac{kC_\delta}{\eta}\left[1 - \mathrm{e}^{-\frac{\eta t}{kI}}\right] H(t). \tag{2-61}$$

As can be seen from Figure 2.3, the displacement approaches an asymptotic value $\frac{kC_\delta}{\eta}$ at a rate dependent on the instrument inertia and geometry as well as the viscosity. Indeed, if $I \to 0$, then

$$\lim_{I\to 0} \chi(t) = \frac{kC_\delta}{\eta} H(t). \tag{2-62}$$

which is essentially the step-strain experiment. Upon application of a constant strain, the Newtonian fluid experiences an infinite stress instantaneously, i.e. in the form of a Delta function and thereafter is equal to zero. This is of course an idealization, since the inertia of the rotating instrument assembly can never be sufficiently small to allow an instantaneous change in angular displacement. It should be noted that the simplified case where $I = 0$ is essentially equivalent to solving the Boltzmann equation (1-35), for which many examples for various applied stress profiles can be found in [94].

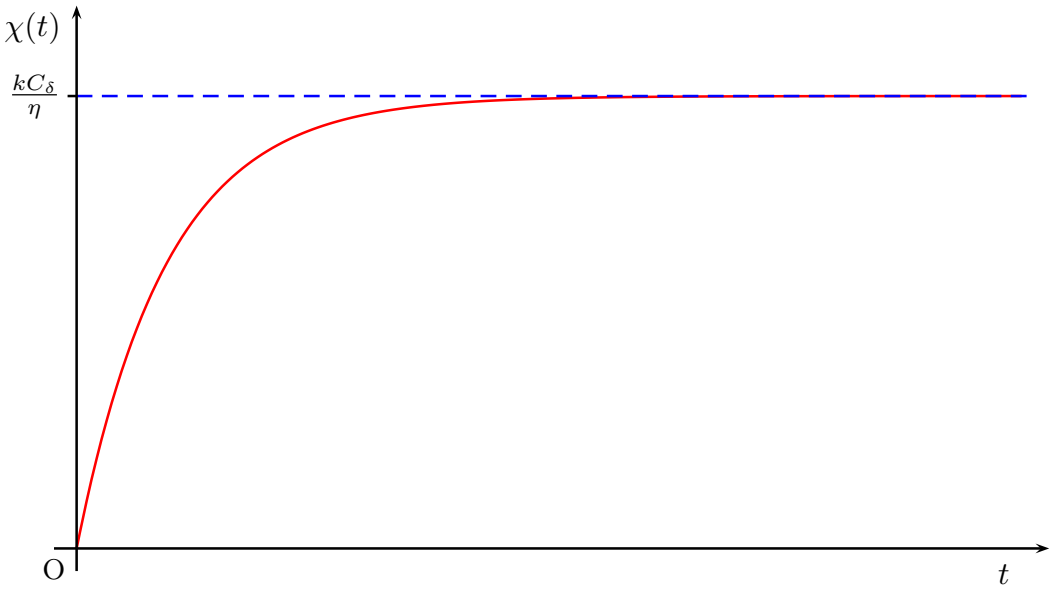

Figure 2.3: Platen displacement: Delta function, Newtonian fluid.

2.2.2 Maxwell Model

The Maxwell model has relaxation modulus with Laplace transform as defined in (2-48) and substituting this expression into (2-42) gives the Laplace transform of the

displacement of the platen

$$\bar{\chi}_0(s) = \frac{s + \lambda^{-1}}{s\left[s^2 + \lambda^{-1}s + \frac{g}{kI}\right]} \tag{2-63}$$

when subjected to a delta function stimulus at $t = 0$. Let the roots of $s^2 + \lambda^{-1}s + \frac{g}{kI}$ be denoted $\{-\xi_1, -\xi_2\}$, then

$$\bar{\chi}_0(s) = \frac{s + \lambda^{-1}}{s(s + \xi_1)(s + \xi_2)} \tag{2-64}$$

where

$$\xi_{1,2} = \frac{1}{2\lambda}\left[1 \pm \sqrt{\frac{kI - 4\eta\lambda}{kI}}\right]. \tag{2-65}$$

The inverse Laplace transform [100] is obtained by calculating the contour integral

$$f(t) = \mathscr{L}^{-1}\left\{\bar{f}(s)\right\}(t) := \frac{1}{2\pi i}\oint \bar{f}(s)\,\mathrm{e}^{st}\,\mathrm{d}s. \tag{2-66}$$

Assuming the function $\bar{f}(s)$ possesses no branch points or essential singularities and the only singularities are a finite number of poles, then it follows that $\bar{f}(s)$ is a *meromorphic* function, i.e. it can be represented as a rational algebraic function. Under such conditions, the inversion of (2-66) may be accomplished using *Cauchy's residue theorem*. Thus $\bar{f}(s)$ can be written in the form $P(s)/Q(s)$, where P and Q are polynomials in s. If $\deg P < \deg Q$, the Laplace transform may be inverted directly, otherwise algebraic long division may be performed until the remainder satisfies the criterion. Linearity of the Laplace integral implies any extra terms may be inverted separately. Thus, provided that the contour integral encloses all of the poles of $\bar{f}(s)$, the inverse Laplace transform is the sum of the residues of $\bar{f}(s)\,\mathrm{e}^{st}$ which are associated with the poles of $\bar{f}(s)$, viz.

$$f(t) = \sum_k \mathrm{Res}_k\left[\bar{f}(s)\,\mathrm{e}^{st}\right]. \tag{2-67}$$

The residue associated with a simple pole located at $s = s_k$ is given by

$$\mathrm{Res}_k = \lim_{s\to s_k}\left[(s - s_k)\bar{f}(s)\,\mathrm{e}^{-st}\right]. \tag{2-68}$$

In the case where $\bar{f}(s)$ possesses poles of multiple order, a more general formula is required. Assuming that $\bar{f}(s)$ has l poles, each with multiplicity $r_k, k = 1, \ldots, l$ located at $s = -s_k$, then it may be decomposed into partial fractions

$$\bar{f}(s) = \sum_{k=1}^{l}\sum_{\nu=1}^{r_k}\frac{c_{k,\nu}}{(s - s_k)^\nu} \tag{2-69}$$

where

$$c_{k,\nu} = \frac{1}{(r_k-\nu)!}\left\{\frac{\mathrm{d}^{(r_k-\nu)}}{\mathrm{d}s^{(r_k-\nu)}}\left[\bar{f}(s)\,(s-s_k)^{r_k}\right]\right\}_{s=s_k}, \tag{2-70}$$

and the inverse Laplace transform of $\bar{f}(s)$ is then

$$f(t) = \sum_{k=1}^{l} \mathrm{e}^{s_k t} \sum_{\nu=1}^{r_k} \frac{c_{k,\nu}\, t^{\nu-1}}{(\nu-1)!}, \quad t > 0 \tag{2-71}$$

The nature of the roots $\{\xi_1, \xi_2\}$, and consequently the response $\chi(t)$ of the system is dependent on the discriminant term $\psi := 1 - 4\frac{\eta\lambda}{kI}$. This reflects the choice of instrumental parameters k and I with respect to the predefined fluid parameters g and λ. This gives rise to two distinct cases:

Case 1. $\psi > 0$: For this problem, the two roots $\{\xi_1, \xi_2\}$ are distinct and real-valued. Now $\bar{\chi}_0(s)$ has only simple poles located at $\{0, -\xi_1, -\xi_2\}$, and using (2-67) and (2-68) the inverse Laplace transform takes the form

$$\chi_0(t) = \gamma_0 + \gamma_1\,\mathrm{e}^{-\xi_1 t} + \gamma_2\,\mathrm{e}^{-\xi_2 t} \tag{2-72}$$

where the constants $\gamma_0, \gamma_1, \gamma_2 \in \mathbb{R}$ are defined

$$\begin{aligned}
\gamma_0 &= \lim_{s\to 0}\{s\bar{\chi}_0(s)\} \\
&= \frac{kI}{\eta} && \text{(2-73a)} \\
\gamma_1 &= \lim_{s\to -\xi_1}\{(s+\xi_1)\bar{\chi}_0(s)\} \\
&= \frac{1-\lambda\xi_1}{\lambda\xi_1(\xi_1-\xi_2)} && \text{(2-73b)} \\
\gamma_2 &= \lim_{s\to -\xi_2}\{(s+\xi_2)\bar{\chi}_0(s)\} \\
&= \frac{\lambda\xi_2-1}{\lambda\xi_2(\xi_1-\xi_2)} && \text{(2-73c)}
\end{aligned}$$

Note that the order in which $\xi_{1,2}$ are chosen is necessarily arbitrary and upon interchanging suffices in the latter expressions the same solution results. The overall solution for $\chi(t)$ corresponding to a Delta function stimulus applied at a time $t = t_0$ is

$$\begin{aligned}
\chi(t) &= \frac{C_\delta}{I}H(t-t_0)\left\{\gamma_0 + \gamma_1\,\mathrm{e}^{-\xi_1(t-t_0)} + \gamma_2\,\mathrm{e}^{-\xi_2(t-t_0)}\right\} \\
&= \frac{C_\delta}{I}H(t-t_0)\left\{\gamma_0 + \gamma_1\,\mathrm{e}^{\xi_1 t_0}\,\mathrm{e}^{-\xi_1 t} + \gamma_2\,\mathrm{e}^{\xi_2 t_0}\,\mathrm{e}^{-\xi_2 t}\right\}
\end{aligned} \tag{2-74}$$

or alternatively in terms of hyperbolic trigonometric functions

$$\chi(t) = \frac{C_\delta}{I} H(t-t_0) \left\{ \gamma_0 + \mathrm{e}^{-\frac{t}{2\lambda}} \left[\gamma_1 \mathrm{e}^{\xi_1 t_0} + \gamma_2 \mathrm{e}^{\xi_2 t_0} \right] \cosh(\zeta t) + \mathrm{e}^{-\frac{t}{2\lambda}} \left[\gamma_2 \mathrm{e}^{\xi_2 t_0} - \gamma_1 \mathrm{e}^{\xi_1 t_0} \right] \sinh(\zeta t) \right\}, \quad (2\text{-}75)$$

where $\zeta = \frac{1}{2\lambda}\sqrt{\frac{kI-4\eta\lambda}{kI}}$. The typical response of a Maxwell fluid with material parameters such that $\psi > 0$ is shown in Figure 2.4. Note that the overall response is similar to that of the Newtonian fluid and the displacement tends to a constant limiting value of the same value as that for the Newtonian fluid.

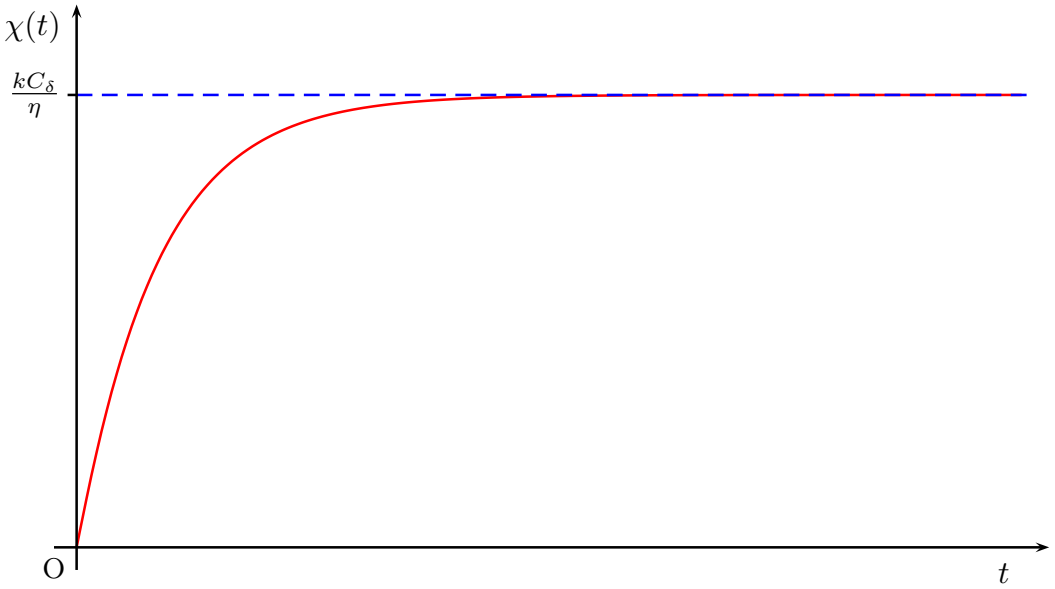

Figure 2.4: Platen displacement: Delta function, Maxwell model, $\psi > 0$.

Case 2. $\psi = 0$: In the case of repeated roots, $\xi_2 = \xi_1 = \frac{1}{2\lambda}$, $\bar{\chi}_0(s)$ has a single pole at $s = 0$ and a double pole at $s = -\xi_1 = \frac{1}{2\lambda}$. Therefore, the solution is of the form

$$\chi_0(t) = \gamma_0' + (\gamma_1' + \gamma_2' t)\, \mathrm{e}^{-\frac{t}{2\lambda}} \quad (2\text{-}76)$$

where the constants $\gamma_0', \gamma_1', \gamma_2' \in \mathbb{R}$ are defined

$$\gamma_0' = \gamma_0 \quad (2\text{-}77a)$$

$$\gamma_1' = \lim_{s\to-\xi_1} \left\{ \frac{\mathrm{d}}{\mathrm{d}s} \left[(s+\xi_1)^2 \bar{\chi}_0(s) \right] \right\} = -4\lambda \quad (2\text{-}77b)$$

$$\gamma_2' = \lim_{s\to-\xi_1} \left\{ (s+\xi_1)^2 \bar{\chi}_0(s) \right\} = -1. \quad (2\text{-}77c)$$

Hence, the overall solution for the displacement is

$$\chi(t) = \frac{C_\delta}{I} H(t - t_0) \left\{ \gamma_0 + \left[(\gamma_1' - \gamma_2' t_0) + \gamma_2' t \right] \, \mathrm{e}^{\frac{t_0}{2\lambda}} \, \mathrm{e}^{-\frac{t}{2\lambda}} \right\} \tag{2-78}$$

The general form of the displacement curve for values of η, λ, kI satisfying the above criterion is shown in Figure 2.5. This limiting case would be extremely unlikely to be observed experimentally, since the probability of the instrumental and fluid parameters assuming the stated exact values is essentially negligible. Note that $\lim_{t\to\infty} \chi(t) = \frac{kC_\delta}{\eta} = \frac{4\lambda C_\delta}{I}$.

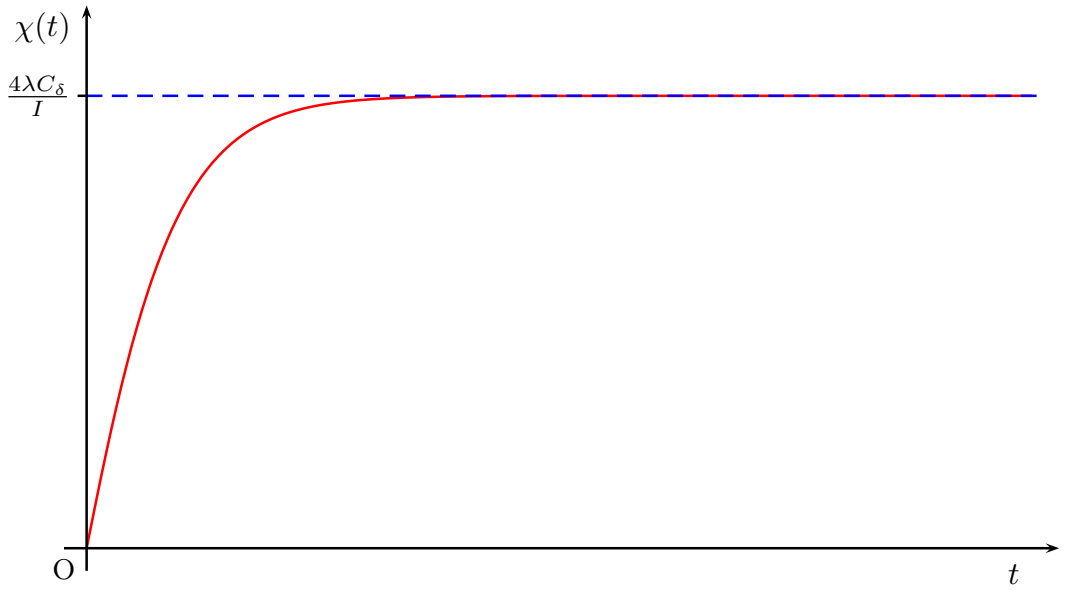

Figure 2.5: Platen displacement: Delta function, Maxwell model, $\psi = 0$.

Case 3. $\psi < 0$: As the quantity kI decreases in magnitude relative to the material parameter $4\eta\lambda$, the roots become complex $\xi_{1,2} \in \mathbb{C}$ and since $\chi(t) : \mathbb{R} \mapsto \mathbb{R}$ it follows that the roots form a conjugate pair so that $\xi_2 = \xi_1^*$. Let $\xi_{1,2} = \frac{1}{2\lambda} \pm i\xi''$. Now $\chi_0(t)$ is of the form

$$\chi_0(t) = \gamma_0'' + \mathrm{e}^{-\frac{t}{2\lambda}} \left[\gamma_1'' \, \mathrm{e}^{-i\xi'' t} + \gamma_2'' \, \mathrm{e}^{i\xi'' t} \right] \tag{2-79}$$

where the constants $\gamma_0'', \gamma_1'', \gamma_2'' \in \mathbb{C}$ are defined

$$\gamma_0'' = \gamma_0 \tag{2-80a}$$

$$\begin{aligned} \gamma_1'' &= \lim_{s\to-\xi_1} \{(s + \xi_1)\bar{\chi}_0(s)\} \\ &= \frac{-4\lambda\xi'' + i\left[4\lambda^2\xi''^2 - 1\right]}{2\xi''\left[1 + (2\lambda\xi'')^2\right]} \end{aligned} \tag{2-80b}$$

$$\begin{aligned}\gamma_2'' &= \lim_{s\to-\xi_1^*}\{(s+\xi_1^*)\bar{\chi}_0(s)\}\\ &= \frac{-4\lambda\xi'' - i\left[4\lambda^2\xi''^2-1\right]}{2\xi''\left[1+(2\lambda\xi'')^2\right]} = \gamma_1''^*\end{aligned} \tag{2-80c}$$

and the overall solution is of the form

$$\chi(t) = \frac{C_\delta}{I}H(t-t_0)\left\{\gamma_0'' + \mathrm{e}^{-\frac{t}{2\lambda}}\left[\gamma_1''\,\mathrm{e}^{\xi_1 t_0}\,\mathrm{e}^{-i\xi''t} + \gamma_2''\,\mathrm{e}^{\xi_1^* t_0}\,\mathrm{e}^{i\xi''t}\right]\right\}, \tag{2-81}$$

which can also be expressed in trigonometric form as

$$\chi(t) = \frac{C_\delta}{I}H(t-t_0)\left\{\gamma_0'' + \mathrm{e}^{-\frac{(t-t_0)}{2\lambda}}\gamma_3''\sin\left[\xi''(t-t_0)+\phi\right]\right\}, \tag{2-82}$$

with new constants

$$\gamma_3'' = 2\left|\gamma_2''\right| \tag{2-83a}$$

and

$$\phi = \arctan\left[\frac{\mathrm{Re}\left\{\gamma_1''\right\}}{\mathrm{Im}\left\{\gamma_1''\right\}}\right]. \tag{2-83b}$$

The envelope of the oscillations is given by the equation

$$E_{1,2}(t) = \frac{C_\delta}{\eta}\left[\gamma_0'' \pm \gamma_3''\,\mathrm{e}^{-\alpha t}\right] \tag{2-84}$$

hence a curve fitted to the envelope will yield a value for $\alpha = -\frac{1}{2\lambda}$ and consequently provide an estimate of the relaxation time for the fluid. The frequency of the oscillations may be used to obtain ξ'' and thus the material parameters η, λ or g additionally. In Figure 2.6 the general form of the displacement curve for values of η, λ, kI satisfying the above criterion is illustrated.

2.2.3 N-mode Maxwell Model

To reasonably describe the response of a real-world viscoelastic material, a model with more degrees of freedom than the single-mode Maxwell model is required. The N-mode Maxwell, with N suitably large but finite, is such a model and the expression for the relaxation modulus assuming $G_\infty \neq 0$ has Laplace transform

$$\bar{G}(s) = \frac{G_\infty}{s} + \sum_{i=1}^{N}\frac{g_i}{s+\frac{1}{\lambda_i}}, \qquad i = 1,\ldots,N. \tag{2-85}$$

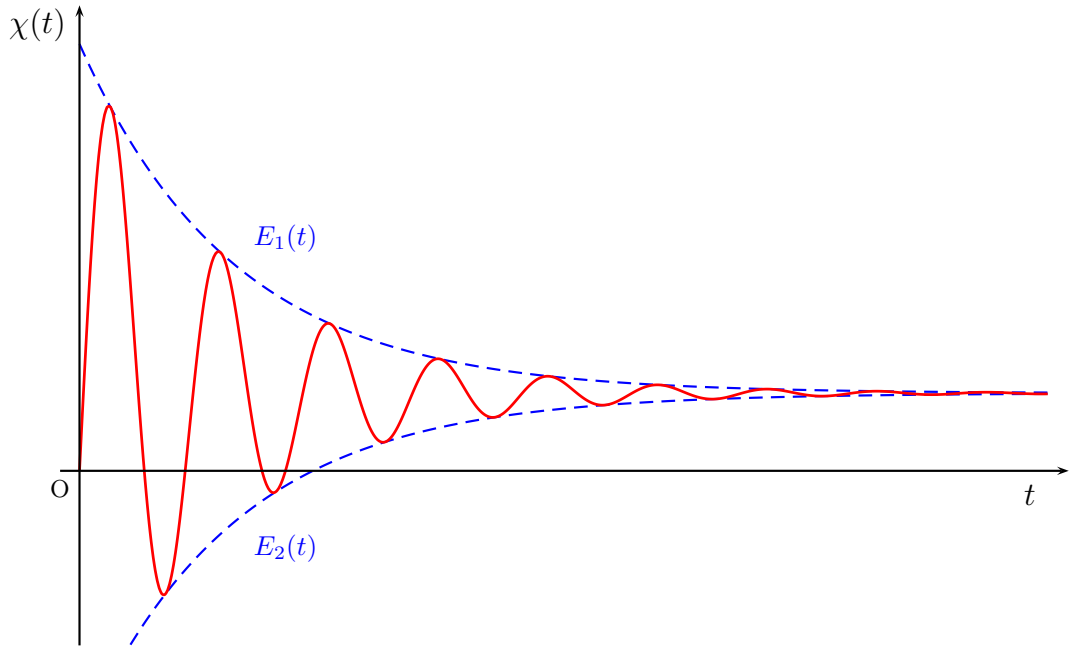

Figure 2.6: Platen displacement: Delta function, Maxwell model, $\psi < 0$.

To simplify the analysis, this is rewritten in the form

$$\bar{G}(s) = \frac{G_\infty \Lambda_{1,N}(s) + s\Lambda_{2,N-1}(s)}{s\Lambda_{1,N}(s)}, \tag{2-86}$$

where $\Lambda_{1,N}(s)$ and $\Lambda_{2,N-1}(s)$ are polynomial functions in s of degree N and $N-1$, respectively, and are defined

$$\Lambda_{1,N}(s) = \prod_{i=1}^{N} \left(s + \frac{1}{\lambda_i} \right) \tag{2-87}$$

$$\Lambda_{2,N-1}(s) = \sum_{i=1}^{N} g_i \prod_{j=1,i}^{N} \left(s + \frac{1}{\lambda_j} \right). \tag{2-88}$$

using the shorthand notation $j = 1, i$ to denote $j = 1, i \neq j$ for the lower limit. There are two cases to consider, corresponding to non-zero and zero values for G_∞, respectively.

Case 1. $G_\infty \neq 0$: Substituting $\bar{C}(s)$ and $\bar{G}(s)$ into (2-42), the Laplace transform of the platen displacement is

$$\bar{\chi}(s) = \frac{C_\delta \Lambda_{1,N}}{I\Lambda_{3,N+2}} \tag{2-89}$$

where the polynomial $\Lambda_{3,N+2}(s)$ of degree $N+2$ is defined

$$\Lambda_{3,N+2} = s^2\Lambda_{1,N}(s) + \frac{1}{kI}\left[G_\infty \Lambda_{1,N}(s) + s\Lambda_{2,N-1}(s) \right]. \tag{2-90}$$

Note that $\bar{\chi}(s)$ is rational and hence of the form $\frac{P(s)}{Q(s)}$ where $P(s)$ and $Q(s)$ are real-valued polynomials in s of degree N and $N+2$, respectively. Denote the roots of $\Lambda_{3,N+2}(s)$ by $\{-\xi_i\}_{i=1}^{N+2}$, where the ξ_i are ordered such that $\mathrm{Re}\,\{\xi_1\} < \mathrm{Re}\,\{\xi_2\} < \cdots < \mathrm{Re}\,\{\xi_{N+2}\}$. Then

$$\bar{\chi}_0(s) = \frac{\prod_{i=1}^{N}(s+\lambda_i^{-1})}{\prod_{i=1}^{N+2}(s+\xi_i)}. \tag{2-91}$$

The $\xi_i, i = 1, \ldots, N+2$ are either real and distinct or some may be complex, but those which are complex must occur in conjugate pairs, since the coefficients of $\prod_{i=1}^{N}(s+\xi_i)$ are real-valued. It is assumed that the ξ_i are distinct and real-valued except for one pair, which may be complex conjugate for $kI > \zeta_c$, where $\zeta_c \in \mathbb{R}$ is a constant dependent upon the material parameters.

Under these assumptions, $\bar{\chi}_0(s)$ has only simple poles and its inverse Laplace transform will be of the form

$$\chi_0(t) = \sum_{i=1}^{N+2} \nu_i \, \mathrm{e}^{-\xi_i t}, \qquad t \in (0, \infty) \tag{2-92}$$

where the residues associated with the simple poles at $\{-\xi_i\}_{i=1}^{N+2}$ are

$$\begin{aligned} \nu_i &= \lim_{s \to -\xi_i} \{(s+\xi_i)\bar{\chi}_0(s)\}, \qquad i = 1, \ldots, N+2 \\ &= \frac{\prod_{j=1}^{N}(\lambda_j^{-1} - \xi_i)}{\prod_{j=1,i}^{N+2}(\xi_j - \xi_i)}. \end{aligned} \tag{2-93}$$

Note that $\lim_{t\to\infty} \chi_0(t) = 0$, so that the platen returns to its original angular displacement at the termination of the experiment.

Case 2. $G_\infty = 0$: If the material is a viscoelastic fluid, then the solution differs subtly in nature from the solid case, although the general solution above is valid. The Laplace transform of the platen displacement is now of the form

$$\bar{\chi}_0(s) = \frac{\Lambda_{1,N}}{s\Lambda_{4,N+1}} \tag{2-94}$$

where the polynomial $\Lambda_{4,N+1}(s)$ of degree $N+1$ is defined

$$\Lambda_{4,N+1} = s\Lambda_{1,N}(s) + \frac{1}{kI}\Lambda_{2,N-1}(s). \tag{2-95}$$

Denoting the $N+1$ roots of $\Lambda_{4,N+1}(s)$ again by $\{-\xi_i'\}_{i=1}^{N+1}$, the inverse Laplace transform yields the solution

$$\chi_0(t) = \mu_0 + \sum_{i=1}^{N+1} \nu_i' \, \mathrm{e}^{-\xi_i' t}, \qquad t \in (0, \infty) \tag{2-96}$$

where

$$\begin{aligned}\mu_0 &= \lim_{s\to 0}\{s\bar{\chi}_0(s)\} \\ &= \frac{1}{\xi'_{N+1}}\prod_{i=1}^{N}\left(\frac{1}{\xi'_i\lambda_i}\right)\end{aligned} \tag{2-97}$$

and

$$\begin{aligned}\nu'_i &= \lim_{s\to -\xi'_i}\left\{(s+\xi'_i)\bar{\chi}_0(s)\right\} \\ &= -\frac{\prod_{j=1}^{N}(\lambda_j^{-1}-\xi'_i)}{\xi'_i\prod_{j=1,i}^{N+1}(\xi'_j-\xi'_i)}, \qquad i=1,\ldots,N+1.\end{aligned} \tag{2-98}$$

Note that $\lim_{t\to\infty}\chi(t) = \frac{C_\delta\mu_0}{I}$, so that in the case of a viscoelastic fluid there is a finite overall flow of the material sample and hence the platen at the end of the experiment, as would be expected.

At this point it is necessary for the purposes of simulation to choose a distribution for the relaxation spectrum in order to provide the values of g_i and λ_i in (2-85). The simplest form is the box spectrum [94], which is defined by

$$H_B(\lambda) = \begin{cases} H_0 & \lambda_{\min} < \lambda < \lambda_{\max} \\ 0 & \lambda < \lambda_{\min}, \lambda > \lambda_{\max}. \end{cases} \tag{2-99}$$

Note that

$$\int_{-\infty}^{\infty} H(\lambda)\,\mathrm{d}\ln\lambda = H_0\int_{\lambda_{\min}}^{\lambda_{\max}}\frac{\mathrm{d}\lambda}{\lambda} = G_0 - G_\infty, \tag{2-100}$$

so the constant H_0 therefore takes the value

$$H_0 = \frac{G_0 - G_\infty}{\ln(\lambda_{\max}/\lambda_{\min})}. \tag{2-101}$$

The discrete values for the relaxation times are assumed to be spaced equally logarithmically in the closed interval $[\lambda_{\min}, \lambda_{\max}]$,

$$\lambda_i = \lambda_{\min}\left(\frac{\lambda_{\max}}{\lambda_{\min}}\right)^{\frac{(i-1)}{(N-1)}}, \qquad i=1,\ldots,N. \tag{2-102}$$

and the numerical values used are: $N = 50, \lambda_{\min} = 0.001s, \lambda_{\max} = 100s$. The fluid parameters were taken to be $G_0 = 4.354$ and $G_\infty = 1$, and the instrumental parameters $k = 1$, $I = 0.1$. The value kI represents a typical experimental setup for the TA-Instruments AR2000, although of course the components and setup may be varied to suit the particular experiment being carried out.

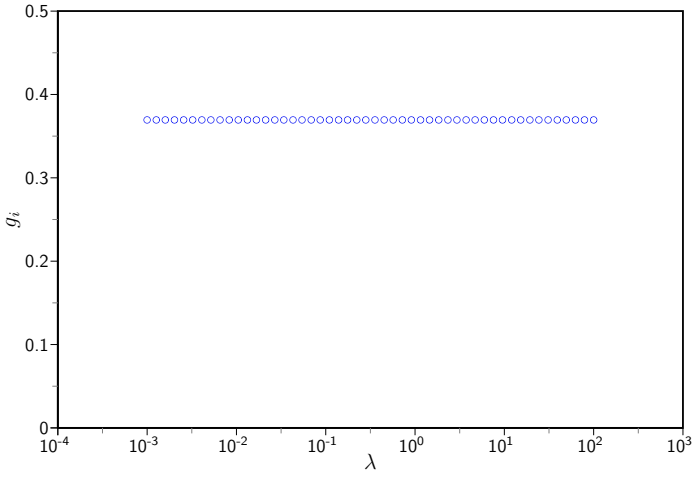

Figure 2.7: Box distribution of discrete relaxation times.

The platen displacement for a viscoelastic fluid with a box relaxation spectrum is shown in Figure 2.9. The qualitative response is similar to that for the Maxwell model case with complex conjugate roots, with a damped oscillation decaying to a fixed value $\frac{C_\delta \mu_0}{I} = 0.006$. The response for a viscoelastic solid is shown in Figure 2.10 and is similar to the response for the viscoelastic fluid, except that the initial displacement of the platen is attained again as $t \to \infty$. Since the limiting value for the viscoelastic fluid is so small, it is difficult to distinguish between the two responses in this case. The recoil may take some considerable time, dependent upon the length of the longest relaxation time of the material.

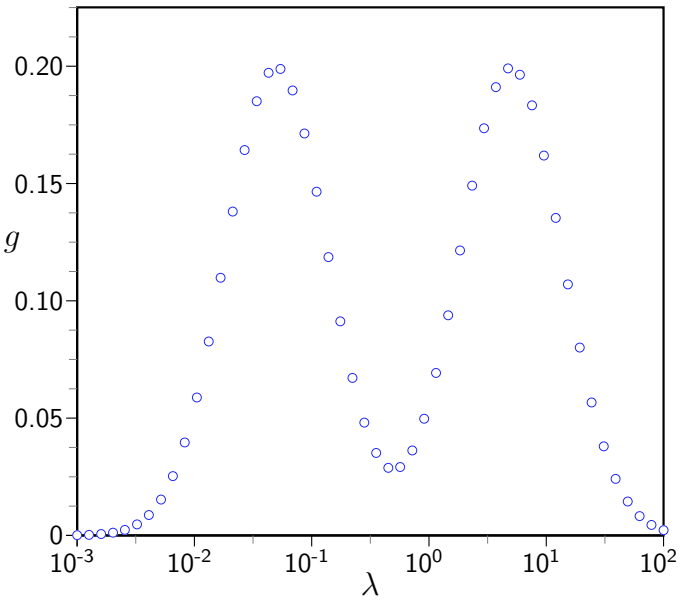

Figure 2.8: Bimodal log-normal distribution of relaxation times of Honerkamp and Weese [36].

The second distribution considered is the double Gaussian spectrum of Honerkamp and Weese [36], which is given by

$$g_i = \frac{1}{2\sqrt{2\pi}} \left[e^{\left[-\frac{1}{2}(\ln\lambda_i - \ln\lambda_\alpha)^2\right]} + e^{\left[-\frac{1}{2}(\ln\lambda_i - \ln\lambda_\beta)^2\right]} \right], \quad i = 1, \ldots, N \tag{2-103}$$

with maxima at λ_α and λ_β, and time constants spaced equally logarithmically according to (2-102). The values of the parameters used in the simulation are as follows. The range of the spectrum is $\lambda_{\min} = 0.001s < \lambda < 100s = \lambda_{\max}$ with local maxima at $\lambda_\alpha = 0.05s$ and $\lambda_\beta = 5s$ and the number of Maxwell elements is $N = 50$. The numerical data used for the relaxation spectrum can be found in Table B-1. The platen displacement shown in Figure 2.11 is for a viscoelastic fluid $G_\infty = 0$ for this relaxation spectrum. In the case of a viscoelastic solid, the equilibrium modulus is taken to be $G_\infty = 1$ and the platen displacement is plotted in Figure 2.12. The method of simulation involves finding the roots of the polynomial equation (2-90), which is of degree 52; the software package Maple was used in this case, but an alternative method using C++ code and the Jenkins-Traub algorithm [71] produced identical results. The output from both spectra are qualitatively very similar, so henceforth only the bimodal Gaussian spectrum needs to be considered.

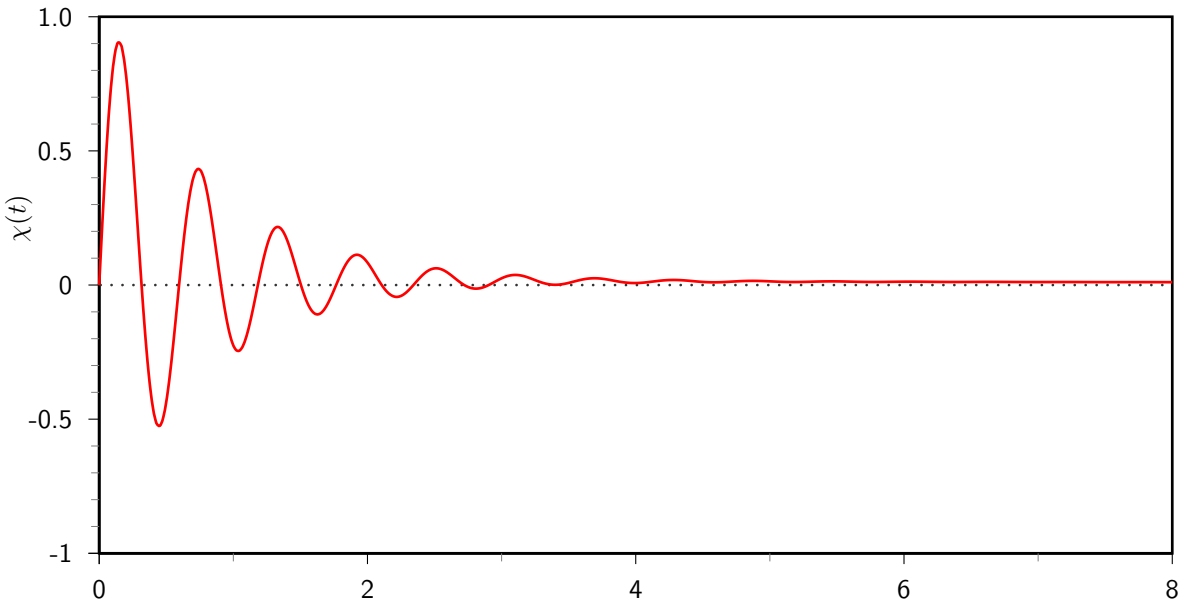

Figure 2.9: Platen displacement: delta function, viscoelastic liquid, box relaxation spectrum.

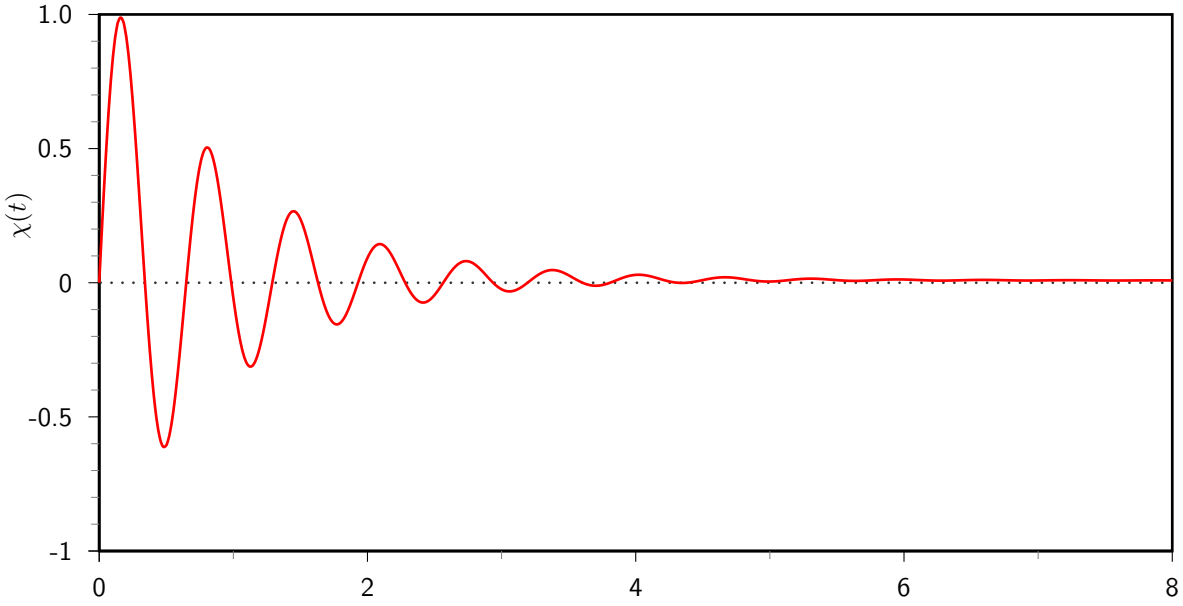

Figure 2.10: Platen displacement: delta function, viscoelastic solid, box distribution relaxation spectrum.

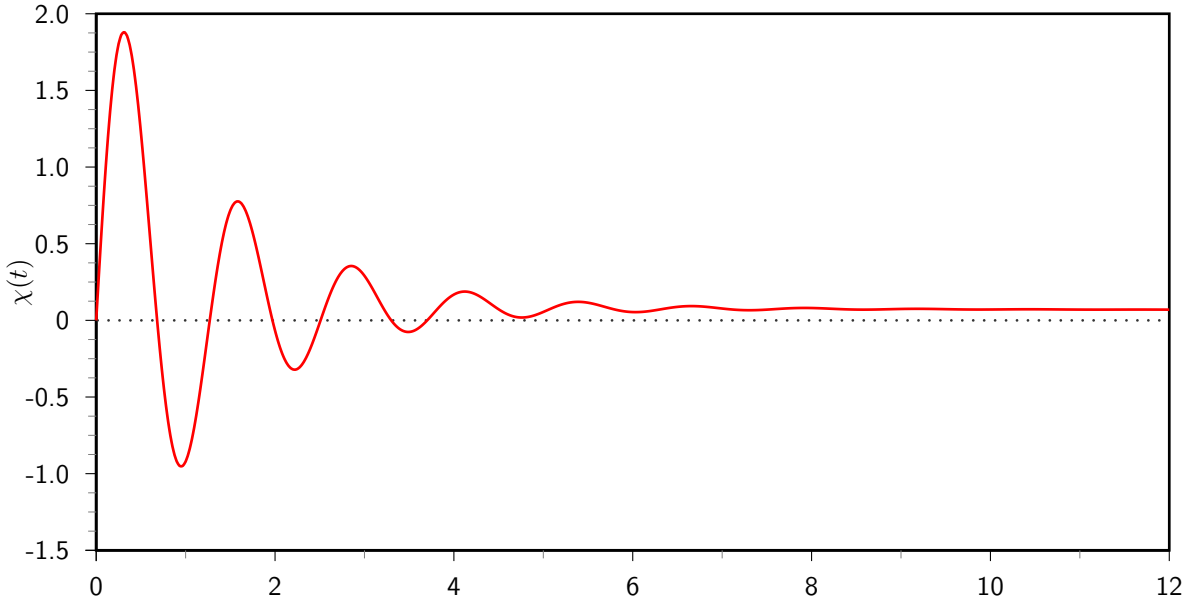

Figure 2.11: Platen displacement: delta function, viscoelastic liquid, double Gaussian spectrum of Honerkamp & Weese.

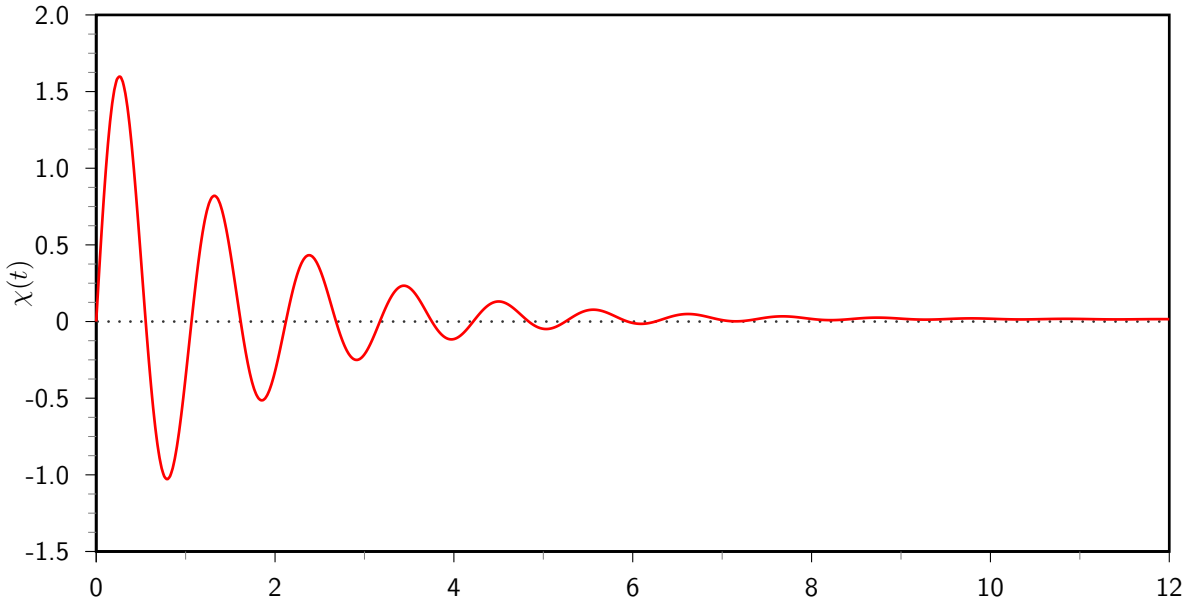

Figure 2.12: Platen displacement: delta function, viscoelastic solid, double Gaussian spectrum of Honerkamp & Weese.

III. STEP & BOX FUNCTIONS

Now consider an applied torque in the form of the Heaviside step function, defined by

$$C(t) = \begin{cases} C_0, & t > t_0 \\ 0, & t < t_0 \end{cases} \tag{2-104}$$

for some constant $t_0 \in [0, \infty)$ and $C_0 \in \mathbb{R}^+$. The function is often defined [41] by taking the limit as $\varepsilon \to 0$ in the expression

$$H(t;\varepsilon) = \frac{1}{2} + \frac{1}{\pi} \tan^{-1}\left(\frac{t}{\varepsilon}\right). \tag{2-105}$$

Since no instrument is capable of producing a perfectly defined jump in stress, the actual stress profile applied will in reality be somewhat similar to the above function with a sufficiently small value of ϵ.

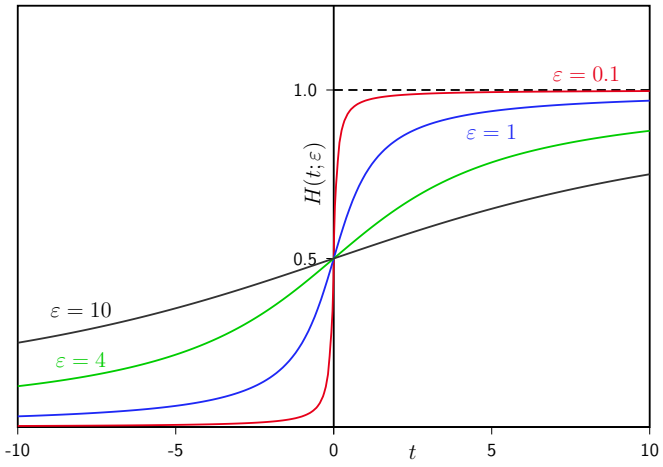

Figure 2.13: Heaviside step function as a limit of sequences.

The applied stress in an experiment is by necessity of finite duration, T, so the actual applied stress will be in the form of a box function,

$$C(t) = \begin{cases} C_0, & t_0 < t < t_1 \\ 0 & \text{otherwise} \end{cases} \tag{2-106}$$

where $0 \leq t_0 < t_1 < T$, or in terms of the Heaviside step function

$$C(t) = C_0 \left[H(t - t_0) - H(t - t_1)\right], \tag{2-107}$$

which results in the displacement with Laplace transform

$$\bar{\chi}_{bf}(s) = \frac{kC_0 \left[\mathrm{e}^{-st_0} - \mathrm{e}^{-st_1}\right]}{s^2 \left[\bar{G}(s) - kIs\right]}. \tag{2-108}$$

Proceeding in a similar manner to the delta function by applying the real-valued shift theorem in (2-57), the overall solution can constructed in terms of a linear combination of the solution for a unit Heaviside step function, which will be denoted $\chi_{sf}(t)$. Hence, for the box function

$$\chi_{bf}(t) = \chi_{sf}(t-t_0)H(t-t_0) - \chi_{sf}(t-t_1)H(t-t_1) \tag{2-109}$$

where

$$\bar{\chi}_{sf}(s) = \frac{kC_0}{s^2\left[\bar{G}(s) + kIs\right]}. \tag{2-110}$$

Now we proceed to consider some specific forms for the relaxation modulus as in the previous section.

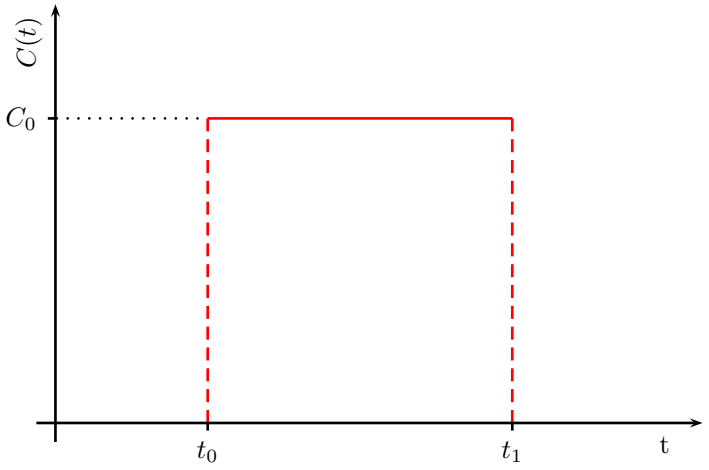

Figure 2.14: Box function applied stress.

2.3.1 Newtonian Fluid Model

The simplest fluid model, upon substituting $\bar{G}(s) = \eta$ into (2-110) yields

$$\bar{\chi}_{sf}(s) = \frac{C_0}{Is^2\left[s + \frac{\eta}{kI}\right]} \tag{2-111}$$

which corresponds in the time domain to

$$\chi_{sf}(t) = \frac{kC_0}{\eta}\left[t - \frac{kI}{\eta} + \frac{kI}{\eta}\,\mathrm{e}^{-\frac{\eta t}{kI}}\right]. \tag{2-112}$$

The angular velocity $\dot{\chi}(t)$ of the platen tends to a constant value $\frac{kC_0}{\eta}$ after an initial period of acceleration where the exponential 'transient' term dominates. Taking the limit as $I \to 0$,

$$\chi_{sf}(t) = \frac{kC_0 t}{\eta}, \tag{2-113}$$

corresponding to a standard creep test where the inertia of the instrument is ignored, results in a constant angular velocity of the platen. Applying (2-109) to (2-112) produces the expression for the box function

$$\chi_{bf}(t) = \begin{cases} 0, & 0 < t < t_0 \\ \frac{kC_0}{\eta}\left[t - t_0 - \frac{kI}{\eta} + \frac{kI}{\eta}\,\mathrm{e}^{-\frac{\eta(t-t_0)}{kI}}\right], & t_0 < t < t_1 \\ \frac{kC_0}{\eta}\left[t_1 - t_0 + \frac{kC_0}{\eta}\left(\mathrm{e}^{\frac{\eta t_0}{kI}} - \mathrm{e}^{\frac{\eta t_1}{kI}}\right)\mathrm{e}^{-\frac{\eta t}{kI}}\right], & t > t_1. \end{cases} \tag{2-114}$$

The response is illustrated in Figure 2.15, where it can be seen that the initial response for $t \in [t_0, t_1]$ is that of the step function, followed by a deceleration to approach a constant value $\frac{kC_0(t_1-t_0)}{\eta}$ after the stress is removed at $t = t_1$.

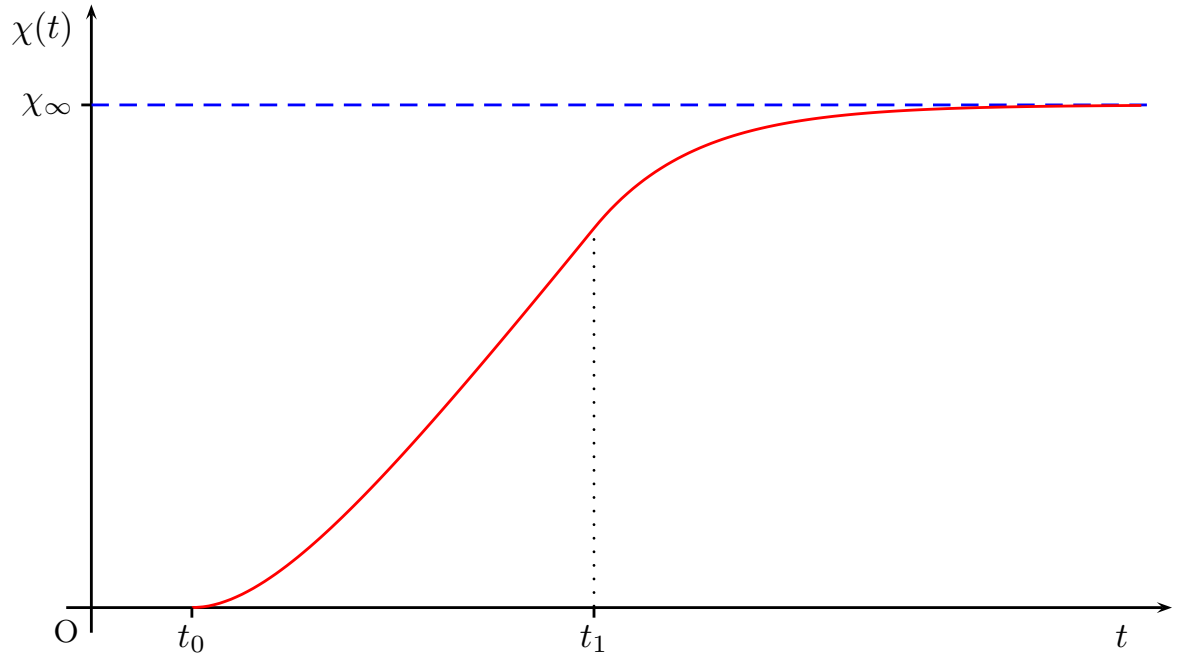

Figure 2.15: Platen displacement: box function, Newtonian fluid. Limiting value $\chi_{bf}(\infty) = \frac{kC_0(t_1-t_0)}{\eta}$

2.3.2 Maxwell Model

Assuming the relaxation modulus corresponds to a single-mode relaxation spectrum $\{g, \lambda\}$, (2-110) becomes

$$\bar{\chi}_{sf}(s) = \frac{C_0(s+\lambda^{-1})}{Is^2(s+\xi_1)(s+\xi_2)} = \frac{C_0}{I}\bar{\chi}_0(s), \tag{2-115}$$

where the roots of the quadratic polynomial in the denominator, $\{-\xi_1, -\xi_2\}$, are as defined in (2-65) and also give rise to three distinct cases dependent upon the value of the parameter $\psi = 1 - 4\frac{\eta\lambda}{kI}$ which are now considered in turn.

Case 1. $\psi > 0$: The roots $\xi_{1,2} \in \mathbb{R}$ and the solution has a double pole at the origin, single poles at $s = -\xi_{1,2}$ and takes the form

$$\chi_{sf}(t) = \frac{C_0}{I}\left\{\gamma_0 + \gamma_1 t + \gamma_2 \mathrm{e}^{-\xi_1 t} + \gamma_3 \mathrm{e}^{-\xi_2 t}\right\} \tag{2-116}$$

where the constants $\gamma_{0,1,2} \in \mathbb{R}$ are defined

$$\begin{aligned}
\gamma_0 &= \lim_{s\to 0}\left\{\frac{\mathrm{d}}{\mathrm{d}s}\left[s^2\bar{\chi}_0(s)\right]\right\} \\
&= \frac{kI(\eta\lambda - kI)}{\eta^2} && \text{(2-117a)} \\
\gamma_1 &= \lim_{s\to 0}\left\{s^2\bar{\chi}_{sf}(s)\right\} \\
&= \frac{kI}{\eta} && \text{(2-117b)} \\
\gamma_2 &= \lim_{s\to -\xi_1}\left\{(s+\xi_1)\bar{\chi}_0(s)\right\} \\
&= \frac{1-\lambda\xi_1}{\lambda\xi_1^2(\xi_2-\xi_1)} && \text{(2-117c)} \\
\gamma_3 &= \lim_{s\to -\xi_2}\left\{(s+\xi_2)\bar{\chi}_0(s)\right\} \\
&= \frac{\lambda\xi_2 - 1}{\lambda\xi_2^2(\xi_2-\xi_1)} && \text{(2-117d)}
\end{aligned}$$

Case 2. $\psi = 0$: Repeated real roots $\xi_1 = \xi_2 = \frac{1}{2\lambda}$. $\bar{\chi}_0(s)$ now has double poles at $s = 0$ and $s = -\xi_1$ and has inverse Laplace transform

$$\chi_{sf}(t) = \frac{C_0}{I}\left\{\gamma_0' + \gamma_1' t + (\gamma_2' + \gamma_3' t)\,\mathrm{e}^{-\frac{t}{2\lambda}}\right\} \tag{2-118}$$

with constants

$$\begin{aligned}
\gamma_0' &= -12\lambda^2 && \text{(2-119a)} \\
\gamma_1' &= 4\lambda && \text{(2-119b)} \\
\gamma_2' &= \lim_{s\to -\xi_1}\left\{\frac{\mathrm{d}}{\mathrm{d}s}\left[(s-\xi_1)^2\bar{\chi}_0(s)\right]\right\} \\
&= 12\lambda^2 && \text{(2-119c)} \\
\gamma_3' &= \lim_{s\to -\xi_1}\left\{(s-\xi_1)^2\bar{\chi}_0(s)\right\} \\
&= 2\lambda && \text{(2-119d)}
\end{aligned}$$

Case 3. $\psi < 0$: The roots are complex $\xi_{1,2} \in \mathbb{C}$ and furthermore $\xi_2 = \xi_1^*$. Let $\xi_1 = \xi + i\xi''$ and $\xi_2 = \xi' - i\xi''$, where $\xi' = \frac{1}{2\lambda}$ and $\xi'' = \frac{1}{2\lambda}\sqrt{|\psi|}$, then the inverse Laplace transform is of the form

$$\chi_{sf}(t) = \frac{C_0}{I}\left\{\gamma_0'' + \gamma_1'' t + \mathrm{e}^{-\xi' t}\left[\gamma_2'' \mathrm{e}^{-i\xi'' t} + \gamma_3'' \mathrm{e}^{i\xi'' t}\right]\right\} \tag{2-120}$$

in addition to constants $\gamma''_{0,1,2,3} \in \mathbb{C}$ defined

$$\gamma''_0 = \gamma_0 \tag{2-121a}$$

$$\gamma''_1 = \gamma_1 \tag{2-121b}$$

$$\begin{aligned}\gamma''_2 &= \frac{\lambda\xi_1 - 1}{\lambda\xi_1^2(\xi_1 - \xi_1^*)} \\ &= \frac{\left[-2\lambda^2\xi''(5 + 4\lambda^2\xi''^2)\right] + i\lambda\left[3 - 4\xi''^2\lambda^2\right]}{\xi''\left[1 + (2\lambda\xi'')^2\right]^2}\end{aligned} \tag{2-121c}$$

$$\begin{aligned}\gamma''_3 &= \frac{1 - \lambda\xi_1^*}{\lambda\xi_1^{*2}(\xi_1 - \xi_1^*)} \\ &= \frac{\left[-2\lambda^2\xi''(5 + 4\lambda^2\xi''^2)\right] - i\lambda\left[3 - 4\xi''^2\lambda^2\right]}{\xi''\left[1 + (2\lambda\xi'')^2\right]^2} = \gamma''^*_2\end{aligned} \tag{2-121d}$$

The limiting case where $I = 0$ results in a displacement

$$\chi_{sf}(t) = \frac{kC_0}{\lambda g}\left[\lambda + t\right] H(t) \tag{2-122}$$

which corresponds to a standard creep test with initial displacement jump and linear temporal increase in platen displacement thereafter.

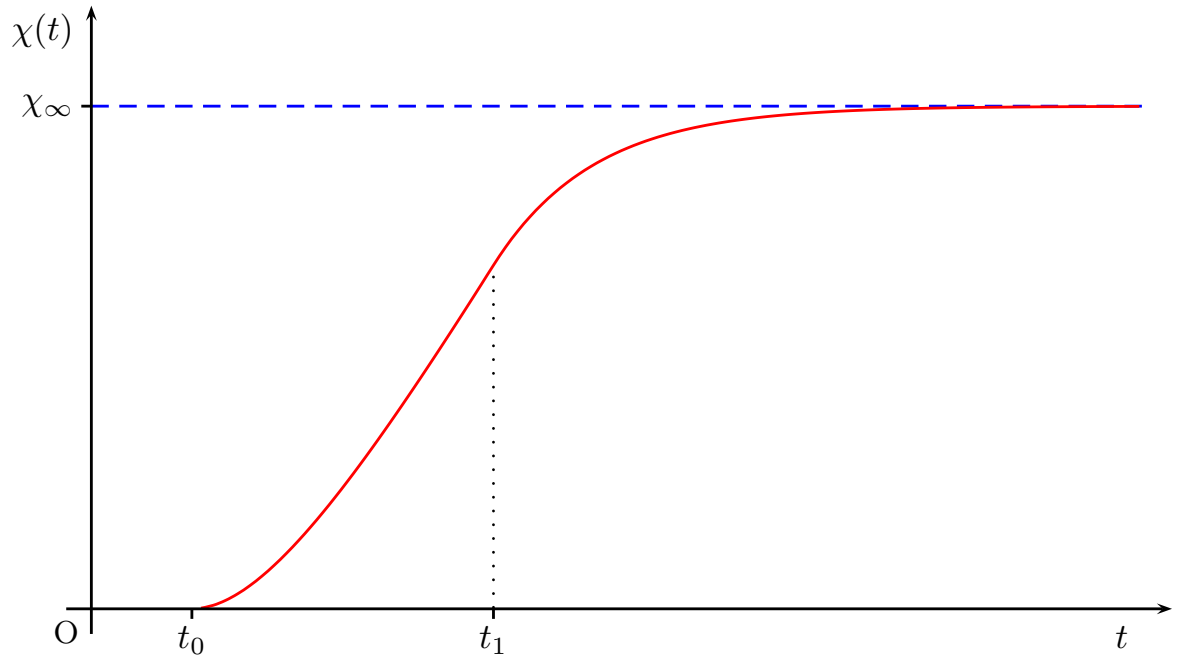

Figure 2.16: Platen displacement: box function, Maxwell model, $\psi > 0$. Limiting value $\chi_{bf}(\infty) = \frac{kC_0(t_1 - t_0)}{\eta}$

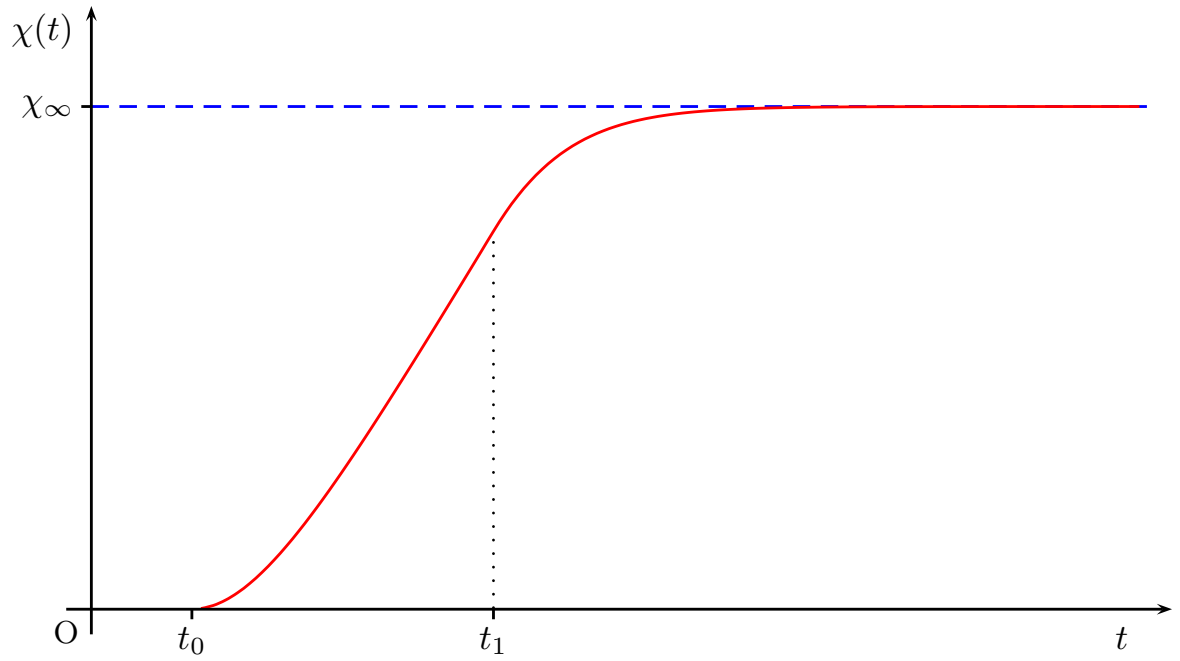

Figure 2.17: Platen displacement: box function, Maxwell model, $\psi = 0$. Limiting value $\chi_{bf}(\infty) = \frac{4\lambda C_0(t_1 - t_0)}{I}$

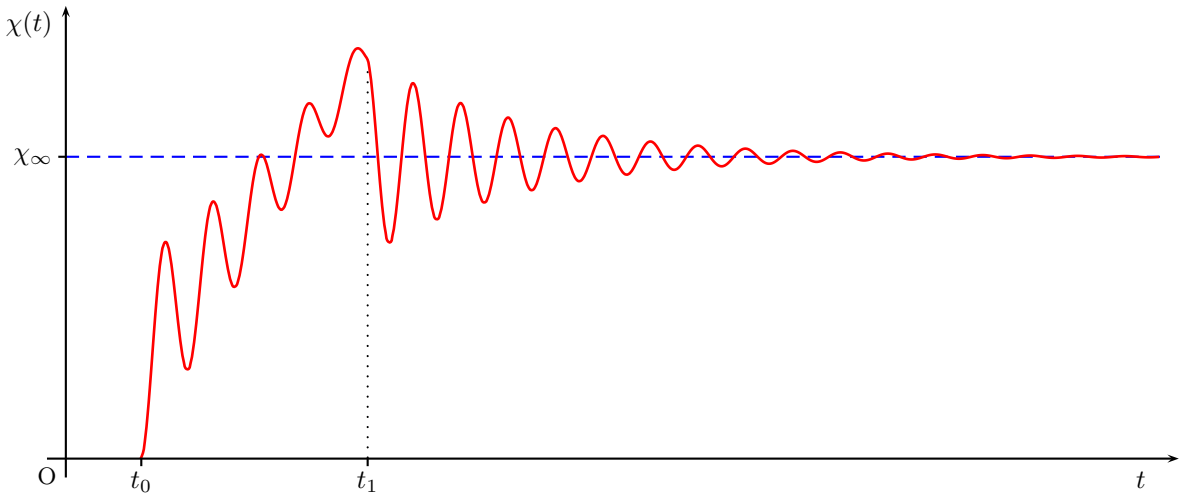

Figure 2.18: Platen displacement: box function, Maxwell model, $\psi < 0$. Limiting value $\chi_{bf}(\infty) = \frac{kC_0(t_1 - t_0)}{\eta}$

2.3.3 N-mode Maxwell Model

As for the delta function applied torque, we now consider the case where the material is modelled by an N-mode relaxation spectrum, individually for viscoelastic fluids and solids.

Case 1. $G_\infty \neq 0$: Using the definitions of $\bar{G}(s)$, $\Lambda_{1,N}(s)$ and $\Lambda_{2,N-1}(s)$ in (2-86)-(2-88), the platen displacement has Laplace transform

$$\bar{\chi}_{sf}(s) = \frac{C_0 \Lambda_{1,N}(s)}{Is\Lambda_{3,N+2}(s)}, \tag{2-123}$$

where $\Lambda_{3,N+2}(s)$ is a polynomial of degree $N+2$ as defined in (2-90). Again, denoting the roots of $\Lambda_{3,N+2}(s)$ by $\{\xi_i\}_{i=1}^{N+2}$, $\chi_{sf}(t)$ has Laplace transform

$$\bar{\chi}_{sf}(s) = \frac{C_0 \prod_{i=1}^{N}(s+\lambda_i^{-1})}{sI\prod_{i=1}^{N+2}(s+\xi_i)}, \tag{2-124}$$

so $\chi_{sf}(t)$ itself is of the general form

$$\chi_{sf}(t) = \frac{C_0}{I}\left\{\mu_0 + \sum_{i=1}^{N+2} \nu_i \, \mathrm{e}^{-\xi_i t}\right\}, \quad t \in [0,T] \tag{2-125}$$

with constants $\mu_0 \in \mathbb{R}$ and $\nu_i \in \mathbb{C}$ defined

$$\begin{aligned} \mu_0 &= \lim_{s\to 0}\{s\bar{\chi}_{sf}(s)\} \\ &= \frac{1}{\xi_{N+1}\xi_{N+2}}\prod_{i=1}^{N}\frac{1}{\lambda_i\xi_i} \end{aligned} \tag{2-126}$$

$$\begin{aligned} \nu_i &= \lim_{s\to -\xi_i}\{(s-\xi_i)\bar{\chi}_{sf}(s)\} \\ &= -\frac{\prod_{j=1}^{N}(\lambda_j^{-1}-\xi_i)}{\xi_i\prod_{j=1,i}^{N+2}(\xi_j-\xi_i)}, \quad i = 1,2,\ldots,N+2. \end{aligned} \tag{2-127}$$

Note that $\lim_{t\to\infty}\chi_{sf}(t) = \frac{C_0}{I}\mu_0 > 0$, so the platen displacement reaches an equilibrium value, as would be expected for a viscoelastic solid under constant stress in the linear regime. Since $\lim_{t\to 0}\chi_{sf}(t) = 0$, additional information about the constants is obtained by the relation $\mu_0 = -\sum_{i=1}^{N+2}\nu_i$. The solution for the box function is obtained by applying (2-109) and the platen displacement is plotted in Figure 2.19 for the double Gaussian spectrum in (2-103) using the same values for the parameters as for the delta function in Section 2.2.3. For $t > t_1$, the displacement is given by $\chi(t) = \chi_{sf}(t-t_0) - \chi_{sf}(t-t_1)$ and although not readily apparent in the figure, $\lim_{t\to\infty}\chi(t) = 0$, the rate of recoil to the initial equilibrium displacement being governed by the magnitude of the longest relaxation time.

Case 2. $G_\infty = 0$: For the viscoelastic fluid case, the platen displacement has Laplace transform

$$\bar{\chi}_{sf}(s) = \frac{C_0 \Lambda_{1,N}(s)}{Is^2\Lambda_{4,N+1}(s)}, \tag{2-128}$$

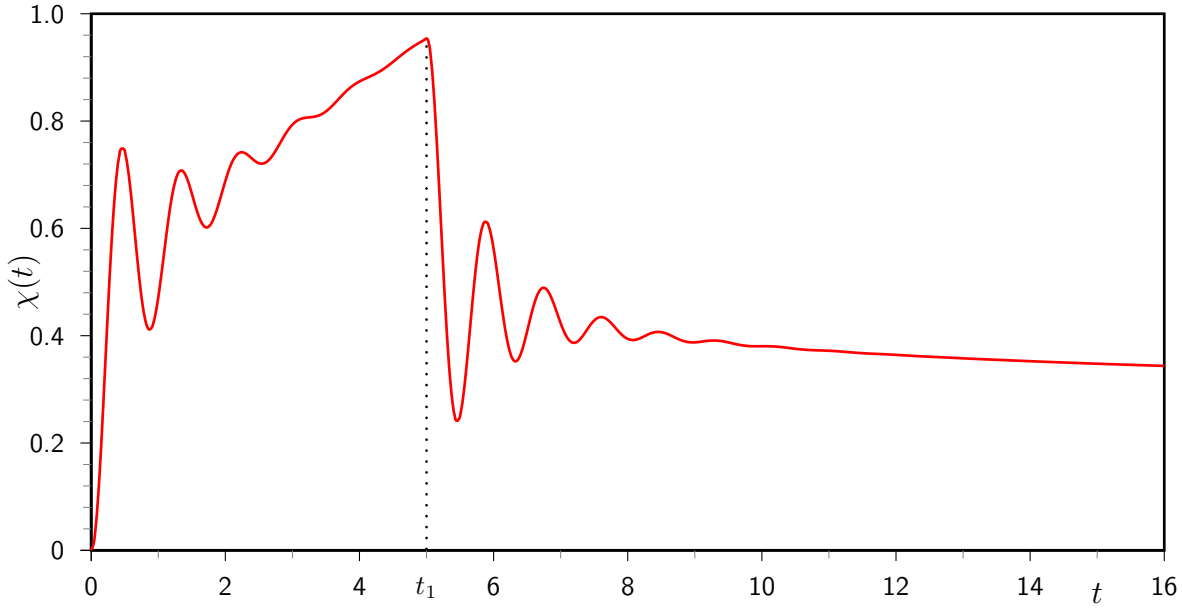

Figure 2.19: Platen displacement: box function, viscoelastic liquid, double Gaussian spectrum of Honerkamp & Weese.

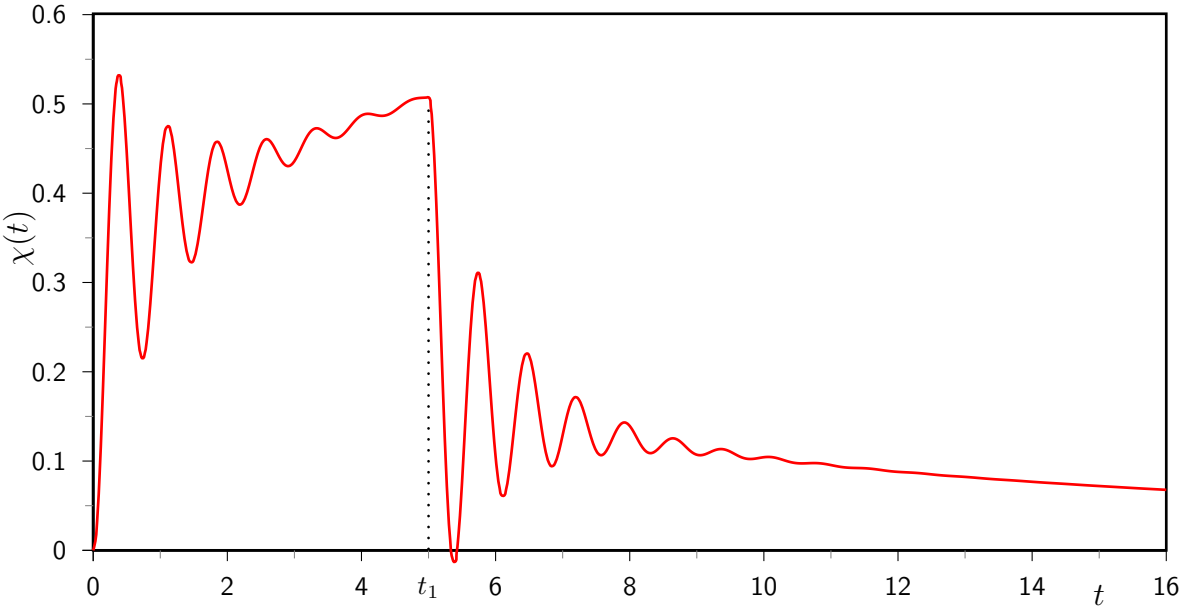

Figure 2.20: Platen displacement: box function, viscoelastic solid, double Gaussian spectrum of Honerkamp & Weese.

where the polynomial functions $\Lambda_{1,N}(s)$ and $\Lambda_{4,N+1}(s)$ are defined as in (2-87) and (2-95), respectively. Denoting the roots of $\Lambda_{4,N+1}(s)$ by $\{-\xi_i'\}_{i=1}^{N+1}$, (2-128) now becomes

$$\bar{\chi}_{sf}(s) = \frac{C_0 \prod_{i=1}^{N}(s+\lambda_i^{-1})}{Is^2 \prod_{i=1}^{N+1}(s+\xi_i')} \tag{2-129}$$

which, upon inversion of the Laplace transform, yields

$$\chi_{sf}(t) = \frac{C_0}{I}\left\{\mu_0' + \mu_1' t + \sum_{i=1}^{N+1} \nu_i' \, \mathrm{e}^{-\xi_i' t}\right\} \tag{2-130}$$

with constants $\nu_i' \in \mathbb{C}$ defined

$$\begin{aligned}\nu_i' &= \lim_{s\to -\xi_i'} \left\{(s+\xi_i')\bar{\chi}_{sf}(s)\right\} \\ &= \frac{\prod_{j=1}^{N}(\lambda_j^{-1} - \xi_i')}{\xi_i'^2 \prod_{j=1,i}^{N+1}(\xi_j' - \xi_i')}, \quad i = 1, 2, \ldots, N+1.\end{aligned} \tag{2-131}$$

The double pole at $s = 0$ gives rise to the remaining constants $\mu_0', \mu_1' \in \mathbb{R}$,

$$\begin{aligned}\mu_0' &= \lim_{s\to 0}\left\{\frac{\mathrm{d}}{\mathrm{d}s}\left[s^2 \bar{\chi}_{sf}(s)\right]\right\} \\ &= \frac{1}{\xi_{N+1}'}\left[\sum_{i=1}^{N}\lambda_i - \sum_{i=1}^{N+1}(\xi_i')^{-1}\right]\prod_{i=1}^{N}\frac{1}{\lambda_i \xi_i'}\end{aligned} \tag{2-132}$$

$$\begin{aligned}\mu_1' &= \lim_{s\to 0}\left\{s^2 \bar{\chi}_{sf}(s)\right\} \\ &= \frac{1}{\xi_{N+1}' \prod_{i=1}^{N}\lambda_i \xi_i'}\end{aligned} \tag{2-133}$$

where μ_0' has been evaluated using the identity

$$\frac{\mathrm{d}}{\mathrm{d}s}\prod_{i=1}^{N} f_i(s) = \left[\sum_{i=1}^{N}\left(\frac{\frac{\mathrm{d}}{\mathrm{d}s} f_i(s)}{f_i(s)}\right)\right]\prod_{i=1}^{N} f_i(s). \tag{2-134}$$

Since $\chi_{sf}(0) = 0$, the coefficients must satisfy $\mu_0 = -\sum_{i=1}^{N+1}\nu_i$ and the step function applied torque results in a linear increase in displacement as $t \to \infty$. The box function solution is obtained as previously described in (2-109) and the displacement for a viscoelastic fluid with double Gaussian relaxation spectrum and parameters as described in Section 2.2.3 is plotted in Figure 2.20. For $t > t_1$, the platen displacement is given by $\chi_{bf}(t) = \chi_{sf}(t - t_0) - \chi_{sf}(t - t_1)$ and it can readily be inferred that $\lim_{t\to\infty}\chi_{bf}(t) = \frac{C_0\mu_1}{I}(t_1 - t_0)$. This result is expected, since a viscoelastic fluid will exhibit a degree of flow overall after the removal of the strictly positive applied stress.

IV. SLOPE & RAMP FUNCTIONS

Consider an applied torque now in the form of a linear function of time. The base function, often called the "slope" function will be defined

$$C_{sl}(t) = C_0 t H(t), \tag{2-135}$$

where $H(t)$ is the Heaviside step function and $C_0 \in \mathbb{R}$, or in Laplace space

$$\bar{C}_{sl}(s) = \frac{C_0}{s^2}. \tag{2-136}$$

which, upon inserting in (2-42) yields the Laplace transform of the platen displacement as

$$\bar{\chi}_{sl}(s) = \frac{kC_0}{s^3\left[\bar{G}(s) + kIs\right]}. \tag{2-137}$$

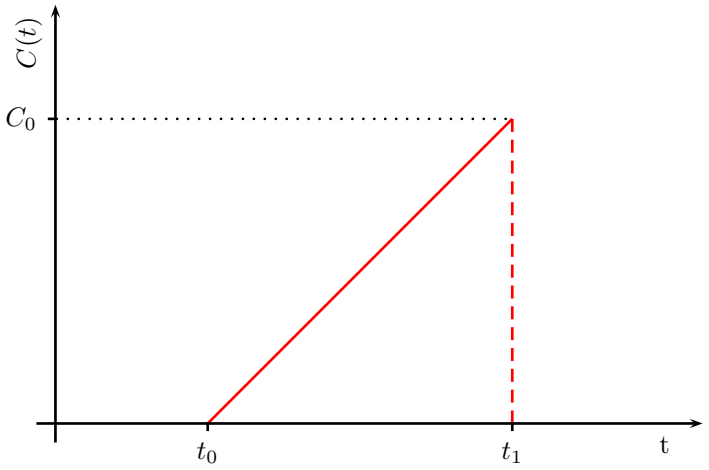

Figure 2.21: Ramp function applied stress.

An experiment of finite duration will necessarily result in the application of a "ramp" function given by

$$C_{rf}(t) = C_0 t\left[H(t) - H(t - t_1)\right] \tag{2-138}$$

for constant $t_1 \in \mathbb{R}^+$ as depicted in Figure 2.21. The Laplace transform is

$$\bar{C}_{rf}(s) = \frac{C_0}{s^2}\left[1 - (1 + st_1)\,\mathrm{e}^{-st_1}\right], \tag{2-139}$$

and the Laplace transform of the platen displacement can be expressed in terms of that of the slope and step function as

$$\bar{\chi}_{rf}(s) = \bar{\chi}_{sl}(s) - \mathrm{e}^{-t_1 s}\left[\bar{\chi}_{sl}(s) - t_1\bar{\chi}_{sf}(s)\right] \tag{2-140}$$

which upon inversion yields

$$\chi_{rf}(t) = \chi_{sl}(t)H(t) - \left[\chi_{sl}(t - t_1) + t_1\chi_{sf}(t - t_1)\right]H(t - t_1) \tag{2-141}$$

As for the previous two sections, we now look at a variety of specific models. Since much of the working is similar, some detail has been omitted to avoid repetition.

2.4.1 Newtonian Fluid Model

The Newtonian model, with relaxation modulus $G(t) = \eta\delta(t)$ produces a platen displacement with Laplace transform

$$\bar{\chi}_{sl}(s) = \frac{C_0}{Is^3\left[s + \frac{\eta}{kI}\right]} \tag{2-142}$$

and in t-space

$$\chi_{sl}(t) = \frac{kC_0}{\eta}\left\{\left(\frac{kI}{\eta}\right)^2 - \frac{kI}{\eta}t + \tfrac{1}{2}t^2 - \left(\frac{kI}{\eta}\right)^2 \mathrm{e}^{-\frac{\eta t}{kI}}\right\}. \tag{2-143}$$

The platen displacement behaves like $\mathcal{O}(t^2)$ as $t \to \infty$ and tends to a constant acceleration $\frac{kC_0}{\eta}$. As $I \to 0$,

$$\chi_{sl}(t) = \frac{kC_0}{\eta}t^2. \tag{2-144}$$

2.4.2 Maxwell Model

For the Maxwell model, with relaxation spectrum $\{g, \lambda\}$, (2-137) becomes

$$\bar{\chi}_{sl}(s) = \frac{C_0(s + \lambda^{-1})}{Is^3(s + \xi_1)(s + \xi_2)} = \frac{C_0}{I}\bar{\chi}_0(s) \tag{2-145}$$

where $\xi_{1,2}$ are defined as in (2-65). As for the previous sections, there are three cases depending upon the value of $\psi = 1 - \frac{4\eta\lambda}{kI}$, but only the case where the roots are distinct is included here.

Assuming $\xi_1 \neq \xi_2$, inversion of the Laplace transform in (2-145) results in a solution of the form

$$\chi_{sl}(t) = \frac{C_0}{I}\left\{\gamma_0 + \gamma_1 t + \gamma_2 t^2 + \gamma_3\,\mathrm{e}^{-\xi_1 t} + \gamma_4\,\mathrm{e}^{-\xi_2 t}\right\} \tag{2-146}$$

with constants $\gamma_{0,1,2} \in \mathbb{R}$ and $\gamma_3 \in \mathbb{C}$ defined

$$\begin{aligned}\gamma_0 &= \lim_{s\to 0}\left\{\frac{\mathrm{d}^2}{\mathrm{d}s^2}\left[\frac{s^3}{2!}\bar{\chi}_0(s)\right]\right\} \\ &= \frac{(kI)^2(kI - 2\eta\lambda)}{\eta^3}\end{aligned} \tag{2-147}$$

$$\begin{aligned}\gamma_1 &= \lim_{s\to 0}\left\{\frac{\mathrm{d}}{\mathrm{d}s}\left[s^3\bar{\chi}_0(s)\right]\right\} \\ &= \frac{kI(\eta\lambda - kI)}{\eta^2}\end{aligned} \tag{2-148}$$

$$\gamma_2 = \frac{1}{2!}\lim_{s\to 0}\left\{s^3\bar{\chi}_0(s)\right\} = \frac{kI}{2\eta} \tag{2-149}$$

$$\begin{aligned}\gamma_3 &= \lim_{s\to -\xi_1}\{(s+\xi_1)\bar{\chi}_0(s)\}\\ &= \frac{\lambda\xi_1 - 1}{\lambda\xi_1^3(\xi_2-\xi_1)}\end{aligned} \tag{2-150}$$

$$\begin{aligned}\gamma_4 &= \lim_{s\to -\xi_2}\{(s+\xi_2)\bar{\chi}_0(s)\}\\ &= \frac{1-\lambda\xi_2}{\lambda\xi_2^3(\xi_2-\xi_1)}\end{aligned} \tag{2-151}$$

In the case where the roots are complex conjugate, it follows that $\gamma_4 = \gamma_3^*$, hence (2-146) can be written in the form

$$\frac{C_0}{I}\left\{\gamma_0 + \gamma_1 t + \gamma_2 t^2 + A\,\mathrm{e}^{-\frac{t}{2\lambda}}\sin(\xi'' t + \phi)\right\}, \tag{2-152}$$

where the constants $A, \phi \in \mathbb{R}$ are defined

$$A = 2\,|\gamma_3| \tag{2-153}$$

$$\tan\phi = \frac{\mathrm{Re}\,\{\gamma_3\}}{\mathrm{Im}\,\{\gamma_3\}}. \tag{2-154}$$

The latter case is plotted in Figure 2.22.

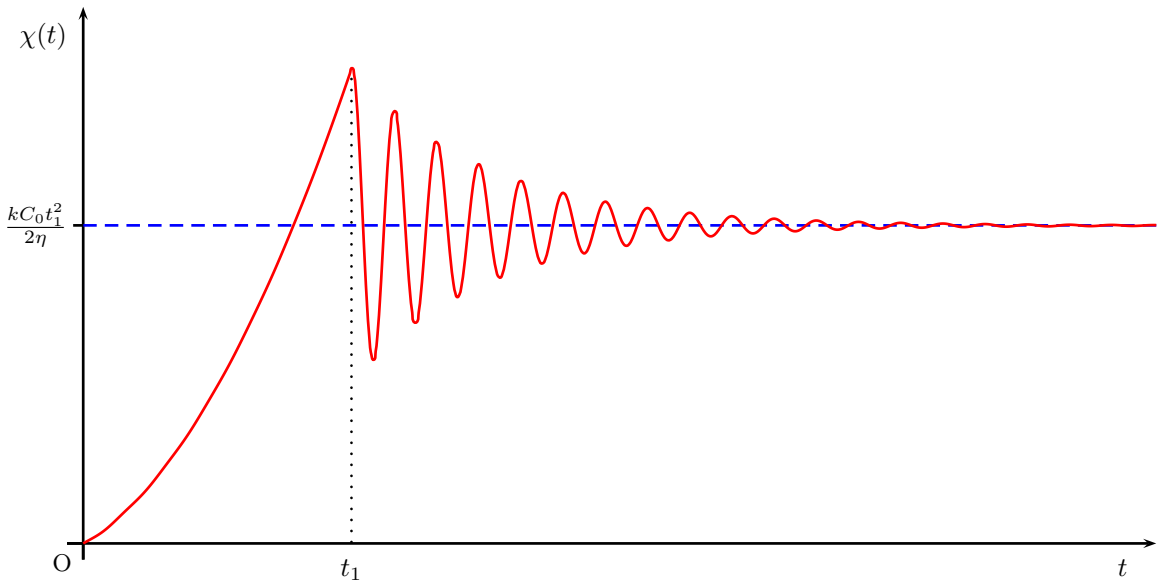

Figure 2.22: Platen displacement: ramp function, Maxwell model, $\psi < 0$, $t_1 = 4$.

2.4.3 N-mode Maxwell Model

Finally, consider a fluid modelled by an N-mode relaxation spectrum for both viscoelastic fluid and solid cases.

Case 1. $G_\infty \neq 0$: Using the definitions of $\bar{G}(s)$, $\Lambda_{1,N}(s)$ and $\Lambda_{2,N-1}(s)$ in (2-86)-(2-88), the platen displacement for a viscoelastic solid has Laplace transform

$$\bar{\chi}_{sl}(s) = \frac{C_0 \Lambda_{1,N}(s)}{I s^2 \Lambda_{3,N+2}(s)} \tag{2-155}$$

where $\Lambda_{3,N+2}(s)$ is a polynomial of degree $N+2$ given by (2-90). Denoting the roots of $\Lambda_{3,N+2}(s)$ by $\{\xi_i\}_{i=1}^{N+2}$, the inverse Laplace transform of (2-155) becomes

$$\chi_{sl}(t) = \frac{C_0}{I}\left\{\mu_0 + \mu_1 t + \sum_{i=1}^{N+2} \nu_i \, \mathrm{e}^{-\xi_i t}\right\} \tag{2-156}$$

where, using the identity (2-134) as necessary, the constants $\mu_0, \mu_1 \in \mathbb{R}$ and $\nu_i \in \mathbb{C} \forall i = 1, 2, \ldots, N+2$ are defined

$$\begin{aligned} \mu_0 &= \lim_{s\to 0}\left\{\frac{\mathrm{d}}{\mathrm{d}s}\left[s^2 \bar{\chi}_0(s)\right]\right\} \\ &= \frac{\sum_{i=1}^{N} \lambda_i - \sum_{i=1}^{N+2} \xi_i^{-1}}{\xi_{N+1}\xi_{N+2}\prod_{i=1}^{N} \xi_i \lambda_i} \end{aligned} \tag{2-157}$$

$$\begin{aligned} \mu_1 &= \lim_{s\to 0}\left\{s^2 \bar{\chi}_0(s)\right\} \\ &= \frac{1}{\xi_{N+1}\xi_{N+2}\prod_{i=1}^{N} \xi_i \lambda_i} \end{aligned} \tag{2-158}$$

$$\begin{aligned} \nu_i &= \lim_{s\to -\xi_i}\left\{(s+\xi_i)\bar{\chi}_0(s)\right\} \\ &= \frac{\prod_{i=1}^{N}(\lambda_i^{-1} - \xi_i)}{\xi_i^2 \prod_{j=1,i}^{N+2}(\xi_j - \xi_i)} \end{aligned} \tag{2-159}$$

Since $\chi_{rf}(0) = 0$, the coefficients must satisfy the property $\mu_0 = -\sum_{i=1}^{N+2} \nu_i$.

Case 2. $G_\infty = 0$: In the case of a viscoelastic fluid, the Laplace transform of the platen displacement is

$$\bar{\chi}_{sl}(s) = \frac{C_0 \Lambda_{1,N}(s)}{I s^3 \Lambda_{4,N+1}(s)} \tag{2-160}$$

where $\Lambda_{4,N+1}(s)$ is defined by (2-95) and is assumed to have $N+1$ distinct roots denoted by $\{-\xi_i\}_{i=1}^{N+1}$, so the solution of (2-160) will be of the general form

$$\chi_{sl}(t) = \frac{C_0}{I}\left\{\mu_0 + \mu_1 t + \mu_2 t^2 + \sum_{i=1}^{N+1} \nu_i' \, \mathrm{e}^{-\xi_i' t}\right\} \tag{2-161}$$

with constants $\mu_0, \mu_1, \mu_2 \in \mathbb{R}$ and $\nu_i' \in \mathbb{C} \forall i = 1, 2, \ldots, N+1$ defined

$$\begin{aligned}
\mu_0 &= \lim_{s\to 0} \{\bar{\chi}_0(s)\} \\
&= \frac{1}{2\xi_{N+1} \prod_{i=1}^{N} \lambda_i \xi_i} \left[\beta_1 - \beta_2 + 2\alpha_2 \left(\alpha_2 - \alpha_1\right)\right] && \text{(2-162)} \\
\mu_1 &= \lim_{s\to} \{\bar{\chi}_0(s)\} \\
&= \frac{\left[\sum_{i=1}^{N} \lambda_i - \sum_{i=1}^{N+1} (\xi_i')^{-1}\right]}{\xi_{N+1}' \prod_{i=1}^{N} \lambda_i \xi_i'} && \text{(2-163)} \\
\mu_2 &= \frac{1}{2!} \lim_{s\to 0} \left\{s^3 \bar{\chi}_0(s)\right\} \\
&= \frac{1}{2\xi_{N+1}' \prod_{i=1}^{N} \lambda_i \xi_i'} && \text{(2-164)} \\
\nu_i' &= \lim_{s\to -\xi_i'} \left\{(s + \xi_i') \bar{\chi}_0(s)\right\} \\
&= -\frac{\prod_{j=1}^{N} (\lambda_j^{-1} - \xi_i')}{(\xi_i')^3 \prod_{j=1,i}^{N+1} (\xi_j' - \xi_i')}, \quad i = 1, 2, \ldots, N+1. && \text{(2-165)}
\end{aligned}$$

where the additional constants are defined $\alpha_1 = \sum_{i=1}^{N} \lambda_i$, $\alpha_2 = \sum_{i=1}^{N+1} (\xi_i')^{-1}$, $\beta_1 = \alpha_1^2 - \sum_{i=1}^{N} \lambda_i^2$ and $\beta_2 = \alpha_2^2 - \sum_{i=1}^{N+1} (\xi_i')^{-2}$. Note that the identity (2-134) has been applied once to obtain μ_1 and twice to obtain μ_0. The initial condition imposed upon $\chi_{sl}(t)$ additionally implies that the constants satisfy the relation $\mu_0 = -\sum_{i=1}^{N+1} \nu_i'$. Figure 2.23 shows a plot of the response for a ramp function applied torque for a viscoelastic fluid with double Gaussian relaxations spectrum and parameters as given in Section 2.2.3.

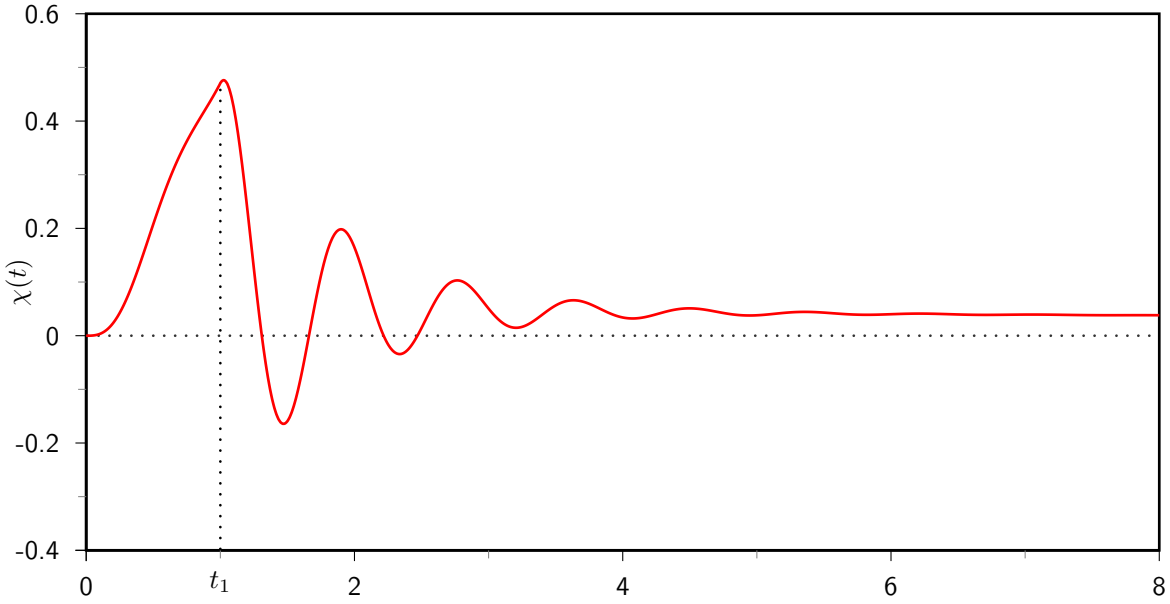

Figure 2.23: Platen displacement: ramp function, viscoelastic liquid, HW relaxation spectrum, $t_1 = 1$.

V. PERIODIC FUNCTIONS

Periodic functions can be handled using the periodicity theorem (A-15) for the Laplace transform. The general result for an arbitrary periodic function of period Ψ with n repetitions is

$$C(t) = \sum_{j=1}^{n} C_r(t - t_j)H(t - t_j), \quad t_j = (j-1)\Psi \tag{2-166}$$

and therefore

$$\begin{aligned} \bar{C}(s) &= \bar{C}_r(s) \sum_{j=1}^{n} \mathrm{e}^{-t_j s} \\ &= \frac{\bar{C}(s)\,\mathrm{e}^{-n\Psi s}}{1 - \mathrm{e}^{-\Psi s}} \end{aligned} \tag{2-167}$$

From (2-167), it can then be deduced that

$$\bar{\chi}(s) = \bar{\chi}_r(s) \sum_{j=1}^{n} \mathrm{e}^{-t_j s} \tag{2-168}$$

and in the time domain

$$\chi(t) = \sum_{j=1}^{n} \chi_r(t - t_j)H(t - t_j) \tag{2-169}$$

2.5.1 Sinusoidal

The standard method for obtaining viscoelastic data in the linear regime for estimation of the relaxation spectrum is to apply a sinusoidally varying stress profile of angular frequency ω, represented in complex notation by

$$C(t) = C_0 \, \mathrm{e}^{i\omega t} \qquad t \in [0, \infty), C_0 \in \mathbb{R} \tag{2-170}$$

The standard approach is to make use of the information that such a stimulus produces a response with a transient component which decays to leave an essentially steady state oscillatory response, also of frequency ω, as t tends to infinity. Thus, it is generally assumed that

$$\lim_{t\to\infty} \chi(t) = \tilde{\chi}(\omega) \, \mathrm{e}^{i\omega t} \qquad \tilde{\chi} \in \mathbb{C} \tag{2-171}$$

where $\tilde{\chi}$ is a complex constant depending on ω. An example of the steady state response is depicted in Figure 1.3.

Now consider the response of a stress-controlled rheometer to an applied stress of the form (2-170). Thus, we have

$$-I\omega^2 \tilde{\chi}(\omega) \, \mathrm{e}^{i\omega t} + k^{-1} \lim_{t\to\infty} \int_0^t G(t-t') i\omega \, \mathrm{e}^{i\omega t'} \, \mathrm{d}t' = C_0 \, \mathrm{e}^{i\omega t} \tag{2-172}$$

or, equivalently

$$-I\omega^2 \tilde{\chi}(\omega) \, \mathrm{e}^{i\omega t} + k^{-1} \lim_{t\to\infty} \int_0^t G(t') i\omega \, \mathrm{e}^{i\omega(t-t')} \, \mathrm{d}t' = C_0 \, \mathrm{e}^{i\omega t} \tag{2-173}$$

$$-I\omega^2 \tilde{\chi}(\omega) \, \mathrm{e}^{i\omega t} + k^{-1} i\omega \tilde{\chi}(\omega) \int_0^\infty G(t') \, \mathrm{e}^{-i\omega t'} \, \mathrm{d}t' = C_0 \, \mathrm{e}^{i\omega t} \tag{2-174}$$

The complex modulus $G^*(\omega)$ is defined in (1-54) and substituting this expression into (2-174), for this problem $G^*(\omega)$ takes the form

$$G^*(\omega) = k \left[\frac{C_0 + I\omega^2 \tilde{\chi}(\omega)}{\tilde{\chi}(\omega)} \right]. \tag{2-175}$$

Assuming a phase difference c between the input and response, (2-175) becomes

$$G^*(\omega) = k \left[\frac{C_0}{\chi_0} \, \mathrm{e}^{-ic} + I\omega^2 \right]. \tag{2-176}$$

However, despite the simplicity of the mathematics produced by ignoring the transient component of the response, this approach to obtaining the linear viscoelastic parameters is not without its disadvantages as noted in Section 1.1. Primarily, the time

required to obtain data at a single frequency is significantly increased if the response of the fluid is neglected until the transient has decayed sufficiently to be assumed negligible and a quasi-steady state has been reached, particularly for low frequencies.

The platen displacement is now simulated in an analogous manner to the previous sections concerning the delta, box and ramp functions, including the transient portion of the response in the analysis.

Maxwell model

For the Maxwell model, which has relaxation modulus with Laplace transform given by (2-46), and using the repetition theorem (2-168), the Laplace transform of the platen displacement is given by

$$\bar{\chi}(s) = \frac{C_0\omega_0\left[1 - \mathrm{e}^{-n\Psi s}\right]}{Is\left(s^2+\omega_0^2\right)\left[s + (kI)^{-1}\bar{G}(s)\right]} \tag{2-177}$$

where $\Psi = \frac{2\pi}{\omega_0}$. Defining $\chi_S(t)$ such that

$$\bar{\chi}(s) = \bar{\chi}_S(s)\left[1 - \mathrm{e}^{-n\Psi s}\right], \tag{2-178}$$

the platen displacement for n cycles of the sinusoidal torque of period Ψ can be expressed as

$$\chi(t) = \chi_S(t)H(t) - \chi_S(t - n\Psi)H(t - n\Psi). \tag{2-179}$$

Assuming $\xi_{1,2}$ are real and distinct and as defined in (2-65), the platen displacement will have the form

$$\chi_S(t) = \frac{C_0}{I}\left\{\gamma_0 + \gamma_1\,\mathrm{e}^{-i\omega t} + \gamma_1^*\,\mathrm{e}^{i\omega t} + \gamma_2\,\mathrm{e}^{-\xi_1 t} + \gamma_3\,\mathrm{e}^{-\xi_2 t}\right\} \tag{2-180}$$

where, defining $\chi_{S0}(t)$ such that $\chi_S(t) = \frac{C_0}{I}\chi_{S0}(t)$,

$$\gamma_0 = \lim_{s\to 0}\{s\bar{\chi}_{S0}\} = \frac{kI}{g\lambda\omega_0} \tag{2-181}$$

$$\gamma_1 = \lim_{s\to -i\omega}\{(s+i\omega)\bar{\chi}_{S0}(s)\} = -\frac{(1-i\omega\lambda)}{2\omega\lambda(\xi_1 - i\omega)(\xi_2 - i\omega)} \tag{2-182}$$

$$\gamma_2 = \lim_{s\to -\xi_1}\{(s+\xi_1)\bar{\chi}_{S0}(s)\} = \frac{\omega_0(\lambda\xi_1 - 1)}{\lambda\xi_1(\omega_0^2+\xi_1^2)(\xi_2 - \xi_1)} \tag{2-183}$$

$$\gamma_3 = \lim_{s\to -\xi_2}\{(s+\xi_2)\bar{\chi}_{S0}(s)\} = \frac{\omega_0(1 - \lambda\xi_2)}{\lambda\xi_2(\omega_0^2+\xi_2^2)(\xi_2 - \xi_1)}. \tag{2-184}$$

This can be expressed in the form

$$\chi_S(t) = \frac{C_0}{I}\left\{\gamma_0 + 2\,|\gamma_1|\sin(\omega_0 t + \phi_1) + \gamma_2\,\mathrm{e}^{-\xi_1 t} + \gamma_3\,\mathrm{e}^{-\xi_2 t}\right\} \tag{2-185}$$

where

$$\tan\phi_1 = \frac{\mathrm{Re}\{\gamma_1\}}{\mathrm{Im}\{\gamma_1\}}, \tag{2-186}$$

so it can be seen that the response consists of a sinusoidal portion out of phase with the applied waveform by ϕ_1 and a transient component expressed as a sum of exponentials, monotone decreasing in the case of real roots. If $\xi_{1,2}$ are complex and distinct, the platen displacement can be rewritten in the form

$$\chi_S(t) = \frac{C_0}{I}\left\{\gamma_0 + 2\left|\gamma_1\right|\sin(\omega_0 t + \phi_1) + 2\left|\gamma_2\right| \mathrm{e}^{-\frac{t}{2\lambda}\sin(\xi'' t + \phi_2}\right\} \tag{2-187}$$

where $\xi'' = \mathrm{Im}\{\gamma_2\}$ and

$$\tan\phi_2 = \frac{\mathrm{Re}\{\gamma_2\}}{\mathrm{Im}\{\gamma_2\}}. \tag{2-188}$$

The typical platen displacement response for a Maxwell fluid with complex roots is shown in Figure 2.24.

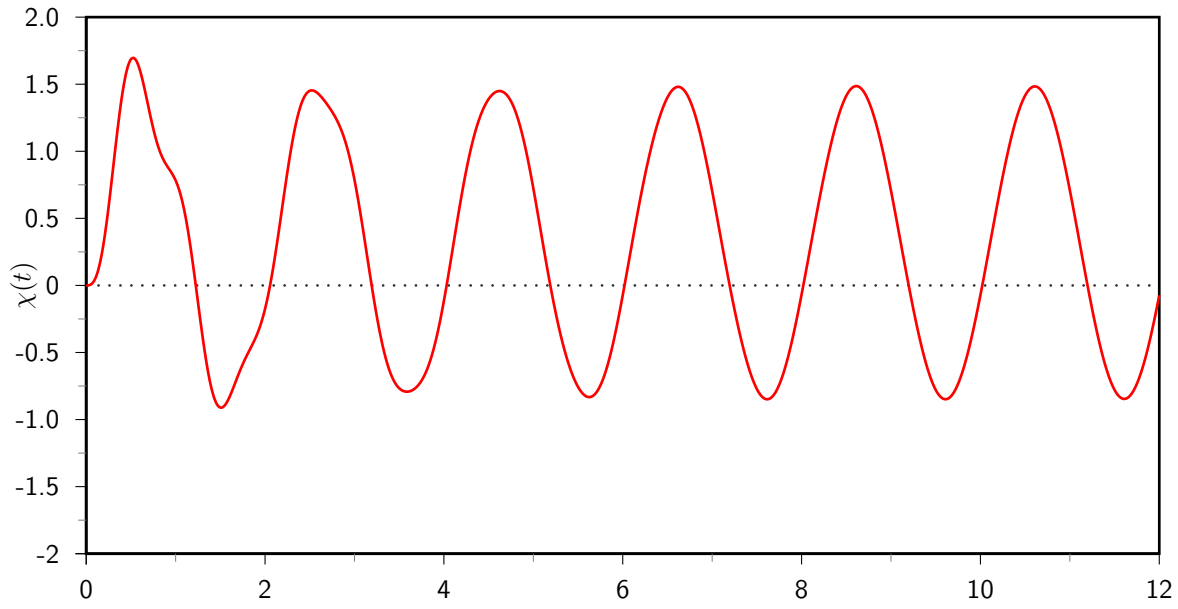

Figure 2.24: Platen displacement: sinusoidal waveform, Maxwell model, $\psi < 0$.

N-mode Maxwell model

The simulation for the N-mode Maxwell case is divided into two parts, depending upon the value of G_∞ which corresponds to viscoelastic solids and fluids, respectively.

Case 1. $G_\infty \neq 0$: For a viscoelastic solid, the Laplace transform of the platen displacement takes the form

$$\bar{\chi}_S(s) = \frac{C_0\omega_0\Lambda_{1,N}(s)}{(s^2+\omega_0^2)\Lambda_{3,N+2}(s)}, \tag{2-189}$$

where $\Lambda_{1,N}(s)$ and $\Lambda_{3,N+2}(s)$ are defined as for (2-87) and (2-90), respectively. In the t-space, this corresponds to

$$\chi_S(t) - \frac{C_0}{I}\left\{2\,|\mu_1|\sin(\omega_0 t+\phi_1) + \sum_{k=1}^{N+2}\nu_k\,\mathrm{e}^{-\xi_k t}\right\} \tag{2-190}$$

with constants are defined

$$\begin{aligned}
\mu_1 &= \lim_{s\to i\omega_0}\{(s-i\omega_0)\bar{\chi}_{S0}(s)\} \\
&= -\frac{i\prod_{j=1}^{N}(i\omega_0+\lambda_j^{-1})}{2\prod_{j=1}^{N+2}(i\omega_0+\xi_j)} \qquad (2\text{-}191)\\
\nu_k &= \lim_{s\to-\xi_k}\{(s+\xi_k)\bar{\chi}_{S0}(s)\} \\
&= \frac{\omega_0\prod_{j=1}^{N}(\lambda_j^{-1}-\xi_k)}{(\omega_0^2+\xi_k^2)\prod_{j=1,k}^{N+2}(\xi_j-\xi_k)}, \quad k=1,\ldots,N+2 \qquad (2\text{-}192)\\
\tan\phi_1 &= \frac{\mathrm{Re}\,\{\mu_1\}}{\mathrm{Im}\,\{\mu_1\}} \qquad (2\text{-}193)
\end{aligned}$$

The response of a viscoelastic solid with relaxation spectrum prescribed according to the double Gaussian spectrum in (2-103) is plotted in Figure 2.25 with parameters as specified in Section 2.2.3.

Case 2. $G_\infty \neq 0$: The viscoelastic fluid is similarly obtained, the Laplace transform of the platen displacement being given by

$$\bar{\chi}_S(s) = \frac{C_0\Lambda_{1,N}(s)}{Is(s^2+\omega_0^2)\Lambda_{4,N+1}(s)} \tag{2-194}$$

where $\Lambda_{1,N}(s)$ and $\Lambda_{4,N+1}(s)$ are defined as for (2-87) and (2-95), respectively. The platen displacement observed would therefore be

$$\chi_S(t) = \frac{C_0}{I}\left\{\mu_0 + 2\,|\mu_1|\sin(\omega_0 t+\phi_1) + \sum_{k=1}^{N+1}\nu_k\,\mathrm{e}^{-\xi_k t}\right\} \tag{2-195}$$

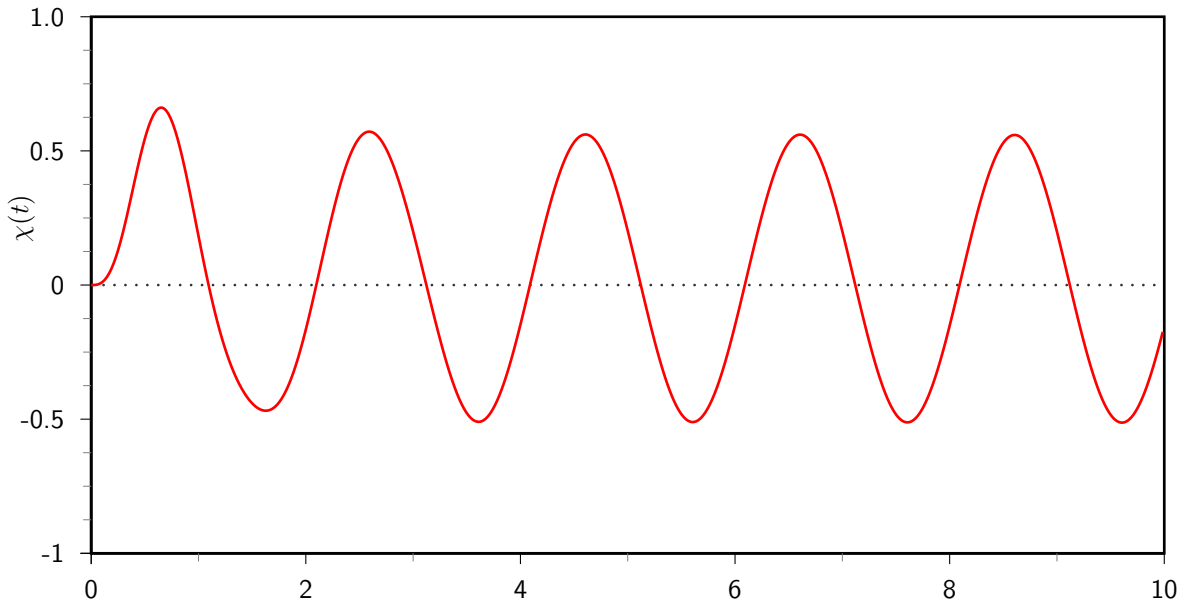

Figure 2.25: Platen displacement: sinusoidal waveform, viscoelastic solid, HW relaxation spectrum.

in terms of the constants defined

$$\mu_0 = \lim_{s\to 0}\{s\bar{\chi}_{S0}(s)\} = \frac{1}{\omega_0\xi_{N+1}\prod_{j=1}^{N}\lambda_j\xi_j} \tag{2-196}$$

$$\mu_1 = \lim_{s\to i\omega_0}\{(s-i\omega-0)\bar{\chi}_{S0}(s)\} = -\frac{\prod_{j=1}^{N}(\lambda_j+i\omega_0)}{2\omega_0\prod_{j=1}^{N+1}(\xi_j+i\omega_0)} \tag{2-197}$$

$$\nu_k = \lim_{s\to -\xi_k}\{(s+\xi_k)\bar{\chi}_{S0}(s)\} = -\frac{\omega_0\prod_{j=1}^{N}}{\xi_k(\xi_k^2+\omega_0^2)\prod_{j=1,k}^{N+1}(\xi_j-\xi_k)} \tag{2-198}$$

$$\tan\phi_1 = \frac{\mathrm{Re}\{\mu_1\}}{\mathrm{Im}\{\mu_1\}}. \tag{2-199}$$

The response of a viscoelastic solid with relaxation spectrum prescribed according to the double Gaussian spectrum in (2-103) is plotted in Figure 2.26 with parameters as specified in Section 2.2.3.

The results from Section 2.2-Section 2.4 can be used to construct the response for certain periodic functions in terms of the response of those functions. Note that experimental interpretation is more appropriate in terms of a frequency-based analysis - FTMS (see Section 1.1), whereby the complex modulus is obtained. However, a steady-state is assumed, which requires several cycles to be applied before measurement can take place. Here, the output is simulated taking into account the transient compo-

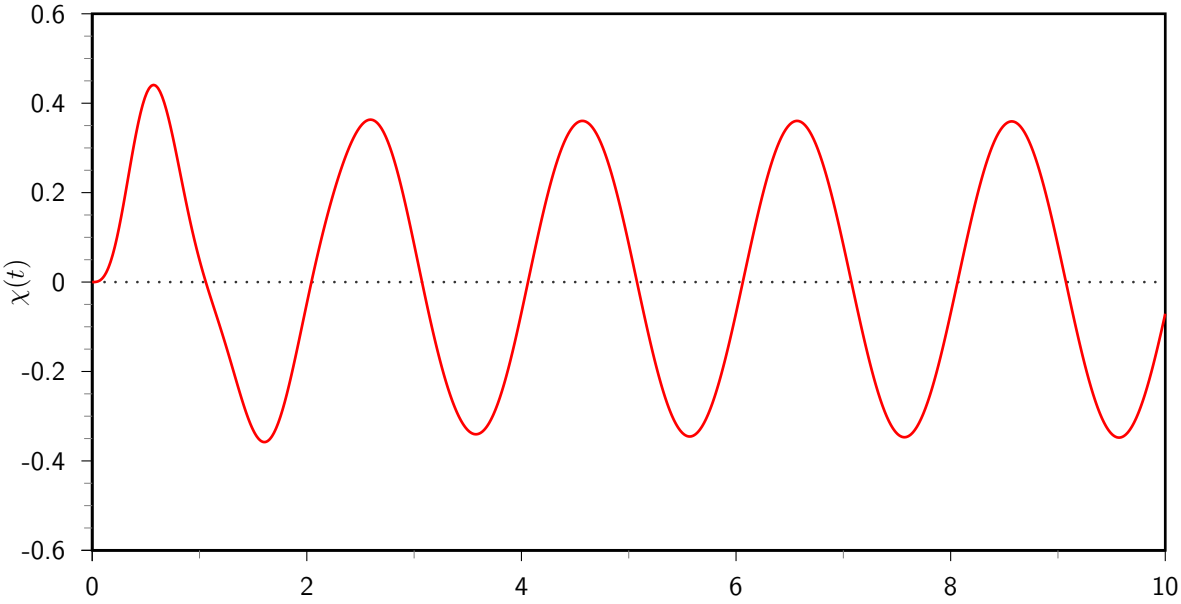

Figure 2.26: Platen displacement: sinusoidal waveform, viscoelastic liquid, HW relaxation spectrum.

nent of the response which any experimental scheme concerned with obtaining data as rapidly as possible should take into account.

1. Multi-frequency waveform: The rationale for combining several sinusoidal waveforms of different frequencies is readily apparent in the frequency domain, whereby the complex modulus can be determined accurately by steady-state theory at several frequencies simultaneously, as considered in [35]. The displacement response when subjected to an applied torque of this form is simply the sum of the responses which would be observed for each of the component frequencies, due to the underlying linear assumption. A typical displacement curve for a multiple frequency sinusoidal applied torque is shown in Figure 2.27 for an N-mode Maxwell fluid with parameters as for Section 2.2.3 and equally weighted component frequencies of 1,2 and 3 rad s^{-1}.

2. Delta function sequence: The absolute values of the displacement decreases rapidly for an applied torque in the form of a delta function, so an obvious extension would be to apply a sequence of delta functions, spaced at a period of Ψ with an initial impulse at $t = t_0$. The torque would take the form

$$C(t) = C_\delta \sum_{j=0}^{n-1} (-1)^j \delta(t - t_j), \quad t_j = t_0 + j\Psi < T \tag{2-200}$$

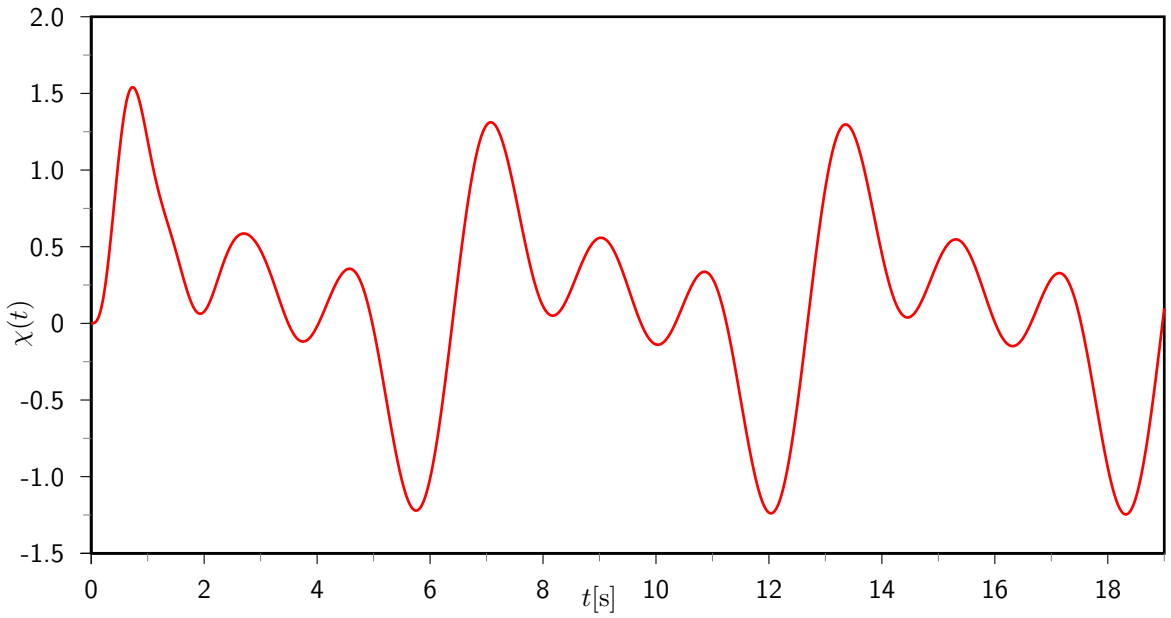

Figure 2.27: Platen displacement: multi-frequency sine wave, viscoelastic liquid, double Gaussian spectrum of Honerkamp & Weese.

and the corresponding displacement, by the linearity assumption, would be the sum of the displacements associated with each of the individual delta functions, viz.

$$\chi(t) = \sum_{j=0}^{n-1} (-1)^j \chi_\delta(t - t_j) H(t - t_j). \tag{2-201}$$

A typical displacement curve for an N-mode Maxwell fluid with parameters as for Section 2.2.3 is shown in Figure 2.28.

3. Square wave: A periodic function based on the box functions is the square wave, with period Ψ, and involves n repetitions of the base function, which is a single cycle of the waveform. The applied torque function is depicted in Figure 2.29.

The applied torque has the form

$$C(t) = C_0 \left[H(t) + H(t - n\Psi) + 2 \sum_{j=1}^{2n-1} (-1)^j H(t - \tfrac{1}{2} j\Psi) \right] \tag{2-202}$$

and using the repetition theorem for the Laplace transform (A-15), the Laplace transform of the platen displacement is

$$\bar{\chi}(s) = \bar{\chi}_{sf}(s) \left[1 + \mathrm{e}^{-n\Psi s} + 2 \sum_{j=1}^{2n-1} (-1)^j \, \mathrm{e}^{-\frac{1}{2} j\Psi s} \right], \tag{2-203}$$

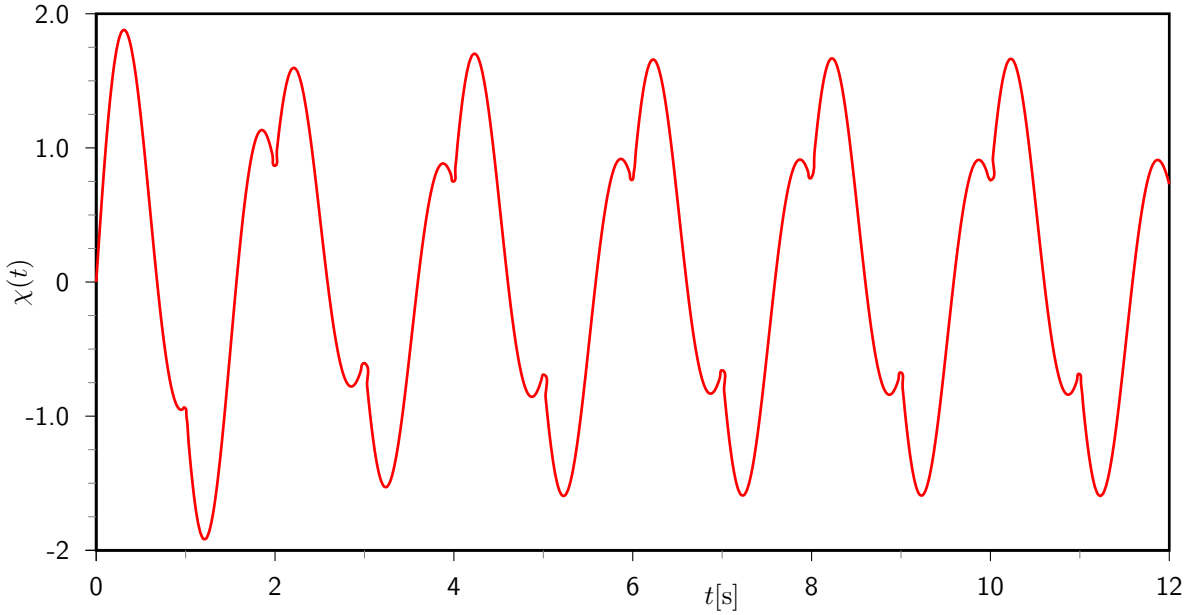

Figure 2.28: Platen displacement: sequence of delta functions, viscoelastic liquid, HW relaxation spectrum.

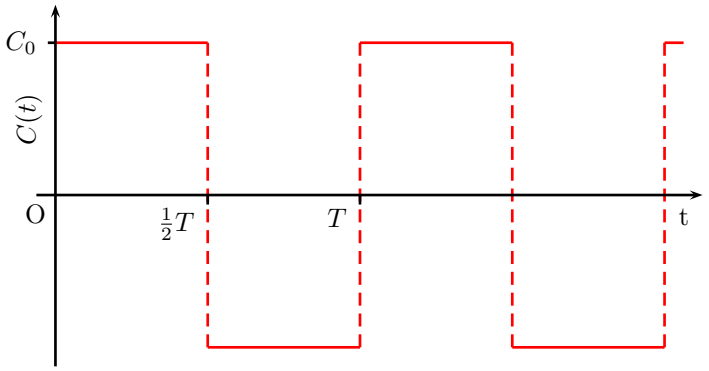

Figure 2.29: Square waveform.

which corresponds in the time domain to the displacement

$$\chi(t) = \chi_{sf}(t)H(t) + \chi_{sf}(t - n\Psi)H(t - n\Psi) + 2\sum_{j=1}^{2n-1}(-1)^j\chi_{sf}(t - \tfrac{1}{2}j\Psi)H(t - \tfrac{1}{2}j\Psi) \tag{2-204}$$

in terms of the displacement for the step function described in Section 2.3. A typical example of the response is shown in Figure 2.30 for an N-mode Maxwell fluid with parameters as in Section 2.2.3.

4. Box function sequence: Another variation on the theme of the box function is an applied torque composed of a sequence of box functions, for which the torque would

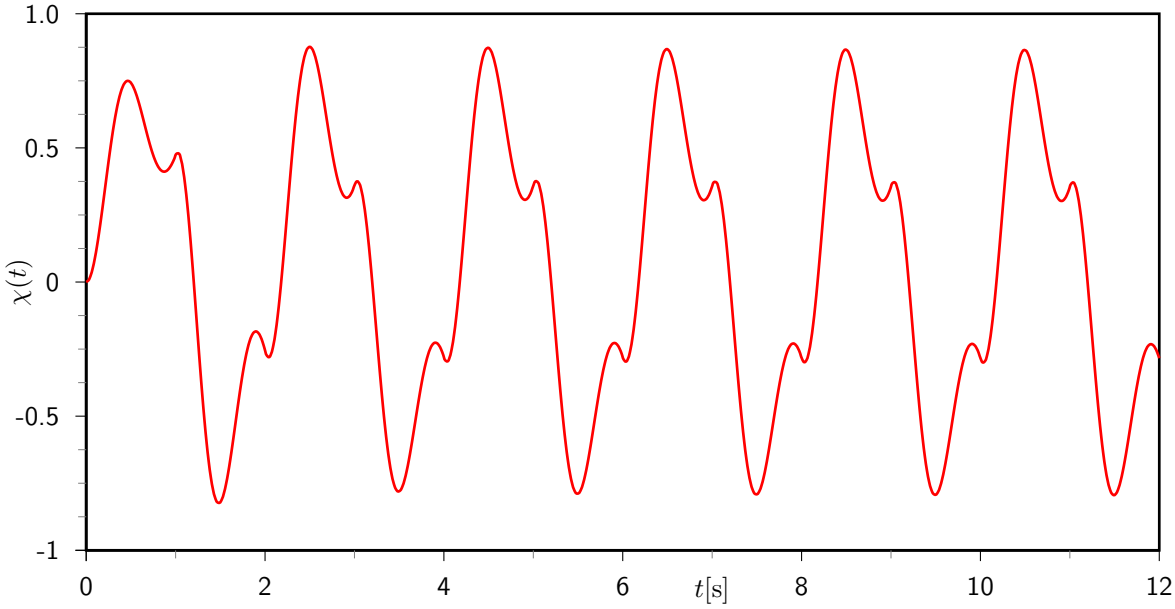

Figure 2.30: Platen displacement: square waveform, viscoelastic liquid, HW relaxation spectrum.

be given by

$$C(t) = C_0 \sum_{j=0}^{n} \left[H(t - j\Psi) - H(t - \tfrac{1}{2}(2j+1))\Psi \right] \tag{2-205}$$

and hence the Laplace transform of the displacement would be

$$\bar{\chi}(s) = \chi_{sf}(s) \left[1 - \tfrac{1}{2} \mathrm{e}^{-\frac{1}{2}\Psi s} \right] \sum_{j=0}^{n} \mathrm{e}^{-j\Psi s}. \tag{2-206}$$

The platen displacement is therefore of the form

$$\chi(t) = \sum_{j=0}^{n} \left[\chi_{sf}(t - j\Psi) H(t - j\Psi) - \chi_{sf}(t - \tfrac{1}{2}(2j+1)\Psi) H(t - \tfrac{1}{2}(2j+1)\Psi) \right]. \tag{2-207}$$

5. Ramp function sequence: A variety of periodic functions for the applied torque can be constructed using the ramp function in Section 2.4. The simplest example is a sequence of ramp functions and the equation for the applied torque in this case is given by

$$C(t) = C_0 \sum_{j=1}^{n} \left\{ (t - (j-1)\Psi) \left[H(t - (j-1)\Psi) - H(t - j\Psi) \right] \right\}. \tag{2-208}$$

The displacement, using the repetition theorem, has Laplace transform

$$\bar{\chi}(s) = \left\{ \bar{\chi}_{sl}(s) \sum_{j=1}^{n} \left[\mathrm{e}^{-(j-1)\Psi s} - \mathrm{e}^{-j\Psi s} \right] - \Psi \bar{\chi}_{sf}(s) \sum_{j=1}^{n} \mathrm{e}^{-j\Psi s} \right\} \tag{2-209}$$

and therefore the platen displacement is

$$\chi(t) = \sum_{j=1}^{n} \left\{ \chi_{sl}(t-(j-1)\Psi) H(t-(j-1)\Psi) - \left[\chi_{sl}(t-j\Psi) + \Psi \chi_{sf}(t-j\Psi) \right] H(t-j\Psi) \right\}. \tag{2-210}$$

Other examples of applied torque functions which can be derived from the slope and step functions are the sawtooth and triangular waves.

CHAPTER 3

General Properties of the Response

This chapter is concerned with the properties of the governing equation in terms of the Laplace transform formulation. The effect of step discontinuities in the platen angular displacement and its derivatives is investigated first. It is demonstrated that it is not possible to apply a physically reproducible torque such that the platen displacement exhibits a step change, however it is possible to induce the angular velocity of the platen to display a step discontinuity, provided the use of the delta function as an applied torque is allowed. Subsequent derivatives of the platen angular displacement can be easily attained using well-behaved functions alone. The motivation for these results is to determine whether it is possible to obtain the relaxation modulus directly from experiment, requiring the minimum of data processing. It then follows that it is only possible to obtain the relaxation modulus as the first and higher-order derivatives of the platen angular displacement, requiring at least one degree of differentiation. Although this may not be the optimal form for the applied torque in terms of the criteria in Chapter 3, it nonetheless represents a desirable form for the output displacement in terms of the amount of data processing which is necessary. This is an example of an adaptive torque profile, whereby the data already obtained is used to improve the accuracy of the data to be acquired during the remainder of the experiment. A more general analysis is made of the case where the relaxation modulus and the displacement *or* velocity of the platen are represented by finite Dirichlet series and it is observed that the torque which must be applied to produce this response consists of a Dirichlet series also, but with an extra term involving a generalized function. Finally, the distribution and relationship between the poles of the torque, displacement and relaxation modulus is investigated, based on the assumption that the Laplace transforms of these three functions are represented by rational functions.

I. OBTAINING G DIRECTLY

An approach to determining an optimal form for the applied torque $C(t)$ is to decide what the most desirable function the displacement should be to provide the most information about the viscoelastic fluid under investigation or in the simplest form which requires a minimum amount of manipulation to obtain the necessary linear viscoelastic functions which characterize the material. Working in the time domain, it is clear that a truly optimal form for the output signal under this criterion would be the relaxation modulus itself, $G(t)$, whence the data could be used in its raw format and absolutely no numerical differentiation or other forms of manipulation are required. The question

which must be posed is whether it is possible to apply a torque such that the platen displacement is of this form, however first it is necessary to analyze the response of the system with respect to discontinuities in $C(t)$, $\chi(t)$ and higher order derivatives of $\chi(t)$. The most desirable output from the system would be for $\chi(t)$ to be a scalar multiple of the relaxation modulus, followed by the corresponding situation for $\dot{\chi}(t)$, since it will be required to perform numerical differentiation on the data, which is an ill-posed process. The concept of ill-posedness will be elaborated upon in the following chapter.

3.1.1 Effect of step discontinuities

It has already been demonstrated in Chapter 1 that it is possible to apply a torque $C(t)$ which possesses a step discontinuity through the analysis of the response of the system to a stimulus in the form of a box function. It was seen that the response of the system is a continuously differentiable function, i.e. $\chi(t) \in C^1[0,T]$. The case where a discontinuity exists in $\chi(t)$ needs to be handled more delicately. The Laplace transform formulation of the problem

$$\bar{C}(s) = I\left[s^2\bar{\chi}(s) - s\chi(0) - \dot{\chi}(0)\right] + k^{-1}\left\{\bar{G}(s)\left[s\bar{\chi}(s) - \chi(0)\right]\right\} \tag{3-1}$$

is insufficient to model the response where the displacement, $\chi(t)$, or any of the higher order derivatives thereof, exhibits a step discontinuity at $t = 0$. The reason for this is the presence of the terms $\chi(0)$ and $\dot{\chi}(0)$ which arise from the Laplace transforms of the derivatives of $\chi(t)$ and are undefined for the case where the discontinuity coincides with the origin. This problem can be circumvented by translating the function along the time axis in a positive direction by a quantity $\alpha > 0$, wherefore the values of $\chi(0)$ and $\dot{\chi}(0)$ are both zero. The case where the discontinuity occurs at $t = 0$ may then be inferred by taking the limit as $\alpha \to 0$. The Laplace transform of the applied stress thus becomes

$$\bar{C}(s) = \bar{\chi}(s)\left[Is^2 + k^{-1}s\bar{G}(s)\right]. \tag{3-2}$$

Discontinuity in $\chi(t)$

First, consider the torque required to produce a displacement with discontinuity located at $t = \alpha$. To represent such a function, define $\chi(t) = H(t-\alpha)\psi(t-\alpha)$ for $\alpha > 0$, where $H(t-\alpha)$ is the Heaviside step function and $\psi(t) \in C^\infty(0,\infty)$ is a continuously differentiable function. The function $\chi(t)$ has a step discontinuity at $t = \alpha$, provided that $\psi(\alpha) \neq 0$. For simplicity in the analysis, consider the case first where

$\psi(t) \equiv 1 \, \forall t \geq 0$. Therefore, we have

$$\bar{\chi}(s) = \frac{1}{s} \mathrm{e}^{-\alpha s} \tag{3-3}$$

and the Laplace transform of the torque becomes

$$\bar{C}(s) = \mathrm{e}^{-\alpha s} \left[Is + k^{-1} \bar{G}(s) \right] \tag{3-4}$$

and inversion yields

$$H(t+\alpha) C(t+\alpha) = I\delta'(t) + k^{-1} G(t) \tag{3-5}$$

or, equivalently

$$C(t) = \left[I\delta'(t-\alpha) + k^{-1} G(t-\alpha) \right] H(t-\alpha), \qquad t \in [0, T]. \tag{3-6}$$

where $\delta'(t)$ denotes the first-order derivative of the delta function, in the sense of distribution. This however has no physical significance and cannot be reproduced experimentally. In the case where $\psi(t)$ is completely arbitrary, provided that the constraint $|\psi(0)| > 0$ is satisfied, the real-valued shift theorem in (A-10) states that $\bar{\chi}(s) = \mathrm{e}^{-\alpha s} \bar{\psi}(s)$ and hence

$$\bar{C}(s) = \mathrm{e}^{-\alpha s} \left[Is^2 \bar{\psi}(s) + k^{-1} s \bar{\psi}(s) \bar{G}(s) \right]. \tag{3-7}$$

Since $\psi(0) \neq 0$, we can write $\psi = \psi(0) + \psi_1(t)$, where $\psi_1(0) = 0$. Thus,

$$\begin{aligned} s^2 \bar{\psi} &= \psi(0) s + s^2 \bar{\psi}_1(s) \\ &= \psi(0) s + \mathscr{L} \left\{ \ddot{\psi}_1 \right\}(s) + \dot{\psi}_1(0) s \end{aligned} \tag{3-8}$$

and noting that the inverse Laplace transform of the latter term on the RHS of equation (3-7) is the convolution of $G(t)$ and $\dot{\psi}(t)$, the applied torque necessary to produce a jump in the platen displacement has the form

$$C(t) = \left\{ I \left[(\psi(0) + \dot{\psi}_1(0)) \, \delta'(t-\alpha) + \ddot{\psi}_1(t-\alpha) \right] - G * \dot{\psi} \right\} H(t-\alpha). \tag{3-9}$$

This demonstrates that $C(t)$ always contains a term containing the unphysical first derivative of the delta function, therefore it is concluded that it is not possible to construct a practical experiment where the output displacement has a step discontinuity. It can be seen however, that taking the limit $I \to 0$ in (3-9) removes the unphysical term $\delta'(t)$, although such an assumption cannot be realized experimentally.

Discontinuity in $\dot{\chi}(t)$

Now consider the effect of a step discontinuity in the first derivative of the displacement $\chi(t)$ at $t = \alpha$, $\alpha > 0$ represented again by the function $\dot{\chi}(t) = H(t-\alpha)\psi(t-\alpha)$. For $\psi(t) \equiv 1\,\forall t \geq 0$, the Laplace transform is

$$s\bar{\chi}(s) = \frac{1}{s}\,\mathrm{e}^{-\alpha s} \tag{3-10}$$

then

$$\bar{C}(s) = \mathrm{e}^{-\alpha s}\left[I + k^{-1}s^{-1}\bar{G}(s)\right] \tag{3-11}$$

which upon inversion yields

$$H(t+\alpha)C(t+\alpha) = I\delta(t) + k^{-1}\int_0^t G(t')\,\mathrm{d}t' \tag{3-12}$$

or equivalently

$$C(t) = \left[I\delta(t-\alpha) + k^{-1}\int_0^{t-\alpha} G(t')\,\mathrm{d}t'\right]H(t-\alpha), \qquad t \in [0,T]. \tag{3-13}$$

For a general function $\psi(t)$, subject to the initial condition $\psi(0) \neq 0$, $\dot{\chi}(t)$ has Laplace transform

$$\mathscr{L}\{\dot{\chi}(t)\} = s\bar{\chi}(s) = \mathrm{e}^{-\alpha s}\bar{\psi}(s) \tag{3-14}$$

and the torque required has Laplace transform

$$\bar{C}(s) = \mathrm{e}^{-\alpha s}\left[Is\bar{\psi} + k^{-1}\bar{G}\bar{\psi}\right]. \tag{3-15}$$

Again, writing $\psi(t) = \psi(0) + \psi_1(t)$, or equivalently $s\bar{\psi} = \psi(0) + s\bar{\psi}_1(s)$, the torque is thus given by

$$C(t) = \left\{I\left[\psi(0)\delta(t-\alpha) + \dot{\psi}_1(t-\alpha)\right] + k^{-1}G(t) * \psi(t)\right\}H(t-\alpha) \tag{3-16}$$

This result demonstrates that is perfectly feasible to obtain a discontinuity in the derivative of $\chi(t)$ experimentally, provided the use of the delta-function as an applied torque is allowed. Again, taking the limit $I \to 0$ removes the generalized function term, and since $G(t)$ and $\psi(t)$ have physical forms, then so will the convolution term.

General result

Now it is possible to generalize the former results to a discontinuity in the nth-order derivative of $\chi(t)$ by considering $\chi^{(n)}(t) = H(t-\alpha)\psi(t-\alpha)$, $\alpha > 0$, $n \in \mathbb{N}$. This has Laplace transform satisfying

$$s^n \bar{\chi}(s) = \mathrm{e}^{-\alpha s}\bar{\psi}(s) \tag{3-17}$$

and the general form for the Laplace transform of $C(t)$ becomes

$$\bar{C}(s) = \mathrm{e}^{-\alpha s}\left\{ I\left[\psi_0 s^{-(n-1)} + s^{-(n-2)}\bar{\psi}_1(s)\right] + k^{-1}\bar{\psi}(s)s^{-(n-1)}\bar{G}(s)\right\}, \tag{3-18}$$

which is valid for $n = 0, 1, 2, \ldots$. For $n > 2$ this corresponds in the time domain to

$$C(t) = \left\{\left[\frac{\psi_0(t-\alpha)^{n-2}}{(n-2)!} + \psi_2(t-\alpha)\right] + k^{-1}\psi * G_1(t-\alpha)\right\} H(t-\alpha), \qquad n \geq 2, \tag{3-19}$$

where $\psi_2(t) = \mathscr{L}^{-1}\left\{s^{-(n-2)}\bar{\psi}_1(s)\right\}$ and $G_1(t) = \mathscr{L}^{-1}\left\{s^{-(n-1)}\bar{G}(s)\right\}$. $G_1(t)$ is obtained by integrating $G(t)$ $(n-1)$ times for $n \geq 2$, while $\psi_2(t)$ is obtained by integrating $\psi_1(t)$ $(n-2)$-times, hence there are no terms containing the delta function or derivatives thereof, and therefore (3-19) represents a physical form for the applied torque.

3.1.2 Relationship between $\chi(t)$ and $G(t)$

Having established the foregoing results concerning discontinuities in $\chi(t)$ and its derivatives, we now proceed to consider the case where $\psi(t)$ has a specific and useful form and present the following two theorems.

Theorem 3.1.1: There is no physical form for the applied torque, $C(t)$, such that the displacement, $\chi(t)$, is equal to the relaxation modulus, $G(t)$.

Proof. To verify this proposition, it is necessary to make use of the results in Section 3.1.1, with the additional assumption that $\psi(t) := G(t)$, $t \in [0, T]$, where $G(t)$ is the relaxation modulus. The displacement is therefore $\chi(t) = H(t-\alpha)G(t-\alpha)$ for $t \in [0, T]$ and has Laplace transform

$$\bar{\chi}(s) = \mathrm{e}^{-\alpha s}\bar{G}(s) \tag{3-20}$$

Since $\chi(0) = \dot{\chi}(0) = 0$, (2-42) gives the expression which we require to determine the applied torque, $C(t)$, which corresponds to the platen displacement with Laplace transform as given by (3-20). In Laplace space, the required function takes the form

$$\bar{C}(s) = \mathrm{e}^{-\alpha s}\left[Is^2\bar{G}(s) + k^{-1}s\left\{\bar{G}\right\}^2\right]. \tag{3-21}$$

The invertibility of (3-21) is dependent upon the form of the relaxation modulus. Making use of the identity for the derivative of the Laplace transform, it is seen that

$$s^2\bar{G}(s) = \mathscr{L}\left\{\ddot{G}(t)\right\}(s) + sG(0) + \dot{G}(0) \tag{3-22}$$

and hence

$$\mathscr{L}^{-1}\left\{s^2\bar{G}(s)\right\}(t) = \ddot{G}(t) + G(0)\delta'(t) + \dot{G}(0)\delta(t). \tag{3-23}$$

Also, note that

$$\begin{aligned}\mathscr{L}^{-1}\left\{s\left\{\bar{G}\right\}^2\right\}(t) &= G(t) * \left(\dot{G}(t) + G(0)\delta(t)\right)\\ &= G(t) * \dot{G}(t) + G(0)G(t) * \delta(t)\\ &= G(t) * \dot{G}(t) + G(0)G(t),\end{aligned} \tag{3-24}$$

hence inversion of (3-21) gives

$$\begin{aligned}C(t) = \{I\left[\dot{G}(t-\alpha) + G(0)\delta'(t-\alpha) + \ddot{G}(t-\alpha)\delta(t-\alpha)\right]\\ +k^{-1}\left(G * \dot{G} + G(0)G(t-\alpha)\right)\}H(t-\alpha).\end{aligned} \tag{3-25}$$

The expression for $C(t)$ contains the first derivative of the delta-function, $\delta'(t)$ and hence cannot be reproduced experimentally and is thus unphysical, which is consistent with the general result in (3-9). □

Theorem 3.1.2: It is possible to apply a torque, $C(t)$, such that the first derivative of the displacement, $\dot{\chi}(t)$ is equal to the relaxation modulus, $G(t)$.

Proof. Proceeding in an analogous manner, with $\dot{\chi}(t) = H(t-\alpha)G(t-\alpha)$, $t \in [0,T]$ and corresponding Laplace transform

$$s\bar{\chi}(s) = \mathrm{e}^{-\alpha s}\bar{G}(s), \tag{3-26}$$

the Laplace transform of the applied torque $C(t)$ in this case has the form

$$\bar{C}(s) = \mathrm{e}^{-\alpha s}\left[Is\bar{G}(s) + k^{-1}\left\{\bar{G}(s)\right\}^2\right]. \tag{3-27}$$

Again, noting that

$$\mathscr{L}^{-1}\left\{s\bar{G}(s)\right\}(t) = \dot{G}(t) + G(0)\delta(t) \tag{3-28}$$

and

$$\mathscr{L}^{-1}\left\{(\bar{G})^2\right\} = G * G \tag{3-29}$$

it follows that the inverse Laplace transform of (3-27) yields

$$C(t) = H(t-\alpha)\left\{I\left[\dot{G}(t) + G(0)\delta(t)\right] + k^{-1}\Gamma(t-\alpha)\right\}, \qquad t \in [0,T] \tag{3-30}$$

where

$$\begin{aligned}\Gamma(t) &= \mathscr{L}^{-1}\left\{[\bar{G}]^2\right\} \\ &= G(t) * G(t).\end{aligned} \tag{3-31}$$

Since $G(0) \neq 0$, by the final value theorem for the Laplace transform $\lim_{s\to\infty} s\bar{G}(s) = G(0)$, or equivalently $s\bar{G}(s) = \mathcal{O}(1)$ as $s \to \infty$. This implies that $\bar{G}(s) = \mathcal{O}(s^{-1})$ as $s \to \infty$ and consequently that $\bar{\Gamma}(s) = [\bar{G}(s)]^2 = \mathcal{O}(s^{-2})$ as $s \to \infty$. This corresponds to the result that $\Gamma(t) = \mathcal{O}(t)$ as $t \to \infty$ in the time domain and also verifies that the inverse Laplace transform of $\bar{\Gamma}$ is a physically realistic function. Provided the use of the delta function is allowed in an experimental context, it is concluded that it is possible to apply a torque of the form (3-30) such that $\dot{\chi} = G(t)$ is satisfied. □

Now an example is provided assuming the material is modelled by a discrete relaxation spectrum $\{g_i, \lambda_i\}$. For general N-mode case, we have

$$\bar{\Gamma}(s) = [\bar{G}(s)]^2 = \frac{\left[\sum_{i=1}^{N} g_i \prod_{j=1,i}^{N}\left(s+\lambda_j^{-1}\right)\right]^2}{\prod_{i=1}^{N}\left(s+\lambda_i^{-1}\right)^2} \tag{3-32}$$

which has poles of order 2 located at $s = \{-\lambda_i^{-1}\}_{i=1}^{N}$ and therefore by the residue theorem the inverse Laplace transform can be expressed as

$$\Gamma(t) = \sum_{i=1}^{N}(\alpha_i + \beta_i t)\,\mathrm{e}^{-\frac{t}{\lambda_i}}. \tag{3-33}$$

Armed with the further information that

$$\dot{G}(t) = -\sum_{i=1}^{N}\frac{g_i}{\lambda_i}\mathrm{e}^{-\frac{t}{\lambda_i}} \tag{3-34}$$

it can be stated that the applied torque necessary to produce $\dot{\chi}(t) = G(t-\alpha)$ is

$$C(t) = H(t-\alpha)\left\{IG(0)\delta(t-\alpha) + \sum_{i=1}^{N}\left[k^{-1}\left(\alpha_i + \beta_i(t-\alpha)\right) - \frac{Ig_i}{\lambda_i}\right]\mathrm{e}^{-\frac{t-\alpha}{\lambda_i}}\right\} \tag{3-35}$$

where the constants $\alpha_i, \beta_i \in \mathbb{R}$ are defined

$$\alpha_i = \lim_{s\to-\frac{1}{\lambda_i}}\left\{\frac{\mathrm{d}}{\mathrm{d}s}\left[\left(s+\lambda_i^{-1}\right)^2\bar{\Gamma}(s)\right]\right\} \tag{3-36a}$$

$$\beta_i = \lim_{s\to-\frac{1}{\lambda_i}}\left\{\left(s+\lambda_i^{-1}\right)^2\bar{\Gamma}(s)\right\}. \tag{3-36b}$$

In the case where $N = 1$, with parameters $\{g, \lambda\}$, the solution can be obtained explicitly without difficulty.

$$C(t) = H(t-\alpha)\left\{Ig\delta(t-\alpha) + \left[k^{-1}g(t-\alpha) - \frac{Ig}{\lambda}\right] \mathrm{e}^{-\frac{(t-\alpha)}{\lambda}}\right\}, \qquad t \in [0, T]. \quad (3\text{-}37)$$

The motivation for obtaining $G(t)$ directly is that since the equation can be solved up to the current time t, perhaps in near real-time, an estimation of the relaxation modulus could then be used in an iterative manner to obtain the solution to greater accuracy than would otherwise be possible. There is scope for more investigation into this concept.

Theorem 3.1.3: It is possible to apply a torque, $C(t)$, such that the displacement, $\dot{\chi}(t)$, is equal to the creep compliance, $J(t)$, in the case where the material under investigation is a viscoelastic fluid, but not for a viscoelastic solid.

Proof. Let $\chi(t) = H(t-\alpha)J(t-\alpha)$, so that $\bar{\chi}(s) = \mathrm{e}^{-\alpha t}\bar{J}(s)$ and from (2-43) the applied necessary torque has Laplace transform

$$\begin{aligned}\bar{C}(s) &= \frac{\bar{\chi}\left[1 + kIs^3\bar{J}(s)\right]}{ks\bar{J}} \\ &= \mathrm{e}^{-\alpha t}\left[ks^{-1} + Is^2\bar{J}(s)\right]. \end{aligned} \quad (3\text{-}38)$$

Using the second order derivative identity for the Laplace transform, note that

$$s^2\bar{J}(s) = \mathscr{L}\left\{\ddot{J}(t)\right\} + sJ(0) + \dot{J}(0) \quad (3\text{-}39)$$

and inversion of (3-38) yields

$$C(t) = H(t-\alpha)\left\{k^{-1} + I\left[\ddot{J}(t-\alpha) + J_0\delta'(t-\alpha) + \dot{J}(0)\delta(t-\alpha)\right]\right\} \quad (3\text{-}40)$$

where

$$\begin{aligned}\frac{\mathrm{d}^2 J}{\mathrm{d}t^2} &= \frac{\mathrm{d}^2}{\mathrm{d}t^2}\left[\int_{\tau=0}^{\infty} L(\tau)\left(1 - \mathrm{e}^{-\frac{t}{\tau}}\right)\mathrm{d}\ln\tau\right] \\ &= \int_{\tau=0}^{\infty} L(\tau)\frac{\mathrm{d}^2}{\mathrm{d}t^2}\left(1 - \mathrm{e}^{-\frac{t}{\tau}}\right)\mathrm{d}\ln\tau \\ &= -\int_{\tau=0}^{\infty}\frac{L(\tau)}{\tau^3}\mathrm{e}^{-\frac{t}{\tau}}\,\mathrm{d}\tau \end{aligned} \quad (3\text{-}41)$$

The creep compliance corresponding to a model with a set of N discrete retardation times $\{\tau_i\}_{i=1}^{N}$ is given by (1-64). The coefficient of the term containing the unphysical first derivative delta function, J_0, is only non-zero in the case of a viscoelastic solid.

If the material is a fluid, then the necessary applied torque would only involve the delta function itself, which it has been established previously, is allowed to represent a physical function. As an example, in this case the torque would take the form

$$C(t) = H(t-\alpha)\left\{k^{-1} + I\left[\sum_{j=1}^{N}\frac{J_i}{\tau_i}\delta(t-\alpha) - \sum_{j=1}^{N}\frac{J_i}{\tau_i}\,\mathrm{e}^{-\frac{t}{\tau}}\right]\right\} \tag{3-42}$$

and it can be seen that $\bar{C}(s)$ and $\bar{J}(s)$ share simple poles located at the origin and the negative reciprocals of the retardation times. □

Theorem 3.1.4: It is possible to apply a torque, $C(t)$, such that the first derivative of the displacement, $\dot{\chi}(t)$ is equal to the creep compliance, $J(t)$, for both viscoelastic liquid and solid materials.

Proof. Let $\dot{\chi}(t) = H(t-\alpha)J(t-\alpha)$, where $\alpha > 0$, with Laplace transform $s\bar{\chi}(s) = \mathrm{e}^{-\alpha t}\bar{J}(s)$. From (2-43), the applied torque to produce the latter angular velocity would have the form

$$\bar{C}(s) = \mathrm{e}^{-\alpha t}\left[k^{-1}s^{-2} + Is\bar{J}(s)\right] \tag{3-43}$$

and since

$$\mathscr{L}^{-1}\left\{s\bar{J}\right\} = \dot{J}(t) + J(0)\delta t \tag{3-44}$$

the applied necessary to produce the aforementioned response is

$$C(t) = H(t-\alpha)\left\{\tfrac{1}{k}(t-\alpha) + I\left[\dot{J}(t-\alpha) + J(0)\delta(t-\alpha)\right]\right\}. \tag{3-45}$$

There are no terms involving derivatives of the delta function, hence a physical form for the applied torque exists. Furthermore, since $J_0 = 0$ for viscoelastic fluids, the delta function term vanishes and the solution is a function of the derivative of the creep compliance with the addition of a linear term in t. In the discrete case, where

$$\dot{J}(t) = \sum_{i=1}^{N} J_i\,\mathrm{e}^{-\frac{t}{\tau}} + \tfrac{1}{\eta}, \tag{3-46}$$

it can be seen that $\bar{C}(s)$ and $\bar{J}(s)$ share simple poles located at the negative reciprocals of the retardation times. □

II. DIRICHLET SERIES REPRESENTATION

It has been established that it is possible to apply a torque to the system such that the response is $\dot{\chi}(t) = G(t)$ for a completely arbitrary relaxation modulus $G(t)$, provided

that the functions $\dot{G}(t)$ and $G * G$ are amenable and provided an example in the case where the relaxation modulus is defined by the Maxwell model or equivalently corresponds to a discrete relaxation spectrum. In this special case, the relaxation modulus takes the form a of a finite *Dirichlet* or *Prony* series.

Definition 3.2.1: Let $\{\lambda_n\}$, $n \in \mathbb{Z}^+$, form an increasing sequence of positive real numbers. A *Dirichlet series* [93] with exponents $\{\lambda_n\}$ is a series of the form

$$f(s) = \sum_n a_n \, \mathrm{e}^{-\lambda_n s} \tag{3-47}$$

where $a_n \in \mathbb{C}$. The more well-known form is a specialization obtaining by setting $\lambda_n = \log n$.

Now the results of the previous section are generalized by considering the relaxation modulus, $G(t)$, and the displacement $\chi(t)$ or its first derivative $\dot{\chi}(t)$ to be of the form (3-47) and investigate the form for the applied torque $C(t)$ which is necessary to produce such a response. The following two propositions consider these two cases, respectively.

Theorem 3.2.1: Let the relaxation modulus $G(t)$ be represented by a finite Dirichlet series $G(t) = G_\infty + \sum_{i=1}^{N} g_i \, \mathrm{e}^{-\frac{t}{\lambda_i}}$ with exponents $\{\lambda_i\}$ ordered such that $\lambda_1 < \lambda_2 < \cdots < \lambda_N$ and $g_i \in \mathbb{R}^+$ for $i = 1, \ldots, N$. Define $G_1(t)$ to be the exponential sum part of $G(t)$, so that $G(t) = G_\infty + G_1(t)$. If the displacement $\chi(t)$ is assumed to be of the same form, with $\chi(t) = \chi_\infty + \sum_{i=1}^{M} \chi_i \, \mathrm{e}^{-\frac{t}{\mu_i}}$, $t \in [0, T]$, $\chi_i \in \mathbb{R}^+$ and $\mu_1 < \mu_2 < \cdots < \mu_N$. Then the torque $C(t)$ required to generate such a response for a general viscoelastic material with an N-mode relaxation spectrum is of the form

$$C(t) = A\delta'(t) + B\delta(t) + C_\infty + \sum_{i=1}^{M+N} \gamma_i \, \mathrm{e}^{-\frac{t}{\theta_i}} \tag{3-48}$$

where the Dirichlet series term has coefficients $\gamma_i \in \mathbb{R}^+$, and exponents $\{\theta_i^{-1}\}$, $i = 1, \ldots, M + N$ and $A, B \in \mathbb{R}$.

Proof. Define the Dirichlet series $\chi_0(t)$ to be

$$\chi_0(t) = \chi_\infty + \sum_{i=1}^{N} \chi_i \, \mathrm{e}^{-t/\mu_i} \tag{3-49}$$

where $\chi_i \in \mathbb{R}$, $i = 1, \ldots, N$ and the $\mu_i \in \mathbb{R}^+$ satisfy $\mu_1 < \mu_2 < \cdots < \mu_N$. To avoid the problems associated with discontinuities at $t = 0$ arising from the Laplace transform

formulation of the problem, consider the function $\chi(t) = H(t-\alpha)\chi_0(t-\alpha)$, for $\alpha \in \mathbb{R}^+$. Then the Laplace transform of the translated function is

$$\bar{\chi}(s) = \mathrm{e}^{-\alpha s}\left[\frac{\chi_\infty}{s} + \sum_{i=1}^{N}\frac{\chi_i}{s+\mu_i^{-1}}\right] \tag{3-50}$$

It is also assumed that the relaxation time $G(t)$ is represented by a Dirichlet series with coefficients $\{g_i\}$ and exponents $\{\lambda_i^{-1}\}$, for $i = 1, \ldots, N$, which has corresponding Laplace transform

$$\bar{G}(s) = \frac{\Lambda_{1,N-1}(s) + G_\infty \prod_{i=1}^{N}(s+\lambda_i^{-1})}{s\prod_{i=1}^{N}(s+\lambda_i^{-1})}. \tag{3-51}$$

where $\Lambda_{1,N-1}$ is defined

$$\Lambda_{1,N-1} := \sum_{i=1}^{N} g_i \prod_{j=1,i}^{N}(s+\lambda_j^{-1}) \tag{3-52}$$

The torque $C(t)$ necessary to generate a response such as that given by (3-49) has Laplace transform

$$\bar{C}(s) = \mathrm{e}^{-\alpha s}\left[Is^2\bar{\chi}_0(s) + k^{-1}s\bar{\chi}_0(s)\bar{G}(s)\right] = \mathrm{e}^{-\alpha s}\bar{C}_0(s). \tag{3-53}$$

Now,

$$\begin{aligned}\mathscr{L}^{-1}\left\{s^2\bar{\chi}_0(s)\right\} &= \ddot{\chi}_0(t) + \chi_0(0)\delta'(t) + \dot{\chi}_0(0)\delta(t)\\ &= \sum_{i=1}^{M}\frac{\chi_i}{\mu_i^2}\mathrm{e}^{-\frac{t}{\mu_i}} + \delta'(t)\left[\chi_\infty + \sum_{i=1}^{M}\chi_i\right] - \delta(t)\sum_{i=1}^{M}\frac{\chi_i}{\mu_i}\end{aligned} \tag{3-54}$$

and consistently with Theorem 3.1.1, the solution involves the first derivative of the delta function, $\delta'(t)$, which cannot be reproduced experimentally. The remaining term

$$\begin{aligned}\mathscr{L}^{-1}\left\{s\bar{\chi}_0(s)\bar{G}(s)\right\} &= \mathscr{L}^{-1}\left\{s\bar{\chi}_0(s)\right\} * G(t)\\ &= \left[\dot{\chi}_0(t) + \chi_0(0)\right] * G(t)\\ &= \chi_0(0)\int_0^t G(t')\,\mathrm{d}t' + \dot{\chi}_0(t) * G(t)\\ &= \chi_0(0)\int_0^t G(t')\,\mathrm{d}t' + G_\infty\int_0^t \dot{\chi}_0(t')\,\mathrm{d}t' + \dot{\chi}_0(t) * G_1(t)\end{aligned} \tag{3-55}$$

must be a finite Dirichlet series, since both $\dot{\chi}_0(t)$ and $G_1(t)$ are sums of exponentials. Thus,

$$\begin{aligned}\mathscr{L}^{-1}\left\{s\bar{\chi}_0(s)\bar{G}(s)\right\} = \chi_0(0)&\left[G_\infty t + \sum_{i=1}^{N} g_i\lambda_i\left(1 - \mathrm{e}^{-\frac{t}{\lambda_i}}\right)\right]\\ &+ G_\infty\left[\chi_0(t) - \chi_0(0)\right] + \dot{\chi}_0(t) * G_1(t).\end{aligned} \tag{3-56}$$

The latter convolution term is determined as follows.

$$\begin{aligned}\mathscr{L}\{\dot{\chi}_0 * G_1\} &= \bar{\dot{\chi}}_0(s)\bar{G}_1(s) \\ &= [\bar{\chi}_1(s)\bar{G}_1(s) + \chi_0(0)]\,\bar{G}_1(s),\end{aligned} \tag{3-57}$$

defining a new function

$$\bar{\chi}_1(s) = \frac{\Lambda_{2,M-1}(s)}{\prod_{i=1}^{M}(s+\mu_i^{-1})} \tag{3-58}$$

where

$$\Lambda_{2,M-1} := -\sum_{i=1}^{N}\frac{\chi_i}{\mu_i}\prod_{j=1,i}^{N}(s+\mu_j^{-1}) \tag{3-59}$$

and additionally using the definition for $\Lambda_{1,N-1}$ in (3-52), it can be seen that

$$\bar{\chi}_1(s)\bar{G}_1(s) = \frac{\Lambda_{1,N-1}(s)\Lambda_{2,M-1}(s)}{\prod_{i=1}^{N}(s+\lambda_i^{-1})\prod_{j=1}^{M}(s+\mu_i^{-1})}, \tag{3-60}$$

which, upon inversion of the Laplace transform yields a solution of the form

$$\mathscr{L}^{-1}\{\bar{\chi}_1(s)\bar{G}_1(s)\} = \sum_{i=1}^{N}\alpha_i\,\mathrm{e}^{-\frac{t}{\lambda_i}} + \sum_{i=1}^{M}\beta_i\,\mathrm{e}^{-\frac{t}{\mu_i}}, \tag{3-61}$$

where the constants $\{\alpha_i\}_{i=1}^{N}$ and $\{\beta_i\}_{i=1}^{M}$ are defined

$$\begin{aligned}\alpha_i &= \lim_{s\to-\lambda_i^{-1}}\left\{(s+\lambda_i^{-1})\bar{\chi}_1(s)\bar{G}_1(s)\right\} \\ &= \frac{\Lambda_{1,N-1}(-\lambda_i^{-1})\Lambda_{2,M-1}(-\lambda_i^{-1})}{\prod_{j=1,i}^{N}(\lambda_j^{-1}-\lambda_i^{-1})\prod_{i=1}^{M}(\lambda_i^{-1}-\mu_i^{-1})}, \quad i=1,2,\ldots,N\end{aligned} \tag{3-62}$$

and

$$\begin{aligned}\beta_i &= \lim_{s\to-\mu_i^{-1}}\left\{(s+\mu_i^{-1})\bar{\chi}_1(s)\bar{G}_1(s)\right\} \\ &= \frac{\Lambda_{1,N-1}(s)(-\mu_i^{-1})\Lambda_{2,M-1}(-\mu_i^{-1})}{\prod_{i=1}^{N}(\lambda_i^{-1}-\mu_i^{-1})\prod_{j=1,i}^{M}(\mu_j^{-1}-\mu_i^{-1})}, \quad j=1,2,\ldots,M.\end{aligned} \tag{3-63}$$

Defining $\{\theta_i\}_{i=1}^{M+N} = \{\mu_i\}_{i=1}^{M}\cup\{\lambda_i\}_{i=1}^{N}$ and corresponding coefficients $\gamma_i = \alpha_i + \chi_0(0)(1-g_i\lambda_i)$ for $i=1,2,\ldots,M$ and $\gamma_i = \frac{I\chi_i}{\mu_i^2} + k^{-1}(G_\infty\chi_i+\beta_i)$ for $i=M+1,M+2,\ldots,M+N$, then $C_0(t)$ has the form

$$\begin{aligned}C_0(t) = I\left[\chi_0(0)\delta'(t)+\dot{\chi}_0(0)\delta(t)\right] + k^{-1}\left[G_\infty\sum_{i=1}^{M}\chi_i + \chi_0(0)\left(\sum_{i=1}^{N}g_i\lambda_i + G_\infty t\right)\right] \\ + \sum_{i=1}^{M+N}\gamma_i\,\mathrm{e}^{-\frac{t}{\theta_i}}.\end{aligned} \tag{3-64}$$

In the case of a viscoelastic fluid ($G_\infty = 0$) and setting $\chi_\infty = 0$, this simplifies to

$$C_0(t) = I\sum_{i=1}^{M}\left[\chi_i\delta'(t) - \frac{\chi_i}{\mu_i}\delta(t)\right] + k^{-1}\chi_0(0)\sum_{i=1}^{N} g_i\lambda_i + k^{-1}\sum_{i=1}^{N}(\alpha_i + \chi_0(0)g_i(1-\lambda_i))\,\mathrm{e}^{-\frac{t}{\lambda_i}} + \sum_{i=1}^{M}\left(\frac{I\chi_i}{\mu_i} + \beta_i\right)\mathrm{e}^{-\frac{t}{\mu_i}}, \quad (3\text{-}65)$$

which is of the required form. □

Theorem 3.2.2: Let the relaxation modulus $G(t)$ be represented by a finite Dirichlet series $G(t) = G_\infty + \sum_{i=1}^{N} g_i\,\mathrm{e}^{-\frac{t}{\lambda_i}}$ with exponents $\{\lambda_i\}$ ordered such that $\lambda_1 < \lambda_2 < \cdots < \lambda_N$ and $g_i \in \mathbb{R}^+$ for $i = 1,\ldots,N$. If the derivative of the displacement $\dot\chi(t)$ is assumed to be of the same form, with $\dot\chi(t) = \chi_\infty + \sum_{i=1}^{N}\chi_i\,\mathrm{e}^{-\frac{t}{\mu_i}}$, for $t \in [0,T]$, $\chi_i \in \mathbb{R}^+$ and $\mu_{i+1} - \mu_i > 0$ for $i = 1,\ldots,N-1$. Then the torque $C(t)$ required to generate such a response for a viscoelastic material with an N-mode relaxation spectrum is of the form

$$C(t) = A\delta(t) + C_\infty + \sum_{i=1}^{M+N}\gamma_i\,\mathrm{e}^{-\frac{t}{\theta_i}} \quad (3\text{-}66)$$

where the Dirichlet series component has coefficients $\gamma_i \in \mathbb{R}^+$, and exponents $\{\theta_i^{-1}\}$, $i = 1,\ldots,M$. For a viscoelastic fluid, the term C_∞ takes the value zero.

Proof. Again, we begin by defining $\chi_0(t)$ as in (3-49), where $\chi_i \in \mathbb{R}$ the $\{\mu_i^{-1}\}_{i=1}^{M}$ form a non-decreasing sequence so that $\dot\chi(t) = H(t-\alpha)\chi_0(t-\alpha)$. The Laplace transform of $\dot\chi(t)$ gives the relation $s\bar\chi(s) = \mathrm{e}^{-\alpha s}\bar\chi_0(s)$, so the applied torque necessary to produce the desired response must have the form

$$\begin{aligned}\bar C(s) &= s\bar\chi(s)\left[Is + k^{-1}\bar G(s)\right]\\ &= \mathrm{e}^{-\alpha s}\left[Is\bar\chi_0(s) + k^{-1}\bar\chi_0(s)\bar G(s)\right]\\ &= \mathrm{e}^{-\alpha s}\bar C_0(s).\end{aligned} \quad (3\text{-}67)$$

Now

$$\begin{aligned}\mathscr{L}^{-1}\{s\bar\chi_0(s)\} &= \dot\chi_0(t) + \chi_0(0)\delta(t)\\ &= -\sum_{i=1}^{M}\frac{\chi_i}{\mu_i}\mathrm{e}^{-\frac{t}{\mu_i}} + \left[G_\infty + \sum_{i=1}^{M}\chi_i\right]\delta(t)\end{aligned} \quad (3\text{-}68)$$

and

$$\begin{aligned}\mathscr{L}^{-1}\{\bar\chi_0\bar G\} &= (\chi_\infty + \chi_1(t)) * (G_\infty + G_1(t))\\ &= \chi_\infty G_\infty + \chi_\infty\sum_{i=1}^{N} g_i\lambda_i\left[1 - \mathrm{e}^{-\frac{t}{\lambda_i}}\right] + G_\infty\sum_{i=1}^{M}\chi_i\mu_i\left[1 - \mathrm{e}^{-\frac{t}{\mu_i}}\right] + \chi_1 * G_1\end{aligned}$$

(3-69)

where $\chi_1(t)$ and $G_1(t)$ are the exponential terms of the functions $\chi_0(t)$ and $G(t)$, respectively. The only term which remains to be determined in explicit form is the last convolution term, which will be an exponential series since both the arguments are of this form,

$$\mathscr{L}\{\chi_1(t) * G_1(t)\} = \frac{\Lambda_{1,N-1}(s)\Lambda_{3,M-1}(s)}{\prod_{i=1}^{M}(s+\mu_i^{-1})\prod_{i=1}^{N}(s+\lambda_i^{-1})} \tag{3-70}$$

with functions $\Lambda_{1,N-1}(s)$ from (3-52) and

$$\Lambda_{3,M-1}(s) = \sum_{i=1}^{M}\chi_i \prod_{j=1,i}^{M}(s+\mu_i^{-1}). \tag{3-71}$$

Then,

$$\chi_1(t) * G_1(t) = \sum_{i=1}^{M}\alpha_i\, \mathrm{e}^{-\frac{t}{\mu_i}} + \sum_{i=1}^{N}\beta_i\, \mathrm{e}^{-\frac{t}{\lambda_i}} \tag{3-72}$$

in terms of the constants

$$\begin{aligned}\alpha_i &= \lim_{s\to-\mu_i^{-1}}\left\{(s+\mu_i^{-1})\bar{\chi}_1(s)\bar{G}_1(s)\right\} \\ &= \frac{\Lambda_{1,N-1}(-\mu_i^{-1})\Lambda_{3,M-1}(-\mu_i^{-1})}{\prod_{j=1,i}^{M}(\mu_j^{-1}-\mu_i^{-1})\prod_{j=1}^{N}(\lambda_j^{-1}-\mu_i^{-1})}, \quad i=1,2,\ldots,M\end{aligned} \tag{3-73}$$

and

$$\begin{aligned}\beta_i &= \lim_{s\to-\lambda_i^{-1}}\left\{(s+\lambda_i^{-1})\bar{\chi}_1(s)\bar{G}_1(s)\right\} \\ &= \frac{\Lambda_{1,N-1}(-\lambda_i^{-1})\Lambda_{3,M-1}(-\lambda_i^{-1})}{\prod_{j=1}^{M}(\mu_j^{-1}-\lambda_i^{-1})\prod_{j=1,i}^{N}(\lambda_j^{-1}-\lambda_i^{-1})}, \quad i=1,2,\ldots,N.\end{aligned} \tag{3-74}$$

Defining $\{\theta_i\}_{i=1}^{M+N} = \{\mu_i\}_{i=1}^{M} \cup \{\lambda_i\}_{i=1}^{N}$, then the applied torque assumes the required form

$$C_0(t) = A\delta(t) + B + \sum_{i=1}^{M+N}\gamma_i\, \mathrm{e}^{-\frac{t}{\theta_i}}, \tag{3-75}$$

where

$$A = I\left[\chi_\infty + \sum_{i=1}^{M}\chi_i\right] \tag{3-76}$$

$$B = k^{-1}\left[\chi_\infty G_\infty + G_\infty\sum_{i=1}^{M}\chi_i\mu_i + \chi_\infty\sum_{i=1}^{N}g_i\lambda_i\right] \tag{3-77}$$

$$\gamma_i = \begin{cases} k^{-1}\left[\alpha_i - G_\infty\chi_i\mu_i\right] - \frac{I\chi_i}{\mu_i} & i=1,2,\ldots,M, \\ k^{-1}\left[\beta_i + \chi_\infty g_i\lambda_i\right] & i=M+1,M+2,\ldots,M+N. \end{cases} \tag{3-78}$$

In the case where the material is a viscoelastic fluid ($G_\infty = 0$) and setting $\chi_\infty = 0$, the torque now becomes

$$C_0(t) = I\sum_{i=1}^{M}\chi_i\delta(t) + \sum_{i=1}^{M}\left[k^{-1}\alpha_i - \frac{I\chi_i}{\mu_i}\right]\mathrm{e}^{-\frac{t}{\mu_i}} + \sum_{i=1}^{N}k^{-1}\beta_i\,\mathrm{e}^{-\frac{t}{\lambda_i}} \tag{3-79}$$

and it can be seen that the limiting value $C_\infty = 0$ as required. □

As a simple example, consider the case where the applied torque has the form $C(t) = C_0\left[\delta(t) + \mathrm{e}^{-at}\right]$ for the Maxwell model. The platen displacement would then have the form

$$\chi(t) = \frac{C_0}{I}\left\{\mu_0 + \gamma_0 + (\mu_1 + \gamma_1)\,\mathrm{e}^{-\xi_1 t} + (\mu_2 + \gamma_2)\,\mathrm{e}^{-\xi_2 t} + \mu_3\,\mathrm{e}^{-at}\right\} \tag{3-80}$$

where $\gamma_{0,1,2}$ are the constants pertaining to the delta function applied torque from (2-73a)-(2-73c) in the case of real $\xi_{1,2}$ or (2-80a)-(2-80c) if they are complex. The new constants $\mu_{0,1,2,3}$ are defined

$$\mu_0 = \frac{kI}{\lambda g a} \tag{3-81a}$$

$$\mu_1 = \frac{\lambda\xi_1 - 1}{\lambda\xi_1(a-\xi_1)(\xi_2-\xi_1)} \tag{3-81b}$$

$$\mu_2 = \frac{1-\lambda\xi_2}{\lambda\xi_2(a-\xi_2)(\xi_2-\xi_1)} \tag{3-81c}$$

$$\mu_3 = \frac{\lambda 1}{\lambda a(\xi_1-a)(\xi_2-a)} \tag{3-81d}$$

Theorem 3.2.3: Let the relaxation modulus $G(t)$ and the second derivative of the displacement $\ddot{\chi}(t)$ be represented by finite Dirichlet series as for Theorem 3.2.2. Then the torque $C(t)$ required to generate such a response for a viscoelastic fluid with an N-mode relaxation spectrum is of the form

$$C(t) = C_\infty + \sum_{i=1}^{M+N}\gamma_i\,\mathrm{e}^{-\frac{t}{\theta_i}} \tag{3-82}$$

where the Dirichlet series component has coefficients $\gamma_i \in \mathbb{R}^+$, and exponents $\{\theta_i^{-1}\}$, $i = 1, \ldots, M$.

Proof. In an analogous manner to the previous two theorems, define $\ddot{\chi}(t) = H(t-\alpha)\chi_0(t-\alpha)$, for $\alpha > 0$, such that $s^2\bar{\chi}(s) = \mathrm{e}^{-\alpha s}\bar{\chi}_0(s)$. The torque required to generate a response of the desired form is given by

$$\bar{C}(s) = \mathrm{e}^{-\alpha s}\bar{\chi}_0(s)\left[I + k^{-1}\frac{\bar{G}(s)}{s}\right] \tag{3-83}$$

Now

$$\frac{\bar{\chi}_0(s)\bar{G}(s)}{s} = \frac{\Lambda_{1,N-1}(s)\Lambda_{3,N-1}(s)}{s\prod_{i=1}^{M}(s+\mu_i^{-1})\prod_{i=1}^{N}(s+\lambda_i^{-1})} \tag{3-84}$$

and

$$\mathscr{L}^{-1}\left\{\frac{\bar{\chi}_0(s)\bar{G}(s)}{s}\right\} = \gamma_0 + \sum_{i=1}^{M}\alpha_i\,\mathrm{e}^{-\frac{t}{\mu_i}} + \sum_{i=1}^{N}\beta_i\,\mathrm{e}^{-\frac{t}{\lambda_i}} \tag{3-85}$$

which can be considered to be a Dirichlet series with one infinite exponent. The constants are defined

$$\begin{aligned}\gamma_0 &= \lim_{s\to 0}\left\{\bar{\chi}_0(s)\bar{G}(s)\right\}\\ &= \left[\sum_{i=1}^{N} g_i\lambda_i\right]\cdot\left[\sum_{i=1}^{M}\chi_i\mu_i\right], \qquad (3\text{-}86)\\ \alpha_i &= \lim_{s\to-\mu_i^{-1}}\left\{(s+\mu_i^{-1})\frac{\bar{\chi}_0(s)\bar{G}(s)}{s}\right\}\\ &= -\frac{\mu_i\Lambda_{1,N-1}(-\mu_i^{-1})\Lambda_{3,M-1}(-\mu_i^{-1})}{\prod_{j=1,i}^{M}(\mu_j^{-1}-\mu_i^{-1})\prod_{j=1}^{N}(\lambda_j^{-1}-\mu_i^{-1})}, \quad i=1,2,\ldots,M, \qquad (3\text{-}87)\end{aligned}$$

and

$$\begin{aligned}\beta_i &= \lim_{s\to-\lambda_i^{-1}}\left\{(s+\lambda_i^{-1})\frac{\bar{\chi}_0(s)\bar{G}(s)}{s}\right\}\\ &= -\frac{\lambda_i\Lambda_{1,N-1}(-\lambda_i^{-1})\Lambda_{3,M-1}(-\lambda_i^{-1})}{\prod_{j=1}^{N}(\mu_j^{-1}-\lambda_i^{-1})\prod_{j=1,i}^{N}(\lambda_j^{-1}-\lambda_i^{-1})}, \quad i=1,2,\ldots,N. \qquad (3\text{-}88)\end{aligned}$$

Then

$$C_0(t) = k^{-1}\gamma_0 + \sum_{i=1}^{M}\left[k^{-1}\alpha_i + I\chi_i\right]\,\mathrm{e}^{-\frac{t}{\mu_i}} + \sum_{i=1}^{N}k^{-1}\beta_i\,\mathrm{e}^{-\frac{t}{\lambda_i}} \tag{3-89}$$

can be rewritten in the form

$$C_0(t) = \sum_{i=0}^{M+N}\gamma_i\,\mathrm{e}^{-\frac{t}{\theta_i}}, \tag{3-90}$$

where $\{\theta_i\}_{i=1}^{M+N} = \{\mu_i\}_{i=1}^{M}\cup\{\lambda_i\}_{i=1}^{N}$ and $\theta_0 = \infty$. □

The results of this section show that if the applied torque and relaxation modulus are prescribed as Dirichlet series, then so is the second-order derivative of the platen displacement. To obtain such a function for the first or zeroth-order derivatives requires the use of a delta function or even the first derivative of the delta function in the latter case.

CHAPTER 4

The Volterra Integral Equation

Well-posedness and Stability

We now proceed to take a detailed look at the nature of the Volterra integro-differential equation in the time domain, particularly with regards to the stability of the equation with respect to experimental, or from a theoretical point of view perturbed data. As has been shown earlier, the system under consideration for this problem is governed by a Volterra integro-differential equation (VIDE). In this chapter, we take a closer look at the properties of this equation and methods and stability of solution for the relaxation function $G(t)$. It is shown that in order to obtain a solution for the relaxation modulus the equation must be recast in the form of a Volterra integral equation of the first kind, the solution is well known to be an ill-posed problem. Defining the concept of well-posedness, it is then demonstrated by considering regular perturbations in the source data $\dot{\chi}(t)$ that stable solutions for the problem can exist and bounds are calculated on the data error under which these conditions are satisfied for a selection of applied torque profiles $C(t)$.

I. VOLTERRA INTEGRAL EQUATIONS

The standard derivation of the governing equation for this system leads to the VIDE encountered in the preceding chapters, which is reproduced here for completeness. Define the experimental time $T \in (0, \infty)$ and let $S := \{(t, t') : 0 \leq t' \leq t \leq T\}$. Consider the VIDE given by

$$I\ddot{\chi}(t) + k^{-1} \int_0^t G(t - t')\dot{\chi}(t')\, \mathrm{d}t' = C(t) \qquad t \in [0, T] \tag{4-1}$$

where $C \in C[0, T]$, $\chi \in C^2[0, T]$ and $G \in C(S)$. Comparison with the general form [16]

$$y'(t) = p(t)y(t) + q(t) + \int_0^t K(t, t')y(t')\, \mathrm{d}t' \qquad t \in [0, T] \tag{4-2}$$

where p, q and K are assumed to be real-valued and continuous on $[0, T]$ and S, indicates that (4-1) is a linear first order VIDE of convolution type with

i. $y(t) \equiv \dot{\chi}(t), \quad t \in [0, T]$

ii. $p(t) \equiv 0, \quad \forall t \in [0, T]$

iii. $q(t) \equiv I^{-1}C(t), \quad t \in [0, T]$

iv. $K(t, t') \equiv -(kI)^{-1}G(t - t'), \quad (t, t') \in S$

Definition 4.1.1: A Volterra equation of the *second* kind [16] is of the form

$$\int_0^t K(t, t')u(t)\, \mathrm{d}t' + g(t) = u(t), \qquad t \in [0, T] \tag{4-3}$$

where K and g are assumed to be real-valued and continuous on S and I, respectively. When $K(t,t') = Q(t-t')$, the kernel is referred to as being of convolution type.

Integration of (4-2) leads to a Volterra integral equation of the 2nd kind,

$$y(t) = g(t) + \int_0^t Q(t-t')y(t')\,\mathrm{d}t', \qquad t \in [0,T] \tag{4-4}$$

with

i. $g(t) := y_0 + \int_0^t q(t')\,\mathrm{d}t', \quad t \in [0,T]$

ii. $Q(t-t') := p(t') + \int_{t'}^t K(\tau - t')\,\mathrm{d}\tau, \quad (t,t') \in S.$

Here we have made use of *Dirichlet's formula* which states that

$$\int_0^t \int_0^\tau \phi(\tau,t')\,\mathrm{d}t'\,\mathrm{d}\tau = \int_0^t \int_{t'}^t \phi(\tau,t')\,\mathrm{d}\tau\,\mathrm{d}t', \qquad (t,t') \in S \tag{4-5}$$

Returning to (4-1), the Volterra-2 equivalent form is

$$\dot{\chi}(t) = I^{-1}\int_0^t C(t')\,\mathrm{d}t' + \int_0^t \int_{t'}^t G(\tau - t')\,\mathrm{d}\tau\,\dot{\chi}(t')\,\mathrm{d}t'. \tag{4-6}$$

The inversion of (4-6) yields a unique solution

$$\dot{\chi}(t) = I^{-1}\int_0^t R(t-t')C(t')\,\mathrm{d}t', \quad t \in [0,T] \tag{4-7}$$

where the *resolvent kernel*, $R(t,t')$, is defined

$$R(t-t') = 1 + \int_{t'}^t r(t-u)\,\mathrm{d}u \tag{4-8}$$

and the iterated kernels which arise from the *Picard method* [64] for constructing successive approximations to the exact solution of (4-6) by

$$r(t-t') = -(kI)^{-1}\left\{\int_{t'}^t G(t-t')\,\mathrm{d}t' + \int_{t'}^t G(t-\tau)r(\tau-t')\,\mathrm{d}\tau\right\}. \tag{4-9}$$

However, the data for $\dot{\chi}(t)$ is assumed to be known and the kernel $G(t-t')$ the function which is required to be determined. An alternative approach is required to yield an expression for the kernel in terms of $\dot{\chi}(t)$ and $C(t)$.

Definition 4.1.2: A Volterra integral equation of the *first* kind [17] is of the form

$$\int_0^t K(t,t')u(t')\,\mathrm{d}t' = f(t), \qquad t \in [0,T] \tag{4-10}$$

where the kernel $K(t,t')$ is continuous on $S := \{(t,t') : 0 \le t' \le t \le T\}$. It is assumed throughout that there exists a unique solution $\bar{u} \in L^2[0,T]$ for a particular choice of $f(t)$ and $K(t,t')$.

It is often more convenient [50] to write (4-10) in the form

$$Au = f, \tag{4-11}$$

where the operator $A \in \mathcal{L}(u)$, the space of linear operators, is defined for $u \in L^2[0,T]$ by

$$Au(t) := \int_0^t K(t,t')u(t')\,\mathrm{d}t', \qquad t \in [0,T]. \tag{4-12}$$

Integral equations involving kernels of the form $K(t,t') \equiv K(t-t')$ are known as Volterra integral equations of convolution type and the method of solution known as *deconvolution*. The corresponding integral equations defined on fixed domains are known as Fredholm integral equations, but do not concern us here.

We now show that the integro-differential equation (4-1) can be rewritten in the form of a Volterra integral equation of the first kind of convolution type. The general form for this class of integral equations is given by

$$\int_0^t K(t-t')y(t')\,\mathrm{d}t' = f(t), \qquad t \in [0,T]. \tag{4-13}$$

First, note that the convolution integral possesses the commutative property

$$f * g := \int_0^t f(t-t')g(t')\,\mathrm{d}t' = \int_0^t f(t')g(t-t')\,\mathrm{d}t' \tag{4-14}$$

which enables (4-1) to be rewritten as a Volterra integral equation of the first kind in G(t), viz.

$$\int_0^t G(t')\dot{\chi}(t-t')\,\mathrm{d}t' = k\left[C(t) - I\ddot{\chi}(t)\right], \qquad t \in [0,T] \tag{4-15}$$

with $f(t) \in C[0,T]$

i. $f(t) \equiv k\left[C(t) - I\ddot{\chi}(t)\right]$

ii. $K(t,t') \equiv \dot{\chi}(t-t')$

iii. $u(t') \equiv G(t')$

in (4-13).

Integration by parts yields an expression in terms of the *memory function*, $M(t) = -\frac{\mathrm{d}G}{\mathrm{d}t}$, and $\chi(t)$, whereby reducing the amount of numerical differentiation required on the data.

$$\int_0^t M(t')\chi(t-t')\,\mathrm{d}t' = k\left[C(t) - I\ddot{\chi}(t)\right] + G(0)\chi(t) \tag{4-16}$$

Although (4-15) and (4-16) describe precisely the same system as (4-1), the inversion procedure to obtain a solution for $\chi(t)$ or $\dot{\chi}(t)$ is considerably more ill-posed and requires a different approach to solution. Before discussing stability of the integral equation however, it is necessary to define the concept of well-posedness.

II. STABILITY AND WELL-POSEDNESS

Consider the Volterra integral equation given by (4-10). The forward or *direct* problem of determining the data function $f(t)$ from the known functions $K(t,t')$ and $u(t')$ for $t \in [0,T]$ generally causes few problems since small errors in the known functions do not result in large errors in the solution; the process of integration smooths out the effects of the errors present in the data. The reverse process of determining $u(t)$ from known functions $K(t,t')$ and $f(t)$ is termed an *inverse* problem and in general is less straightforward than the forward process. Inverse problems are commonly encountered in the modelling of physical phenomena where the model parameters or material are unknown and need to be determined from the known input and observed response (see [24], for examples).

The term well-posedness was first defined by Hadamard [34], a well-posed mathematical problem being one that satisfies the following three criteria:

i) A solution exists (existence)

ii) The solution is unique (uniqueness)

iii) The solution depends continuously on the data (stability).

Inverse problems are typically continuous and hence satisfy all the criteria for well posedness, however when discretized the finite precision implicitly necessary means the latter criterion fails to be satisfied and the problem becomes ill posed. For such problems, the solution is highly sensitive to small changes in the data and regularization methods are often required to obtain an acceptable solution.

In practice only an approximation of the data $f^\varepsilon \in U$ is available, which satisfies $\|f - f^\varepsilon\|_2 \leq \varepsilon$ for some $\varepsilon > 0$, so the ill posedness means that the computed solution u^ε of $Au = f^\varepsilon$ may be arbitrarily far from the solution of the unperturbed problem.

The degree of ill-posedness of Volterra integral equations of the first kind is dependent upon the behaviour of the kernel at $t = t'$ and we shall use the classification given in [50] in terms of ν-smoothing kernels as follows.

Definition 4.2.1: The Volterra equation (4-10) is a *ν-smoothing* problem for $\nu \geq 1$ if the operator A defined in (4-12) is a ν-smoothing operator and $f \in C^{\nu}[0,T]$. A Volterra operator A is said to be ν-smoothing if the kernel K is such that $\frac{\partial^l K}{\partial t^l}(t,t) = 0$ for $0 \leq t \leq T$ and $l = 0, \ldots, \nu - 2$ and such that $\frac{\partial^{\nu-1} K}{\partial t^{\nu-1}} = 1$ for $0 \leq t \leq T$, with $\frac{\partial^{\nu} K}{\partial t^{\nu}}$ continuous on $[0,T] \times [0,T]$. Extending the definition to infinite values of ν, the Volterra integral equation (4-10) is an *infinitely-smoothing* problem if $\frac{\partial^l K}{\partial t^l}(t,t) = 0$ for $0 \leq t \leq T$ and all $l = 1, 2, \ldots$.

Therefore, if (4-10) is a ν-smoothing problem it can be differentiated ν times to give

$$K^{(\nu-1)}(t,t)u(t) + \int_0^t \frac{\partial^{\nu}}{\partial t^{\nu}} K(t,t')u(t')\,\mathrm{d}t' = f^{\nu}(t), \qquad t \in [0,T] \tag{4-17}$$

which is equivalent to (4-10) provided that $f(0) = f'(0) = \cdots = f^{(\nu-1)}(0) = 0$. (4-17) is a Volterra integral equation of the second kind, the solution of which is a well-posed problem. It appears that an ill-posed problem has been converted into one which is well-posed. The ill-posedness, however, is inherent to the problem and in this case the ill-posedness is manifest in the determination of the derivatives in the Volterra-2 form, since perturbations of the data $f^{\varepsilon}(t) = f(t) + \varepsilon(t)$ are not necessarily differentiable. The one-smoothing problem exhibits the least degree of ill-posedness, since only one differentiation of the data is required. It readily apparent that the degree of ill-posedness of ν-smoothing problems increases with increasing ν and it is therefore desirable to deal with as small a value for ν as possible, should any degree of control be possible in the matter. The applied torque functions considered in Chapter 2 all produce kernel functions with finite values for ν and are therefore only exhibit slight to moderate ill-posedness. An example of an infinitely-smoothing problem is the inverse heat conduction problem (IHCP), where an undefined heat source is determined from internal temperature measurements in a solid, and is consequently a highly ill-posed problem.

In the case of this problem, the degree of smoothing ν is determined by the choice of applied torque $C(t)$. Using definition 4.2.1, it can be seen that if $C(t)$ is chosen such that the kernel function $\dot{\chi}(t)$ is a 1-smoothing kernel, then this choice of $C(t)$ produces the least ill-posed problem possible. Such a function could arguably be defined as the optimal applied torque for this experimental setup. In practical terms however, this narrows down the possible choices for an optimal applied torque, since there are a whole class of functions which satisfy this criterion.

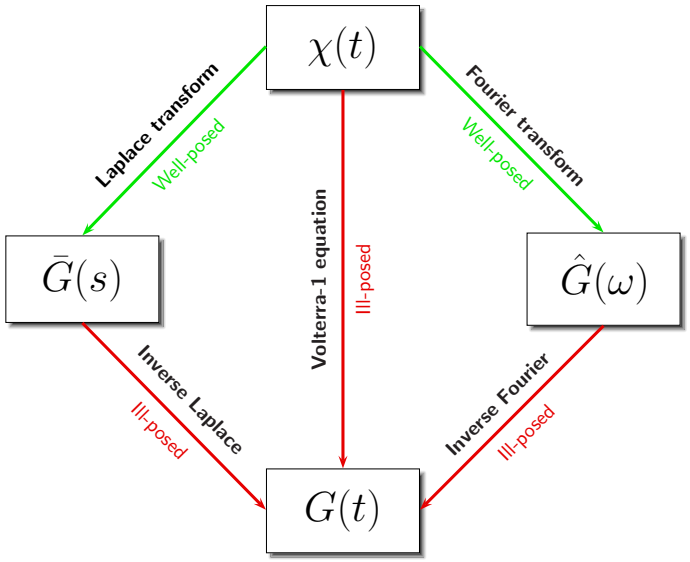

Figure 4.1: Summary of solution methods for the Volterra-1 equation.

Various methods of solution exist, but the ill-posedness still remains in the presence of perturbed data. Figure 4.1 illustrates some possibilities. The Volterra integral equation may be solved directly to obtain $G(t)$ in a single step, the ill-posedness being inherent in this process. Alternatively, integral transforms may used, such as the Fourier, Laplace or wavelet transform, resulting in an intermediate solution function. In the case of the Fourier transform, the functions $G'(\omega)$ and $G''(\omega)$ would be determined. The forward integral transform is well-posed, since the process of integration has a smoothing effect on the data perturbations and although it appears that the ill-posedness has been circumvented, it has merely been transferred to the inverse transform which may need to be performed to obtain $G(t)$ or equivalently the relaxation spectrum. Here, the direct method is considered, since it is always desirable to reduce the number of computational steps to the basic minimum.

III. STABILITY ANALYSIS

Before looking at the numerical discretization of the Volterra integral equation, it is first necessary to investigate whether conditions exist for which a stable solution to the problem can be found. This is achieved by calculating theoretical estimates for the bounds on the error in the solution in terms of the error in the measured data. The method used here is based upon the analysis in [3], in which the stability estimates of the interconversion condition (1-52) between $G(t)$ and $J(t)$ are obtained. This is a Volterra integral equation of the first kind, with data function $f(t)$ which is known

precisely and noisy kernel function $G(t-t')$ or $J(t-t')$, depending upon which of the two functions is required to be calculated. The main difference for this problem is the additional presence of noise in the data function $f(t)$, which will always be greater in magnitude than that of the kernel, since an extra degree of differentiation is involved.

To give a general overview of the method, regular perturbations are considered to represent the error in the measured data. For sake of convenience, denote the kernel function by $\Omega(t) = \dot{\chi}(t)$, so that $f(t) = k[C(t) - I\dot{\Omega}(t)]$. The noise in the measured data $\Omega(t)$ is modelled by a perturbation $\phi(t)$, for $t \in [0,T]$, so that $\left|\Omega - \Omega^{\phi}\right| \leq \|\phi\|_{\infty}$, where the L_{∞}-norm is defined $\|f\|_{\infty} = \operatorname{ess\,sup}_{t\in[0,T]} |f(t)|$. Similarly, the noisy data function f^{ε} possesses a perturbation $\varepsilon(t)$, which is related to $\phi(t)$ through differentiation of first order. The relaxation modulus, which is the function to be calculated, is assumed to have a resulting perturbation $\gamma(t)$, for which bounds in terms of $\varepsilon(t)$ and $\phi(t)$ are required to answer questions concerning stability. This produces a pair of equations, one exact and one perturbed,

$$G * \Omega = f \tag{4-18}$$

$$(G+\gamma) * (\Omega+\phi) = f + \varepsilon \tag{4-19}$$

and using the distributive property of the linear convolution operator this can be expanded to

$$G * \Omega + G * \phi + \Omega * \gamma + \phi * \gamma = f + \varepsilon. \tag{4-20}$$

Subtracting the unperturbed from the perturbed equation, performing an extra convolution with $G(t)$ and replacing $G * \Omega$ by f, the equation

$$f * \gamma = G * \epsilon - G * G * \phi - G * \phi * \gamma \tag{4-21}$$

is obtained. The remainder of the analysis is dependent upon the exact nature of the data function and may involve differentiation, the degree of which reflects the degree necessary in the solution of the Volterra-1 equation. Applying the triangular inequality and additionally Young's inequality for convolution,

$$|f * g| \leq \|f\|_1 \|g\|_{\infty} \tag{4-22}$$

where the L_1-norm on $[0,T]$ is defined

$$\|f\|_1 = \int_0^T |f| \, \mathrm{d}t, \tag{4-23}$$

a bound for $\gamma(t)$ is obtained in terms of the perturbations in the measured functions and constraints on the parameters such that the equation is consistent can be deduced.

Now, we proceed to look at some specific forms for the data function, f, using the results of Chapter 2 and determine the relative ill-posedness for each example.

4.3.1 Step Function

First, consider the step function applied torque, $C(t) = C_0 H(t - t_0)$, which produces a platen angular displacement dependent upon the model assumed for the relaxation modulus as calculated in Section 2.3.1-Section 2.3.3. Using the standard form of the analysis, problems are encountered with the exponentials in the transient function, so firstly assume that these terms can be absorbed into the perturbation term.

General form

The response for all discrete models is of the general form

$$\chi(t) = C_0 \left[\gamma_0 + \gamma_1 t + \mu(t)\right] \tag{4-24}$$

where $\gamma_0, \gamma_1 \in \mathbb{R}$ and $\mu(t)$ represents the transient function, which is a sum of exponentials, with real or complex coefficients and exponents such that overall $\mu(t)$ is a real function of t. Differentiating twice w.r.t. t, results in the data function

$$f(t) = kC_0 \left[1 - I\ddot{\mu}(t)\right], \tag{4-25}$$

and under the assumption that the term $\mu(t)$ is incorporated into the perturbation in $\Omega(t)$, i.e. $\phi(t) = -kC_0 I\ddot{\mu}(t) + \phi_0(t)$ for $t \in [0, T]$, where $\phi_0(t)$ now represents the noise, the pair of equations

$$\dot{\chi} * G = kC_0 \tag{4-26a}$$

$$G * \Omega + G * \phi + \Omega * \gamma + \phi * \gamma = kC_0 + \varepsilon(t) \tag{4-26b}$$

are obtained. Subtracting (4-26a) from (4-26b) and performing an extra convolution with $G(t)$,

$$G * \Omega * \gamma = G * \varepsilon - G * G * \phi - G * \phi * \gamma. \tag{4-27}$$

Replacing $G * \Omega$ by $f(t)$, (4-27) becomes

$$kC_0 \cdot 1 * \gamma = G * \varepsilon - G * G * \phi - G * \phi * \gamma. \tag{4-28}$$

Differentiation of (4-28), noting that

$$\frac{\mathrm{d}}{\mathrm{d}t}\left[1 * \gamma\right] = \frac{\mathrm{d}}{\mathrm{d}t}\int_0^t \gamma(t')\,\mathrm{d}t' = \gamma(t) \tag{4-29}$$

produces

$$kC_0\gamma(t) = \frac{\mathrm{d}}{\mathrm{d}t}\left[G * \varepsilon\right] - \frac{\mathrm{d}}{\mathrm{d}t}\left[G * G * \phi\right] - \frac{\mathrm{d}}{\mathrm{d}t}\left[G * \phi * \gamma\right]. \tag{4-30}$$

Applying the triangular inequality, we obtain

$$|kC_0\gamma(t)| \leq \left|\frac{\mathrm{d}}{\mathrm{d}t}\left[G * \varepsilon\right]\right| + \left|\frac{\mathrm{d}}{\mathrm{d}t}\left[G * G * \phi\right]\right| + \left|\frac{\mathrm{d}}{\mathrm{d}t}\left[G * \phi * \gamma\right]\right|. \tag{4-31}$$

The following identities are now used: the derivative identities

$$\frac{\mathrm{d}}{\mathrm{d}t}\left[f * g\right] = f_0 g(t) + \dot{f} * g \tag{4-32}$$

$$\frac{\mathrm{d}}{\mathrm{d}t}\left[f * g * h\right] = f_0 g * h + \dot{f} * g * h \tag{4-33}$$

and also Young's inequality [105] for the convolution integral, which states that

$$|f * g| \leq \|f\|_1 \|g\|_\infty \tag{4-34}$$

for $f, g \in L^1[0,T]$ and $h \in L_\infty[0,T]$ and in the case of a triple convolution

$$|f * g * h| \leq \|f\|_1 \|g\|_1 \|h\|_\infty \tag{4-35}$$

for functions $f, g \in L_1[0,T]$ and $g \in L_\infty[0,T]$. Thus, (4-31) becomes

$$kC_0\,|\gamma(t)| \leq \left[G_0 + \|\dot{G}\|_1\right]\left\{\|\varepsilon\|_\infty + \|G\|_1\|\phi\|_\infty + \|\phi\|_1\|\gamma\|_\infty\right\}. \tag{4-36}$$

Thus, we have an inequality relating the supremum of the perturbation γ in the relaxation modulus in terms of those in the measured variables,

$$\|\gamma\|_\infty \leq \frac{G_0 + \|\dot{G}\|_1}{kC_0 - (G_0 + \|\dot{G}\|_1)\|\phi\|_1}\left[\|\varepsilon\|_\infty + \|G\|_1\|\phi\|_\infty\right]. \tag{4-37}$$

For (4-37) to be consistent, the RHS must be positive and this imposes the constraint

$$\|\phi\|_1 < \frac{kC_0}{G_0 + \|\dot{G}\|_1} \tag{4-38}$$

where

$$\|\dot{G}\|_1 = \int_0^T \left|\dot{G}(t)\right|\,\mathrm{d}t = G_0 - G(T) \tag{4-39}$$

for the problem to be well-posed. Provided (4-38) is satisfied, as $\|\phi\|_\infty \to 0$ and $\|\epsilon\|_\infty \to 0$, then $\|\gamma\|_\infty \to 0$ also and a stable solution can be obtained. Conversely, if the constraint is not fulfilled, then it is indeterminate whether a stable solution exists. Note that the problem can be well-posed for both viscoelastic fluids ($G_\infty = 0$) and viscoelastic solids. Taking $T \to \infty$, it can be seen that the bound in (4-39) is less tight when $G_\infty \neq 0$, implying that the problem is more stable for a viscoelastic solid, assuming the materials being compared possess the same value for G_0.

Maxwell Model

The platen displacement for a Maxwell fluid subjected to a step function applied torque $C(t) = C_0 H(t - t_0)$ is given by (2-116) for the case where both roots are real and distinct, but this can be taken to apply to any case where the roots are distinct without loss of generality. Thus, the data function for this problem will be

$$f(t) = kC_0 \left[1 - \alpha_1 \mathrm{e}^{-\xi_1(t-t_0)} - \alpha_2 \mathrm{e}^{-\xi_2(t-t_0)}\right], \quad t \in [t_0, T] \tag{4-40}$$

where $\alpha_1 = \gamma_2 \xi_1^2$ and $\alpha_2 = \gamma_3 \xi_2^2$ in terms of the coefficients defined in (2-117c) and (2-117d). This gives rise to the pair of perturbed and unperturbed equations

$$G * \Omega = kC_0 \left[1 - \alpha_1 \mathrm{e}^{-\xi_1(t-t_0)} - \alpha_2 \mathrm{e}^{-\xi_2(t-t_0)}\right] \tag{4-41a}$$

$$(G + \gamma) * (\Omega + \phi) = kC_0 \left[1 - \alpha_1 \mathrm{e}^{-\xi_1(t-t_0)} - \alpha_2 \mathrm{e}^{-\xi_2(t-t_0)}\right] + \varepsilon(t), \quad t \in [t_0, T]. \tag{4-41b}$$

Subtracting (4-41a) from (4-41a) and performing an extra convolution with $G(t)$ results in

$$kC_0 \left[1 - \alpha_1 \mathrm{e}^{-\xi_1(t-t_0)} - \alpha_2 \mathrm{e}^{-\xi_2(t-t_0)}\right] * \gamma = G * \varepsilon - G * G * \phi - G * \phi * \gamma. \tag{4-42}$$

Noting that

$$\frac{\mathrm{d}}{\mathrm{d}t}\left[\mathrm{e}^{-\xi t} * \gamma(t)\right] = \gamma(t) - \xi \mathrm{e}^{-\xi t} * \gamma, \tag{4-43}$$

upon differentiating once, the LHS of (4-42) becomes

$$\frac{\mathrm{d}}{\mathrm{d}t}[f * \gamma] = kC_0 \left[(1 - \alpha_1 - \alpha_2)\gamma(t) + \alpha_1 \xi_1 \mathrm{e}^{-\xi_1 t} * \gamma + \alpha_2 \xi_2 \mathrm{e}^{-\xi_2 t} * \gamma\right], \tag{4-44}$$

but since $1 - \alpha_1 - \alpha_2 = 0$, the first term vanished to leave the terms involving the convolution of exponential terms with $\gamma(t)$.

Applying the triangular inequality, and using the derivative identities (4-32)-(4-33),

$$kC_0 \left| \left[\alpha_1 \xi_1 \, \mathrm{e}^{-\xi_1 (t-t_0)} + \alpha_2 \xi_2 \, \mathrm{e}^{-\xi_2 (t-t_0)} \right] * \gamma \right| \leq G_0 \left| \varepsilon(t) \right| + \left| \dot{G} * \varepsilon \right| + G_0 \left| G * \phi \right| + \left| \dot{G} * G * \phi \right| + G_0 \left| \phi * \gamma \right| + \left| \dot{G} * \phi * \gamma \right| . \quad (4\text{-}45)$$

Using the convolution inequalities from (4-34) and (4-35),

$$kC_0 \left| \left[\alpha_1 \xi_1 \, \mathrm{e}^{-\xi_1 (t-t_0)} + \alpha_2 \xi_2 \, \mathrm{e}^{-\xi_2 (t-t_0)} \right] * \gamma \right| \leq \left[G_0 + \| \dot{G} \|_1 \right] \left[\| \varepsilon \|_\infty + \| G \|_1 \| \phi \|_\infty + \| \phi \|_1 \| \gamma \|_\infty \right] . \quad (4\text{-}46)$$

Furthermore, using the sharp form of Young's inequality with suitably defined $0 < \beta \leq 1$, (see (A-27)), this can be rewritten in the form

$$\| \gamma \|_\infty \leq \frac{\left[G_0 + \| \dot{G} \|_1 \right]}{C_1 - C_2} \left[\| \varepsilon \|_\infty + \| G \|_1 \| \phi \|_\infty \right] \quad (4\text{-}47)$$

where the constants $C_{1,2} \in \mathbb{R}$ are defined

$$C_1 = kC_0 \beta \| \alpha_1 \xi_1 \, \mathrm{e}^{-\xi_1 t} + \alpha_2 \xi_2 \, \mathrm{e}^{-\xi_2 t} \|_1 \quad (4\text{-}48)$$

$$C_2 = \left[G_0 + \| \dot{G} \|_1 \right] \| \phi \|_1 \quad (4\text{-}49)$$

and

$$\| \dot{G} \|_1 = \int_0^{T-t_0} \left| \dot{G}(t) \right| \, \mathrm{d}t = g \left[1 - \mathrm{e}^{-\frac{T-t_0}{\lambda}} \right] . \quad (4\text{-}50)$$

For (4-47) to be consistent, it is required that $C_1 - C_2 > 0$. In the case where the roots $\xi_{1,2}$ are real and distinct, a more specific form can be obtained. The integrand in C_1 is a monotone decreasing function, since the Laplace transform has poles which lie on the negative real axis, so

$$C_1 = kC_0 \beta \left[\alpha_1 \left(1 - \mathrm{e}^{-\xi_1 (T-t_0)} \right) + \alpha_2 \left(1 - \mathrm{e}^{-\xi_2 (T-t_0)} \right) \right] \quad (4\text{-}51)$$

hence for well-posedness, it is sufficient that

$$\| \phi \|_1 < \frac{kC_0 \beta}{g \left(2 - \mathrm{e}^{-\frac{T-t_0}{\lambda}} \right)} \left[1 - \alpha_1 \, \mathrm{e}^{-\xi_1 (T-t_0)} - \alpha_2 \, \mathrm{e}^{-\xi_2 (T-t_0)} \right] . \quad (4\text{-}52)$$

For the complex case, this represents a minimum value for C_1, since the absolute integral of the decaying oscillatory function will be larger in magnitude than integral of the standard function. In the case where $I = 0$, the problem reduces to the canonical example with $f(t) = 1$ and the restriction on the error is

$$\| \phi \|_1 < \frac{kC_0}{g \left(2 - \mathrm{e}^{-\frac{T-t_0}{\lambda}} \right)} \quad (4\text{-}53)$$

which indicates that the range for which $\| \phi \|_1$ allows a stable solution is less tight than for a finite value for the inertia.

N-mode Maxwell

Generalizing to a Maxwell model with N relaxation times, the platen displacement from (2-130) and (2-125) gives a data function of the form

$$f(t) = kC_0 \left[1 - \sum_{i=1}^{N+1} \alpha_i' \, \mathrm{e}^{-\xi_i'(t-t_0)} \right] \tag{4-54}$$

for a viscoelastic fluid ($G_\infty = 0$) with $\alpha_i' = \nu_i' \xi_i'^2, i = 1, 2, \ldots, N+1$ and

$$f(t) = kC_0 \left[1 - \sum_{i=1}^{N+2} \alpha_i \, \mathrm{e}^{-\xi_i(t-t_0)} \right] \tag{4-55}$$

for a viscoelastic solid ($G_\infty \neq 0$) with $\alpha_i = \nu_i \xi_i^2, i = 1, 2, \ldots, N+1$, respectively. Since these are similar in nature, we need only consider the analysis for the first case.

The pair of perturbed and unperturbed equations for this problem are

$$G * \Omega = kC_0 \left(1 - \sum_{i=1}^{N+1} \alpha_i' \, \mathrm{e}^{-\xi_i'(t-t_0)} \right) \tag{4-56a}$$

$$(G + \gamma) * (\Omega + \phi) = kC_0 \left(1 - \sum_{i=1}^{N+1} \alpha_i' \, \mathrm{e}^{-\xi_i'(t-t_0)} \right) + \varepsilon \tag{4-56b}$$

and proceeding in the usual manner by taking the difference of the pair and performing an extra convolution with $G(t)$ results in

$$kC_0 \left(1 - \sum_{i=1}^{N+1} \alpha_i' \, \mathrm{e}^{-\xi_i'(t-t_0)} \right) * \gamma = G * \varepsilon - G * G * \phi - G * \phi * \gamma. \tag{4-57}$$

Differentiation is required to remove the $1 * \gamma$ term, whence the LHS becomes

$$\frac{\mathrm{d}}{\mathrm{d}t} \left[\left(1 - \sum_{i=1}^{N+1} \alpha_i' \, \mathrm{e}^{-\xi_i'(t-t_0)} \right) * \gamma \right] = \left(1 - \sum_{i=1}^{N+1} \alpha_i' \right) \gamma(t) + \sum_{i=1}^{N+1} \alpha_i' \xi_i' \, \mathrm{e}^{-\xi_i'(t-t_0)} * \gamma. \tag{4-58}$$

Now, $\ddot{\chi}(0) = \frac{C_0}{I} \sum_{i=1}^{N+1} \alpha_i'$. Applying the initial value theorem to the Laplace transform in (2-128), $\lim_{t \to 0} \ddot{\chi}(t) = \lim_{s \to \infty} s \bar{\ddot{\chi}}(s) = \lim_{s \to \infty} s^3 \bar{\chi}(s) = \frac{C_0}{I}$, so the coefficient of $\gamma(t)$ is zero, leaving only the convolution of the exponential terms with γ. The derivative of the RHS is evaluated using (4-32)-(4-33) and after applying Young's inequality (4-34) for the convolution integral, we obtain

$$kC_0 \left| \sum_{i=1}^{N+1} \alpha_i' \, \mathrm{e}^{-\xi_i'(t-t_0)} * \gamma \right| \leq \left[G_0 + \|\dot{G}\|_1 \right] \left[\|\varepsilon\|_\infty + \|G\|_1 \|\phi\|_\infty + \|\phi\|_1 \|\gamma\|_\infty \right]. \tag{4-59}$$

Using the sharp form for Young's inequality with suitably defined $0 < \beta \leq 1$ as in (4-145), this can be rearranged into the form

$$\|\gamma\|_\infty \leq \left[\frac{G_0 + \|\dot{G}\|_1}{C_1 - C_2}\right] [\|\varepsilon\|_\infty + \|G\|_1 \|\phi\|_\infty] \tag{4-60}$$

where the constants $C_{1,2} \in \mathbb{R}$ are defined

$$\begin{aligned} C_1 &= k\beta C_0 \| \sum_{i=1}^{N+1} \alpha_i' \xi_i' \, \mathrm{e}^{-\xi_i'(t-t_0)} \|_1 \\ &= k\beta C_0 \int_{t_0}^{T} \left| \sum_{i=1}^{N+1} \alpha_i' \xi_i' \, \mathrm{e}^{-\xi_i'(t-t_0)} \right| \mathrm{d}t \end{aligned} \tag{4-61}$$

$$C_2 = \left[G_0 + \|\dot{G}\|_1\right] \|\phi\|_1 \tag{4-62}$$

For the problem to be well-posed, (4-60) must be consistent, hence $C_1 - C_2 > 0$. At least $N - 1$ of the parameters ξ_i' must be real-valued and the remaining pair can be either real and distinct, real and repeated or complex conjugate. If all $N + 1$ roots are real and distinct, the integrand in (4-61) is monotone decreasing to 0 as $t \to \infty$, thus

$$\|\phi\|_1 < \frac{k\beta C_0}{\sum_{i=1}^{N} g \left(2 - \mathrm{e}^{-\frac{T-t_0}{\lambda}}\right)} \left| \sum_{i=1}^{N+1} \alpha_i' \left(1 - \mathrm{e}^{-\xi_i'(T-t_0)}\right) \right|. \tag{4-63}$$

Similarly, for a viscoelastic solid ($G_\infty > 0$), the criterion for well-posedness is

$$\|\phi\|_1 < \frac{k\beta C_0}{G_\infty + \sum_{i=1}^{N} g \left(2 - \mathrm{e}^{-\frac{T-t_0}{\lambda}}\right)} \left| \sum_{i=1}^{N+2} \alpha_i \left(1 - \mathrm{e}^{-\xi_i(T-t_0)}\right) \right|, \tag{4-64}$$

which can be satisfied for suitably chosen parameters, hence the problem can be well-posed for both viscoelastic fluid and solid materials.

Newtonian Fluid

Although the problem for a Newtonian fluid is not a Volterra integral equation of the first kind *sensu stricto*, since the relaxation modulus may be obtained directly by evaluating the first and second order derivatives of $\chi(t)$, error bounds can still be obtained by the same method as that applied to the viscoelastic models.

The expression for $\chi(t)$ in (2-112) indicates that the data function for this problem takes the form

$$f(t) = kC_0 \left[1 - \mathrm{e}^{-\frac{\eta(t-t_0)}{kI}}\right], \quad t \in [0, T] \tag{4-65}$$

and the pair of equations are now

$$G * \Omega = kC_0 \left[1 - \mathrm{e}^{-\frac{\eta(t-t_0)}{kI}}\right] \tag{4-66a}$$

$$(G+\gamma) * (\Omega+\phi) = kC_0 \left[1 - \mathrm{e}^{-\frac{\eta(t-t_0)}{kI}}\right] + \varepsilon(t). \tag{4-66b}$$

Subtracting the former from the latter, performing an extra convolution with $G(t)$ and replacing the exact $f(t)$ by the expression in (4-65),

$$kC_0 \left[1 - \mathrm{e}^{-\frac{\eta(t-t_0)}{kI}}\right] * \gamma = G * \varepsilon - G * G * \phi - G * \phi * \gamma. \tag{4-67}$$

The relaxation modulus for the Newtonian fluid is $G(t) = \eta\delta(t)$, and since the delta function represents the identity w.r.t. convolution, i.e.

$$\delta * f = \int_0^t \delta(t'-t) f(t')\,\mathrm{d}t = f(t), \tag{4-68}$$

then (4-67) reduces to

$$kC_0 \left[1 - \mathrm{e}^{-\frac{\eta(t-t_0)}{kI}}\right] * \gamma = \eta\varepsilon(t) - \eta^2\phi(t) - \eta\phi * \gamma. \tag{4-69}$$

Upon differentiation of first order,

$$\frac{\eta C_0}{I}\,\mathrm{e}^{-\frac{\eta(t-t_0)}{kI}} * \gamma = \eta\frac{\mathrm{d}\varepsilon}{\mathrm{d}t} - \eta^2\frac{\mathrm{d}\phi}{\mathrm{d}t} - \eta\phi_0\gamma(t) - \eta\dot{\phi} * \gamma \tag{4-70}$$

and applying the triangular inequality and the convolution identities (4-34)-(4-35),

$$\begin{aligned}\frac{C_0}{I}\left|\mathrm{e}^{-\frac{\eta(t-t_0)}{kI}} * \gamma\right| &\leq |\dot{\varepsilon}| + \eta\,|\dot{\phi}| + |\phi_0|\,|\dot{\phi} * \gamma| \\ &\leq \|\dot{\varepsilon}\|_\infty + \eta\|\dot{\phi}\|_\infty + |\phi_0|\,\|\gamma\|_\infty + \|\dot{\phi}\|_1\|\gamma\|_\infty.\end{aligned} \tag{4-71}$$

Using the sharp form of the convolution inequality with suitably chosen $0 < \beta \leq 1$ (see (4-145)), the following bound is obtained for the perturbation in the solution $G(t)$.

$$\|\gamma\|_\infty \leq \frac{1}{C_1 - C_2}\left[\|\dot{\varepsilon}\|_\infty + \|\phi\|_\infty\right] \tag{4-72}$$

where the constants $C_{1,2} \in \mathbb{R}$ are defined

$$\begin{aligned}C_1 &= \frac{C_0\beta}{I}\left\|\mathrm{e}^{-\frac{\eta(t-t_0)}{kI}}\right\|_1 \\ &= \frac{kC_0\beta}{\eta}\left[1 - \mathrm{e}^{-\frac{\eta(T-t_0)}{kI}}\right]\end{aligned} \tag{4-73}$$

$$C_2 = |\phi_0| + \|\dot{\phi}\|_1 \tag{4-74}$$

and hence for well-posedness, it is required that

$$|\phi_0| + \|\dot{\phi}\|_1 \leq \frac{kC_0\beta}{\eta}\left[1 - \mathrm{e}^{-\frac{\eta(T-t_0)}{kI}}\right]. \tag{4-75}$$

Note that the maximum value for the RHS is achieved as $T \to \infty$, indicating that the longer the experimental time the larger the maximum data error can be while still remaining well-posed. Note that the Newtonian problem is more ill-posed than that for the Maxwell model, since it is required that $\dot{\phi} \in L_1[0,T]$ rather than $\phi \in L_1[0,T]$.

4.3.2 Box Function

Now consider an applied torque in the form of the box function $C(t) = C_0[H(t-t_0) - H(t-t_1)]$, which is also a 2-smoothing problem with $\chi(t_0) = \dot{\chi}(t_0) = 0$. In this case, only the analysis for the Maxwell model is included.

Maxwell Model

The platen displacement was determined in (2.3.2) in terms of the displacement for the step function. The data function for this problem is therefore

$$f_{bf}(t) = kC_0\left[B(t) - \left(\dot{\Omega}(t-t_0)H(t-t_0) - \dot{\Omega}(t-t_1)H(t-t_1)\right)\right] \tag{4-76}$$

where $B(t) = H(t-t_0) - H(t-t_1)$ denotes the unit box function. The pair of exact and perturbed equations are therefore

$$G * \Omega = kC_0\left[B(t) - \left(\dot{\Omega}(t-t_0)H(t-t_0) - \dot{\Omega}(t-t_1)H(t-t_1)\right)\right] \tag{4-77a}$$

$$(G+\gamma) * (\Omega+\phi) = kC_0\left[B(t) - \left(\dot{\Omega}(t-t_0)H(t-t_0) - \dot{\Omega}(t-t_1)H(t-t_1)\right)\right] + \varepsilon(t) \tag{4-77b}$$

Subtracting the exact from the perturbed equation, performing an extra convolution with $G(t)$ and replacing $G * \Omega$ by $f_{bf}(t)$, we obtain

$$f_{bf}(t) * \gamma = G * \varepsilon - G * G * \phi - G * \phi * \gamma \tag{4-78}$$

and after differentiation,

$$\frac{\mathrm{d}}{\mathrm{d}t}\left[f_{bf} * \gamma\right] = G_0\varepsilon(t) + \dot{G} * \varepsilon - G_0 G * \phi - \dot{G} * G * \phi - G_0\phi * \gamma - \dot{G} * \phi * \gamma \tag{4-79}$$

where

$$\frac{\mathrm{d}}{\mathrm{d}t}\left[f_{bf} * \gamma\right] = kC_0\left\{\left[\alpha_1\xi_1\,\mathrm{e}^{-\xi_1(t-t_0)} + \alpha_2\xi_2\,\mathrm{e}^{-\xi_2(t-t_0)}H(t-t_0) * \gamma\right] - \left[\alpha_1\xi_1\,\mathrm{e}^{-\xi_1(t-t_0)} + \alpha_2\xi_2\,\mathrm{e}^{-\xi_2(t-t_1)}\right] * \gamma\right\} \tag{4-80}$$

since $1 - \alpha_1 - \alpha_2 = 0$. Denoting the RHS of (4-80) by $kC_0D_1(t)$ and applying the triangular inequality,

$$kC_0 \left| D_1 * \gamma \right| \leq G_0 \left| \varepsilon(t) \right| + \left| \dot{G} * \varepsilon \right| + G_0 \left| G * \phi \right| + \left| \dot{G} * G * \phi \right| + G_0 \left| \phi * \gamma \right| + \left| \dot{G} * \phi * \gamma \right| \tag{4-81}$$

and additionally the convolution inequalities (4-34)-(4-35),

$$kC_0 \left| D_1 * \gamma \right| \leq \left[G_0 + \|\dot{G}\|_1 \right] \left[\|\varepsilon\|_\infty + \|G\|_1 \|\phi\|_\infty + \|\phi\|_1 \|\gamma\|_\infty \right]. \tag{4-82}$$

For an appropriate value for $0 < \beta \leq 1$ (see (4-146)), this can be expressed in the form

$$\|\gamma\|_\infty \leq \frac{g\left(2 - \mathrm{e}^{-\frac{T-t_0}{\lambda}}\right)}{C_1 - C_2} \left[\|\varepsilon\|_\infty + \lambda g \left(1 - \mathrm{e}^{-\frac{T-t_0}{\lambda}}\right) \|\phi\|_\infty \right] \tag{4-83}$$

where the constants $C_{1,2} \in \mathbb{R}$ are defined

$$C_1 = kC_0\beta \|D_1\|_1 \tag{4-84a}$$

$$C_2 = g\left(2 - \mathrm{e}^{-\frac{T-t_0}{\lambda}}\right) \|\phi\|_1 \tag{4-84b}$$

For well-posedness, the RHS must be strictly positive, so $C_1 - C_2 > 0$ or equivalently

$$\|\phi\|_1 < \frac{kC_0\beta \|D_1\|_1}{g\left(2 - \mathrm{e}^{-\frac{T-t_0}{\lambda}}\right)}. \tag{4-85}$$

The norm $\|D_1\|_1$ is evaluated from

$$\begin{aligned} \|D\|_1 = &\int_{t_0}^{t_1} \left| \alpha_1\xi_1 \mathrm{e}^{-\xi_1(t-t_0)} + \alpha_2\xi_2 \mathrm{e}^{-\xi_2(t-t_0)} \right| \mathrm{d}t \\ &+ \int_{t_1}^{T} \left| \alpha_1\xi_1 \left(\mathrm{e}^{-\xi_1(t-t_0)} - \mathrm{e}^{-\xi_1(t-t_1)} \right) + \alpha_2\xi_2 \left(\mathrm{e}^{-\xi_1(t-t_0)} - \mathrm{e}^{-\xi_1(t-t_1)} \right) \right| \mathrm{d}t \end{aligned} \tag{4-86}$$

and noting that

$$\|D_1\|_1 \leq \int_0^T \left| \alpha_1\xi_1 \mathrm{e}^{-\xi_1 t} + \alpha_2\xi_2 \mathrm{e}^{-\xi_2 t} \right| \mathrm{d}t \tag{4-87}$$

it can be seen that the value $\|D_1\|_1$ is maximized by letting $t_0 \to 0$ and $t_1 \to T$, or equivalently maximizing the quantity $t_1 - t_0$. Essentially, this implies that the solution for the step function is more stable in general than that for the box function. If the box function is used as an applied torque, the quantity $t_1 - t_0$ should be increased as to as long a time as the experimental setup will allow. Provided $\phi \in L_1[0, T]$ and the constraint in (4-85) is satisfied, a stable solution should exist.

4.3.3 Slope/Ramp Function

Now consider the slope function $C(t) = C_0 t H(t)$ as an applied torque, using the results of Section 2.4 to provide the relevant functions in the foregoing analysis. In a similar fashion to the step function analysis, first consider the simpler case where the transient component of the response is assumed to be incorporated into the perturbation in the data function, $f(t)$, for a general viscoelastic material.

General form

In general the response for a discrete viscoelastic model corresponds to a data function of the form

$$f(t) = kC_0 \left[t - I\ddot{\mu}(t)\right], \tag{4-88}$$

where $\mu(t)$ represents the transient function compose of a sum of exponentials. Assuming the noisy data is represented by a perturbation $\varepsilon(t)$ in the data function $f(t)$ and $\phi(t)$ in the measured data for $\dot{\chi}(t)$, and that the transient function is incorporated into the former perturbation, the following pair of equations are obtained:

$$\dot{\chi} * G = kC_0 t \tag{4-89a}$$

$$G * \Omega + G * \phi + \Omega * \gamma + \phi * \gamma = kC_0 t + \varepsilon(t). \tag{4-89b}$$

Subtracting (4-89a) from (4-89b), performing an extra convolution with $G(t)$ and replacing $G * \Omega$ by $f(t)$, we obtain

$$t * \gamma = G * \epsilon - G * G * \phi. \tag{4-90}$$

Differentiation of second order is required to reduce the LHS to a more amenable form, reflecting the additional degree of differentiation required over the step function to solve the Volterra-1 problem. First, note that

$$\frac{\mathrm{d}^2}{\mathrm{d}t^2}\left[t * \gamma\right] = \frac{\mathrm{d}}{\mathrm{d}t}\left[1 * \gamma\right] = \gamma(t). \tag{4-91}$$

Applying the triangular inequality,

$$kC_0 \left|\gamma(t)\right| \leq \left|\frac{\mathrm{d}^2}{\mathrm{d}t^2}\left[G * \varepsilon\right]\right| + \left|\frac{\mathrm{d}^2}{\mathrm{d}t^2}\left[G * G * \phi\right]\right| + \left|\frac{\mathrm{d}^2}{\mathrm{d}t^2}\left[G * \phi * \gamma\right]\right| \tag{4-92}$$

and the remaining terms can be evaluated using derivative identities for convolution integrals are given by

$$\frac{\mathrm{d}^2}{\mathrm{d}t^2}\left[f * g\right] = g_0 \frac{\mathrm{d}f}{\mathrm{d}t} + f_0 \frac{\mathrm{d}g}{\mathrm{d}t} + \dot{f} * \dot{g} \tag{4-93}$$

$$\frac{\mathrm{d}^2}{\mathrm{d}t^2}\left[f * g * h\right] = f_0 g_0 h(t) + f_0 \dot{g} * h + g_0 \dot{f} * h + \dot{f} * \dot{g} * h. \tag{4-94}$$

Additionally, using Young's inequality (4-34)

$$kC_0\,|\gamma(t)| \leq G_0\|\dot{\varepsilon}\|_\infty + \left|\dot{G}_0\right|\left[1+\|\ddot{G}\|_1\right]\|\varepsilon\|_\infty + \left[G_0+\|\dot{G}\|_1\right]^2\|\phi\|_\infty + \left[|\phi_0|+\|\dot{\phi}\|_1\right]\left[G_0+\|\dot{g}\|_1\right]\|\gamma\|_\infty \quad (4\text{-}95)$$

which is of the equivalent form

$$\|\gamma\|_\infty \leq \frac{1}{kC_0-C_1}\left\{G_0\|\dot{\varepsilon}\|_\infty + \left|\dot{G}_0\right|\left[1+\|\ddot{G}\|_1\right]\|\varepsilon\|_\infty + \left[G_0+\|\dot{G}\|_1\right]^2\|\phi\|_\infty\right\}, \quad (4\text{-}96)$$

where the constant $C_1 \in \mathbb{R}$ is defined

$$C_1 = \left[|\phi_0|+\|\dot{\phi}\|_1\right]\left[G_0+\|\dot{G}\|_1\right]. \quad (4\text{-}97)$$

and since the domain is finite on $[0,T]$, the L_1-norms are defined

$$\|\dot{G}\|_1 = \int_0^T \left|\dot{G}\right|\,\mathrm{d}t = G(0)-G(T) \quad (4\text{-}98)$$

$$\|\ddot{G}\|_1 = \int_0^T \left|\ddot{G}\right|\,\mathrm{d}t = \dot{G}(T)-\dot{G}(0) \quad (4\text{-}99)$$

by monotonicity of the relaxation modulus and its derivatives. For the problem to be well-posed, it is required that $kC_0 - C_1 > 0$, i.e.

$$|\phi_0|+\|\dot{\phi}\|_1 < \frac{1}{2G_0-G(T)}. \quad (4\text{-}100)$$

Thus, when considering an applied torque in the form of $C(t) = tH(t)$, it is not only required that the perturbation $\phi(t)$ in $\Omega(t)$ is differentiable, but also that the L_1-norm on $[0,T]$ is sufficiently small. This is a notably stricter requirement than for the case where the applied torque takes the form of a step function, since the perturbations in the measured data are not necessarily differentiable. Taking $T \to \infty$, it can be seen that the problem can be well-posed for both viscoelastic solids and liquids, although the latter is more ill-posed since the RHS of (4-100) will be smaller, provided materials with the same value for $G(0)$ are compared.

Although the analysis is not included here, it can be inferred that higher order polynomials for the applied torque will impose stricter constraints on the admissible noise levels. For $C(t) = t^2$, the perturbation would be required to satisfy $\ddot{\phi} \in L_1[0,T]$ and be twice differentiable, and so on. Thus, it is unproductive to consider higher orders for this problem.

Now we proceed to consider each of the viscoelastic models considered in Section 2.4 to obtain stability estimates which take into account the transient function.

Maxwell Model

When subjected to a slope function $C(t) = C_0 t H(t)$, the form of the platen response was calculated for the Maxwell model in Section 2.4.2. Thus, in this case the data function takes the form

$$f(t) = kC_0 \left[t - 2\gamma_2 - \alpha_1 \mathrm{e}^{-\xi_1 t} - \alpha_2 \mathrm{e}^{-\xi_2 t} \right], \tag{4-101}$$

where $\alpha_1 = \gamma_3 \xi_1^2$ and $\alpha_2 = \gamma_4 \xi_2^2$, and the pair of working equations are

$$G * \Omega = kC_0 \left[t - 2\gamma_2 - \alpha_1 \xi_1^2 \mathrm{e}^{-\xi_1 t} - \alpha_2 \mathrm{e}^{-\xi_2 t} \right] \tag{4-102a}$$

$$(G + \gamma) * (\Omega + \phi) = kC_0 \left[t - 2\gamma_2 - \alpha_1 \xi_1^2 \mathrm{e}^{-\xi_1 t} - \alpha_2 \mathrm{e}^{-\xi_2 t} \right] + \varepsilon(t). \tag{4-102b}$$

Subtracting (4-102a) from (4-102b) and performing an extra convolution with $G(t)$,

$$kC_0 \left[t - 2\gamma_2 - \alpha_1 \xi_1^2 \mathrm{e}^{-\xi_1 t} - \alpha_2 \mathrm{e}^{-\xi_2 t} \right] * \gamma = G * \varepsilon - G * G * \phi - G * \phi * \gamma. \tag{4-103}$$

Comparison with the canonical case (4-90) indicates that second order differentiation is required to remove the $t * \gamma$, whence the LHS becomes

$$\frac{\mathrm{d}^2}{\mathrm{d}t^2} \left[f * \gamma \right] = -(\alpha_1 + \alpha_2 + 2\gamma_2)\dot{\gamma}(t) + (1 + \alpha_1 \xi_1 + \alpha_2 \xi_2)\gamma(t) - \left[\alpha_1 \xi_1^2 \mathrm{e}^{-\xi_1 t} + \alpha_2 \xi_2^2 \mathrm{e}^{-\xi_2 t} \right] * \gamma \tag{4-104}$$

which simplifies considerably, since $\alpha_1 + \alpha_2 + 2\gamma_2 = 0$ and $1 + \alpha_1 \xi_1 + \alpha_2 \xi_2 = 0$. The second derivative of the RHS is evaluated using (4-93)-(4-94) and after applying the triangular inequality and convolution inequalities (4-34)-(4-35), (4-103) becomes the inequality

$$kC_0 \left| \left[\alpha_1 \xi_1^2 \mathrm{e}^{-\xi_1 t} + \alpha_2 \xi_2^2 \mathrm{e}^{-\xi_2 t} \right] * \gamma \right| \leq G_0 \|\dot{\varepsilon}\|_\infty + \left[G_0 + \|\ddot{G}\|_1 \right] \|\varepsilon\|_\infty + \left[G_0 + \|\dot{G}\|_1 \right]^2 \|\phi\|_\infty + \left[G_0 + \|\dot{G}\|_1 \right] \left[|\phi_0| + \|\dot{\phi}\|_1 \right] \|\gamma\|_\infty. \tag{4-105}$$

This can be rearranged, using a suitably chosen value for $0 < \beta \leq 1$ (see (4-145)), to give

$$\|\gamma\|_\infty \leq \frac{1}{C_1 - C_2} \left\{ g \|\dot{\varepsilon}\|_\infty + \left[g + \tfrac{g}{\lambda} \left(1 - \mathrm{e}^{-\frac{T}{\lambda}} \right] \right) \|\varepsilon\|_\infty + \left[g \left(2 - \mathrm{e}^{-\frac{T}{\lambda}} \right) \right]^2 \|\phi\|_\infty \right\} \tag{4-106}$$

with constants $C_{1,2} \in \mathbb{R}$ defined by

$$C_1 = kC_0\beta\left\|\alpha_1\xi_1^2\,\mathrm{e}^{-\xi_1 t} + \alpha_2\xi_2^2\,\mathrm{e}^{-\xi_2 t}\right\|_1 \tag{4-107}$$

$$C_2 = \left[G_0 + \|\dot{G}\|_1\right]\left[|\phi_0| + \|\dot{\phi}\|_1\right]. \tag{4-108}$$

For the problem to be well-posed, $C_1 - C_2 > 0$ must be satisfied, i.e.

$$|\phi_0| + \|\dot{\phi}\|_1 < \frac{kC_0\beta}{g\left(2 + \mathrm{e}^{-\frac{T}{\lambda}}\right)}\left\|\alpha_1\xi_1^2\,\mathrm{e}^{-\xi_1 t} + \alpha_2\xi_2^2\,\mathrm{e}^{-\xi_2 t}\right\|_1 \tag{4-109}$$

Thus, for a stable solution to the problem to exist, the perturbations in the measured data must not only be differentiable, but also it is a requirement that $\dot{\phi} \in L_1[0,T]$. In the case where $\xi_{1,2} \in \mathbb{R}$ and are distinct, the L_1-norm in C_1 can be evaluated easily since the function is a monotonically decreasing function, wherefore the stability criterion becomes

$$|\phi_0| + \|\dot{\phi}\|_1 < \frac{kC_0\beta}{g\left(2 + \mathrm{e}^{-\frac{T}{\lambda}}\right)}\left|\alpha_1\xi_1\left(1 - \mathrm{e}^{-\xi_1 t}\right) + \alpha_2\xi_2\left(1 - \mathrm{e}^{-\xi_2 t}\right)\right|. \tag{4-110}$$

As $T \to \infty$, and assuming that since $\Omega(0) = 0$ then $\phi(0) = 0$, this reduces to

$$\|\dot{\phi}\|_1 < \frac{kC_0\beta}{g}. \tag{4-111}$$

N-Mode Maxwell Model

Extending the analysis to a general discrete N-mode relaxation spectrum, the platen displacement from (2-156) gives a data function of the form

$$f(t) = kC_0\left[t - \sum_{i=1}^{N+2}\alpha_i\,\mathrm{e}^{-\xi_i t}\right] \tag{4-112}$$

for a viscoelastic solid ($G_\infty > 0$) and

$$f(t) = kC_0\left[t - 2\mu_2 - \sum_{i=1}^{N+1}\alpha_i'\,\mathrm{e}^{-\xi_i' t}\right] \tag{4-113}$$

for a viscoelastic liquid ($G_\infty = 0$), where $\alpha_i = \nu_i\xi_i^2$ and $\alpha_i' = \nu_i'\xi_i'$.

Case 1. $G_\infty > 0$: For a viscoelastic solid, the pair of unperturbed and perturbed equations are

$$G * \Omega = kC_0\left[t - \sum_{i=1}^{N+2}\alpha_i\,\mathrm{e}^{-\xi_i t}\right] \tag{4-114a}$$

$$(G + \gamma) * (\Omega + \phi) = kC_0\left[t - \sum_{i=1}^{N+2}\alpha_i\,\mathrm{e}^{-\xi_i t}\right] + \varepsilon(t). \tag{4-114b}$$

Proceeding in the usual manner, by subtracting the first from the last equation and performing an extra convolution with $G(t)$, we obtain

$$kC_0\left[t-\sum_{i=1}^{N+2}\alpha_i\,\mathrm{e}^{-\xi_i t}\right]*\gamma = G*\varepsilon - G*G*\phi - G*\phi*\gamma. \tag{4-115}$$

Differentiating twice to remove the $t*\gamma$ term, the LHS becomes

$$\frac{\mathrm{d}^2}{\mathrm{d}t^2}\left[f*\gamma\right] = kC_0\left[\left(1-\sum_{i=1}^{N+2}\alpha_i\nu_i\right)\gamma(t) - \sum_{i=1}^{N+2}\alpha_i\dot{\gamma}(t) - \sum_{i=1}^{N+2}\alpha_i\nu_i^2\,\mathrm{e}^{-\xi_i t}*\gamma\right] \tag{4-116}$$

Note that $\sum_{i=1}^{N+2}\alpha_i = \frac{I}{C_0}\ddot{\chi}(0) = 0$ and also that $\sum_{i=1}^{N+2}\alpha_i\nu_i = -\frac{I}{C_0}\chi^{(3)}(0) = -1$, so the LHS simplifies to the convolution of $\gamma(t)$ with the exponential terms. The second derivative of the RHS is obtained using (4-93)-(4-94), and after applying the triangular inequality and additionally the convolution inequalities (4-34)-(4-35), the following inequality is attained.

$$kC_0\left|\sum_{i=1}^{N+1}\alpha_i\xi_i^2\,\mathrm{e}^{-\xi_i t}*\gamma\right| \le G_0\|\ddot{\varepsilon}\|_\infty + \left[\left|\dot{G}_0\right| + \|\ddot{G}\|_1\right]\|\varepsilon\|_\infty + \left[G_0+\|\dot{G}\|_1\right]^2\|\phi\|_\infty$$
$$+\left[G_0+\|\dot{G}\|_1\right]\left[|\phi_0|+\|\dot{\phi}\|_1\right] \tag{4-117}$$

Using the sharp form of Young's inequality for the convolution integral on the LHS with an appropriate choice of $0<\beta\le 1$ (see (4-145)), the bound on $\gamma(t)$ obtained is of the form

$$\|\gamma\|_\infty \le \frac{1}{C_1-C_2}\left\{G_0\|\ddot{\varepsilon}\|_\infty + \left[\left|\dot{G}_0\right| + \|\ddot{G}\|_1\right]\|\varepsilon\|_\infty + \left[G_0+\|\dot{G}\|_1\right]^2\|\phi\|_\infty\right\} \tag{4-118}$$

with constants $C_{1,2}\in\mathbb{R}$ defined by

$$C_1 = kC_0\beta\left\|\sum_{i=1}^{N+2}\nu_i\xi_i^4\,\mathrm{e}^{-\xi_i t}\right\|_1 \tag{4-119a}$$

$$C_2 = \left[G_0+\|\dot{G}\|_1\right]\left[|\phi_0|+\|\dot{\phi}\|_1\right] \tag{4-119b}$$

and

$$\|\dot{G}\|_1 = \sum_{i=1}^{N} g_i\left(1-\mathrm{e}^{-\frac{T}{\lambda_i}}\right) \tag{4-120}$$

$$\|\ddot{G}\|_1 = \sum_{i=1}^{N}\frac{g_i}{\lambda_i}\left(1-\mathrm{e}^{-\frac{T}{\lambda_i}}\right). \tag{4-121}$$

For well-posedness, $C_1-C_2>0$ must be satisfied, i.e.

$$|\phi_0|+\|\dot{\phi}\|_1 < \frac{kC_0\beta L}{\sum_{i=1}^{N} g_i\left(2-\mathrm{e}^{-\frac{T}{\lambda_i}}\right)}, \tag{4-122}$$

where L denotes the L_1-norm in (4-119a). In the case where all the roots ξ_i are real and distinct, the transient is monotone decreasing, so this can be expressed as

$$L = \int_0^T \left| \sum_{i=1}^{N+2} \alpha_i \xi_i^2 \, \mathrm{e}^{-\xi_i t} \right| \, \mathrm{d}t = \left| \sum_{i=1}^{N+2} \alpha_i \xi_i \left(1 - \mathrm{e}^{\xi_i T} \right) \right|. \tag{4-123}$$

Again, it can be seen that for a stable solution to exist for an applied torque of the form $C(t) = C_0 t$, the perturbations in the data $f(t)$ must be differentiable and satisfy $\phi \in L_1[0, T]$.

Case 2. $G_\infty = 0$: The analysis is similar in the case of a viscoelastic liquid, but from (2-161) it can be seen that the data function is now of the form

$$f(t) = kC_0 \left[t - 2\mu_2 - \sum_{i=1}^{N+1} \alpha_i' \, \mathrm{e}^{-\xi_i' t} \right], \quad t \in [0, T] \tag{4-124}$$

where $\alpha_i' = \nu_i' \xi_i'$ and hence the pair of working equations is

$$G * \Omega = kC_0 \left[t - 2\mu_2 - \sum_{i=1}^{N+1} \alpha_i' \, \mathrm{e}^{-\xi_i' t} \right] \tag{4-125a}$$

$$(G + \gamma) * (\Omega + \phi) = kC_0 \left[t - 2\mu_2 - \sum_{i=1}^{N+1} \alpha_i' \, \mathrm{e}^{-\xi_i' t} \right] + \varepsilon. \tag{4-125b}$$

Taking the same approach as for the viscoelastic solid, the second order derivative of the $f * \gamma$ is found to be

$$\frac{\mathrm{d}^2}{\mathrm{d}t^2} \left[f * \gamma \right] = \left(1 + \sum_{i=1}^{N+1} \alpha_i' \xi_i' \right) \gamma(t) - \left(2\mu_2 + \sum_{i=1}^{N+1} \alpha_i' \right) \dot{\gamma}(t) - \sum_{i=1}^{N+1} \alpha_i' \xi_i'^2 \, \mathrm{e}^{-\xi_i' t} * \gamma. \tag{4-126}$$

Noting that $\ddot{\chi}(0) = \frac{C_0}{I} \left(2\mu_2 + \sum_{i=1}^{N+1} \alpha_i' \right) = 0$ and also that $\sum_{i=1}^{N+1} \alpha_i' \xi_i' = -\frac{I}{C_0} \chi^{(3)}(0) = \lim_{s \to \infty} s^4 \bar{\chi}(s) = -1$, this simplifies to the convolution of the exponential terms with $\gamma(t)$. Thus, the analysis is basically the same as for the viscoelastic solid case and thus a bound can be obtained on $\gamma(t)$ of the same form as (4-117), but with $G_0 = G_\infty + \sum_{i=1}^{N} g_i$ and

$$C_1 = kC_0 \beta \int_0^T \left| \sum_{i=1}^{N+1} \alpha_i' \xi_i'^2 \right| \, \mathrm{d}t. \tag{4-127}$$

Thus, for well-posedness, the inequality to be satisfied is

$$|\phi_0| + \|\dot{\phi}\|_1 < \frac{kC_0 \beta \int_0^T \left| \sum_{i=1}^{N+1} \alpha_i' \xi_i'^2 \right| \, \mathrm{d}t}{G_\infty + \sum_{i=1}^{N} g_i \left(2 - \mathrm{e}^{-\frac{T}{\lambda_i}} \right)} \tag{4-128}$$

and the requirement $\dot{\phi} \in L_1[0, T]$ must be satisfied.

Newtonian Fluid

In the case where the material is assumed to be Newtonian in character with viscosity η, the applied torque $C(t) = C_0 t$ gives rise to a platen displacement in the form of (2-143) and a data function for this problem

$$f(t) = \frac{kC_0}{\eta}\left\{\eta t - kI\left[1 - \mathrm{e}^{-\frac{\eta t}{kI}}\right]\right\}, \quad t \in [0, T]. \tag{4-129}$$

The standard problem with exact data, coupled with the same equation with perturbed data produces the pair

$$G * \Omega = \frac{kC_0}{\eta}\left\{\eta t - kI\left[1 - \mathrm{e}^{-\frac{\eta t}{kI}}\right]\right\} \tag{4-130a}$$

$$(G + \gamma) * (\Omega + \phi) = \frac{kC_0}{\eta}\left\{\eta t - kI\left[1 - \mathrm{e}^{-\frac{\eta t}{kI}}\right]\right\} + \varepsilon(t). \tag{4-130b}$$

Subtracting the former from the latter, performing a convolution with $G(t)$ and using the identity property of the delta function w.r.t convolution in the relaxation modulus $G(t) = \eta\delta(t)$ for the Newtonian model, we obtain

$$\frac{kC_0}{\eta}\left[\eta t - kI\left(1 - \mathrm{e}^{-\frac{\eta t}{kI}}\right)\right] * \gamma = \eta\left[\varepsilon(t) - \eta\phi(t) - \phi * \gamma\right]. \tag{4-131}$$

Differentiating twice, this becomes

$$\frac{\eta C_0}{I}\mathrm{e}^{-\frac{\eta t}{kI}} * \gamma = \eta\left[\ddot{\varepsilon}(t) - \eta\ddot{\phi}(t) - (\phi_0 + \dot{\phi}_0)\gamma + \dot{\phi} * \gamma\right] \tag{4-132}$$

and after applying the triangular inequality

$$\frac{\eta C_0}{I}\left|\mathrm{e}^{-\frac{\eta t}{kI}} * \gamma\right| \leq \eta\left[|\ddot{\varepsilon}(t)| + \eta\,|\ddot{\phi}(t)| + (|\phi_0| + |\dot{\phi}_0|)\,|\gamma| + |\dot{\phi} * \gamma|\right] \tag{4-133}$$

and the convolution inequalities (4-32)-(4-33),

$$\frac{\eta C_0}{I}\left|\mathrm{e}^{-\frac{\eta t}{kI}} * \gamma\right| \leq \eta\left[\|\ddot{\varepsilon}\|_\infty + \eta\|\ddot{\phi}\|_\infty + (|\phi_0| + |\dot{\phi}_0|)\,\|\gamma\|_\infty + \|\dot{\phi}\|_1\|\gamma\|_\infty\right]. \tag{4-134}$$

This can be rearranged to give a bound on the perturbation in $G(t)$, viz.

$$\|\gamma\|_\infty \leq \frac{\eta}{C_1 - C_2}\left[\|\ddot{\varepsilon}\|_\infty + \eta\|\ddot{\phi}\|_\infty\right] \tag{4-135}$$

where

$$C_1 = \frac{\eta\beta C_0}{I}\left\|\mathrm{e}^{-\frac{\eta t}{kI}}\right\|_1 = kC_0\beta\left[1 - \mathrm{e}^{-\frac{\eta T}{kI}}\right] \tag{4-136a}$$

$$C_2 = \eta\left[|\phi_0| + |\dot{\phi}_0| + \|\ddot{\phi}\|_1\right] \tag{4-136b}$$

and $0 < \beta \leq 1$ is a constant defined by the sharp form of Young's inequality (see (4-145)). Thus, for the problem to be well-posed, the inequality

$$|\phi_0| + |\dot{\phi}_0| + \|\ddot{\phi}\|_1 < \frac{kC_0\beta}{\eta}\left[1 - \mathrm{e}^{-\frac{\eta T}{kI}}\right] \tag{4-137}$$

when satisfied, guarantees consistency in (4-135). As $T \to \infty$, and additionally assuming that since $C(0) = 0$, then the data at $t = 0$ is exactly equal to zero, i.e. $\phi_0 = \dot{\phi}_0 = 0$, then

$$\|\ddot{\phi}\|_1 < \frac{kC_0\beta}{\eta}. \tag{4-138}$$

The RHS of the inequality in (4-137) is obviously maximized as T increases towards infinity, however since the rate of change is exponential with a negative exponent, beyond a certain value of T there is little to be gained in terms of stability by increasing the experimental time further. Note that for well-posedness, it is required that perturbations in the data be twice differentiable and furthermore that $\ddot{\phi} \in L_1[0, T]$. Therefore, the problem is notably more ill-posed for the Newtonian fluid than the Maxwell and N-mode Maxwell models when subjected to a torque in the form $C(t) = C_0 t$.

4.3.4 Delta Function

When subjected to an applied torque in the form of a delta function $C(t) = C_\delta \delta(t - t_0)$, the data function $f(t)$ is merely the transient function, denoted by $\mu(t)$. Assuming that the transient is incorporated into the perturbation in the noisy data function, $\varepsilon(t)$, then the exact part of the data function is equal to zero. However, it should be noted that $\|\mu\|_\infty \leq |\varepsilon| \leq \|\varepsilon\|_\infty$, so the actual value can only be zero if $\varepsilon(t) < 0$ on $[0, T]$. The pair of unperturbed and perturbed equations for this problem, respectively, are

$$G * \Omega = 0 \tag{4-139a}$$

$$G * \Omega + G * \phi + \Omega * \gamma + \phi * \gamma = \varepsilon(t). \tag{4-139b}$$

Proceeding in the usual manner, by subtracting the unperturbed from the perturbed equation, performing an extra convolution with $G(t)$ and using the fact that $G * \Omega = 0$, we obtain

$$G * \varepsilon - G * G * \phi - G * \phi * \gamma = 0. \tag{4-140}$$

Here, a slightly different approach must be taken, since the term $f * \gamma = 0$. Rearranging and applying the triangular inequality,

$$|G * \phi * \gamma| \leq |G * \varepsilon| + |G * G * \phi| \tag{4-141}$$

and using Young's convolution inequality (4-34)

$$|G * \phi * \gamma| \leq \|G\|_1 \left[\|\varepsilon\|_\infty + \|G\|_1 \|\phi\|_\infty\right]. \tag{4-142}$$

To proceed, it is necessary to make use of the sharp form of Young's inequality, which is given by

$$|f * g| \leq \beta \|f\|_1 \|g\|_\infty \tag{4-143}$$

for $f \in L_1[0,T]$, $g \in L_\infty[0,T]$ or in the case of a triple convolution

$$|f * g * h| \leq \beta \|f\|_1 \|g\|_1 \|h\|_\infty \tag{4-144}$$

for $f, g \in L_1[0,T]$ and $h \in L_\infty[0,T]$, and constant $0 < \beta \leq 1$. The inequality is *sharp* in the sense that the RHS is the minimum value possible such that the inequality still holds. More precisely, the value of β is defined by

$$\beta = \frac{\|f * g\|_\infty}{\|f\|_1 \|g\|_\infty}. \tag{4-145}$$

Applying (4-144) and (4-145) to (4-142), can thus be written in the form

$$\|\gamma\|_\infty \leq \frac{1}{\beta \|\phi\|_1} \left[\|\varepsilon\|_\infty + \|G\|_1 \|\phi\|_\infty\right] \tag{4-146}$$

where

$$\|G\|_1 = \int_0^{T-t_0} |G(t)| \, \mathrm{d}t. \tag{4-147}$$

For well-posedness and to guarantee consistency in (4-146), it is required that $\beta\|\phi\|_1 > 0$, or since $0 < \beta \leq 1$, $\|\phi\|_1 > 0$. Essentially, if the perturbation in the data $\phi \in L_1[0,T]$, then a stable solution to the problem should exist. Note also that in the case where exact data is used, i.e. $\|\phi\|_\infty, \|\varepsilon\|_\infty \to 0$, then the perturbation in the solution also tends to zero.

Maxwell Model

An applied torque in the form of a delta function $C(t) = C_0\delta(t - t_0)$ was found to produce a platen displacement (2-72) for a material conforming to the Maxwell model and assuming the roots $\xi_{1,2}$ in the Laplace transform are distinct. This gives rise to the data function for this problem of the form

$$f(t) = -kC_\delta \left\{\alpha_1 \, \mathrm{e}^{-\xi_1(t-t_0)} + \alpha_2 \, \mathrm{e}^{-\xi_2(t-t_0)}\right\}, \quad t \in [t_0, T] \tag{4-148}$$

where $\alpha_1 = \gamma_1\xi_1^2$ and $\alpha_2 = \gamma_2\xi_2^2$ in terms of the appropriate constants from Section 2.2.2. Hence, for this problem the pair of unperturbed and perturbed equations are

$$G * \Omega = -kC_\delta \left\{ \alpha_1 \, \mathrm{e}^{-\xi_1(t-t_0)} + \alpha_2 \, \mathrm{e}^{-\xi_2(t-t_0)} \right\} \tag{4-149a}$$

$$(G+\gamma) * (\Omega+\phi) = -kC_\delta \left\{ \alpha_1 \, \mathrm{e}^{-\xi_1(t-t_0)} + \alpha_2 \, \mathrm{e}^{-\xi_2(t-t_0)} \right\} + \varepsilon(t) \tag{4-149b}$$

Taking the difference of (4-149a) and (4-149b) and performing an extra convolution with the relaxation modulus $G(t)$,

$$kC_\delta \left[\alpha_1 \, \mathrm{e}^{-\xi_1(t-t_0)} + \alpha_2 \, \mathrm{e}^{-\xi_2(t-t_0)} \right] * \gamma = G * G * \phi + G * \phi * \gamma - G * \varepsilon. \tag{4-150}$$

Applying the triangular inequality,

$$kC_\delta \left| \left[\alpha_1 \, \mathrm{e}^{-\xi_1(t-t_0)} + \alpha_2 \, \mathrm{e}^{-\xi_2(t-t_0)} \right] * \gamma \right| \leq |G * \varepsilon| + |G * G * \phi| + |G * \phi * \gamma| \tag{4-151}$$

and additionally the convolution inequalities (4-34)-(4-35),

$$\begin{aligned} kC_\delta \left| \left[\alpha_1 \, \mathrm{e}^{-\xi_1(t-t_0)} + \alpha_2 \, \mathrm{e}^{-\xi_2(t-t_0)} \right] * \gamma \right| \leq \|G\|_1 \|\varepsilon\|_\infty + \|G\|_1^2 \|\phi\|_\infty \\ + \|G\|_1 \|\phi\|_1 \|\gamma\|_\infty. \end{aligned} \tag{4-152}$$

The sharp form of Young's inequality for the convolution integral (4-143) with a suitable value of $0 < \beta \leq 1$ (see (4-145)) then allows the inequality to be recast as

$$\begin{aligned} kC_\delta \beta \left\| \alpha_1 \, \mathrm{e}^{-\xi_1(t-t_0)} + \alpha_2 \, \mathrm{e}^{-\xi_2(t-t_0)} \right\|_1 \|\gamma\|_\infty \leq \|G\|_1 \|\varepsilon\|_\infty + \|G\|_1^2 \|\phi\|_\infty \\ + \|G\|_1 \|\phi\|_1 \|\gamma\|_\infty \end{aligned} \tag{4-153}$$

and rearranging, a bound on the supremum of the perturbation in the solution is obtained of the form

$$\|\gamma\|_\infty \leq \frac{\lambda g \left(1 - \mathrm{e}^{-\frac{(T-t_0)}{\lambda}} \right)}{C_1 - C_2} \left[\|\varepsilon\|_\infty + \lambda g \left(1 - \mathrm{e}^{-\frac{(T-t_0)}{\lambda}} \right) \|\phi\|_\infty \right] \tag{4-154}$$

with constants $C_{1,2} \in \mathbb{R}$ defined by

$$C_1 = kC_\delta \beta \left\| \alpha_1 \, \mathrm{e}^{-\xi_1(t-t_0)} + \alpha_2 \, \mathrm{e}^{-\xi_2(t-t_0)} \right\|_1 \tag{4-155a}$$

$$C_2 = \lambda g \left(1 - \mathrm{e}^{-\frac{(T-t_0)}{\lambda}} \right) \|\phi\|_1. \tag{4-155b}$$

For the problem to be well-posed, (4-154) must be consistent, so $C_1 - C_2 > 0$ must be satisfied. This leads to a constraint on the perturbation in the data ϕ of the form

$$\|\phi\|_1 < \frac{kC_\delta \beta L}{\lambda g \left(1 - \mathrm{e}^{-\frac{(T-t_0)}{\lambda}}\right)} \tag{4-156}$$

where L denotes the L_1-norm in C_1. Assuming that $\xi_{1,2}$ are real and distinct, the integrand in L will be monotone decreasing to 0 as $t \to \infty$ and therefore can be evaluated as follows

$$\begin{aligned} L &= \int_{t_0}^{T} \left| \alpha_1 \mathrm{e}^{-\xi_1(t-t_0)} + \alpha_2 \mathrm{e}^{-\xi_2(t-t_0)} \right| \mathrm{d}t \\ &= \gamma_1 \xi_1 \left(1 - \mathrm{e}^{-\xi_1(T-t_0)}\right) + \gamma_2 \xi_2 \left(1 - \mathrm{e}^{-\xi_2(T-t_0)}\right). \end{aligned} \tag{4-157}$$

When the roots are complex, such that $\xi_2 = \xi_1^*$ and $\alpha_2 = \alpha_1^*$, L is determined as the value of

$$L = 2\,|\alpha_1| \int_{t_0}^{T} \left| \mathrm{e}^{-\frac{t}{2\lambda}} \sin(\xi'' t + a) \right| \mathrm{d}t, \tag{4-158}$$

where $\xi'' = \mathrm{Im}\,\{\xi_1\}$ and $\tan a = \frac{\mathrm{Re}\{\xi_1\}}{\mathrm{Im}\{\xi_1\}}$. In both cases, it can be seen that as $T - t_0 \to \infty$ the stability criterion attains its maximal value. To summarize, for the problem to be well-posed, it is required that $\phi \in L_1[0, T]$ and that the norm is sufficiently small in compliance with (4-156).

N-Mode Maxwell Model

The rheometer response for the N-mode Maxwell model when subjected to an applied torque in the form of a delta function $C(t) = C_0\delta(t - t_0)$ is described in Section 2.2.3. Consequently, the data functions for this problem are

$$f(t) = -kC_\delta \sum_{i=1}^{N+1} \alpha_i' \mathrm{e}^{-\xi_i'(t-t_0)}, t \in [0, T] \tag{4-159}$$

where $\alpha_i' = \nu_i' \xi_i'^2, i = 1, \ldots, N+1$, for a viscoelastic liquid ($G_\infty = 0$), and

$$f(t) = -kC_\delta \sum_{i=1}^{N+2} \alpha_i \mathrm{e}^{-\xi_i(t-t_0)}, t \in [0, T] \tag{4-160}$$

for a viscoelastic solid, with $\alpha_i = \nu_i \xi_i^2, i = 1, \ldots, N+2$. The similarity between the two solutions for this problem allows the same form of the analysis to be applied to both

cases. Firstly, consider the viscoelastic fluid, for which the set of exact and perturbed equations are

$$G * \Omega = -kC_\delta \sum_{i=1}^{N+1} \alpha_i' \, \mathrm{e}^{-\xi_i'(t-t_0)} \tag{4-161a}$$

$$(G+\gamma) * (\Omega+\phi) = -kC_\delta \sum_{i=1}^{N+1} \alpha_i' \, \mathrm{e}^{-\xi_i'(t-t_0)} + \varepsilon(t). \tag{4-161b}$$

Subtracting the exact from the perturbed equations, performing an extra convolution with $G(t)$ and replacing $G * \Omega$ by $f(t)$, the working equation becomes

$$-kC_\delta \sum_{i=1}^{N+1} \alpha_i' \, \mathrm{e}^{-\xi_i'(t-t_0)} * \gamma = G * \varepsilon - G * G * \phi - G * \phi * \gamma \tag{4-162}$$

and by the triangular inequality

$$kC_\delta \left| \sum_{i=1}^{N+1} \alpha_i' \, \mathrm{e}^{-\xi_i'(t-t_0)} * \gamma \right| \leq |G * \varepsilon| + |G * G * \phi| + |G * \phi * \gamma| \,. \tag{4-163}$$

The convolution inequalities (4-34)-(4-35) provide a loose bound for the RHS, so (4-163) now becomes

$$kC_\delta \left| \sum_{i=1}^{N+1} \alpha_i' \, \mathrm{e}^{-\xi_i'(t-t_0)} * \gamma \right| \leq \|G\|_1 \left[\|\varepsilon\|_\infty + \|G\|_1 \|\phi\|_\infty + \|\phi\|_1 \|\gamma\|_\infty \right]. \tag{4-164}$$

Using the sharp form of the convolution inequality with corresponding value of $0 < \beta \leq 1$ (see (4-143),(4-145)) on the LHS, (4-164) can be rewritten as

$$kC_\delta \beta \left\| \sum_{i=1}^{N+1} \alpha_i' \, \mathrm{e}^{-\xi_i' t} * \gamma \right\|_1 \leq \|G\|_1 \left[\|\varepsilon\|_\infty + \|G\|_1 \|\phi\|_\infty + \|\phi\|_1 \|\gamma\|_\infty \right] \tag{4-165}$$

or, equivalently

$$\|\gamma\|_\infty \leq \frac{\sum_{i=1}^{N} g_i \lambda_i \left(1 - \mathrm{e}^{-\frac{T}{\lambda}}\right)}{C_1 - C_2} \left[\|\varepsilon\|_\infty + \sum_{i=1}^{N} g_i \lambda_i \left(1 - \mathrm{e}^{-\frac{T}{\lambda}}\right) \|\phi\|_\infty \right] \tag{4-166}$$

where the constants $C_{1,2} \in \mathbb{R}$ are defined

$$C_1 = kC_\delta \beta \left\| \sum_{i=1}^{N+1} \alpha_i' \, \mathrm{e}^{-\xi_i' t} \right\|_1 \tag{4-167a}$$

$$C_2 = \sum_{i=1}^{N} g_i \lambda_i \left(1 - \mathrm{e}^{-\frac{T}{\lambda}}\right). \tag{4-167b}$$

For the problem to be well-posed, the criterion $C_1 - C_2 > 0$ must be satisfied, which implies that

$$\|\phi\|_1 < \frac{kC_\delta\beta\left\|\sum_{i=1}^{N+1}\alpha_i' \mathrm{e}^{-\xi_i' t}\right\|_1}{\sum_{i=1}^{N} g_i\lambda_i\left(1-\mathrm{e}^{-\frac{T}{\lambda}}\right)}. \tag{4-168}$$

If the $\xi_i' \in \mathbb{R}$ for $i = 1, 2, \ldots, N+1$, then the integrand of the norm is monotone, so the norm may be explicitly determined as

$$\begin{aligned}\left\|\sum_{i=1}^{N+1}\alpha_i' \mathrm{e}^{-\xi_i' t}\right\|_1 &= \int_{t_0}^{T}\left|\sum_{i=1}^{N+1}\alpha_i' \mathrm{e}^{-\xi_i' t}\right| \mathrm{d}t \\ &= \sum_{i=1}^{N+1}\nu_i'\xi_i'\left[1-\mathrm{e}^{-\xi_i'(T-t_0)}\right].\end{aligned} \tag{4-169}$$

The more common case is that where $N-1$ of the roots are real and the remaining pair are complex conjugate. Assuming $\xi_i' \in \mathbb{R}$ for $i = 1, 2, \ldots, N-1$ and $\xi_N', \xi_{N+1}' \in \mathbb{C}$ such that $\xi_{N+1}' = \xi_i'^*$ and $\alpha_{N+1}' = \alpha_N'^*$, then the equivalent form for (4-169) in this case is

$$\begin{aligned}\left\|\sum_{i=1}^{N+1}\alpha_i' \mathrm{e}^{-\xi_i' t}\right\|_1 = \sum_{i=1}^{N-1}\nu_i'\xi_i'\left(1-\mathrm{e}^{-\xi_i'(T-t_0)}\right) \\ + 2\left|\alpha_N'\right|\int_{t_0}^{T}\left|\mathrm{e}^{-\xi_{re}t}\sin(\xi_{im}t+a)\right| \mathrm{d}t,\end{aligned} \tag{4-170}$$

since the function of the first $N-1$ of the ξ_i' forms a monotone decreasing and strictly positive function. Here, the real part of ξ_N' is denoted by ξ_{re} and the imaginary part by ξ_{im}, the constant a being defined by $\tan a = \frac{\xi_{re}}{\xi_{im}}$.

The analysis for the viscoelastic solid is very similar, hence only the end result needs to be stated here. The inequality obtained by the method above in this case is

$$\begin{aligned}\|\gamma\|_\infty \leq \frac{G_\infty(T-t_0)+\sum_{i=1}^{N} g_i\lambda_i \mathrm{e}^{-\frac{(T-t_0)}{\lambda_i}}}{C_1-C_2}\Big[\|\varepsilon\|_\infty + G_\infty(T-t_0) \\ + \sum_{i=1}^{N} g_i\lambda_i \mathrm{e}^{-\frac{(T-t_0)}{\lambda_i}}\|\phi\|_\infty\Big]\end{aligned} \tag{4-171}$$

where the constant $C_1 \in \mathbb{R}$ is defined

$$C_1 = kC_\delta\beta\left\|\sum_{i=1}^{N+2}\alpha_i \mathrm{e}^{-\xi_i t}\right\|_1 \tag{4-172a}$$

$$C_2 = \left[G_\infty(T-t_0) + \sum_{i=1}^{N} g_i\lambda_i \mathrm{e}^{-\frac{(T-t_0)}{\lambda_i}}\right]\|\phi\|_1 \tag{4-172b}$$

and the criterion for well-posedness is

$$\|\phi\|_1 < \frac{kC_\delta\beta\left\|\sum_{i=1}^{N+2}\alpha_i\,\mathrm{e}^{-\xi_i t}\right\|_1}{G_\infty(T-t_0)+\sum_{i=1}^{N}g_i\lambda_i\,\mathrm{e}^{-\frac{(T-t_0)}{\lambda_i}}}. \tag{4-173}$$

Note that the denominator in (4-173) increases without bound as $(T-t_0)\to\infty$ and also that $\frac{\|G\|_1}{C_1-C_2}\to -1$, so in the case of a viscoelastic solid it is an open problem as to whether a stable solution can exist for this problem.

Newtonian Fluid

Continuing the analysis to cover all classes of fluids, a Newtonian fluid with relaxation modulus $G(t)=\eta\delta(t)$ produces a platen response of the form (2-61) when subjected to a torque of the form $C(t)=C_\delta\delta(t-t_0)$. Thus the data function for this problem is

$$f(t)=\frac{\eta C_\delta}{I}\,\mathrm{e}^{-\frac{\eta(t-t_0)}{kI}},\quad t\in[t_0,T] \tag{4-174}$$

and the pair of exact and perturbed convolution equations are

$$G*\Omega=\frac{\eta C_\delta}{I}\,\mathrm{e}^{-\frac{\eta(t-t_0)}{kI}} \tag{4-175a}$$

$$(G+\gamma)*(\Omega+\phi)=\frac{\eta C_\delta}{I}\,\mathrm{e}^{-\frac{\eta(t-t_0)}{kI}}+\varepsilon(t). \tag{4-175b}$$

Subtracting the former from the latter, performing an extra convolution with $G(t)$ and substituting $f(t)$ for $G*\Omega$, the working equation for the problem is

$$\frac{\eta C_\delta}{I}\,\mathrm{e}^{-\frac{\eta(t-t_0)}{kI}}*\gamma=G*\varepsilon-G*G*\phi-G*\phi*\gamma. \tag{4-176}$$

Using the identity property of the delta function with respect to convolution, substitution of $G(t)=\eta\delta(t)$ into (4-176) transforms this into

$$\frac{\eta C_\delta}{I}\,\mathrm{e}^{-\frac{\eta(t-t_0)}{kI}}*\gamma=\eta\left[\varepsilon(t)-\eta\phi(t)-\phi*\gamma\right]. \tag{4-177}$$

By the triangular inequality,

$$\frac{\eta C_\delta}{I}\left|\mathrm{e}^{-\frac{\eta(t-t_0)}{kI}}*\gamma\right|\le\eta\left[|\varepsilon(t)|+\eta\,|\phi(t)|+|\phi*\gamma|\right] \tag{4-178}$$

and applying the convolution inequality (4-34),

$$\frac{\eta C_\delta}{I}\left|\mathrm{e}^{-\frac{\eta(t-t_0)}{kI}}*\gamma\right|\le\eta\left[\|\varepsilon\|_\infty+\eta\|\phi\|_\infty+\|\phi\|_1\|\gamma\|_\infty\right]. \tag{4-179}$$

The sharp form of Young's convolution inequality with appropriate constant $0 < \beta \leq 1$ (see (4-145)), allows this to be recast in the form

$$\|\varepsilon\|_\infty \leq \frac{\eta}{C_1 - C_2} \left[\|\varepsilon\|_\infty + \eta\|\phi\|_\infty\right] \tag{4-180}$$

where the constants $C_{1,2} \in \mathbb{R}$ are defined

$$C_1 = \frac{\eta\beta C_\delta}{I} \left\| \mathrm{e}^{-\frac{\eta(t-t_0)}{kI}} \right\|_1 \tag{4-181a}$$

$$C_2 = \eta\|\phi\|_1 \tag{4-181b}$$

For the problem to be well-posed, consistency in (4-180) is required, so $C_1 - C_2 > 0$ must be satisfied, or equivalently

$$\|\phi\|_1 < \frac{\beta C_\delta}{I\eta} \left[1 - \mathrm{e}^{-\frac{\eta(t-t_0)}{kI}}\right]. \tag{4-182}$$

Taking $T \to \infty$, the RHS attains its maximal value and hence the restrictions on the perturbation in the error are relaxed as much as possible. Therefore, for a stable solution for this problem to exist, it is required that $\phi \in L_1[0, T]$ and the norm is bounded according to (4-182).

4.3.5 Delta Function Sequence

As an example of a periodic function derived from one of the basic applied torque functions considered in Chapter 2, now consider a sequence of delta functions of alternating sign and period Ψ given by $C(t) = C_\delta \sum_{j=0}^{n-1} (-1)^j \delta(t - t_j)$, where $t_j = t_0 + j\Psi \leq T$.

Maxwell Model

The platen displacement was determined in (2-201) for an applied torque in the form of a sequence of delta functions, given in terms of the base solution for a single delta function, $\chi_\delta(t)$. The data function can then be determined as

$$f(t) = kC_\delta \sum_{j=0}^{n-1} f_i(t) = kC_\delta \sum_{j=0}^{n-1} (-1)^{j+1} \left[\alpha_1 \mathrm{e}^{-\xi_1(t-t_j)} + \alpha_2 \mathrm{e}^{-\xi_2(t-t_j)}\right] \tag{4-183}$$

where $\alpha_1 = \gamma_1\xi_1^2$ and $\alpha_2 = \gamma_2\xi_2^2$. Proceeding in the same manner, it is found that the perturbation in the solution, $\gamma(t)$, has the bound

$$\|\gamma\|_\infty \leq \frac{g\lambda\left(1 - \mathrm{e}^{-\frac{T-t_0}{\lambda}}\right)}{C_1 - C_2} \left[\|\varepsilon\|_\infty + \|\phi\|_\infty\right] \tag{4-184}$$

where the constants $C_{1,2} \in \mathbb{R}$ are defined

$$C_1 = kC_0L \tag{4-185a}$$

$$C_2 = g\lambda\left(1 - \mathrm{e}^{-\frac{T-t_0}{\lambda}}\right)\|\phi\|_\infty \tag{4-185b}$$

and therefore to be well-posed, $C_1 - C_2 > 0$, i.e.

$$\|\phi\|_1 < \frac{kC_\delta\beta L}{g\lambda\left(1 - \mathrm{e}^{-\frac{T-t_0}{\lambda}}\right)}. \tag{4-186}$$

Thus, we require $\phi \in L_1[0,T]$ and to be suitably small. The quantity L is defined

$$\begin{aligned} L &= \int_{t_0}^{T}\left|\sum_{j=0}^{n-1}(-1)^{j+1}\left[\alpha_1\,\mathrm{e}^{-\xi_1(t-t_j)} + \alpha_2\,\mathrm{e}^{-\xi_2(t-t_j)}\right]\right|\mathrm{d}t \\ &= \int_{t_0}^{T}\left|\alpha_1\sum_{j=0}^{n-1}(-1)^{j+1}\,\mathrm{e}^{-\xi_1(t-t_j)} + \alpha_2\sum_{j=0}^{n-1}(-1)^{j+1}\,\mathrm{e}^{-\xi_2(t-t_j)}\right|\mathrm{d}t. \end{aligned} \tag{4-187}$$

Compare this to the L_1-norm for a single delta function:

$$\|f_\delta\|_1 = kC_\delta\int_{t_0}^{T}\left|\alpha_1\,\mathrm{e}^{-\xi_1(t-t_0)} + \alpha_2\,\mathrm{e}^{-\xi_2(t-t_0)}\right|\mathrm{d}t. \tag{4-188}$$

For any $t \in (t_m, t_{m+1})$, $0 < m < n-1$, the values of $(t - t_j)$ form a decreasing sequence for $j = 0, 1, \ldots, m$, so the corresponding values of $\mathrm{e}^{-\xi_1(t-t_j)}$ therefore form an increasing sequence. Hence the absolute value of the alternating sequence increases and L increases with increasing n. Therefore there exists some $n_c > 1$ such that $L > \|f_\delta\|_1$ when $n \geq n_c$. Regarding this problem, this implies that if a sufficient number of delta functions are incorporated in the applied torque, then the problem gains increased stability over the standard problem where only a single delta function is utilized as an applied torque.

4.3.6 Other 1-Smoothing Problems

In Chapter 3 a number of functions for the applied torque related to the discrete form of the relaxation modulus were investigated. The stability analysis for the cases where the torque is chosen such that $\dot{\chi}(t) = G(t)$ and a simple exponential series combined with a delta function is included here using the Maxwell model. These are both 1-smoothing problems and belong to the optimal class of functions along with the delta function for the Volterra-1 problem.

Relaxation Modulus

The form for the applied torque such that $\Omega(t) = G(t)$ determined in (3-37) for the Maxwell model. The data function is then easily determined and gives rise to the pair of equations

$$G * \Omega = gt\,\mathrm{e}^{-\frac{t}{\lambda}} \tag{4-189a}$$

$$(G+\gamma) * (\Omega+\phi) = gt\,\mathrm{e}^{-\frac{t}{\lambda}} + \varepsilon(t) \tag{4-189b}$$

and using the same technique as for the delta function applied torque, the inequality

$$g\left|t\,\mathrm{e}^{-\frac{t}{\lambda}} * \gamma\right| \leq \|G\|_1\|G\|_1\left[\|\varepsilon\|_\infty + \|G\|_1\|\phi\|_\infty + \|\phi\|_1\|\gamma\|_\infty\right] \tag{4-190}$$

is obtained, where

$$\|G\|_1 = \int_0^T |G(t)|\,\mathrm{d}t = g\lambda\left(1-\mathrm{e}^{-\frac{T}{\lambda}}\right). \tag{4-191}$$

Therefore, the bound on the perturbation in the solution has the form

$$\|\gamma\|_\infty \leq \frac{g\lambda\left(1-\mathrm{e}^{-\frac{T}{\lambda}}\right)}{C_1-C_2}\left[\|\varepsilon\|_\infty + g\lambda\left(1-\mathrm{e}^{-\frac{T}{\lambda}}\right)\|\phi\|_\infty\right] \tag{4-192}$$

with constants $C_{1,2} \in \mathbb{R}$ defined by

$$C_1 = \beta\lambda g\left[\lambda + (\lambda - T)\,\mathrm{e}^{-\frac{T}{\lambda}}\right] \tag{4-193a}$$

$$C_2 = \lambda g\left[1-\mathrm{e}^{-\frac{T}{\lambda}}\right]\|\phi\|_1 \tag{4-193b}$$

for $0 < \beta \leq 1$ defined in (4-145). For well-posedness $C_1 - C_2 > 0$ must be satisfied, which implies that

$$\|\phi\|_1 < \frac{\beta\left[\lambda + (\lambda - T)\,\mathrm{e}^{-\frac{T}{\lambda}}\right]}{1-\mathrm{e}^{-\frac{T}{\lambda}}}. \tag{4-194}$$

Thus, well-posedness requires that the perturbations in the data $\phi \in L_1[0,T]$ and are sufficiently small in compliance with (4-194). Note that as $T \to \infty$, the criterion becomes

$$\|\phi\|_1 < \beta\lambda. \tag{4-195}$$

Exponential Series

An applied torque in the form of a Dirichlet series with the addition of a delta function was found to produce a platen displacement in the form of a Dirichlet series - see Theorem 3.2.2. Taking a simple example, with $C(t) = C_0\left[\delta(t) + \mathrm{e}^{-at}\right]$ and assuming the material is a Maxwell fluid, then it can be determined without difficulty that the data function is of the form

$$f(t) = -kC_0\left\{\alpha_0\,\mathrm{e}^{-at} + \alpha_1\,\mathrm{e}^{-\xi_1 t} + \alpha_2\,\mathrm{e}^{-\xi_2 t}\right\} \tag{4-196}$$

where $\alpha_0 = 1 - \mu_0 a^2$, $\alpha_1 = (\mu_1 + \gamma_1)\xi_1^2$, $\alpha_2 = (\mu_2 + \gamma_2)\xi_2^2$, $\gamma_{1,2}$ are the coefficients of the exponential terms in the solution for the delta function torque from (2-72)/(2-79) and $\mu_{0,1,2}$ are the coefficients for platen displacement pertaining to the torque $C(t) = C_0\,\mathrm{e}^{-at}$ in (3-80). The standard form of the analysis gives the bound on the perturbation in the solution as

$$\|\gamma\|_\infty \leq \frac{g\lambda\left(1 - \mathrm{e}^{-\frac{T}{\lambda}}\right)}{C_1 - C_2}\left[\|\varepsilon\|_\infty + g\lambda\left(1 - \mathrm{e}^{-\frac{T}{\lambda}}\right)\|\phi\|_\infty\right] \tag{4-197}$$

where $0 < \beta \leq 1$ is defined as in (4-145) and the constants $C_{1,2} \in \mathbb{R}$ are defined by

$$C_1 = kC_0\beta\int_0^T \left|\alpha_0\,\mathrm{e}^{-at} + \alpha_1\,\mathrm{e}^{-\xi_1 t} + \alpha_2\,\mathrm{e}^{-\xi_2 t}\right| \mathrm{d}t \tag{4-198a}$$

$$C_2 = g\lambda\left(1 - \mathrm{e}^{-\frac{T}{\lambda}}\right)\|\phi\|_1. \tag{4-198b}$$

For well-posedness, it is required that $\phi \in L_1[0,T]$ and additionally that the constraint

$$\|\phi\|_1 < \frac{kC_0\beta\int_0^T \left|\alpha_0\,\mathrm{e}^{-at} + \alpha_1\,\mathrm{e}^{-\xi_1 t} + \alpha_2\,\mathrm{e}^{-\xi_2 t}\right| \mathrm{d}t}{g\lambda\left(1 - \mathrm{e}^{-\frac{T}{\lambda}}\right)} \tag{4-199}$$

is satisfied. Note that the integrand in (4-198a) will always be greater than that for a delta function applied torque with the same parameters, therefore additional stability is gained by adding the exponential term, or indeed a sequence of exponential terms if an N-mode Maxwell model is considered.

It can be seen that in general for a 1-smoothing problem, under the assumption that the relaxation modulus is a Dirichlet series, the bound on the perturbation $\gamma(t)$ in the solution $G(t)$ will always be of the form

$$\|\gamma\|_\infty \leq \frac{\|G\|_1}{\beta\|f\|_1 - \|G\|_1\|\phi\|_1}, \quad t \in [0,T] \tag{4-200}$$

and the stability criterion is therefore

$$\|\phi\|_1 < \frac{\beta\|f\|_1}{\|G\|_1}. \tag{4-201}$$

Provided $\phi \in L_1[0,T]$, then maximizing the value of $\|f\|_1$ provides an optimal bound in terms of stability for the problem. In terms of choice of an applied torque, this favours functions which assume a non-zero value for as much of the duration of the experimental time as possible.

IV. SUMMARY

In this chapter it has been established that although the governing equation is a Volterra integro-differential equation in the variable $\dot{\chi}(t)$, when the function $G(t)$ is to be determined the problem is actually a Volterra integral equation of the first kind, the solution of which is ill-posed w.r.t. perturbations in the data. The third of Hadamard's criteria for well-posedness, that the solution depends continuously on the data (i.e. stability), is the one that often fails to be satisfied for this type of problem, manifest in highly oscillatory solutions in the presence of even small amounts of noise. The degree of ill-posedness is quantified by the concept of a ν-smoothing problem, which is a measure of the degree of differentiation required to convert the problem to a well-posed Volterra integral equation of the second kind. Under this definition, the delta function belongs to the class of 1-smoothing problems, the step function, box function and square waves are 2-smoothing problems and the most ill-posed problems considered here are the 3-smoothing kernels which comprise the slope and ramp functions. Using this as a definition of optimality, the 1-smoothing problem is the best possible choice with respect to stability in the solution for the relaxation modulus $G(t)$.

The stability analysis which was adapted to this problem attempts to determine the maximum permissible amount of error in the measured data which will allow a stable solution to be obtained. In each case, both a bound on the maximum error $\|\gamma\|_\infty$ in the solution $G(t)$ in terms of the magnitude of the errors in $\dot{\chi}(t)$ and $f(t)$, which are denoted by $\|\phi\|_\infty$ and $\|\varepsilon\|_\infty$, respectively, and also conditions on ϕ are determined for which a stable solution can exist. Generally, larger values for the torque amplitude C_0 or C_δ increase stability, subject to the linear viscoelastic restraints in practice. The specific cases are summarized as follows:

Case 1. **1-smoothing problems**: This group includes the delta function and sequence of delta functions. It was shown in Section 3.1.1 that the 1-smoothing problem requires

the presence of a delta function in the applied torque to produce the step jump in the angular velocity of the platen at $t = 0$. Also, the torque such that $\dot{\chi}(t) = G(t)$ is a 1-smoothing problem and is therefore optimal in that sense. In general, the bound on the supremum of the perturbation in $G(t)$ for the 1-smoothing problem is given by

$$\|\gamma\|_\infty \leq \frac{\|G\|_1}{C_1 - C_2} \left[\|\varepsilon\|_\infty + \|G\|_1 \|\phi\|_\infty\right], \quad t \in [0, T]$$

wherefore it can be seen that an exact solution can be obtained as $\|\varepsilon\|_\infty \to 0$ and $\|\phi\|_\infty \to 0$ provided the constants satisfy $C_1 - C_2 > 0$. This gives rise to a further bound on the perturbation in the platen angular velocity $\phi(t)$, whereby $\|\phi\|_1$ must be less than a constant value which is proportional to the value kC_δ and the L_1-norm of the data function.

Case 2. **2-smoothing problems**: The step function and box function applied torques belong to the 2-smoothing class of problems along with the sum of exponentials mentioned in Theorem 3.2.3. The 2-smoothing case is slightly less stable than the 1-smoothing case, but not as much as would be expected considering the extra degree of differentiation required. The bound on the perturbation in the solution $G(t)$ has the general form

$$\|\gamma\|_\infty \leq \frac{G_0 + \|\dot{G}\|_1}{C_1 - C_2} \left[\|\varepsilon\|_\infty + \|G\|_1 \|\phi\|_\infty\right], \quad t \in [0, T]$$

which is similar to the 1-smoothing case, except that the criterion $C_1 - C_2 > 0$ places a tighter restriction on the allowable values for $\|\phi\|_1$. It is well-established that the 2-smoothing case is more ill-posed than the 1-smoothing case by a degree equivalent to that of first-order differentiation. This discrepancy might be explained by the fact that the stability analysis does not adapt particularly well to the case where the applied torque is a generalized function.

Case 3. **3-smoothing problems**: The 3-smoothing group of problems comprising the slope and ramp functions is the most ill-posed considered here and the bounds on the perturbation in the solution $G(t)$ are correspondingly worse. The inequality in this case is of the form

$$\|\gamma\|_\infty \leq \frac{1}{C_1 - C_2} \left\{G_0 \|\dot{\varepsilon}\|_\infty + \left|\dot{G}_0\right| \left[1 + \|\ddot{G}\|_1\right] \|\varepsilon\|_\infty + \left[G_0 + \|\dot{G}\|_1\right]^2 \|\phi\|_\infty\right\}, \quad t \in [0, T]$$

where the RHS now contains a term concerning the error in the derivative of the data function, $\|\varepsilon\|_\infty$, which will be greater in general than $\|\varepsilon\|_\infty$ and in the presence of very noisy data may even be unbounded. Also, the criterion $C_1 - C_2 > 0$ requires that

$\|\dot{\phi}\|_1$ is bounded - a condition unlikely to be satisfied in the presence of noisy data, since the perturbations in the data are not necessarily differentiable. Note that the sinusoidal waveform would also fall into this category, indicating that when obtaining $G(t)$ directly by this method it is not the best choice.

To conclude, it has been demonstrated that the best choice of applied torque, where stability of the solution is concerned and within a purely theoretical framework, is that which is associated with a 1-smoothing kernel $\dot{\chi}(t)$. Applied torque functions which give rise to 2- or 3-smoothing problems require progressively more restrictive conditions on the level of data error for which a stable solution exists, therefore it is desirable to choose a ν-smoothing problem with as small a value for ν as possible. The question then arises whether the 1-smoothing case can ever be achieved experimentally, since the delta function is really a mathematical abstraction representing a force of infinite magnitude for an infinitesimal duration. Any experimentally produced torque would resemble a box function in reality, which does not share the optimal properties of the delta function, wherefore from a purely practical point of view, the optimal case must be the 2-smoothing case corresponding to the step and box functions, etc.

CHAPTER 5

Numerical Solution

In this chapter the issues concerning the discretization of the governing equation in Volterra-1 form are investigated. Initially, the equation is solved using a basic piecewise constant collocation method for various applied torque functions, however the solution for the relaxation modulus is unstable in the presence of noisy data and some sort of regularization scheme is shown to be necessary. A brief overview of potential regularization schemes is given, then two examples are implemented; it is then demonstrated that the future-constant and future-polynomial regularization methods are effective in stabilizing the solution.

I. DISCRETIZATION METHODS

There are a number of options for discretization of Volterra integral equations of the first kind. Here, several potential methods are outlined, more detail being available in [16] and [7]. The basic underlying method is to replace the integral with a numerical quadrature scheme with the requirement that the resulting equation be satisfied exactly at a finite number of grid points, R, in $[0, T]$. Any reasonable discretization method for Volterra integral equations of the first kind results in a matrix equation of the form

$$\mathsf{A}^R \boldsymbol{u}^R = \boldsymbol{f}^R \tag{5-1}$$

where A^R is a lower-triangular matrix containing entries dependent upon the kernel function, $\boldsymbol{u}^R$ and $\boldsymbol{f}^R$ are vectors containing the solution and data values at the grid-points defined by $\boldsymbol{u}^R = (u_0, u_1, \ldots, u_{R-1})^T$ and $\boldsymbol{f}^R = (f_0, f_1, \ldots, f_{R-1})^T$, respectively.

5.1.1 Midpoint Rule

The midpoint rule entails approximating the integral at time t_i, on a uniform grid with number of grid-points R and time-step $h = \frac{T}{R}$ by

$$\int_0^{t_i} \phi(t)\,\mathrm{d}t \approx h \sum_{j=0}^{i-1} \phi(t_{j+\frac{1}{2}}), \quad i = 1, \ldots, R, \tag{5-2}$$

where $t_{j+\frac{1}{2}} = t_j + \frac{h}{2}$. Applying this to (4-10), the approximate solution

$$h \sum_{j=0}^{i-1} K(t_i, t_{j+\frac{1}{2}}) u_{j+\frac{1}{2}} = f(t_i), \quad i = 1, \ldots, R \tag{5-3}$$

is obtained. This leads to a matrix system of equations of the form (5-1), where A^R is a lower-triangular matrix containing entries dependent upon the kernel function according to (5-3), while $\boldsymbol{u}^R$ and $\boldsymbol{f}^R$ are vectors defined by $\boldsymbol{u}^R = (u_{\frac{1}{2}}, u_{\frac{3}{2}}, \ldots, u_{R+\frac{1}{2}})^T$ and $\boldsymbol{f}^R = (f_1, f_2, \ldots, f_r)^T$, respectively.

5.1.2 Trapezoidal Rule

The trapezoidal rule uses an affine function to interpolate the integrand, leading to the approximation

$$\int_0^{t_i} \phi(t)\,\mathrm{d}t \approx \tfrac{h}{2}\left[\phi(0) + 2\sum_{j=1}^{i-1}\phi(t_j) + \phi(t_i)\right] \tag{5-4}$$

for a general integral, and

$$\int_0^{t_i} K(t,t')u(t')\,\mathrm{d}t' \approx \tfrac{h}{2}\left[K(t_i,0)u(0) + 2\sum_{j=1}^{i-1}K(t_i,t_j)u(t_j) + K(t_i,t_i)u(t_i)\right], \quad i = 1,\ldots,R \tag{5-5}$$

for a Volterra integral. The Volterra integral equation of the first kind is thus approximated by

$$\tfrac{h}{2}\left[K(t_i,0)u(0) + 2\sum_{j=1}^{i-1}K(t_i,t_j)u(t_j) + K(t_i,t_i)u(t_i)\right] = f(t_i), \quad i = 1,2,\ldots,R. \tag{5-6}$$

It should be noted that the trapezoidal rule and higher order quadrature rules are in general numerically unstable for Volterra integral equations of the first kind as noted in [28] and are therefore of limited use for this problem.

5.1.3 Euler Method (Rectangular Rule)

The Euler method, sometimes known as the Rectangular rule, approximates the integral for $R \geq 1$ by

$$\int_0^{t_i} \phi(t)\,\mathrm{d}t = h\sum_{j=0}^{i-1}\phi(t_j) \tag{5-7}$$

and the Volterra integral becomes

$$\int_0^{t_i} K(t_i,t_j)u(t')\,\mathrm{d}t' = h\sum_{j=1}^{i-1}K(t_i,t_j)u(t_j). \tag{5-8}$$

The discretized version of (4-10) is then

$$h\sum_{j=0}^{i-1}K(t_i,t_j)u(t_j) = f(t_i), \quad i = 1,2,\ldots,R \tag{5-9}$$

which can be expressed as a matrix equation of the form (5-1), where the vectors $\boldsymbol{f}^R, \boldsymbol{u}^R \in \mathbb{R}^R$ are defined $\boldsymbol{f}^R = [f(t_1), f(t_2), \ldots, f(t_R)]^T$ and $[u(t_0), u(t_1), \ldots, u(t_{R-1})]^T$. The matrix A^R is lower triangular with non-zero entries given by $[\mathsf{A}^R]_{i,j} = hK(t_i, t_{j-1}), i \leq j$.

5.1.4 Collocation

Collocation methods represent a class of approximations which can be generalized to arbitrarily high order. The method of choice for solving this problem is the simplest form using piecewise constant polynomials, but a short overview of the general background theory is included here - good references for an in-depth examination of the subject can be found in [16] and [7].

The basis for the method is to obtain an approximate solution $\boldsymbol{u}^R$ in the space of piecewise polynomials $S_{m-1}^{(-1)}(R)$, given intervals $\sigma_i = (t_{i-1}, t_i], i = 1, 2, \ldots, R$, where

$$S_{m-1}^{(-1)}(R) = \{u : u|_{\sigma_i} \in \Pi_{m-1}, i = 1, \ldots, R\} \tag{5-10}$$

and Π_k is the space of real polynomials of degree $\leq k$. Now $\dim S_{m-1}^{(-1)}(R) = Rm$, so the same number of conditions need to be imposed on the approximate solution to obtain a unique solution by defining Rm collocation points

$$X_m(R) = \left\{t_{i,j} = t_{i-1} + c_j h : j = 1, \ldots, m, i = 1, \ldots, R\right\} \tag{5-11}$$

where $\{c_j\}_{j=1}^m$ are the *collocation parameters* which satisfy $0 < c_1 < \cdots < c_m \leq 1$. Additionally, the solution $\boldsymbol{u}^R \in S_{m-1}^{(-1)}(R)$ must satisfy $Au = f$ exactly at each collocation point in $X_m(R)$. This results in a system of linear equations of the standard form $\mathsf{A}^R \boldsymbol{u}^R = \boldsymbol{f}^R$ with $R \times m$ block-triangular matrix A^R (i.e. it has R diagonal $m \times m$ blocks each nonsingular for $h > 0$ sufficiently small if the problem is 1-smoothing), leading to a block-sequential solution method. Analysis for the optimal choice of the collocation parameters where convergence is concerned may be found in [16].

The simplest form of collocation corresponds to a choice of $c_m = 1$, so that collocation occurs at each of the grid-points $t_j, j = 1, \ldots, R$. This is the method chosen for this problem, whereby collocation is considered in the space of piecewise constant polynomials, denoted $S_0^{(-1)}(R)$. Defining the characteristic function $\Psi_i(t)$ on σ_i for $i = 1, \ldots, R$ by

$$\Psi_i(t) = \begin{cases} 1 & t \in \sigma_i, \\ 0 & \text{otherwise}, \end{cases} \tag{5-12}$$

then the collocation solution u^R is given by

$$u^R(t) = \sum_{i=1}^{R} c_i \Psi_i(t), \quad t \in [0, T]. \tag{5-13}$$

Noting that for the convolution kernel [44]

$$\begin{aligned} Au(t_j) &= \int_0^{t_j} K(t_j - t') \sum_{i=1}^{R} c_i \Psi_i(t') \, \mathrm{d}t' \\ &= \sum_{i=1}^{j} c_i \int_{t_{i-1}}^{t_i} K(t_j - t') \, \mathrm{d}t' \\ &= \sum_{i=1}^{j} c_i \int_0^{t_1} K(t_{j-i+1} - s) \, \mathrm{d}s = f(t_j) \end{aligned} \tag{5-14}$$

where the substitution $s = t' - t_{i-1}$ has been used. Therefore, the matrix equation $\mathsf{A}^R \boldsymbol{c}^R = \boldsymbol{f}^R$ is obtained, where A^R is an $R \times R$ lower triangular matrix and additionally of Toeplitz type with constant diagonal values. More explicitly,

$$\begin{bmatrix} \Delta_1 & 0 & 0 & \cdots & 0 \\ \Delta_2 & \Delta_1 & 0 & \cdots & 0 \\ \Delta_3 & \Delta_2 & \Delta_1 & \cdots & 0 \\ \vdots & \vdots & \ddots & \ddots & \vdots \\ \Delta_R & \Delta_{R-1} & \cdots & \Delta_2 & \Delta_1 \end{bmatrix} \begin{bmatrix} c_1 \\ c_2 \\ c_3 \\ \vdots \\ c_R \end{bmatrix} = \begin{bmatrix} f_1 \\ f_2 \\ f_3 \\ \vdots \\ f_R \end{bmatrix} \tag{5-15}$$

where

$$\Delta_i := \int_0^{t_1} K(t_i - t') \, \mathrm{d}t'. \tag{5-16}$$

The c_i are then calculated using forward substitution and are given by

$$c_i = \frac{f_i - \sum_{j=1}^{i-1} c_j \Delta_{i-j+1}}{\Delta_1}, \quad i = 1, \ldots, R. \tag{5-17}$$

The moment integrals Δ_i can be determined analytically for simple kernel functions or by a discrete quadrature rule, the optimal choice of rule in terms of stability being discussed in [16]. However, for this problem, note that

$$\begin{aligned} \int_0^{t_1} K(t_i - t') \, \mathrm{d}t' &= \int_0^{t_1} \dot{\chi}(t_i - t') \, \mathrm{d}t' \\ &= \left[-\chi(t_i - t') \right]_0^{t_1} \\ &= \chi(t_i) - \chi(t_{i-1}), \quad i = 1, \ldots, R. \end{aligned} \tag{5-18}$$

This discretization method therefore has the advantage that the data $\chi(t)$ can be used directly instead of the kernel $\dot{\chi}(t)$; since differentiation is an ill-posedness process, this should reduce the potential amount of error involved in the method of solution. The solution $u^R(t)$ obtained by this process is then a piecewise constant solution that converges uniformly to the exact solution $\bar{u}$ at a rate of $\mathcal{O}(h)$.

5.1.5 Condition Number

Standard discretization schemes for ill-posed Volterra problems generally result in systems of linear equations which are ill-conditioned, i.e. the matrix in (5-1) is close to singularity, hence simple inversion of the matrix may result in unacceptably large errors in the solution. The stability of the linear system (5-1) can be quantified using a *condition number*. This is essentially a measure of a problem's amenity to digital computation; a high condition number indicates the problem is ill-conditioned and thus the matrix A^R is close to being singular. There are several types of condition number depending upon the matrix norm which is used; here the ∞-norm version is used.

$$\kappa(A) = \|\mathsf{A}\|_\infty \cdot \|\mathsf{A}^{-1}\|_\infty \tag{5-19}$$

where $\|\mathsf{A}\|_\infty$ is the matrix ∞-norm defined as the maximum absolute row sum

$$\|\mathsf{A}\|_\infty = \max_{1\le i\le n} \sum_{j=1}^{n} |A_{ij}| \tag{5-20}$$

for a square matrix A. An approximate method for estimating the condition number without evaluating the inverse matrix A^{-1} can be found in [30], but here Maple is used to calculate the exact values.

II. REGULARIZATION OF VOLTERRA-1 EQUATIONS

In Chapter 4 it was established that the solution of the problem in the form of a Volterra integral equation of the first kind is ill-posed. It is insufficient merely to replace the measured data $f(t)$ and $\Omega(t)$ with their perturbed forms and use standard solution methods, since this usually results in highly oscillatory solutions. Therefore to obtain a stable solution some form of regularization procedure is required. A short summary of the available options pertinent to this problem is included in this section, but for a comprehensive overview of regularization methods for Volterra integral equations of the first kind the papers [50] and [52] should be consulted.

The standard approach for stabilizing the solution of ill-posed first kind integral equations has been to use Tikhonov regularization [31]. In common with most regularization methods, the underlying technique is to transform the Volterra integral of the first kind, which is ill-posed in nature, into a well-posed equation of the second kind by imposing assumptions about the nature of the solution. The Tikhonov method approaches the problem in a least squares sense, given a perturbation f^ε of the data,

by minimizing the quantity

$$\min_u \|Au - f^\varepsilon\|^2 + \alpha\|\mathcal{L}u\|^2 \tag{5-21}$$

where the Volterra operator A is defined as in (4-12) and $\mathcal{L}$ is an operator used to stabilize the solution such as the identity or differential operator, for example. The parameter $\alpha > 0$ is known as the *Tikhonov regularization parameter* and balances the bias towards accuracy of model-fitting or stability achieved by the extra operator term and there are well-established conditions for choosing an optimal value. This is equivalent, using the identity operator in place of $\mathcal{L}$, to solving the normal equations

$$\left(A^\dagger A + \alpha I\right) u = f^\varepsilon \tag{5-22}$$

where $A^\dagger$ is the adjoint operator, defined as

$$A^\dagger u := \int_t^T K(t,t')u(t')\,\mathrm{d}t'. \tag{5-23}$$

Therefore, the Tikhonov method requires that the data is known on the whole domain of solution $[0,T]$, indicating that only once the data for the whole experiment has been collected can the solution process commence. However, this does not take advantage of the important *causal* or *non-anticipatory* property of Volterra integral equations, which means that at any point in time $t \in [0,T]$ the solution depends only upon the past data $[0,t]$ and is independent of future data in $[t,T]$. The consequences of this attribute are that solution methods which preserve the causal property can be solved in near real-time as the data is accumulated. Discretization methods of "Volterra-type" generally result in a lower-triangular matrix A^R as noted in (5-1) which can be solved efficiently by sequential methods, whereas $(\mathsf{A}^R)^T\mathsf{A}^R$ will typically be a full matrix which is more computationally expensive to solve and in general more poorly conditioned than A^R.

A veritable plethora of regularization methods exist for integral equations (see [50] for an overview and references), some of which preserve the causal nature of Volterra equations. One disadvantage of regularization methods of Volterra type is that convergence is more difficult to prove, since the spectral properties of $A^\dagger A$ cannot be used, and is generally limited to low ν values (see Definition 4.2.1). In discrete form, the ill-posedness is manifest in the value of the diagonal entries, which are close to zero, wherefore the general idea in Volterra methods is to augment those values. In an infinite-dimensional setting this corresponds to

$$\alpha u(t) + \int_0^t K(t,t')u(t')\,\mathrm{d}t' = f^\varepsilon(t), \quad t \in [0,T], \tag{5-24}$$

which is a second-kind equation with a unique solution u_α^ε which depends continuously on the data.

Differentiation ν-times of the Volterra-1 equation results in an equation of the second kind of the form (4-17), but since differentiation is an ill-posed process additional steps must be taken to ensure the derivative of the perturbed data is obtained in a stable manner. Some examples of methods of this type are mentioned in [50] with references to the literature.

The process of discretization itself, has the effect of a basic form of regularization; the regularization parameter in this case is the step-size which can be coordinated to the level of noise present in the data. An ill-posed infinite dimensional equation is thereby transformed into a well-posed finite dimensional problem, although the resulting matrix may be ill-conditioned, the degree of ill-conditioning increasing with increasing dimension. As the error level $\varepsilon \to 0$, then the step size can be reduced to an arbitrarily small size $h \to 0$. However, for $\varepsilon > 0$, there is a lower limit to the practicable value of h. This "self-regularization" property consequently often leads to an unacceptably coarse grid in the presence of noisy data or for highly ill-posed problems and in practice further regularization is usually required. The midpoint and Euler methods are the only reasonable quadrature methods; the trapezoidal, higher-order Gregory and Newton-Cotes integration rules being numerically unstable for Volterra-1 problems [28]. This is an example of how the ill-posedness of Volterra-1 equations influences the solution method, in comparison with the Volterra-2 equation for which any standard numerical approximation produces a stable solution. A discretization method is *robust* for a 1-smoothing problem if the amplification of the data error is of $\mathcal{O}(\varepsilon/h)$ as $h \to 0$. The midpoint method is robust for 1-smoothing problems [5] and thus can handle the error level for 1-smoothing problems by varying the step-size. Most standard discrete methods when taken in isolation are only effective for 1-smoothing problems at best, since they result in a diagonal term $K(t,t)$ which is zero for $\nu > 1$. Exceptions to this are collocation [23] and linear multistep methods [4] (for $\nu = 2$). For ill-posed problems the best approach is to combine a discretization method with a continuous regularization method, both of which preserve the Volterra nature of the problem.

5.2.1 Local Regularization

A significant class of regularization methods of Volterra type can be termed *local regularization methods*, the basic underlying principle being to decompose the operator A

into "local" and "nonlocal" components, then the local part alone is inverted by a regularized procedure. Recent papers dealing with this group of methods are [44], [45], [46], [47], [55], [18], [53] and [54]. This is the type of method which has been chosen here as most pertinent and simplest to apply to this particular problem. First, an overview of the theory of the continuous regularization version is given, then the details of the discretization are described and adapted to apply to the stress-controlled rheometry integral equation.

The underlying idea in an infinite-dimensional (continuous) setting first introduced in [44] and [46] is to construct a well-posed Volterra integral equation of the second kind by assuming that the solution on $[t, t+\Delta_r]$ for some $\Delta_r > 0$ is "regular" in some fashion, in this case it is assumed to be constant in that interval. The constant Δ_r fulfills the role of the regularization parameter here. Extending the domain from $[0, T]$ to $[0, T+\Delta_r]$, (4-13) becomes

$$\int_0^{t+\rho} K(t+\rho-t')u(t')\,\mathrm{d}t' = f(t+\rho), \quad t \in [0,T], \rho \in [0,\Delta_r] \tag{5-25}$$

or equivalently, by splitting the domain and a change of variable $t' \to t'+t$,

$$\int_0^{t} K(t+\rho-t')u(t')\,\mathrm{d}t' + \int_0^{\rho} K(\rho-t')u(t+t')\,\mathrm{d}t' = f(t+\rho). \tag{5-26}$$

The equation is extended slightly into the future by an amount ρ. Integrating w.r.t. ρ and changing the order of integration in the first integral,

$$\int_0^{t}\int_0^{\Delta_r} K(t+\rho-t')\,\mathrm{d}\rho u(t')\,\mathrm{d}t' + \int_0^{r}\int_0^{\rho} K(\rho-t')u(t+t')\,\mathrm{d}t'\,\mathrm{d}\rho = \int_0^{\Delta_r} f(t+\rho)\,\mathrm{d}\rho. \tag{5-27}$$

Replacing the data function with a perturbed function f^ε, and since the solution is assumed to be constant on the interval $[t, t+\Delta_r]$, $u(t+t')$ becomes $u(t)$, it can be seen that (5-27) is actually a Volterra equation of the second kind, viz.

$$\alpha(t;\Delta_r) + \int_0^{t} \tilde{K}(t-t';\Delta_r)u(t')\,\mathrm{d}t' = \tilde{f}^\varepsilon(t;\Delta_r), \quad t \in [0,T]. \tag{5-28}$$

The new functions can be generalized to the Stieltjes integrals

$$\alpha(t;\Delta_r) = \int_0^{\Delta_r}\int_0^{\rho} K(\rho-t')\,\mathrm{d}t'\,\mathrm{d}\eta_{\Delta_r}(\rho), \quad 0 \le t' \le t \le T \tag{5-29a}$$

$$\tilde{K}(t-t';\Delta_r) = \int_0^{\Delta_r} K(t+\rho-t')\,\mathrm{d}\eta_{\Delta_r}(\rho) \tag{5-29b}$$

$$\tilde{f}^\varepsilon(t;\Delta_r) = \int_0^{r} f^\varepsilon(t+\rho)\,\mathrm{d}\eta_{\Delta_r}(\rho), \tag{5-29c}$$

where $\eta_{\Delta_r}(\rho)$ is a positive Borel-Stieltjes measure, the choice of which can rise rise to a family of regularization methods. Conditions guaranteeing convergence for general ν-smoothing problems with convolution kernels can be found in [47]. One potential disadvantage of this method is that the solution can only be obtained on a contracted interval $[0, T - \Delta_r]$, but since the experimental duration could easily be extended to $[0, T + \Delta_r]$ this is only a minor consideration.

III. PREDICTOR-CORRECTOR REGULARIZATION

We now proceed to look at the discrete form of the regularization algorithm formulated in [47] and apply it to this particular problem. Consider a uniform grid with $R + 1$ grid-points and time-step $h = 1/R$. Thus $t_j = jh$ for $j = 0, 1, \ldots R$. It is useful to extend the solution range beyond the normal value for T to allow for the utilization of a small amount of future information of length $\Delta_r = (r-1)h, r \geq 2$ in the solution process towards the end of the duration of the experiment, so take $j = 0, 1, \ldots, R, R+1, \ldots, R+r-1$. Alternatively, a restricted solution range could be taken if the data has already been obtained.

Incorporating the collocation algorithm described in Section 5.1.4, (5-28) becomes

$$\alpha(\Delta_r)c_j + \int_0^{t_j} \tilde{K}(t_j - t'; \Delta_r) \left[\sum_{i=1}^{j} c_i \Psi(t') \right] \mathrm{d}t' = \int_0^{\Delta_r} f^{\varepsilon}(t_j + \rho)\, \mathrm{d}\eta_{\Delta_r}(\rho) \tag{5-30}$$

which is a lower triangular system with non-zero diagonal entries and therefore possesses a unique solution. The solution is held constant on $[t, t + \Delta_r]$, leading to the specific choice $\sum_{i=1}^{r} s_i \delta(t - \tau_i \Delta_r)$ for the measure $\eta_{\Delta_r}(\rho)$. The theoretical matters pertaining to convergence for this particular choice of the measure for Volterra-1 equations in general are discussed in some detail [47]. The relevant constants are defined

$$s_i = \frac{\int_0^{t_i} K(t_i - t')\, \mathrm{d}t'}{\int_0^{t_1} K(t_1 - T')\, \mathrm{d}t'}, \quad i = 1, \ldots, r \tag{5-31}$$

and

$$\tau_i = \frac{i-1}{r-1}, \quad r \geq 2. \tag{5-32}$$

The unregularized case corresponds to $r = 1$ and the definition $\tau_1 = 0$ is required. For this problem, $K \equiv \dot{\chi}$, so the specific value

$$s_i = \frac{\chi(t_i)}{\chi(t_1)}, \quad i = 1, \ldots, r \tag{5-33}$$

will be used. The piecewise constant solution obtained by this process is denoted $u_r^R = \sum_{j=1}^{R} c_{j,r}\Psi(\tau_i\Delta_r)$, in which the collocation parameters $c_{j,r}$ are found sequentially, being held constant over the interval $[t_j, t_j + \Delta_r]$. Once the solution has been determined for each time-step t_j, the constant portion of the solution (the "predictor" step) on the future interval $[t_j, t_{j+\Delta_r}]$ is discarded (the "corrector" step) and the procedure moves on to the the next time-step.

The end result is a system of linear equations which can be represented in matrix form by

$$\mathsf{A}_r^R \boldsymbol{u}^R = \boldsymbol{f}_r^R \tag{5-34}$$

where A_r^R is a lower triangular, Toeplitz matrix, $\boldsymbol{u}_r^R = [c_1, c_2, \ldots, c_R]^T$ and $\boldsymbol{f}_r^R = [\tilde{f}_1, \tilde{f}_2, \ldots, \tilde{f}_R]^T$. The modified data function vector components are given by

$$\tilde{f}_i = \sum_{j=1}^{r} s_j f(t_{i+j-1}), \quad i = 1, \ldots, R \tag{5-35}$$

in terms of the s_j in (5-33). The elements of the matrix A_r^R can be expressed in the form

$$\mathsf{A}_r^R = \begin{bmatrix} s_1\tilde{\Delta}_1 + \cdots + s_r\tilde{\Delta}_r & 0 & 0 & 0 \\ s_1\Delta_2 + \cdots + s_r\Delta_{r+1} & s_1\tilde{\Delta}_1 + \cdots + s_r\tilde{\Delta}_r & 0 & 0 \\ s_1\Delta_3 + \cdots + s_r\Delta_{r+2} & s_1\Delta_2 + \cdots + s_r\Delta_{r+1} & \ddots & 0 \\ \vdots & \vdots & \ddots & \vdots \\ s_1\Delta_R + \cdots + s_r\Delta_{R+r-1} & s_1\Delta_{R-1} + \cdots + s_r\Delta_{R+r-2} & \ldots & s_1\tilde{\Delta}_1 + \cdots + s_r\tilde{\Delta}_r \end{bmatrix} \tag{5-36}$$

where $\tilde{\Delta}_i := \sum_{j=1}^{i} \Delta_j, i = 1, \ldots, r$. Note that for $r = 1$, the matrix is consistent with the standard collocation formulation in (5-15). Since A_r^R is Toeplitz in nature, it takes the form

$$\mathsf{A}_r^R = \begin{bmatrix} x_1 & 0 & 0 & 0 \\ x_2 & x_1 & 0 & 0 \\ x_3 & x_2 & \ddots & \vdots \\ \vdots & \vdots & \ddots & \vdots \\ x_R & x_{R-1} & \ldots & x_1 \end{bmatrix} \tag{5-37}$$

so it can be represented by a single vector $\boldsymbol{x}$ with entries given by

$$x_1 = \sum_{j=1}^{r} s_j\tilde{\Delta}_j = \sum_{j=1}^{r} \frac{[\chi(t_j)]^2}{\chi(t_1)} \tag{5-38}$$

and

$$x_i = \sum_{j=1}^{r} s_j \Delta_{i+j-1} = \sum_{j=1}^{i} \frac{\chi(t_j)}{\chi(t_1)} \left[\chi(t_{i+j-1}) - \chi(t_{i+j-2})\right], \quad i = 2, \ldots, R \tag{5-39}$$

since, from (5-18) and under the assumption that $\chi(0) = 0$ we have

$$\begin{aligned} \tilde{\Delta}_i &= \sum_{j=1}^{i} \Delta_j \\ &= \sum_{j=1}^{i} \left[\chi(t_j) - \chi(t_{j-1})\right] \\ &= \chi(t_i), \quad i = 1, \ldots, r \end{aligned} \tag{5-40}$$

whereby the memory storage requirements are reduced to $\mathcal{O}(R)$ rather than $\mathcal{O}(R^2)$. Finally, the solution is obtained by forward substitution using

$$c_i = \frac{f_1 - \sum_{j=1}^{i-1} x_{i-j+1} c_j}{x_1}, \quad i = 1, 2, \ldots, R. \tag{5-41}$$

The future-constant algorithm is now applied to the stress-controlled rheometry problem. First, the conditioning of the system is analysed for exact data, exact in the sense that the only error present is that due to the limitations of machine precision; here Maple was used with a precision of 40 digits. To simulate the effect of experimental error, random noise is added to the synthesized data which is uniformly distributed in $[-1, 1]$. Denoting the maximum error level by α, then the actual error added to the exact value will lie in the interval $[-\alpha\|f\|_\infty, \alpha\|f\|_\infty]$. An error level of approximately 1% is considered to represent normal experimental conditions; a value of 5% represents an extreme case. Since $\chi(0) = 0$ for any physical form for the applied torque, the error in the error in the platen displacement data is assumed to be zero for $t = 0$. Note that the data function requires differentiation of the data and therefore will always contain a higher level of noise than the directly measured platen displacement which is used to evaluate the matrix. In these examples, the second derivative in the data function is obtained analytically before the noise is added to the data, but in practice this will need to be calculated numerically. Since differentiation is an ill-posed process, additional regularization may be required to acquire a reasonable solution - much literature can be found on this subject, a good synopsis being found in [73] and [74].

5.3.1 Delta function

Consider first the delta function applied torque as described in Section 2.2. Assuming the material is a Maxwell fluid, the platen displacement is given by (2-79) in the case

of complex roots, and the data function by (4-148). Applying the simple piecewise-constant collocation discretization described in Section 5.1.4, it can be seen in Figure 5.1 that a stable solution for $G(t)$ exists with exact data. The solution is actually piecewise constant on each interval $[t_{i-1}, t_i], i = 1, \ldots, R$, but for the sake of clarity the graphs are constructed by joining the values of the solution at the midpoints of each interval. A range of grid sizes are depicted, reflecting the dimension of the matrix A^R and it appears that the numerical solution converges to the exact solution as $h \to 0$, or equivalently $R \to \infty$. This however represents the best possible choice of applied torque combined with precisely known data - a scenario impossible to achieve in reality.

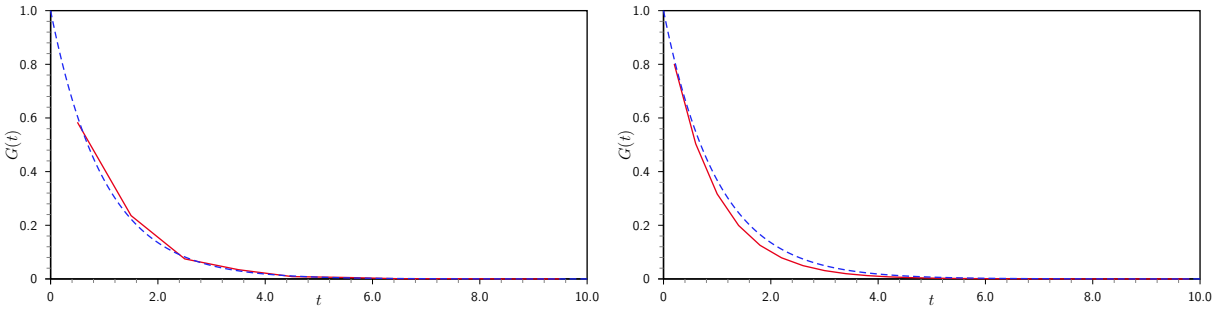

(a) $R = 10$

(b) $R = 25$

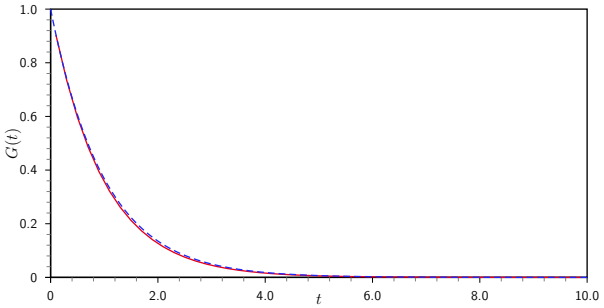

(c) $R = 50$

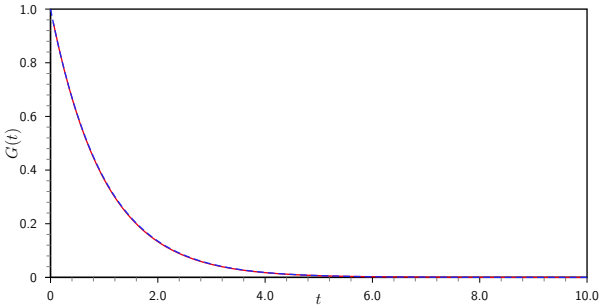

(d) $R = 100$

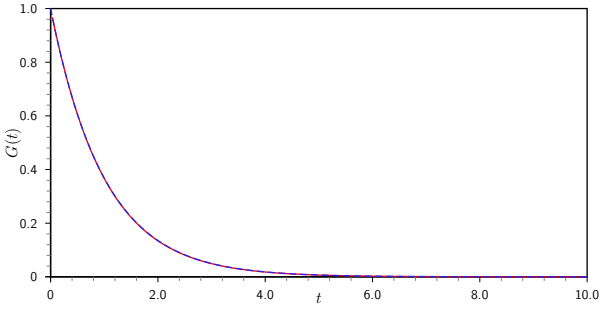

(e) $R = 150$

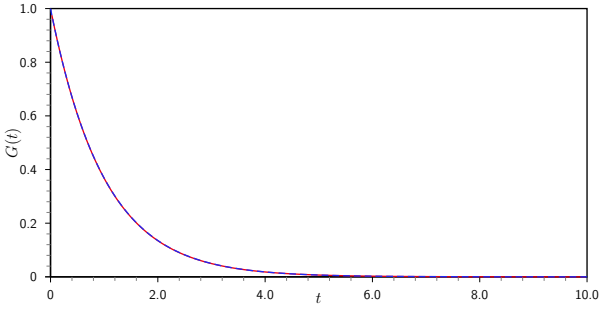

(f) $R = 200$

Figure 5.1: Numerical solution: delta function, Maxwell model $(\psi < 0)$, exact data.

The condition number of A^R as defined in (5-19) is generally small ($\mathcal{O}(10^1)$), so the linear system (5-15) is well-conditioned in the case of exact data and the matrix can be inverted in a stable manner. The matrix A^R, the elements of which are defined in (5-15), depends only upon the kernel function $\dot{\chi}(t)$ and can be determined directly from the measured platen displacement $\chi(t)$, wherefore the condition number will be independent of the error in the data function. This is fortuitous, since the error level in the kernel will generally be lower than that in the data function, which involves evaluation of the second derivative of the platen displacement. In Table 5.1 condition numbers are given for various values from 0-5% of the maximum error level in the measured data $\chi(t)$, which is denoted by $\|\rho(t)\|_\infty$. It can be seen that increasing the error level in the kernel generally produces a moderate increase in the condition number, except for very large values for the number of grid-points and the extreme value of 5% for the error level. The solution for $R = 100$ is shown for each of the error levels in Figure 5.2. The solution is reasonable except in the 5% error case, which corresponds to a matrix system with condition number of $\mathcal{O}(10^4)$. For comparison, the number of grid-points is increased to $R = 150$ in Figure 5.3, where as expected the errors in the solution are visibly greater and the solution is more oscillatory in nature for comparable values of the maximum error $\|\rho(t)\|_\infty$ in the measured $\chi(t)$ data. The condition numbers for the N-mode Maxwell model are calculated in Table 5.2 and since the same qualitative behaviour is shown, only the analysis for the single mode Maxwell model is considered henceforth.

$\|\rho\|_\infty$ (%)	R=10	R=25	R=50	R=100	R=150	R=200
0.00	$4.4873\ 10^0$	$1.2010\ 10^1$	$2.1995\ 10^1$	$2.5598\ 10^1$	$3.8776\ 10^1$	$5.1924\ 10^1$
0.01	$4.4874\ 10^0$	$1.2008\ 10^1$	$2.2008\ 10^1$	$2.5551\ 10^1$	$3.9175\ 10^1$	$5.0533\ 10^1$
0.05	$4.4876\ 10^0$	$1.2021\ 10^1$	$2.2230\ 10^1$	$2.6257\ 10^1$	$3.8787\ 10^1$	$5.0254\ 10^1$
0.10	$4.4940\ 10^0$	$1.2092\ 10^1$	$2.2271\ 10^1$	$2.5556\ 10^1$	$4.3958\ 10^1$	$4.8096\ 10^1$
0.50	$4.5304\ 10^0$	$1.2185\ 10^1$	$2.4358\ 10^1$	$5.9262\ 10^1$	$2.8277\ 10^2$	$9.8362\ 10^2$
1.00	$4.6109\ 10^0$	$1.2272\ 10^1$	$2.5871\ 10^1$	$9.3634\ 10^1$	$6.4967\ 10^2$	$4.5399\ 10^3$
5.00	$4.7966\ 10^0$	$1.4012\ 10^1$	$4.7230\ 10^1$	$1.2239\ 10^4$	$1.2034\ 10^{10}$	$5.3879\ 10^{25}$

Table 5.1: Condition numbers for A^R, delta function applied torque, Maxwell model ($\psi < 0$).

The effect of the error in the data function is depicted in Figure 5.4, which shows the solution for the same relative error values for the error $\varepsilon(t)$ in the data function $f(t)$ as previously used for the $\chi(t)$ data, the kernel data being assumed to be exact. As

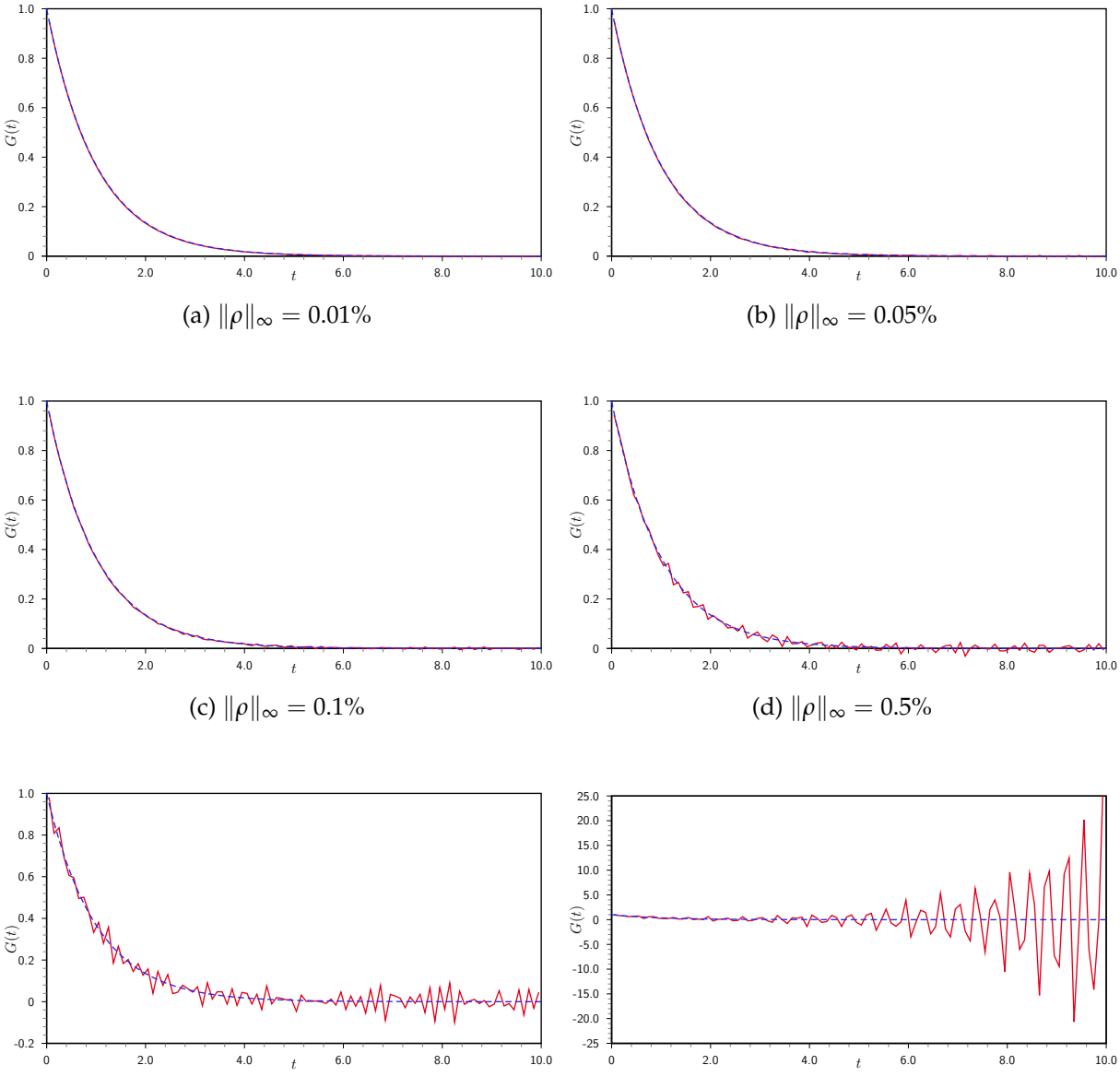

(a) $\|\rho\|_\infty = 0.01\%$ (b) $\|\rho\|_\infty = 0.05\%$

(c) $\|\rho\|_\infty = 0.1\%$ (d) $\|\rho\|_\infty = 0.5\%$

(e) $\|\rho\|_\infty = 1\%$ (f) $\|\rho\|_\infty = 5\%$

Figure 5.2: Numerical solution: delta function, Maxwell model ($\psi < 0$), $R = 100$, noisy data.

expected, the instability worsens as the error level is increased, but the apparent effect on the accuracy of solution is less than that of the kernel error. The combined effect of noise in both the platen displacement data and data function is illustrated in Figure 5.5 for various combinations of error level, subject to the specification that $\|\rho\|_\infty < \|\varepsilon\|_\infty$ as mentioned previously. Henceforth, the values 1% and 5% for the relative errors in $\chi(t)$ and $f(t)$ shall be assumed to be representative of typical experimental data.

A basic form of regularization can be implemented by varying the step-size, since for problems exhibiting a low degree of ill-posedness reducing the step-size often re-

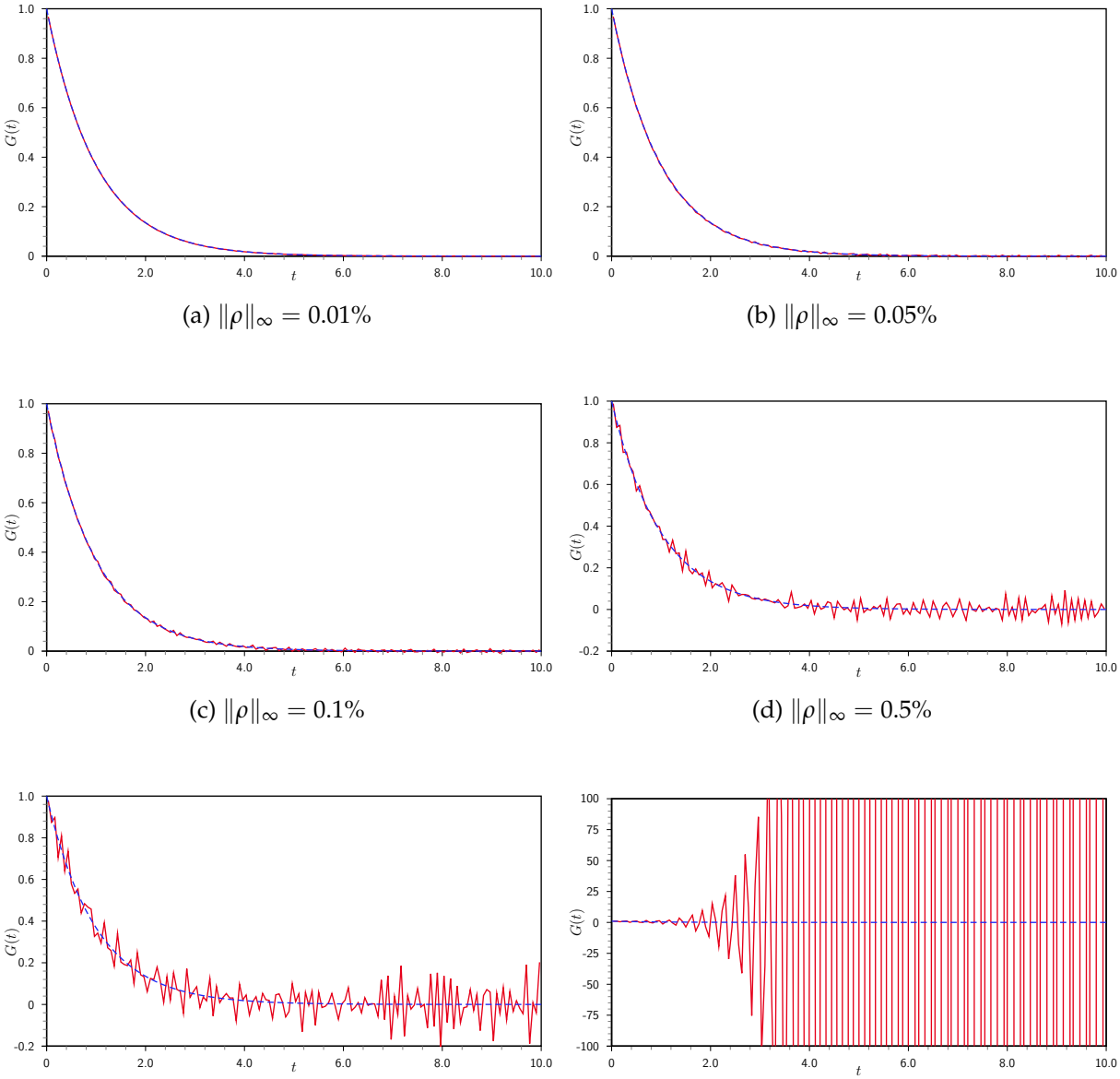

(a) $\|\rho\|_\infty = 0.01\%$ (b) $\|\rho\|_\infty = 0.05\%$

(c) $\|\rho\|_\infty = 0.1\%$ (d) $\|\rho\|_\infty = 0.5\%$

(e) $\|\rho\|_\infty = 1\%$ (f) $\|\rho\|_\infty = 5\%$

Figure 5.3: Numerical solution: delta function, Maxwell model ($\psi < 0$), $R = 150$, noisy data.

sults in a sufficiently stable solution. The effect of this approach is shown in Figure 5.6. For the smallest step-size, the solution is unacceptably oscillatory with considerable relative error. Reducing the step-size results in convergence to the true solution, although sufficiently accurate results are only achieved by using a very coarse grid with 10 points, or one grid-point per second in this case. One consequence of this is that the value of $G(0)$ can not be estimated with any accuracy.

The implementation of the future-constant algorithm described in Section 5.3 is illustrated in Figure 5.7 for various values of the regularization parameter, r, which is a

$\|\rho\|_\infty$ (%)	R=10	R=25	R=50	R=100	R=150	R=200
0	4.2147 10^1	8.4185 10^1	8.7363 10^1	1.0283 10^2	1.1389 10^2	1.2424 10^2
0.01	4.2148 10^1	8.4172 10^1	8.7358 10^1	1.0281 10^2	1.1392 10^2	1.2424 10^2
0.05	4.2121 10^1	8.4086 10^1	8.7372 10^1	1.0282 10^2	1.1404 10^2	1.2469 10^2
0.10	4.2148 10^1	8.4395 $10^1$1	8.7411 10^1	1.0273 10^2	1.1456 10^2	1.2490 10^2
0.50	4.2403 10^1	8.4861 10^1	8.7718 10^1	1.0532 10^2	1.2690 10^2	2.4018 10^2
1.00	4.2082 10^1	8.1848 10^1	8.6870 10^1	1.1605 10^2	1.6400 10^2	6.4673 10^2
5.00	4.0824 10^1	1.0629 10^2	1.0168 10^2	1.5226 10^3	5.5984 10^3	1.6521 10^{12}

Table 5.2: Condition numbers for A^R, delta function applied torque, N-mode Maxwell model.

r	R=10	R=25	R=50	R=100	R=150	R=200
1	4.5398 10^0	1.2276 10^1	2.6641 10^1	1.4785 10^2	4.9554 10^2	2.6721 10^3
2	3.1084 10^0	1.0654 10^1	1.5252 10^1	2.6210 10^1	6.2197 10^1	2.3790 10^1
3		9.9685 10^0	1.2021 10^1	1.9058 10^1	3.0930 10^1	4.7456 10^1
4			1.1432 10^1	1.5816 10^1	2.2897 10^1	3.1652 10^1
5			1.1068 10^1	1.3672 10^1	1.8956 10^1	2.4473 10^1
6			1.0732 10^1	1.2592 10^1	1.6645 10^1	2.0699 10^1
7			1.1037 10^1	1.2236 10^1	1.5246 10^1	1.8285 10^1
8			1.1679 10^1	1.1968 10^1	1.3685 10^1	1.6627 10^1
9			1.1789 10^1	1.1606 10^1	1.3085 10^1	1.5457 10^1
10			1.1137 10^1	1.1440 10^1	1.2742 10^1	1.4070 10^1

Table 5.3: Condition numbers for A_r^R, delta function applied torque, Maxwell model $(\psi < 0)$, (1%,5%) error, future constant regularization.

measure of the length of the future interval which is used to stabilize the solution. The first graph in the sequence shows the solution for $r = 1$, i.e. no regularization is occurring, which is unacceptably oscillatory. For $r = 2$, one future interval is used and has a noticeable smoothing effect on the solution, which has already achieved reasonable stability. The best result in this case is probably achieved by using $r = 3$, for which a reasonable approximation to the true solution is obtained. Increasing the value of r further results in an increasingly smooth solution, however the solution departs from the true solution for small values of t. There is therefore an optimal value for the choice of the regularization parameter r beyond which over-regularization may occur. It should be noted that the flat part of the solution appears to benefit from large values of r, while the steep section near $t = 0$ gains more accuracy for smaller values of r, suggesting that

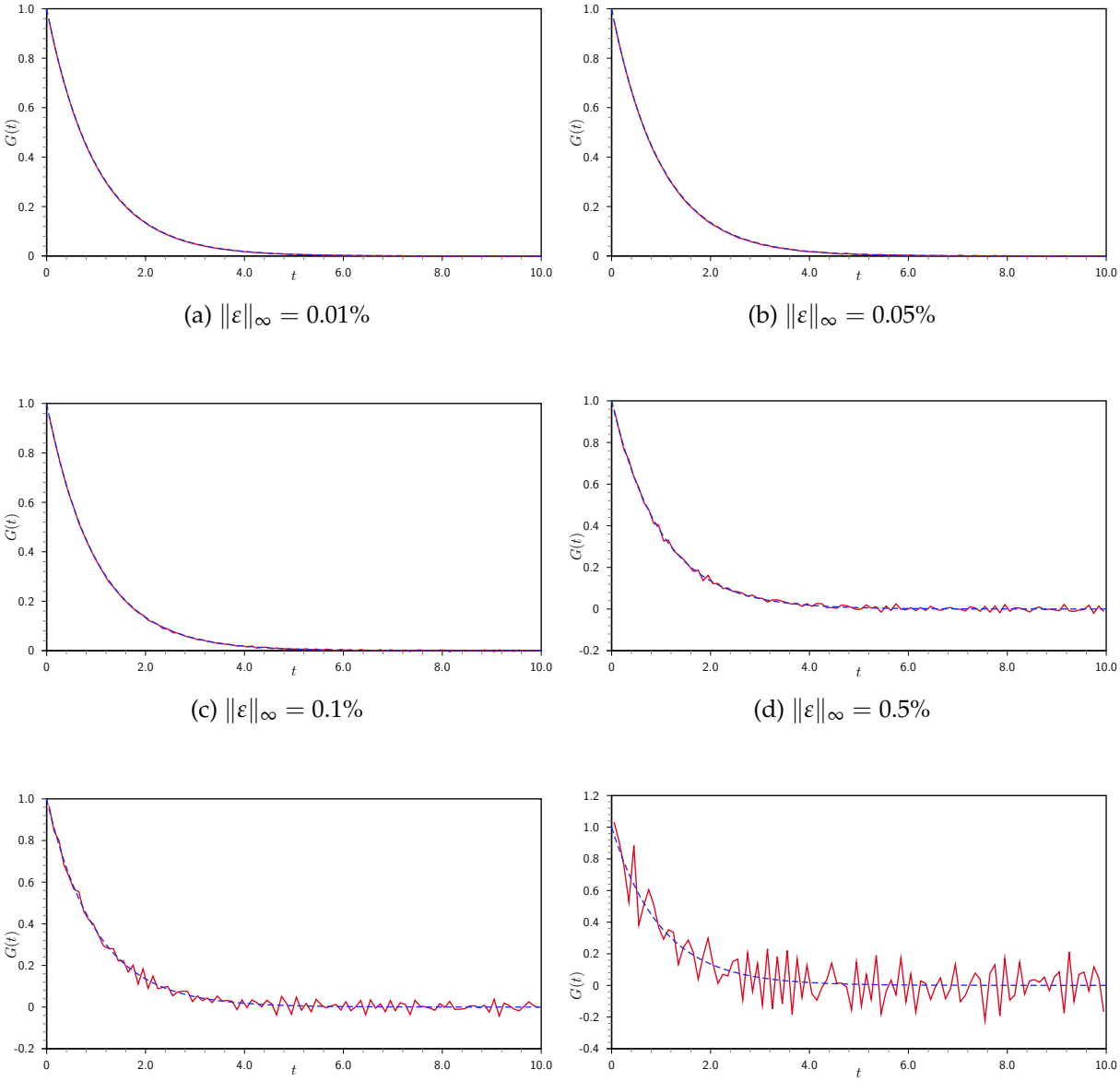

(a) $\|\varepsilon\|_\infty = 0.01\%$ (b) $\|\varepsilon\|_\infty = 0.05\%$

(c) $\|\varepsilon\|_\infty = 0.1\%$ (d) $\|\varepsilon\|_\infty = 0.5\%$

(e) $\|\varepsilon\|_\infty = 1\%$ (f) $\|\varepsilon\|_\infty = 5\%$

Figure 5.4: Numerical solution: delta function, Maxwell model ($\psi < 0$), $R = 100$, noisy data ($\|\rho\|_\infty = 0$).

selecting separate values of r for the two regions may produce better results, although the choice of intervals would depend on the exact nature of relaxation modulus for a specific material. The effect of the regularization parameter on the conditioning of the system is indicated by Table 5.3, demonstrating that increasing the value of r has the effect of decreasing the condition number of A_r^R. It should be noted that a small condition number does not necessarily guarantee that an accurate solution can be obtained, as exemplified by the results of Figure 5.7.

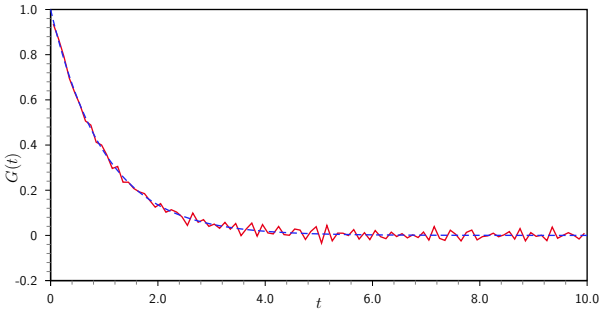

(a) $\|\rho\|_\infty = 0.5\%$, $\|\varepsilon\|_\infty = 0.5\%$

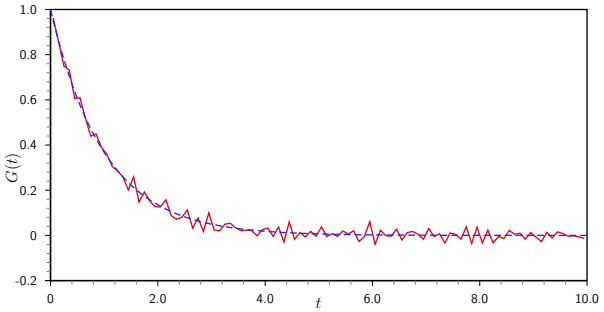

(b) $\|\rho\|_\infty = 0.5\%$, $\|\varepsilon\|_\infty = 1\%$

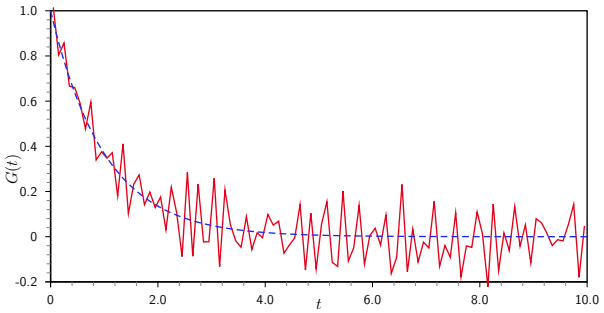

(c) $\|\rho\|_\infty = 0.5\%$, $\|\varepsilon\|_\infty = 5\%$

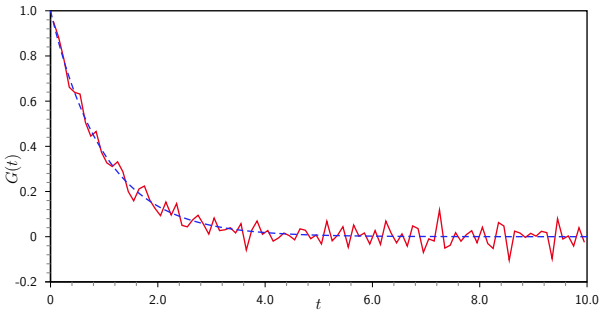

(d) $\|\rho\|_\infty = 1\%$, $\|\varepsilon\|_\infty = 1\%$

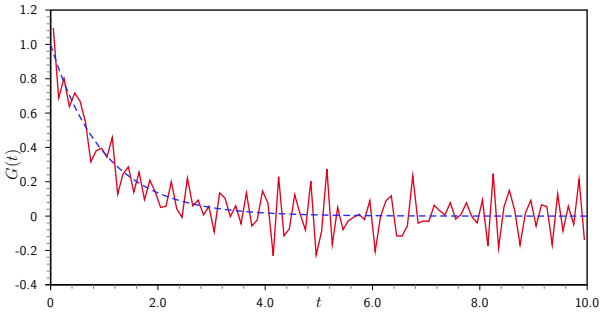

(e) $\|\rho\|_\infty = 1\%$, $\|\varepsilon\|_\infty = 5\%$

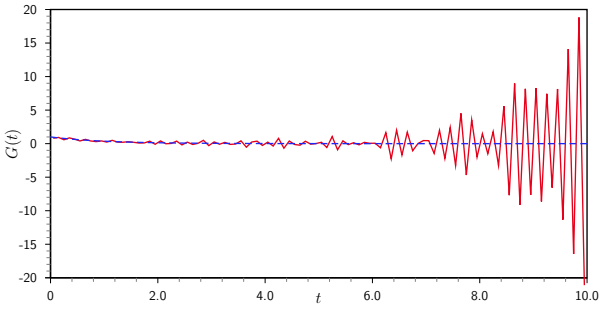

(f) $\|\rho\|_\infty = 5\%$, $\|\varepsilon\|_\infty = 5\%$

Figure 5.5: Numerical solution: delta function, Maxwell model ($\psi < 0$), $R = 100$, noisy data.

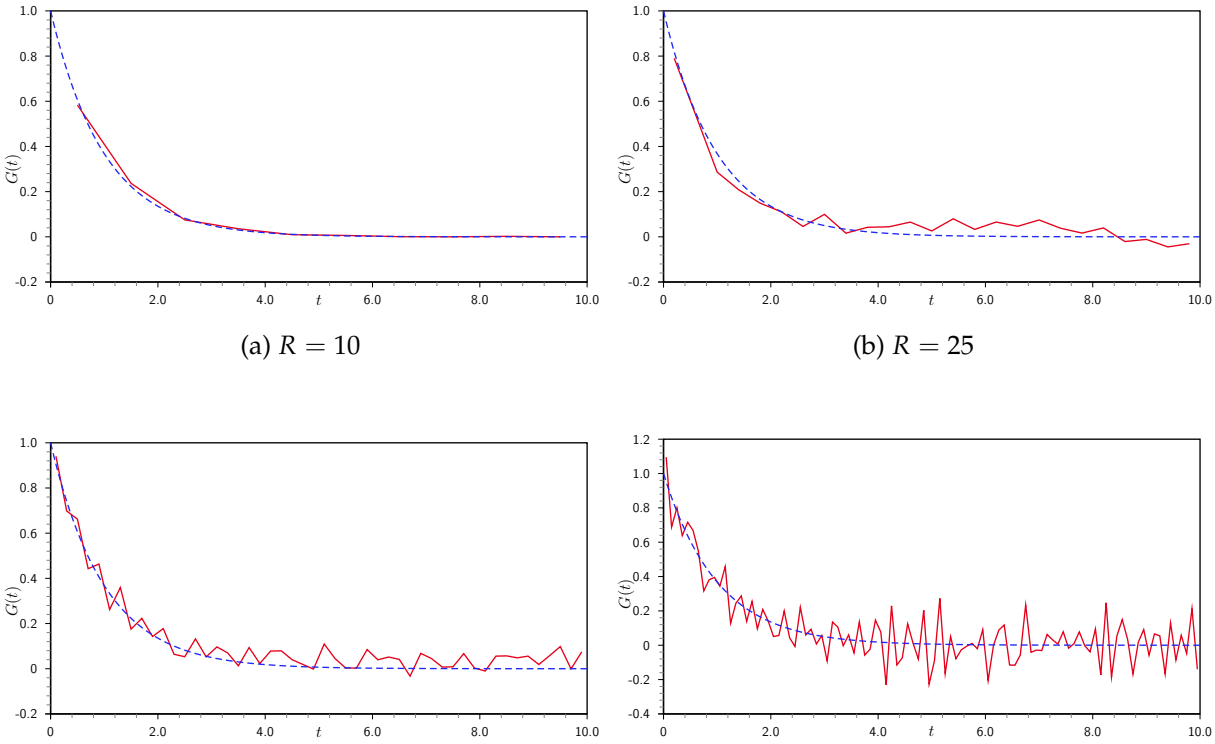

(a) $R = 10$ (b) $R = 25$

(c) $R = 50$ (d) $R = 100$

Figure 5.6: Numerical solution: delta function, Maxwell model $(\psi < 0)$, (1%,5%) error.

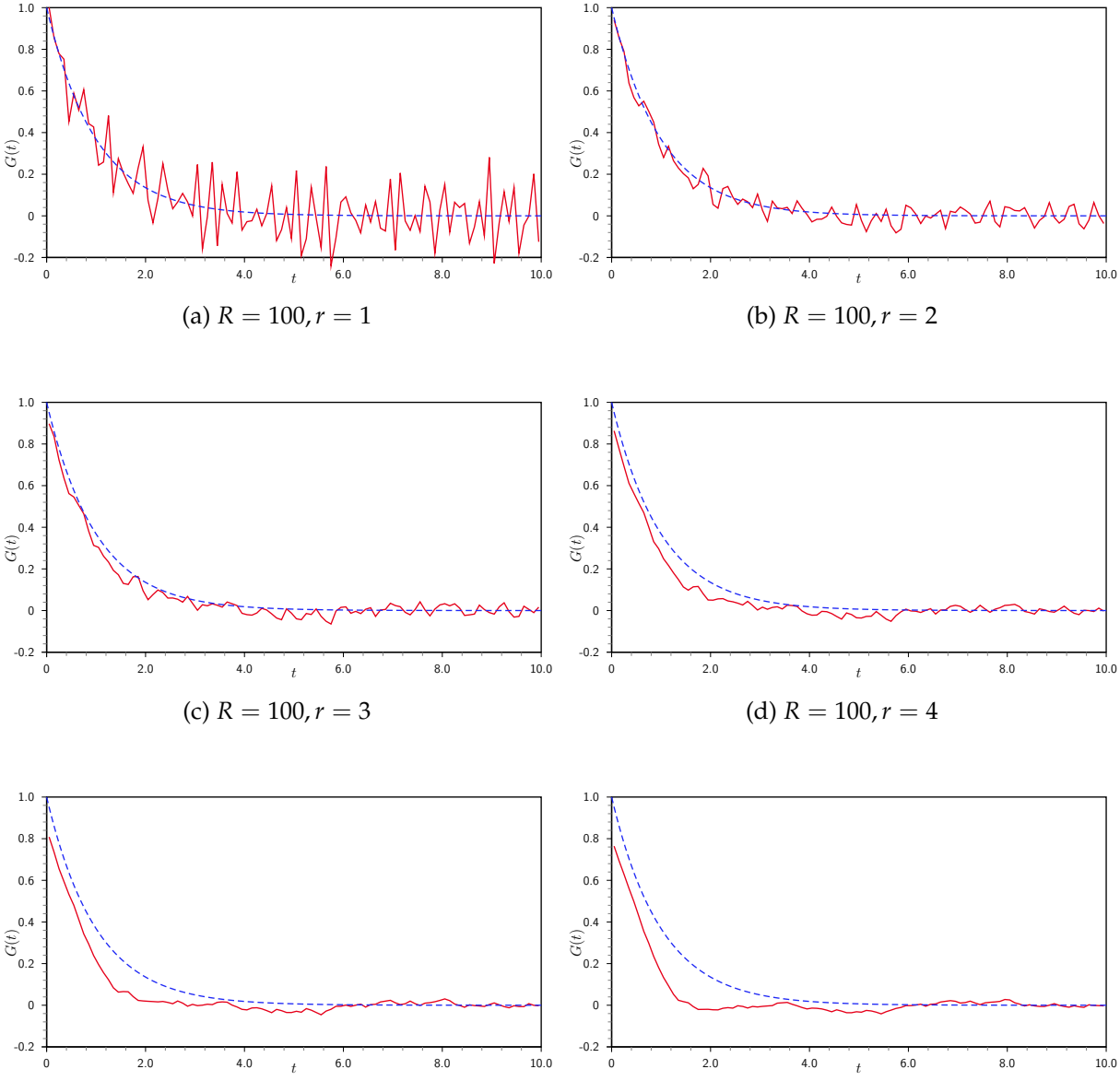

(a) $R = 100, r = 1$

(b) $R = 100, r = 2$

(c) $R = 100, r = 3$

(d) $R = 100, r = 4$

(e) $R = 100, r = 5$

(f) $R = 100, r = 6$

Figure 5.7: Numerical solution: delta function, Maxwell model $(\psi < 0)$, (1%,5%) error, future-constant regularization.

Other 1-smoothing problems

The class of 1-smoothing problems with applied torques which produce a step discontinuity in the angular velocity of the platen $\dot{\chi}(t)$ at $t = 0$ should all share similar properties to the case where the delta function was considered. Instability and large condition numbers result when the diagonal elements are small relative to the remaining non-zero entries in the matrix A^R. This corresponds to the value of platen displacement at $t = t_1$, i.e. $\chi(t_1)$, so the more rapid the increase in $\chi(t)$ at the commencement of the experiment, the more stable the solution will be.

As an example of another 1-smoothing problem, consider the applied torque in Section 3.1.2 which produces a platen displacement such that $\dot{\chi}(t) = G(t)$, using the Maxwell model. The standard collocation approach with error levels of 1% for the platen displacement and 5% for the data function is shown in the first plot in Figure 5.8 and can be seen to be of limited use for determining the relaxation modulus alone. The remaining plots show the effect of varying the regularization parameter r in the future-constant algorithm in Section 5.3. Merely using one future interval ($r = 2$) has a dramatic effect on the stability of the solution; although some oscillations still exist, they are much reduced in amplitude. The best overall solution is achieved when $r = 4$ or $r = 5$ and increasing r futher improves the solution in the flatter part of the curve, but over-regularizes the solution in the steeper part of the solution near $t = 0$.

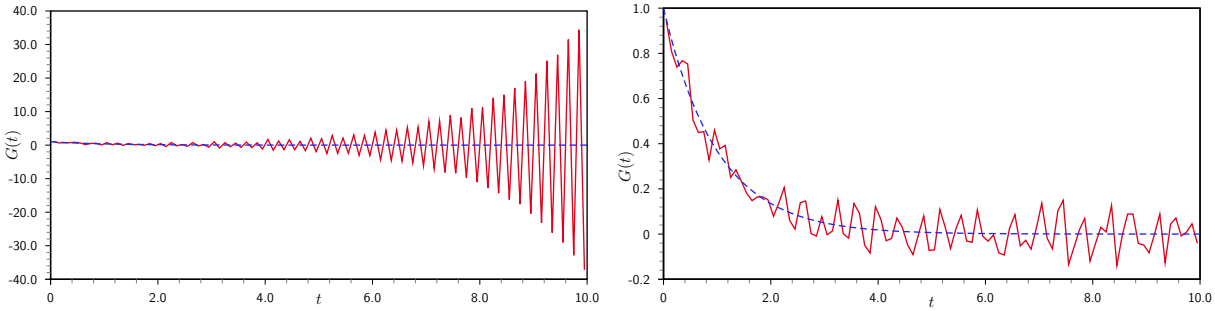

(a) $R = 100, r = 1$

(b) $R = 100, r = 2$

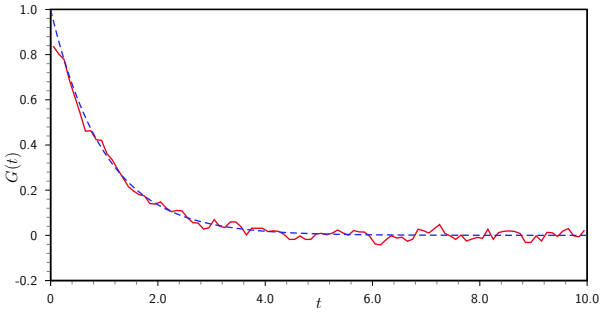

(c) $R = 100, r = 4$

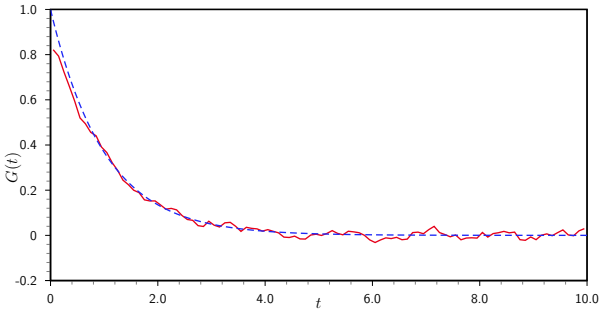

(d) $R = 100, r = 5$

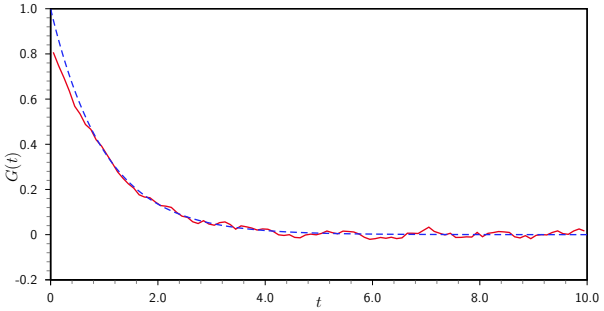

(e) $R = 100, r = 6$

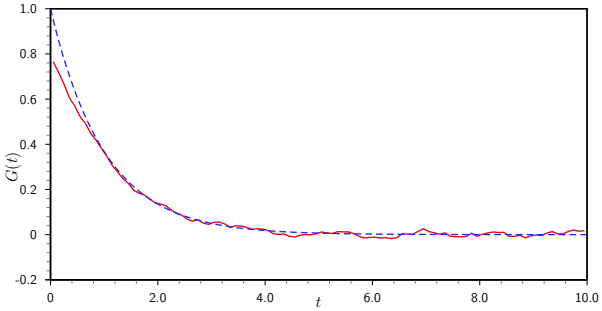

(f) $R = 100, r = 7$

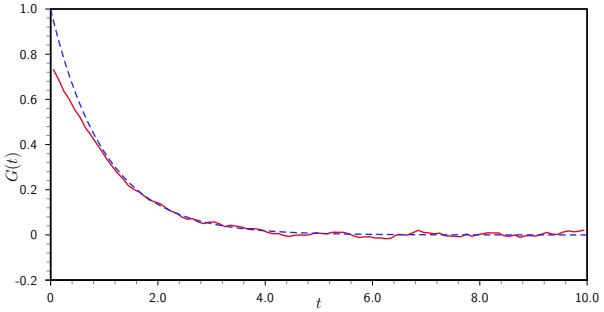

(g) $R = 100, r = 8$

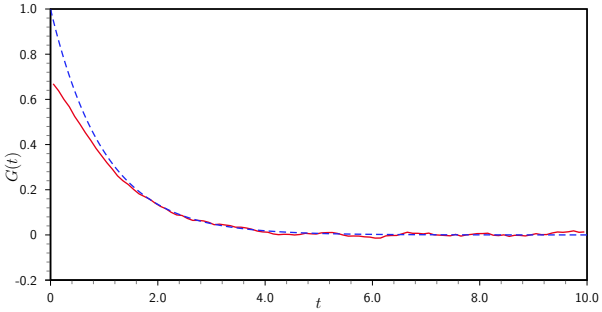

(h) $R = 100, r = 10$

Figure 5.8: Numerical solution: relaxation modulus ($G(t) = \dot{\chi}(t)$), Maxwell model ($\psi < 0$), (1%,5%) error, future-constant regularization.

5.3.2 Step & box functions

The next class of functions considered are those which produce a 2-smoothing kernel function, namely the step and box functions, and in the oscillatory case, the square wave. These functions are more practicable for experimental use than the 1-smoothing case and are therefore perhaps the most useful to consider. The solution for $G(t)$ using exact data is plotted for selected values of the number of grid-points in Figure 5.10 for the Maxwell model and Figure 5.11 for the N-mode Maxwell model. Even in the absence of noise, it is not possible to obtain a smooth solution in general, reflecting the additional degree of ill-posedness over the 1-smoothing case. The data in Table 5.4 demonstrates the effect of the error in $\chi(t)$ on the condition number of the matrix A^R. For exact data, the condition numbers are larger than for the 1-smoothing case, accounting for the decrease in stability observed in Figure 5.10. Increasing the number of grid-points R and the error level in the kernel produces extremely large condition numbers for reasonable values of R and hence the matrix A^R will be close to singularity and the solution extremely unstable. The condition numbers for the box function are somewhat larger than for the step function, suggesting inferior stability in comparison with the step function, although the difference is not obvious in general in the exact data solutions plotted in Figure 5.13.

$\|\rho\|_\infty$ (%)	R=10	R=25	R=50	R=100	R=150	R=200
0.00	$1.5342\ 10^{1}$	$4.0137\ 10^{1}$	$5.9394\ 10^{1}$	$1.2825\ 10^{2}$	$1.7908\ 10^{2}$	$2.3173\ 10^{2}$
0.01	$1.5362\ 10^{1}$	$4.0221\ 10^{1}$	$6.8980\ 10^{1}$	$1.4207\ 10^{2}$	$2.1621\ 10^{2}$	$5.1601\ 10^{2}$
0.05	$1.9067\ 10^{1}$	$4.2762\ 10^{1}$	$7.8138\ 10^{1}$	$3.5594\ 10^{2}$	$9.9365\ 10^{2}$	$4.2632\ 10^{3}$
0.10	$1.8290\ 10^{1}$	$4.7444\ 10^{1}$	$9.3179\ 10^{1}$	$6.3218\ 10^{2}$	$3.4352\ 10^{3}$	$2.6609\ 10^{5}$
0.50	$2.0492\ 10^{1}$	$8.4132\ 10^{1}$	$2.6393\ 10^{5}$	$7.0014\ 10^{4}$	$4.4406\ 10^{8}$	$8.1454\ 10^{14}$
1.00	$2.5878\ 10^{1}$	$8.8729\ 10^{1}$	$8.2968\ 10^{5}$	$4.2808\ 10^{23}$	$2.4576\ 10^{8}$	$7.3077\ 10^{24}$
5.00	$3.0944\ 10^{1}$	$1.8960\ 10^{3}$	$2.1861\ 10^{10}$	$2.0916\ 10^{42}$	$2.6636\ 10^{43}$	$1.1644\ 10^{45}$

Table 5.4: Condition numbers for A^R, step function applied torque, Maxwell model ($\psi < 0$).

In the presence of perturbed data, modelled by error levels of 1% and 5% in the platen displacement and data functions, respectively, decreasing the number of grid-points is not particularly effective in stabilizing the solution. Figure 5.9 demonstrates that even a coarse grid with $R = 10$ is not quite sufficient to obtain a useful solution. Clearly, additional regularization is required for the 2-smoothing problem. The effect of applying the future-constant regularization algorithm to the step function case is

illustrated in Figure 5.12 for the step function, Figure 5.14 for the box function and Figure 5.15 for the square wave. Collocation alone $r = 1$ is completely unable to produce a meaningful solution for the 2-smoothing case in the presence of perturbed data and in all cases the best overall solution is obtained by using $r = 6$ to 8. The square waveform clearly produces the least stable solution. As with the one-smoothing case, higher values of r appear to produce better results in the flatter part of the curve for large t, while the solution becomes over-regularized for smaller values of t. The condition numbers for the step function are given in Table 5.5 and clearly demonstrate the effectiveness of the future-constant method in reducing the condition numbers to values which correspond to stable solutions of the Volterra integral equation. The effect of changing the elasticity or relxation time parameters in the Maxwell model is essentially equivalant to assuming that the material parameters are held constant and varying the instrumental parameters k and I. The distinction in the behaviour of the platen displacement is determined by the nature of ψ as defined in Section 2.3.2; if $\psi < 0$ then the displacement will be oscillatory in nature and if $\psi > 0$ the displacement will be monotone increasing. The effect of changing the instrumental parameters is inestigated in Section 6.1.3, therefore it is unnecessary to examine the effect of varying the material parameters separately here.

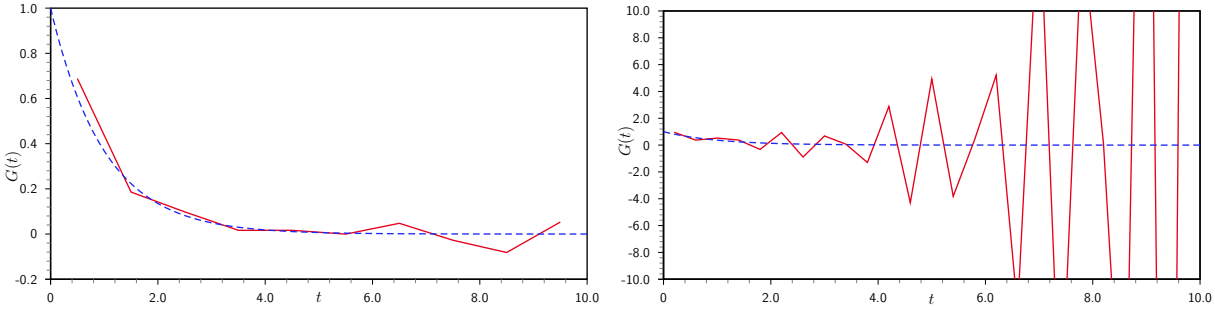

(a) $R = 10$ (b) $R = 25$

Figure 5.9: Numerical solution: step function, Maxwell model $(\psi < 0)$, (1%,5%) error.

r	R=10	R=25	R=50	R=100	R=150	R=200
1	$9.0339\ 10^{0}$	$1.2369\ 10^{4}$	$3.0342\ 10^{17}$	$1.4550\ 10^{44}$	$4.7905\ 10^{43}$	$4.1717\ 10^{44}$
2	$7.5093\ 10^{0}$	$1.7748\ 10^{1}$	$1.1947\ 10^{5}$	$6.9714\ 10^{8}$	$1.4395\ 10^{43}$	$2.0255\ 10^{43}$
4		$9.5097\ 10^{0}$	$2.1351\ 10^{1}$	$1.8758\ 10^{5}$	$4.0041\ 10^{4}$	$1.9277\ 10^{14}$
6			$7.6588\ 10^{0}$	$5.5985\ 10^{1}$	$2.5184\ 10^{2}$	$1.2257\ 10^{5}$
8				$1.9991\ 10^{1}$	$6.2724\ 10^{1}$	$4.9471\ 10^{2}$
10				$1.3062\ 10^{1}$	$3.0640\ 10^{1}$	$9.6899\ 10^{1}$
12				$6.5374\ 10^{0}$	$1.9527\ 10^{1}$	$4.3193\ 10^{1}$
14					$1.4980\ 10^{1}$	$1.8801\ 10^{1}$
16					$1.0773\ 10^{1}$	$1.5017\ 10^{1}$
18					$7.2703\ 10^{0}$	$1.5426\ 10^{1}$
20						$9.5351\ 10^{0}$

Table 5.5: Condition numbers for A_r^R, step function applied torque, Maxwell model $(\psi < 0)$, (1%,5%) error, future constant regularization.

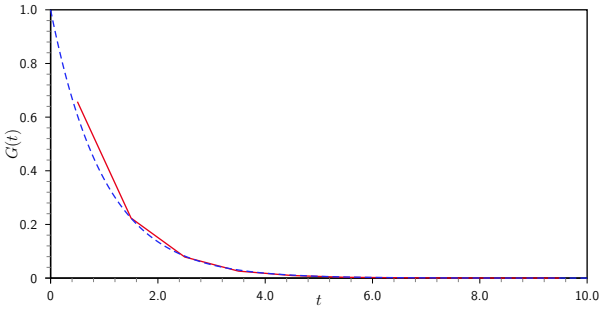

(a) $N = 10$

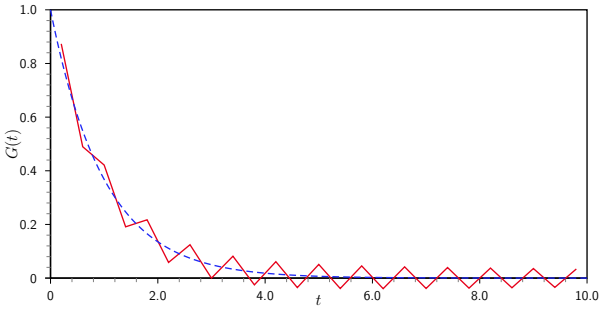

(b) $R = 25$

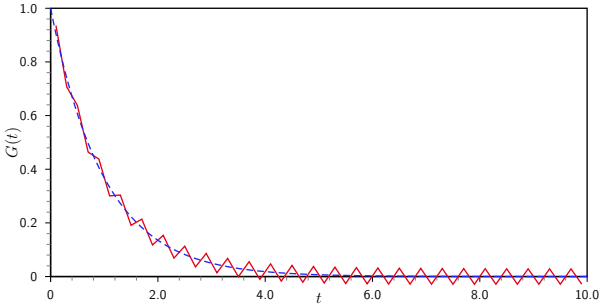

(c) $R = 50$

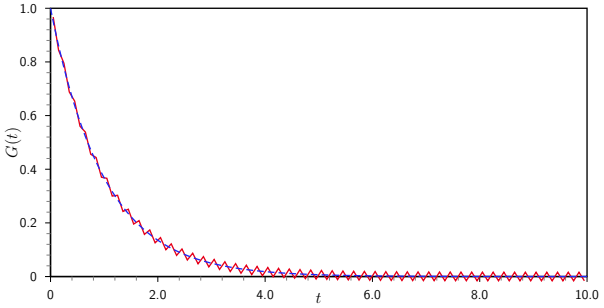

(d) $R = 100$

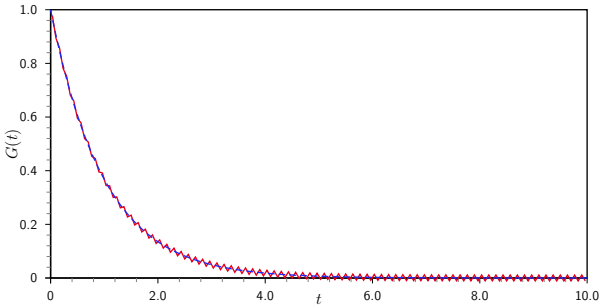

(e) $R = 150$

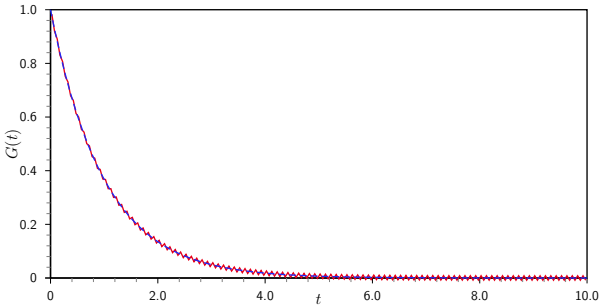

(f) $R = 200$

Figure 5.10: Numerical solution: step function, Maxwell model $(\psi < 0)$, exact data.

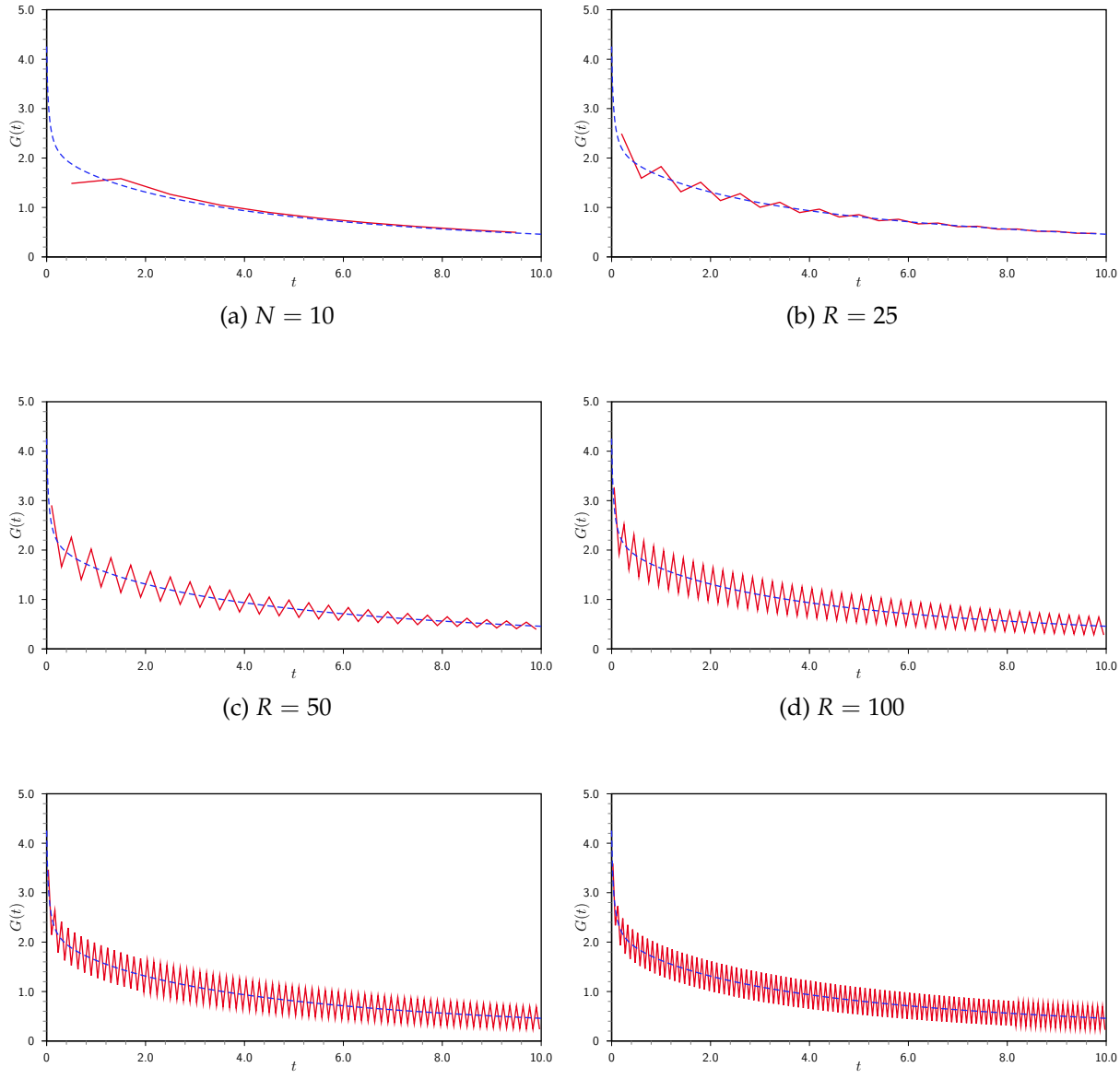

(a) $N = 10$ (b) $R = 25$

(c) $R = 50$ (d) $R = 100$

(e) $R = 150$ (f) $R = 200$

Figure 5.11: Numerical solution: step function, N-mode Maxwell model ($\psi < 0$), exact data.

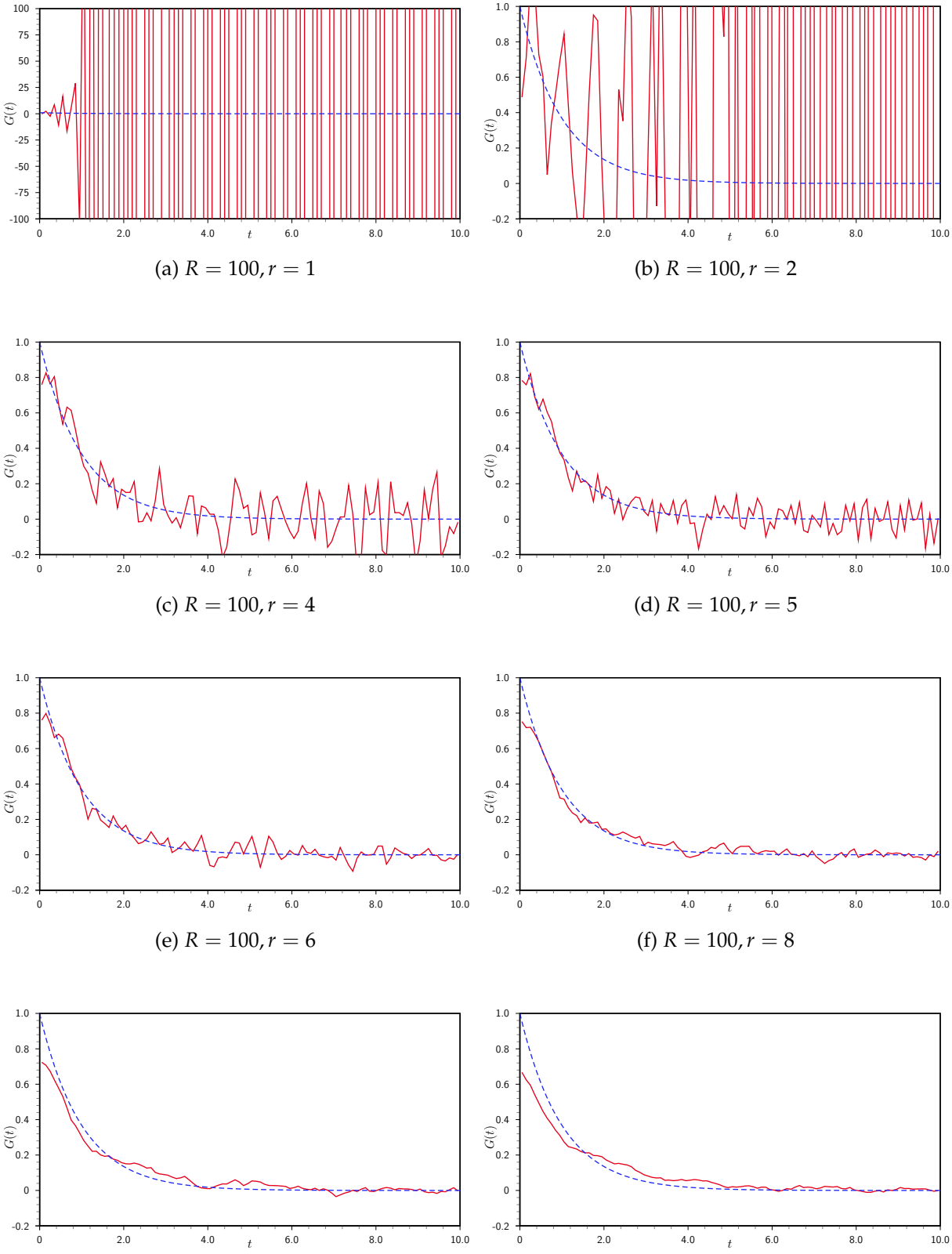

(a) $R = 100, r = 1$

(b) $R = 100, r = 2$

(c) $R = 100, r = 4$

(d) $R = 100, r = 5$

(e) $R = 100, r = 6$

(f) $R = 100, r = 8$

(g) $R = 100, r = 10$

(h) $R = 100, r = 12$

Figure 5.12: Numerical solution: step function, Maxwell model ($\psi < 0$), (1%,5%) error, future-constant regularization.

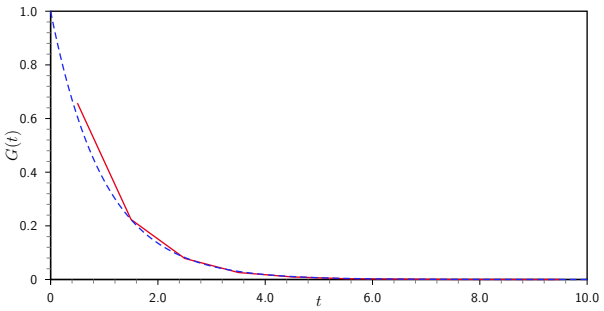

(a) $N = 10$

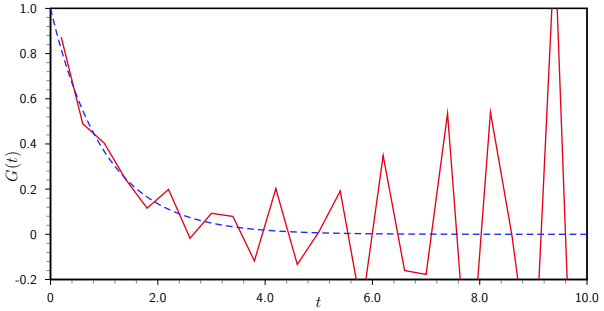

(b) $R = 25$

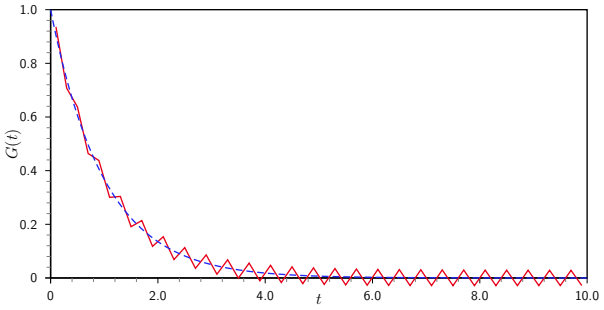

(c) $R = 50$

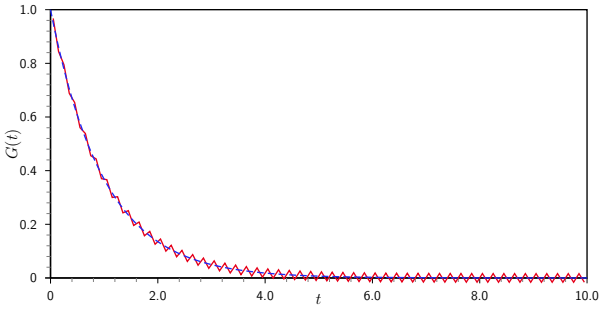

(d) $R = 100$

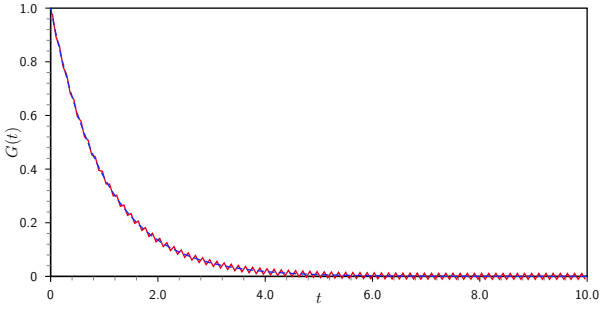

(e) $R = 150$

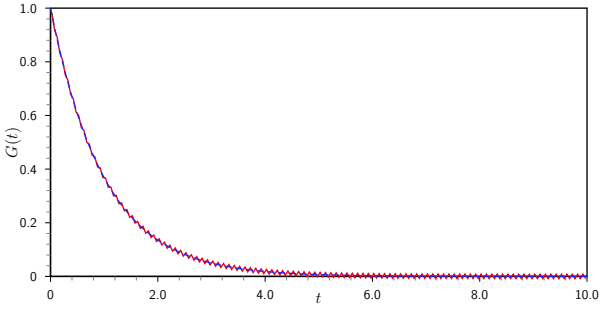

(f) $R = 200$

Figure 5.13: Numerical solution: box function, Maxwell model ($\psi < 0$), exact data.

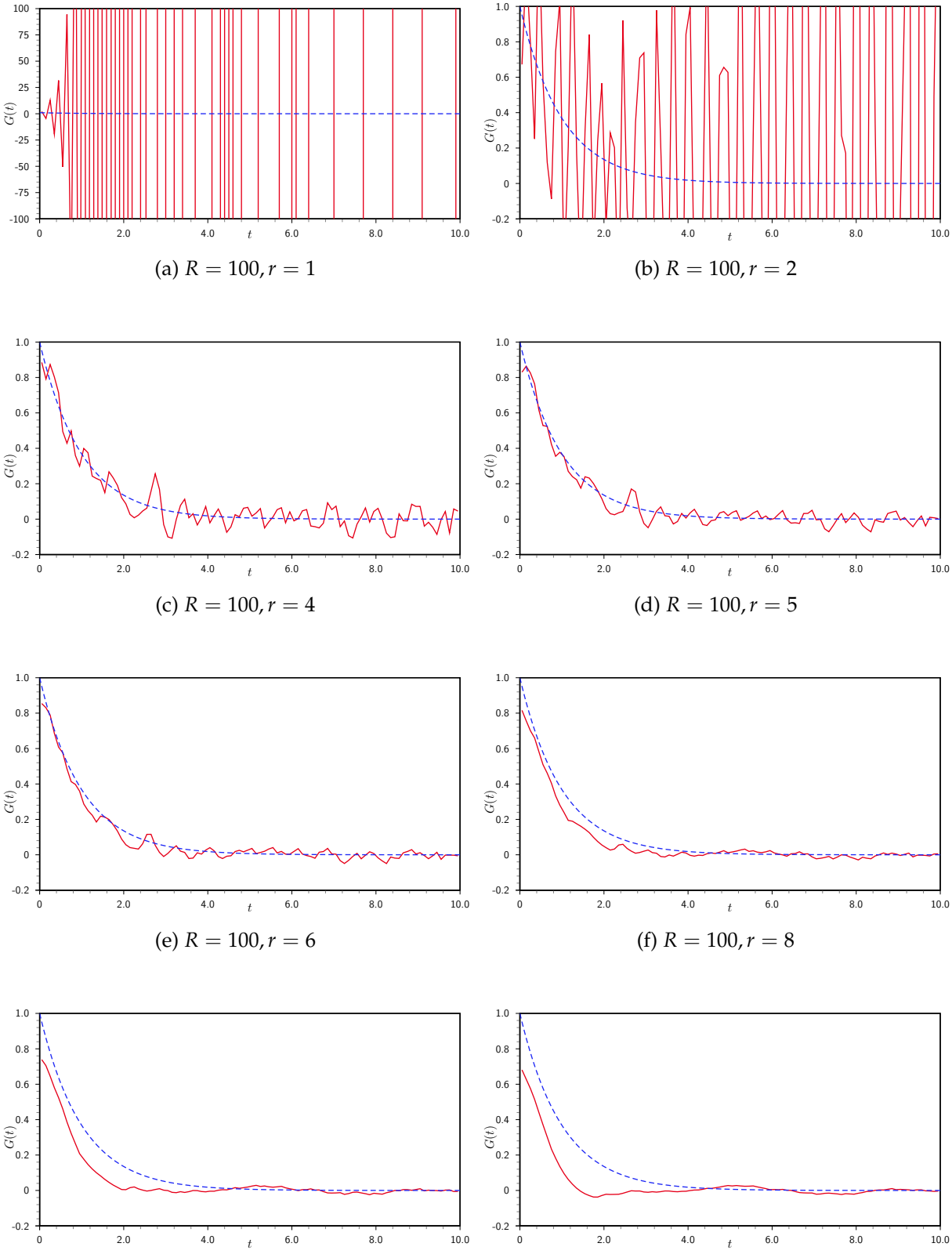

(a) $R = 100, r = 1$

(b) $R = 100, r = 2$

(c) $R = 100, r = 4$

(d) $R = 100, r = 5$

(e) $R = 100, r = 6$

(f) $R = 100, r = 8$

(g) $R = 100, r = 10$

(h) $R = 100, r = 12$

Figure 5.14: Numerical solution: box function, Maxwell model ($\psi < 0$), (1%,5%) error, future-constant regularization.

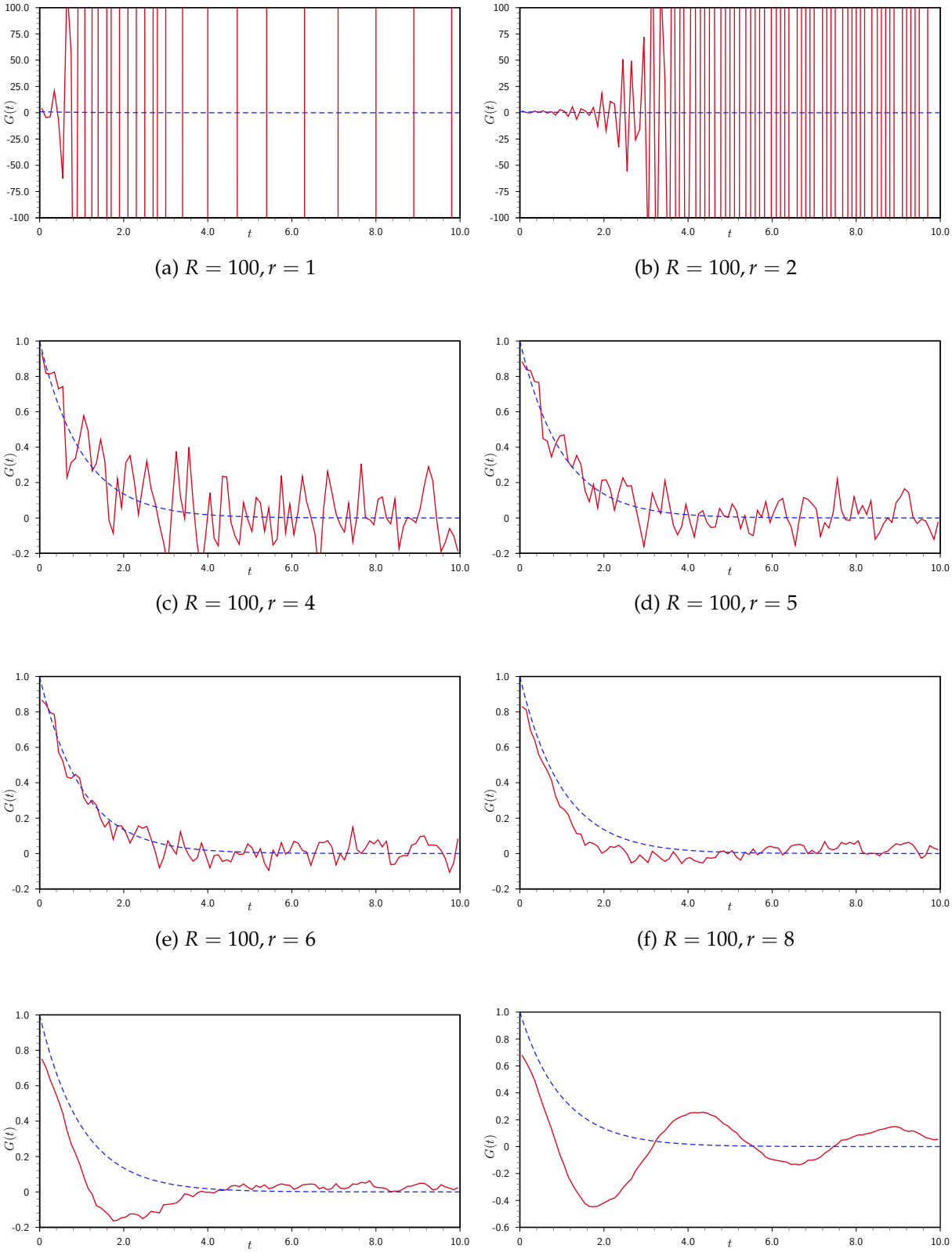

(a) $R = 100, r = 1$

(b) $R = 100, r = 2$

(c) $R = 100, r = 4$

(d) $R = 100, r = 5$

(e) $R = 100, r = 6$

(f) $R = 100, r = 8$

(g) $R = 100, r = 10$

(h) $R = 100, r = 12$

Figure 5.15: Numerical solution: square wave, Maxwell model ($\psi < 0$), (1%,5%) error, future-constant regularization.

5.3.3 Slope & ramp functions

The most ill-posed case considered here is the 3-smoothing problem, corresponding to the slope function, $C(t) = C_0 t$, and the ramp function as described in Section 2.4. The degree of instability produced by this class of problem is manifest in highly oscillatory solutions even where the data is exact as demonstrated in Figure 5.16. Obviously, none of the choices of step-size produces usable data for the solution $G(t)$ and it can be inferred that regularization by reducing the number of grid-points is not applicable here with exact or perturbed data. The kernel $\dot{\chi}(t)$ behaves like $\mathcal{O}(t)$ as $t \to 0$, hence the diagonal values will be small relative to the other non-zero matrix elements of A^R and the relative error much more significant. The solution is built up sequentially using previous values of $\chi(t_i)$, therefore the error propagates throughout the solution, growing without bound as t increases. The condition numbers are tabulated in Table 5.6 for various relative errors in the platen displacement. The large values even for noise-free data indicate that the matrix A^R is close to singularity and that inversion of the matrix is unlikely to produce a stable solution. Note that the addition of random error does not always increase the condition number, since a large error may augment the diagonal value sufficiently in this case to decrease the condition number, however this does not imply that a more accurate solution will be obtained.

$\|\rho\|_\infty$ (%)	R=10	R=25	R=50	R=100	R=150	R=200
0.00	4.1563 10^3	7.3024 10^{15}	4.2604 10^{31}	1.4804e 10^{46}	5.3375 10^{47}	6.1659 10^{46}
0.01	4.1872 10^3	4.3006 10^{14}	7.4638 10^{42}	6.1721 10^{46}	3.1037 10^{45}	9.6751 10^{44}
0.05	5.1371 10^3	2.9993 10^{19}	6.6659 10^{26}	7.3492 10^{42}	4.6666 10^{43}	1.6730 10^{44}
0.10	6.1703 10^3	1.1272 10^{11}	4.2331 10^{25}	1.0923 10^{22}	3.6589 10^{40}	2.1479 10^{40}
0.50	3.2353 10^5	7.5878 10^{25}	1.8205 10^{18}	4.3159 10^{31}	8.0351 10^{40}	2.7415 10^{19}
1.00	1.5622 10^4	8.0599 10^{18}	2.8050 10^{20}	7.1495 10^{18}	5.6823 10^{37}	3.5478 10^{22}
5.00	4.4839 10^5	1.1810 10^6	9.8867 10^{36}	9.8528 10^{29}	8.9834 10^{42}	7.2174 10^{43}

Table 5.6: Condition numbers for A^R, slope function applied torque, Maxwell model ($\psi < 0$).

Clearly, regularization is required to obtain a reasonable solution even with exact data. The solution obtained using the future-constant algorithm from Section 5.3 is plotted for various values of the regularization parameter r in Figure 5.17 using error levels of 1% and 5% for the platen displacement and data functions, respectively. Much larger values of r are necessary to obtain a reasonable solution than for the step or delta function applied torques, reflecting the extra degree of ill-posedness inherent

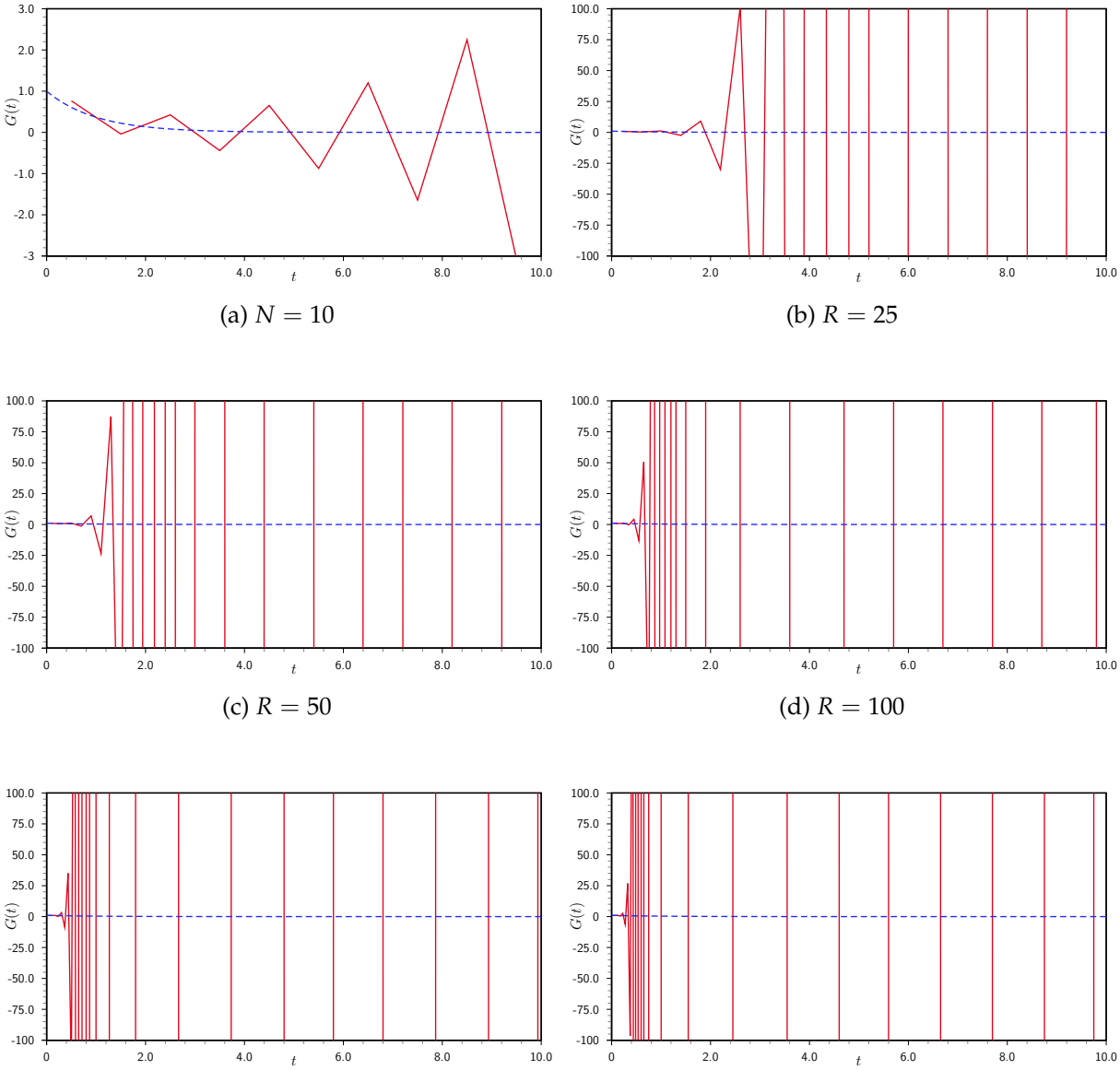

(a) $N = 10$ (b) $R = 25$

(c) $R = 50$ (d) $R = 100$

(e) $R = 150$ (f) $R = 200$

Figure 5.16: Numerical solution: slope function, Maxwell model ($\psi < 0$), exact data.

in the 3-smoothing problem. A value of approximately $r = 20$ is required to stabilize the solution, but even this is less than satisfactory, suggesting that it is undesirable to choose a form for the applied torque which leads to a 3-smoothing problem or higher. The condition numbers are displayed in Table 5.7 for various grid dimensions and demonstrate a dramatic decrease in the condition number as an increasing number of future intervals are used to construct the solution. In this case, although the solution becomes over-smoothed for small values of t, the ability of the algorithm to reconstruct a reasonable solution from the wildly oscillatory unregularized solution is still impressive.

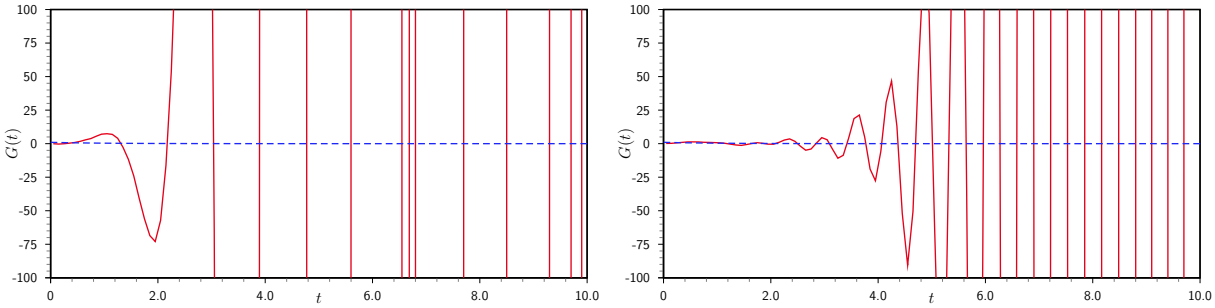

(a) $R = 100, r = 1$ (b) $R = 100, r = 6$

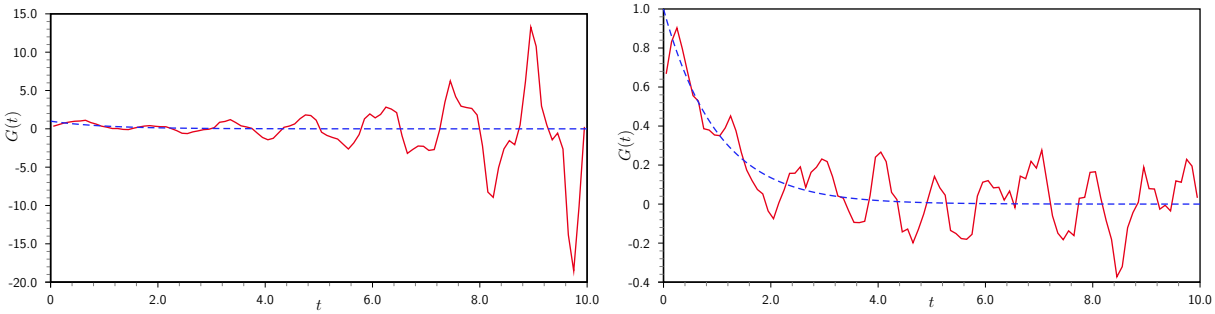

(c) $R = 100, r = 8$ (d) $R = 100, r = 12$

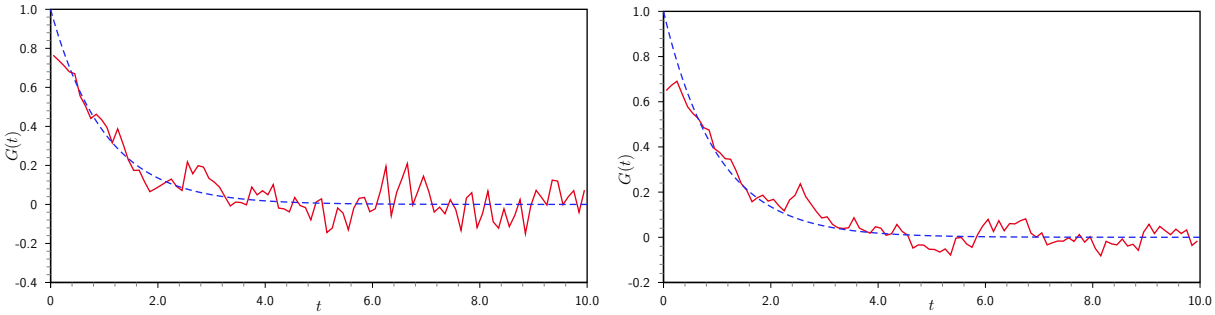

(e) $R = 100, r = 14$ (f) $R = 100, r = 16$

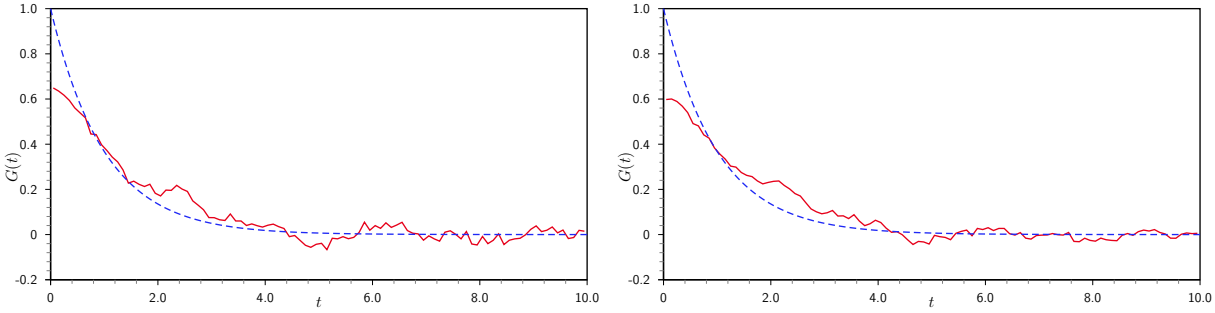

(g) $R = 100, r = 18$ (h) $R = 100, r = 20$

Figure 5.17: Numerical solution: slope function, Maxwell model ($\psi < 0$), (1%,5%) error, future-constant regularization.

r	R=10	R=25	R=50	R=100	R=150	R=200
1	$3.4595\ 10^{3}$	$9.0853\ 10^{9}$	$1.1787\ 10^{23}$	$1.0675\ 10^{14}$	$2.8513\ 10^{27}$	$2.3370\ 10^{41}$
2	$6.8335\ 10^{2}$	$3.4112\ 10^{8}$	$1.9229\ 10^{9}$	$5.0249\ 10^{11}$	$5.7807\ 10^{32}$	$1.7720\ 10^{40}$
4	$3.4964\ 10^{1}$	$1.7978\ 10^{3}$	$4.0300\ 10^{7}$	$4.9204\ 10^{16}$	$6.7308\ 10^{8}$	$4.4342\ 10^{10}$
6	$1.7857\ 10^{1}$	$5.9438\ 10^{1}$	$1.3228\ 10^{4}$	$1.0445\ 10^{9}$	$2.0060\ 10^{9}$	$1.0582\ 10^{9}$
8	$8.8187\ 10^{0}$	$3.5552\ 10^{1}$	$3.6618\ 10^{2}$	$3.4830\ 10^{4}$	$7.0904\ 10^{8}$	$9.6164\ 10^{9}$
10		$2.6291\ 10^{1}$	$1.3546\ 10^{2}$	$2.7741\ 10^{3}$	$1.2960\ 10^{6}$	$1.1119\ 10^{7}$
12		$2.0407\ 10^{1}$	$8.8978\ 10^{1}$	$6.1154\ 10^{2}$	$1.6413\ 10^{5}$	$1.7355\ 10^{5}$
14		$1.7422\ 10^{1}$	$5.7273\ 10^{1}$	$4.8353\ 10^{2}$	$6.8359\ 10^{3}$	$3.8372\ 10^{4}$
16		$1.4593\ 10^{1}$	$4.0435\ 10^{1}$	$1.9274\ 10^{2}$	$9.7375\ 10^{2}$	$2.2781\ 10^{4}$
18		$1.2435\ 10^{1}$	$3.3512\ 10^{1}$	$1.4285\ 10^{2}$	$5.7657\ 10^{2}$	$7.3648\ 10^{3}$
20		$1.0892\ 10^{1}$	$2.8389\ 10^{1}$	$1.0362\ 10^{2}$	$2.5895\ 10^{2}$	$4.0840\ 10^{3}$
25		$7.2448\ 10^{0}$	$2.0926\ 10^{1}$	$6.9740\ 10^{1}$	$1.3829\ 10^{2}$	$3.5420\ 10^{2}$
30			$1.6648\ 10^{1}$	$4.7805\ 10^{1}$	$9.4523\ 10^{1}$	$2.0004\ 10^{2}$
35			$1.3634\ 10^{1}$	$3.6728\ 10^{1}$	$7.2746\ 10^{1}$	$1.3504\ 10^{2}$

Table 5.7: Condition numbers for A_r^R, slope function applied torque, Maxwell model $(\psi < 0)$, (1%,5%) error, future constant regularization.

The effect of the regularization parameter in the future-constant algorithm is illustrated in Figure 5.18 for the ramp function described in Section 2.4.2. The unregularized case using simple collocation is similar to that for the slope function, being highly oscillatory in nature and of little practical use. Somewhat surprisingly, the future-constant algorithm is more effective at obtaining an accurate solution than with the slope function. A value of the regularization parameter of $r = 8$ provides quite a reasonable solution over the whole domain of solution.

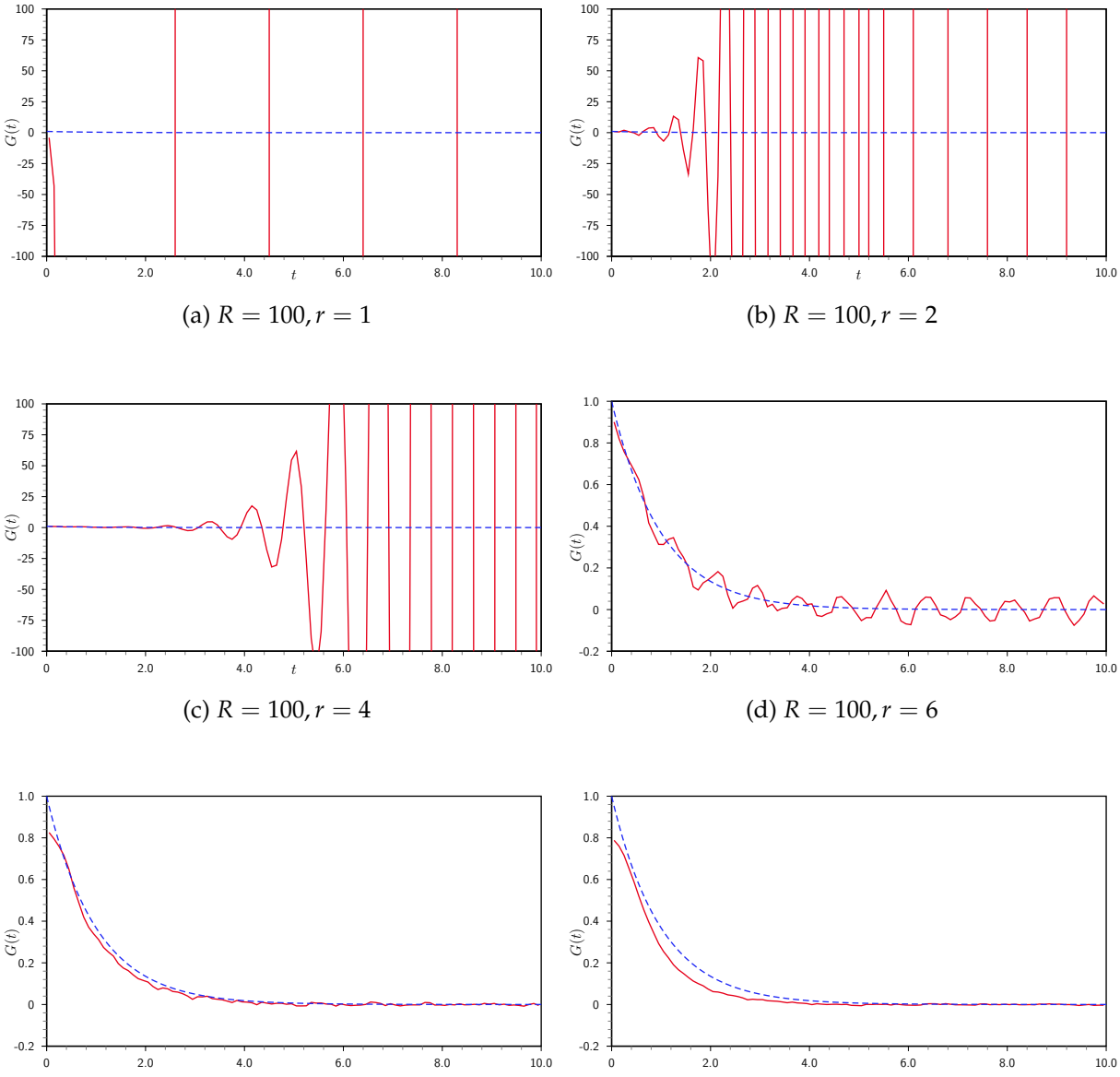

(a) $R = 100, r = 1$

(b) $R = 100, r = 2$

(c) $R = 100, r = 4$

(d) $R = 100, r = 6$

(e) $R = 100, r = 8$

(f) $R = 100, r = 10$

Figure 5.18: Numerical solution: ramp function, Maxwell model ($\psi < 0$), (1%,5%) error, future-constant regularization.

IV. FUTURE POLYNOMIAL REGULARIZATION

The second regularization method utilized for this problem is a generalization of the future-constant algorithm, where the solution is held constant on the small future interval $[t, t + (r-1)h]$, to the case where the solution is approximated by a polynomial of low degree on that interval. A brief description of the implementation of the method is given here, but the original paper [18] should be consulted for the full detail and convergence analysis. The motivation for using a polynomial rather than a constant value for the future interval is due to the fact that the future-constant algorithm tends to oversmooth regularized solutions, as has been noted for the steeper part of the relaxation modulus solution curve in the preceding experiments due to the amount of rigidity which is imposed on the solution.

Let $d \geq 0$ and $r \geq d + 2$ be integers. Assuming the solution has been obtained up to t_{i-1}, the collocation parameters $c_1, \ldots, c_{i-1}$ will already have been determined, the problem is to find $c_i \in \mathbb{R}$ such that $c_i = p_{i,r,d}(t_i)$ where the polynomial $p \in \mathcal{P}^d$, the space of polynomials of degree at most d, is defined

$$p_{i,r,d}(t) = \sum_{j=0}^{d} \frac{1}{h^j} b_{i,j} (t - t_{i-1})^j \tag{5-42}$$

and $b_{i,0}, \ldots, b_{i,d} \in \mathbb{R}$. The algorithm is formulated in a least squares setting using the piecewise collocation discretization described in Section 5.1.4, the function $p_{i,r,d}$ being determined as

$$p_{i,r,d} = \arg\min_{p \in \mathcal{P}^d} J_{i,r,d}(p) \tag{5-43}$$

where

$$J_{i,r,d}(p) = \sum_{l=0}^{r-1} \left[\left(\sum_{j=1}^{i-1} c_j \Delta_{i+l-j+1} \right) + \sum_{m=0}^{l} p(t_{i+m}) \Delta_{l-m+1} - f_{i+l} \right]^2 \tag{5-44}$$

Noting that advancing the solution slightly forward in time, $p_{i,r,d}(t_{i+m}) = \sum_{j=0}^{d} b_{i,j}(m+1)^j$, the necessary conditions for minimization are given by

$$\mathsf{K}^T \mathsf{K} \boldsymbol{b}_i = \mathsf{K}^T \left(\boldsymbol{f}_{i,r} - \sum_{j=1}^{i-1} c_j \boldsymbol{v}_{i+1-j,r} \right) \tag{5-45}$$

where

$$\boldsymbol{b}_i = (b_{i,0}, b_{i,1}, \ldots, b_{i,d})^T \tag{5-46a}$$

$$\boldsymbol{v}_{l,r} = (\Delta_l, \Delta_{l+1}, \ldots, \Delta_{l+r-1})^T \tag{5-46b}$$

$$\boldsymbol{f}_{l,r} = (f_l, f_{l+1}, \ldots, f_{l+r-1})^T \tag{5-46c}$$

and the $r \times (d+1)$ matrix K is defined by

$$\mathsf{K} = \begin{bmatrix} \Delta_1 & \Delta_1 & \dots & \Delta_1 \\ \Delta_1 + \Delta_2 & 2\Delta_1 + \Delta_2 & \dots & 2^d\Delta_1 + \Delta_2 \\ \Delta_2 + \ldots + \Delta_r & r\Delta_1 + \ldots + \Delta_r & \dots & r^d\Delta_1 + \ldots + \Delta_r \end{bmatrix} \tag{5-47}$$

This matrix can be decomposed into a product of a lower-triangular Toeplitz matrix L, which has an inverse if $\Delta_1 \neq 0$, and a Vandermonde matrix V, which is by definition of full rank, so therefore $\mathsf{K}^T\mathsf{K}$ is invertible and the polynomial coefficients can be found from

$$\boldsymbol{b}_i = \mathsf{K}^+ \left(\boldsymbol{f}_{i,r} - \sum_{j=1}^{i-1} c_j \boldsymbol{v}_{i+1-j,r} \right) \tag{5-48}$$

where $\mathsf{K}^+ = (\mathsf{K}^T\mathsf{K})^{-1}\mathsf{K}^T$ is the (Moore-Penrose) pseudo-inverse. Now, setting $c_i = p_{i,r,d}(t_i)$, i.e.

$$\begin{aligned} c_i &= \sum_{j=0}^{d} \frac{1}{h^j} b_{i,j}(t_i - t_{i-1})^j \\ &= \boldsymbol{b}_i^T (1, \ldots, 1)^T \\ &= \left(f_{i,r} - \sum_{j=1}^{i-1} c_j \boldsymbol{v}_{i+1-j,r} \right)^T (\mathsf{K}^T)^+ (1, \ldots, 1)^T \end{aligned} \tag{5-49}$$

and using the identity $(\mathsf{K}^+)^T = (\mathsf{K}^T)^+$, the c_i's can be obtained by the equation

$$\sum_{j=1}^{i-1} c_j \boldsymbol{v}_{i+1-j,r}^T (\mathsf{K}^T)^+ (1, \ldots, 1)^T + c_i = \boldsymbol{f}_{i,r}^T (K^T)^+ (1, \ldots, 1)^T. \tag{5-50}$$

This is equivalent to solving the matrix equation

$$\left[\tilde{\mathsf{A}} + \tilde{\alpha} \mathsf{I} \right] \boldsymbol{c} = \tilde{\boldsymbol{f}} \tag{5-51}$$

where $\boldsymbol{c} = (c_1, \ldots, c_R)^T$ is the solution vector and I is the $R \times R$ identity matrix. Note that this is the discrete form of a Volterra integral equation of the second kind for which a stable solution exists. Since $\tilde{\alpha} = 1 - \tilde{\Delta}_1$, (5-51) becomes

$$\begin{bmatrix} 1 & 0 & \dots & 0 \\ \tilde{\Delta}_2 & 1 & \ddots & \vdots \\ \vdots & \vdots & \ddots & 0 \\ \tilde{\Delta}_R & \tilde{\Delta}_{R-1} & \dots & 1 \end{bmatrix} \begin{bmatrix} c_1 \\ c_2 \\ \vdots \\ c_R \end{bmatrix} = \begin{bmatrix} \tilde{f}_1 \\ \tilde{f}_2 \\ \vdots \\ \tilde{f}_R \end{bmatrix} \tag{5-52}$$

with the parameters

$$\tilde{\Delta}_i = \sum_{l=1}^{r} \tau_l \Delta_{i+l-1} = \sum_{l=1}^{r} [\tau_l \chi(t_{i+l-1}) - \chi(t_{i+l-2})] \tag{5-53a}$$

$$\tilde{f}_i = \sum_{l=1}^{r} \tau_l f_{i+l-1}, \quad i = 1, \ldots, R \tag{5-53b}$$

and τ_i is the $i-$th row sum of the (Moore-Penrose) pseudo-inverse of the matrix K^T, i.e.

$$\tau_i = \sum_{j=1}^{d+1} \left[\left(\mathsf{K}^T \right)^+ \right]_{i,j}, \quad i = 1, \ldots, r. \tag{5-54}$$

Hence, the regularization method results in a lower-triangular matrix Toeplitz matrix system which preserves the causal structure of the original Volterra integral equation and can be solved easily by forward substitution. This algorithm is more resource intensive than the future-constant algorithm, particularly in the calculation of the pseudo-inverse, but should still be practicable for near real-time solution. Note that when $r \leq d + 1$, the algorithm reduces to simple collocation.

The numerical experiments performed for the future-constant regularization algorithm are now repeated for the more general future-polynomial method and a comparison of the effectiveness at obtaining an accurate solution is made for a selection of values for the regularization parameters, the future interval length r and polynomial degree d.

5.4.1 Delta function

The least ill-posed class of functions for the applied torque, which the delta function function belongs to, require little in the way of regularization to obtain a stable solution. In Figure 5.19, the effect of the choice of polynomial degree d on the solution, $G(t)$, is illustrated. The number of grid-points is taken to be $R = 100$ and the relative error in the platen displacement and data functions are taken to be 1% and 5%, respectively. The unregularized case ($r = 0$) is included first for comparison and verifies that regularization is actually necessary. For small values of $d = 0, 1, 2$, the value of the regularization parameter r was varied to determine the optimal value, the solution for which is plotted in the remaining three subfigures. Taking a value for the polynomial degree of $d = 0$, which corresponds to the future-constant algorithm, the optimal value for the future interval is $r = 3$ which represents a compromise between supression of the spurious oscillations seen in the unregularized case and over-regularization which flattens the curve excessively for higher values of r.

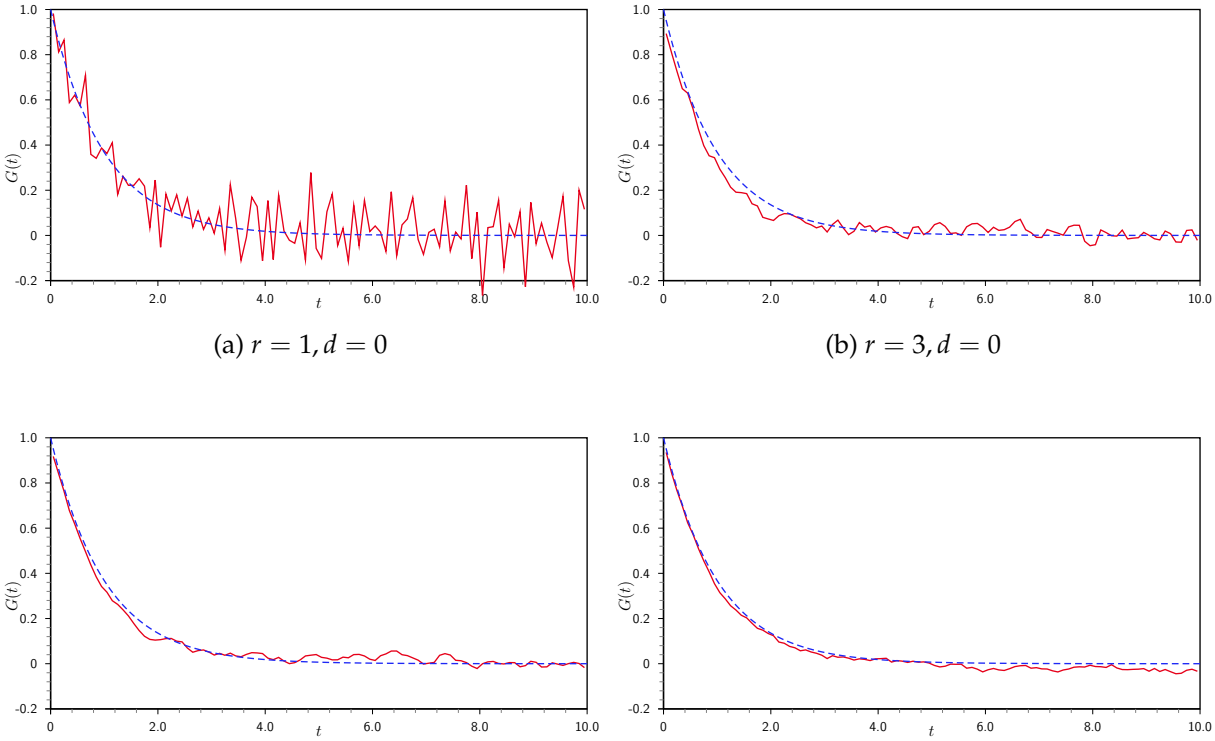

(a) $r = 1, d = 0$

(b) $r = 3, d = 0$

(c) $r = 9, d = 1$

(d) $r = 16, d = 2$

Figure 5.19: Numerical solution: delta function, Maxwell model $(\psi < 0)$, (1%,5%) error, future-polynomial regularization method.

Increasing the polynomial degree to $d = 1$, the solution is now assumed to be constrained to be a linear function of time on the future interval $[t, t + (r - 1)h]$. A much higher value of $r = 9$ can be used without over-smoothing the solution in this case and in general it can be seen that the solution is slightly more accurate than the future-constant case $d = 0$. Increasing the polynomial degree to $d = 2$ improves the solution further, providing the best approximation to the true solution in the steep section of the curve near $t = 0$, the optimal value for the future interval being higher than for the other cases with $r = 16$. For $R = 100$, or 10 data points per second this only corresponds to an extension of 1.6s to the experiment however.

As another example of a 1-smoothing problem, the applied torque which corresponds to $\dot{\chi}(t) = G(t)$ is used to determine the relaxation modulus in Figure 5.20. The solution is obtained by differentiation of the platen displacement data and the degree of ill-posedness is therefore equivalent to the 1-smoothing problem. All forms of the regularization algorithm for $d = 0, 1, 2$ produce reasonable solutions, although the future-constant algorithm performs slightly less effectively near $t = 0$. Note that with each integer increase in the polynomial degree, the number of future intervals required

to obtain an optimal stable solution is approximately doubled.

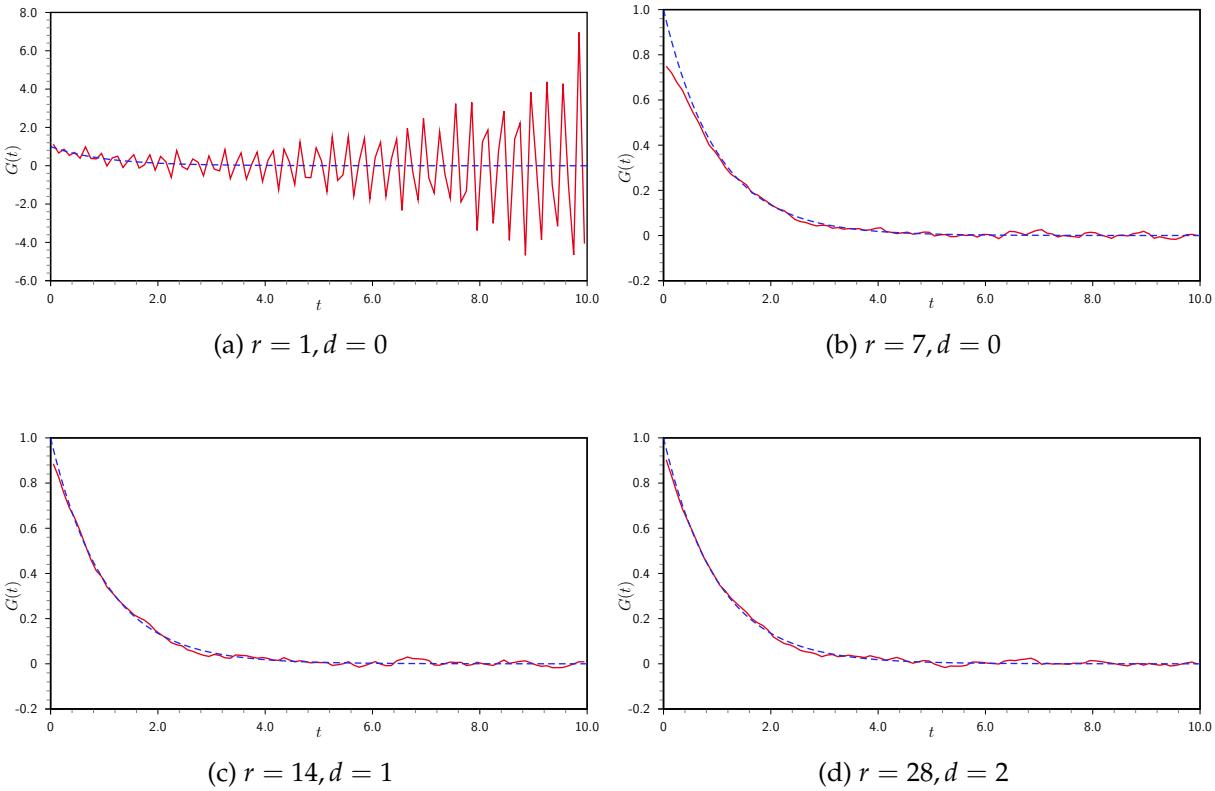

(a) $r = 1, d = 0$ (b) $r = 7, d = 0$

(c) $r = 14, d = 1$ (d) $r = 28, d = 2$

Figure 5.20: Numerical solution: relaxation modulus (such that $G = \dot{\chi}$) torque, Maxwell model ($\psi < 0$), (1%,5%) error, future-polynomial regularization method.

5.4.2 Step and box functions

The effect of regularization for the two-smoothing case is illustrated in Figure 5.21 for the step function and in Figure 5.22 for the box function. For all values of $d = 0, 1, 2$ a higher value of the regularization parameter r is required to stabilize the solution relative to the 1-smoothing case. In both cases, the unregularized solution is completely inadequate for determining the relaxation modulus. For the step function, $r = 10$ is necessary when $d = 0$, providing an accurate solution for longer time values, but over-regularizing slightly on shorter timescales. Much better performance is attained near $t = 0$ for the linear and quadratic polynomial cases, but the flatter part of the curve is approximated less accurately than for the future-constant case $d = 0$. The box function appears to be slightly more stable, requiring lower values of r to obtain better results than the step function. For $r = 24$ and $d = 2$ an accurate solution can be obtained using the prescribed data.

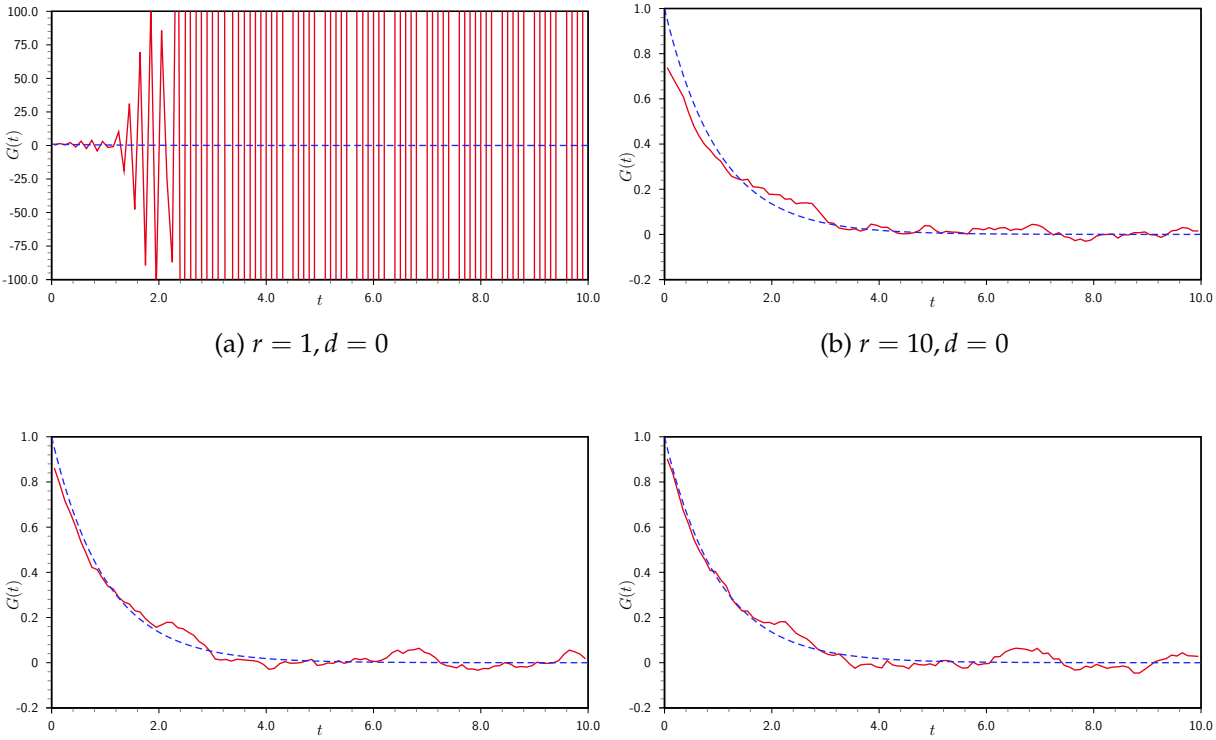

(a) $r = 1, d = 0$

(b) $r = 10, d = 0$

(c) $r = 18, d = 1$

(d) $r = 26, d = 2$

Figure 5.21: Numerical solution: step function torque, Maxwell model ($\psi < 0$), (1%,5%) error, future-polynomial regularization method.

5.4.3 Ramp function

The most ill-posed class of 3-smoothing problems is represented in Figure 5.23 by the ramp function applied torque. As expected, the unregularized case $r = 1$ is highly oscillatory and regularization is required to obtain meaningful results. Somewhat surprisingly, the future-constant algorithm produces a reasonable solution for a relatively low value of $r = 3$. Accuracy is improved by increasing the polynomial degree to $d = 1$ and the future interval to $r = 15$ and a further improvement is observed for the quadratic case with $r = 21$ future intervals.

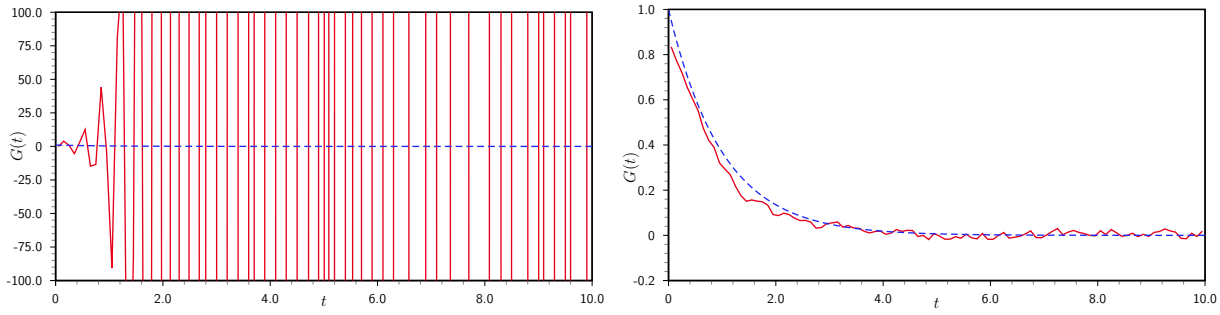

(a) $r = 1, d = 0$ (b) $r = 7, d = 0$

(c) $r = 14, d = 1$ (d) $r = 24, d = 2$

Figure 5.22: Numerical solution: box function applied torque, Maxwell model ($\psi < 0$), (1%,5%) error, future-polynomial regularization method.

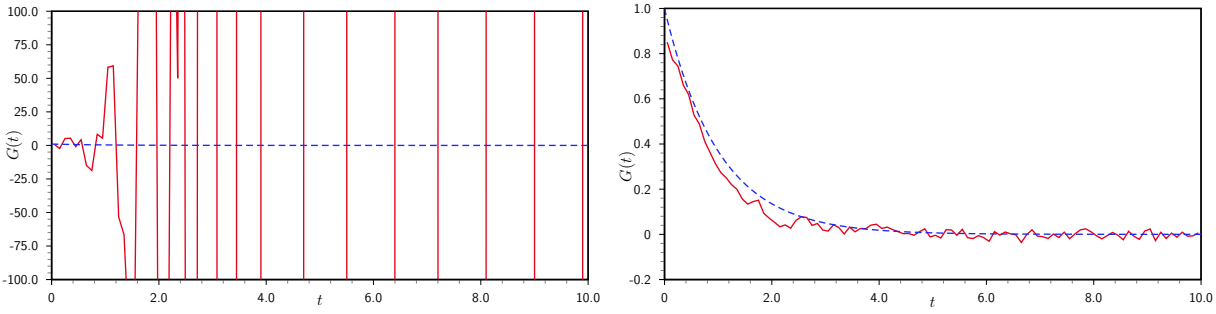

(a) $r = 1, d = 0$ (b) $r = 3, d = 0$

(c) $r = 15, d = 1$ (d) $r = 21, d = 2$

Figure 5.23: Numerical solution: ramp function applied torque, Maxwell model ($\psi < 0$), (1%,5%) error, future-polynomial regularization method.

V. SUMMARY

In this chapter the issues concerning numerical solution of the governing equation in the form of a Volterra integral equation of the first kind have been investigated. A choice of simple discretization methods are available for this type of equation, these being more stable than the more complex higher-order methods which can be devised. In the examples, the piecewise constant collocation method was used, both in isolation and paired with one of two regularization methods of the predictor-corrector type which preserve the characteristic causal property of the Volterra equation, to obtain the most stable and accurate solution possible for each of the applied torque functions introduced previously. The functions are classified according to the ν-smoothing definition in Chapter 4, so the delta function belongs to the 1-smoothing class, the step and box functions to the 2-smoothing class and the slope and ramp functions to the 3-smoothing class.

Using collocation alone, reasonable solutions can be obtained for the 1-smoothing and 2-smoothing cases when exact data is used. However, in the presence of noisy data for the platen displacement and derived data functions a stable solution can not be obtained in general for every choice of step-size. For 1-smoothing problems, varying the step-size can result in a reasonable solution, although this often results in an unacceptably coarse grid. The 2-smoothing problem cannot be satisfactorily stabilized by this method alone and additional regularization is required. The most ill-posed problem considered here is the 3-smoothing problem, which in this case is highly unstable even using exact data.

The two examples of a predictor-corrector type regularization method implemented here were found to be effective in determining a stable solution for all of the applied torque functions considered here. Acceptable results can even be achieved for 3-smoothing problems, but in general it is desirable to choose an applied torque which minimizes the ill-posedness of the problem, i.e a 1-smoothing or 2-smoothing problem. The future-constant method implemented first regularizes the problem by holding the solution constant on $(r-1)$ future intervals. For the delta function, only a small amount of future information is required, corresponding to $r = 3$ for the best solution. As the degree of ill-posedness increases, a large value for r is required to stabilize the solution. For the 2-smoothing kernels pertaining to the step and box functions, a larger value of r is required to stabilize the solution, typically $r = 7$ or $r = 8$ provides the optimal solution. The most ill-posed 3-smoothing problem, the slope

function applied torque requires a much longer future interval of $r = 18$ to obtain an acceptable solution and even then the solution is not as accurate as for the 1- and 2-smoothing cases. Somewhat unexpectedly, the ramp function only required $r = 8$ to obtain a much better solution than for the slope function.

Although the algorithms described in [47] and [18] were only considered for noise in the data function, it has been demonstrated here that they are effective at regularizing the problem when the kernel function is contaminated with noise additionally. Perturbations in the kernel function often have the effect of increasing the condition number of the matrix A^R for this problem, leading to an even less well-conditioned system and consequently an unstable solution. The regularization methods used here stabilize the problem by reducing the condition number of A^R to obtain a smooth solution, so it is intuitive that kernel noise can also be handled, although a larger value of the regularization parameter is often required than the examples given in the papers.

It was noted in all cases that the future-constant algorithm tends to over-regularize the steep section of curve where short relaxation times are dominant when the value of r is increased beyond an optimal value, although good performance is generally obtained in the flatter part of curve dominated by longer relaxation times for large r values. This was the motivation for trying the future-polynomial regularization algorithm of [18], whereby the solution is assumed to be a d-th degree polynomial rather than a constant on the future interval. The future-polynomial algorithm for $d = 1, 2$ was compared with the future-constant algorithm ($d = 0$) and in all examples it was found to approximate the solution much more accurately near $t = 0$. For higher polynomial degrees, the optimal value of r increases, requiring the use of more future information. In general $d = 2$ produced the most accurate results, although in some cases the future-constant algorithm handles the more rigid part of the curve near the end of the solution interval. It may be advantageous to solve the equation for both $d = 0$ and $d = 2$ and combine the results using the latter for shorter timescales and the former for longer timescales.

In agreement with the conclusions of Chapter 4, the best applied torque in terms of stability is the delta function and other functions belonging to the 1-smoothing class of problems. The experiments in this chapter suggest that reasonable solutions for the relaxation modulus may be obtained for applied torques corresponding to general ν-smoothing problems provided ν is not too large. However, the best results will always be obtained by choosing ν as small as possible.

As an addendum, a few alternative methods are mentioned which may be suitable

for this problem, although the predictor-corrector methods used here appear to be perfectly adequate. Firstly, analogously to the method of obtaining an exact solution in Chapter 2, the Laplace transform could be discretized to provide a solution. The forward Laplace transform is well-posed w.r.t. perturbations in the data and can be found without too much difficulty, the ill-posedness of the problem lying in the inversion of the transform equation. Various regularization procedures may be found in the literature for the inverse Laplace transform and a Fortran program known as *Contin* [1] is available which has been used successfully for some rheological interconversion problems. Another form of the predictor-corrector algorithm by the same author which involves using Tikhonov regularization sequentially using a prescribed amount of future information can be found in [45],[55],[48],[49],[53].

[1] Contin: http://s-provencher.com/pages/contin.shtml

CHAPTER 6

Experimental Design & Conclusion

In this final chapter, matters pertaining to the design of an experimental investigation are considered. Questions concerning the choice of applied torque to use in order to characterize a linear viscoelastic material, the choice of instrumental setup to produce the most stable data and the numerical interpretation of the data thus acquired are discussed. The second part of the chapter contains a detailed summary of the results presented in the preceding chapters of the thesis and concluding remarks.

I. EXPERIMENTAL DESIGN

6.1.1 Standard Procedure

The standard procedure, as discussed in Chapter 1, for obtaining the linear viscoelastic functions is to apply a sinusoidally varying applied torque, or strain, and observe the response of the part of the rheometer that undergoes the resulting motion. Taking a fairly modern instrument such as the TA Instruments AR2000 as an example, there are a number of steps involved in performing an experiment to determine the characteristic material functions. The principal consideration when performing an experiment to determine the material functions is to ensure that the applied stress is chosen such that the displacement response is sufficiently small to ensure that the linear assumption is valid. The limit beyond which the behaviour of the material is non-linear depends upon the specific material under investigation and can only be determined by experimentation. Where sinusoidal stress profiles are concerned, the first step would be to perform a "stress sweep", where a fixed frequency waveform is applied to the same material which is under investigation, for a range of amplitudes. Solution for the complex modulus will then demonstrate the range of stresses that can be utilized, each giving the same solution for the complex modulus. If the linear viscoelastic limit is exceeded, a plot of G' or G'' as a function of stress will reveal a departure from a horizontal line. This will need to be repeated for several frequencies representing the range of frequencies for which the solution is desired for the most accurate results, consequently adding considerable time to the duration of the experiment. This step is generally necessary however; if it is omitted there is essentially no way of determining whether the solution obtained conforms to the linear viscoelastic assumption and therefore may be inaccurate. The main body of the experiment can take place once the stress amplitudes have been selected by performing a "frequency sweep", whereby the sinusoidal stress is applied over a specified range of frequencies for which the complex modulus is desired.

Calibration of the instrumental setup also comprises an important step before any measurements can take place. Firstly, the gap between the two plates must be determined accurately by establishing a zero reference point for which the plates are in direct contact. The TA Instruments AR2000 rheometer possesses a fixed lower platen, which has Peltier apparatus for controlling the temperature of the sample and is much larger in diameter than the upper platen, which is part of the rotating assembly of the rheometer used to apply the specified torque or strain and provide measurement of the required variable. It has been assumed throughout that the damping factor, d, in the governing equations for the parallel plate geometry is small enough to be negligible. However, it requires only a minor modification to incorporate this into the analysis should it be considered necessary, by the addition of a term $d\dot{\chi}(t)$ in the data function. The air bearings used on modern rheometers typically produce frictive torques of $\leq 1\,10^{-11}$ Nm, so it can safely be assumed that $d \approx 0$. A side-effect of the use of air bearings is that there frequently exists a small rotational torque due to the air current which must be compensated for by an auxiliary jet of air or a small bias current in the drive. Another disadvantage is the relative delicacy of the structure which in some cases necessitates the use of a clamp while loading or removing samples to prevent damage. The damping factor is typically determined automatically by the rheometer during the initial calibration step along with the determination of the inertia of the rotating assembly. This step must be performed after the geometry has been chosen and is dependent upon the density of the material used in the manufacture of the platen and also the diameter.

The use of applied torque profiles of types other than a fixed frequency sinusoidal waveform is only partially implemented in current rheometers. Many instruments, including the TA Instruments AR2000, have the facility to apply a torque consisting of a small number of superimposed frequencies with specified amplitudes and built-in capabilities for obtaining the complex modulus at the relevant frequencies via use of the discrete Fourier transform. The problems concerning the choice of the individual stress amplitudes has been discussed in Section 1.1 subject to the linear constraint and the sensitivity of the instrument sensors. The use of completely arbitrary applied torque profiles requires the modification of current rheometers and can not be considered to be currently mainstream. The TA Instruments AR2000 at Aberystwyth University possesses a specially written software application known as "Torque Table" which allows the application of a discrete torque signal in the form of a tabular data file, the strain data being written to a separate file for corresponding time points. The first step to

take in any experimental investigation involving non-standard procedure is to verify whether the use of a sinusoidal waveform produces the same results as those determined automatically by the rheometer software. A concise experimental investigation to this purpose was carried out in [8], however a slight discrepancy was experienced between the data produced by the rheometer software and that obtained by applying a fixed frequency sinusoidal waveform using the software modification, the deviation being more pronounced for higher frequencies. The damping factor was excluded from the analysis and may partially account for the discrepancy, but the more likely explanation may lie with the approach the machine takes to data acquisition. Many rheometers use alternating data acquisition, the stress being measured at the time expected and the strain being measured at a time offset by an amount equal to half the sampling time. Thus, for higher frequencies this would result in an apparently more significant time shift than for lower frequencies. This is one of the problems which must be overcome when performing experiments with non-standard torque or strain profiles. The alternative is a simultaneous acquisition method, where the stress and strain are measured at exactly the same point in time - in this case no compensation is necessary.

The effect of fluid inertia was considered to be negligible in the analysis and this is a reasonable assumption for viscoelastic fluids in general. However, for torques that produce sudden changes in the fluid velocity, or fluids that possess a very low viscosity, it may be worthwhile investigating whether fluid inertia is a significant factor. Measurements in the linear viscoelastic region generally involve small displacements and gradients, therefore the incorporation of fluid inertia into the theory is less important than for non-linear measurements such as steady-shear with the cone and plate geometry. When fluid inertia is taken into account, the solution of the governing equations is no longer trivial, and involves determination of a correction term to the standard solution where the fluid inertia term is assumed to be zero. An example of the implementation of a model incorporating fluid inertia for small amplitude oscillatory shear may be found in [96].

The considerations pertaining to the design of a stress-controlled experiment to determine the linear viscoelastic functions are now discussed.

6.1.2 Choice of Applied Torque

The wide variety of functions which are suitable for use as applied torques have been grouped into classes of functions in terms of optimality with respect to numerical sta-

bility, as defined using the ν-smoothing classification in Section 4 and examples were used for simulation of the displacement response in Chapter 2. Using the method outlined in this dissertation, practically any function which can be physically applied on a rheometer can be used in an experiment to determine the relaxation modulus, although the stability of the solution process will be determined by the particular choice of function. Applied torques which produce more ill-posed problems require a greater degree of regularization to produce a reasonable solution in the time domain and there is no guarantee that a stable solution can be found, therefore it is always desirable to use a torque profile which minimizes the ill-posedness of the problem. From a purely theoretical perspective, it was shown that the optimal form for the applied torque would be the 1-smoothing case, of which the canonical form is the delta function. In Section 3.1.1 it was shown that the 1-smoothing case requires a step discontinuity in the platen angular velocity and that the applied torque must contain a delta function. However, it is arguable whether an infinitely large force applied over an infinitesimal time can ever be realistically reproduced in an experimental situation. The actual torque applied would resemble a narrow box function, limited in width by the sampling time of the experiment, but the box function was shown to correspond to a 2-smoothing problem and hence does not share the optimal properties of the delta function.

Incorporating practical considerations into the argument, the best or optimal choice for the applied torque function must be the 2-smoothing problem, the canonical case for which is the box function. Although it is reasonable to simulate experiments for the step function, which takes the value C_0 for all values of time $t > 0$, since any experiment will be of finite duration T the actual torque will take the form of a box function. In fact, this implies that all applied torques must be compact functions defined on $[0, T]$. Thus, in the absence of *a posteriori* information pertaining to instrumental output, the optimal form for the applied torque would be the box function. In a stress-controlled framework it is reasonable to assume that step changes in the torque can be applied, whereas for strain-controlled experiments it is difficult to achieve an accurate step change due to the inertia of the rotating instrument assembly. Since the ill-posedness of the problem is related to the rapidity with which the kernel function $\dot{\chi}(t)$ increases near $t = 0$, the more ponderous growth in the strain actually representing a step increase will result in decreased stability in the solution. This is a further example of the advantages of stress-controlled over strain-controlled measurements.

Since there is a predilection for analysis in the frequency domain to obtain the storage and loss moduli, further constraints on the applied torque function can be em-

ployed from experimental considerations. In both the time and frequency domains, it is desirable to maintain the magnitude of the measured platen displacement in the region bounded above by the linear viscoelastic limit beyond which the governing equations are no longer valid, and below by the smallest strain values that the instrument sensors can reliably measure to an acceptable degree of accuracy. In the frequency domain this infers that all of the frequency components for which the complex modulus solution is required must have displacements large enough to be measured accurately. As mentioned in Section 1.1, the optimal form the applied torque where a frequency domain analysis is concerned was stated in [58] to be the sinc function, whose Fourier transform is the box function and thus contains equal amplitudes for all frequencies in a specified range. This definition is compatible with the smoothing definition utilized here, since the sinc function as an applied torque, when taken on the interval $[0, T]$, is also a member of the class of functions corresponding to the 2-smoothing problem. Should the complex modulus only be required at a small number of discrete frequencies, the Fourier transform should consist of several sharp spikes at the frequencies of interest or equivalently a combination of superimposed sinusoidal waveforms at the relevant frequencies as described in [35].

The next step in designing an experimental investigation would be to determine the magnitude of the applied torque, C_0, the best choice being suitably large that the platen displacement is measured in the most accurate range of the instrument sensor. However, the displacement must be sufficiently small such that the linear viscoelastic limit is adhered to, otherwise the governing equations can no longer be considered to be valid. Unfortunately, there is no theoretical means for calculating the maximum displacement which the material can be subjected to whilst still adhering to the linear viscoelastic regime, so only an empirical approximation can be obtained for the limiting value by trying a selection of applied torque magnitudes. If the values lie within linear viscoelastic range, the torque and displacement will exhibit a directly proportional relationship and hence indistinguishable solutions for the relaxation modulus or complex modulus will be obtained. When the applied torque is increased beyond the linear limit, the solution obtained will begin to depart from the true solution. The torque magnitude should also be chosen to ensure that the displacements are adequately large to be measured with acceptable accuracy over the entire experimental time, otherwise particular parts of the curve may be subject to noise, which in the case of solution in the time domain may propagate to the solution function at subsequent time-steps.

The final design choice, assuming that the box function is to be used as an applied torque function, is concerned with the relative values of the experimental time T and the cut-off time t_1, after which the torque is zero. The options are to take the cut-off time to be equal to the experimental time, in which case the torque is non-zero for the whole duration of the experiment, or to take the cut-off time to be less than the experimental time. In the latter case it is possible that the platen displacement may become zero or too small to measure with any degree of accuracy before the end of the experiment at $t = T$. This corresponds to a small value for the data function $f(t)$ for the latter part of the experiment, since the platen displacement tends to a linear function and the second derivative tends to zero. Theoretically, there does not appear to be an optimal value for the cut-off time relative to the experimental time, leaving only an empirical approach to determining which option provides the best quality data.

As a case study, the single-mode Maxwell model is taken to represent the material subjected to an applied torque in the form of a box function, as described in Section 2.3.2. The material parameters are taken to be $g = 1$ and $\lambda = 1$, and the instrumental parameters $kI = 0.1$, the torque magnitude being $C_0 = 1$. The cut-off time has been varied to take the values $\{0.01, 0.1, 0.5, 1, 2, 4, 8, 10\}$ in seconds, where the experimental time $T = 10$ seconds. Noise is added to the data by the method described in Section 5.3, with levels of 1% in the kernel function $\dot{\chi}(t)$ and 5% in the data function $f(t)$. The simple collocation method, without any form of regularization as described in Section 5.1.4, is first used to gain an idea of the inherent degree of stability involved in the solution for each of the values for the cut-off time. The condition numbers for the linear system of equations are shown in Table 6.1 for each of the cut-off times specified, both for exact and noisy data. It can clearly be seen that in the case of exact data the condition number of the matrix increases with increasing cut-off time, and is distinctly smaller for the shortest cut-off time than any of the others, probably due to the similarity to the optimal delta function torque. For the noisy data, the shortest cut-off time again has a distinctly smaller condition number and hence represents the most stable, well-conditioned system of equations. The case where the cut-off time coincides with the experimental time is clearly the most poorly-conditioned example.

It is apparent that solely in terms of stability, it is best to choose the cut-off time as short as possible in relation to the experimental time. However, there are further experimental considerations to take into account concerning the accuracy with which the resulting platen displacement can be measured. The solutions obtained for noisy data using the box function with variable cut-off time are shown in Figure 6.1 using

the future-polynomial regularization method described in the previous chapter. It can be seen that the best results are obtained in the range $t_1 = 0.5$ to $t_1 = 2$ seconds, with the solution being perceptibly worse for the case where the cut-off and experimental times coincide. The best solution is for the shortest cut-off time, but it should be noted that the platen displacement suffers from rapid diminution relatively early in the course of the experiment, therefore the displacements may be too small to measure with sufficient accuracy towards the end of the experiment and could be contaminated with noise of a magnitude potentially larger than that simulated here. It was noted in [97] that the data produced by free oscillations, which are essentially the response being observed in this case after the cessation of the applied torque, are generally not as accurate as those produced by forced oscillations for this very reason. The rate of decay depends on the real part of the complex root of (2-95) for an N-mode Maxwell fluid, and since this may be considerably smaller than the longest relaxation times, the platen displacement may be essentially zero for much of the latter parts of the experiment if the cut-off time is too short. For the Maxwell model, the rate of decay of the oscillations is equal to half the reciprocal of the relaxation time, hence the effect of small platen displacements is less obvious than for models with a widely distributed relaxation spectrum.

The best choice of applied torque appears to be one that allows free oscillations to occur after the cut-off time and before the end of the experiment, whereby making use of all the time-varying displacement data. For materials with widely-spaced and long relaxation times, it may be necessary to apply a sequence of box functions such that the longer end of the relaxation spectrum is probed, since the oscillations may decay to diminutive levels too rapidly to allow these relaxation times and equivalently the relaxation modulus for longer timescales to be resolved accurately. The relatively poor performance of the case where the cut-off and experimental times are coincident may be due to the fact that the data function, which depends on the term $\ddot{\chi}(t)$ becomes relatively small as the displacement tends to a linear function of time and is thus contaminated with noise for the latter part of the experiment. When the torque is removed, the same effect on the second derivative of $\chi(t)$ occurs, suggesting that applied torques which produce non-zero values for $\ddot{\chi}(t)$ throughout the duration of the experiment may be of more practical use.

A further consideration is the sampling rate, or number of data points to use. A smaller number of time-steps will result in greater stability, since discretization has a regularizing effect on the solution of the Volterra-1 equation, the regularization pa-

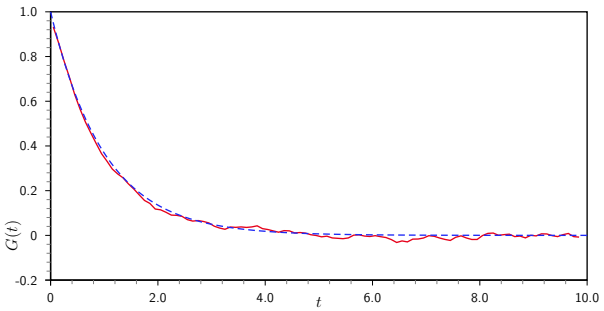

(a) $t_1 = 0.01$, $r = 18$, $d = 2$

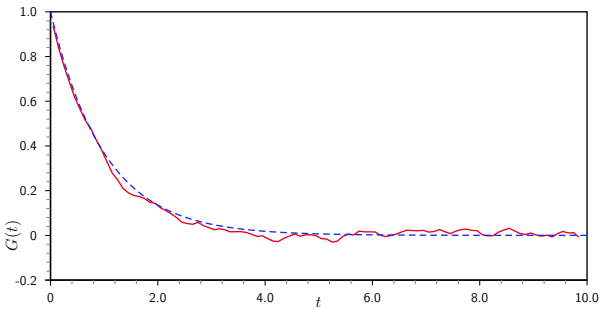

(b) $t_1 = 0.1$, $r = 16$, $d = 2$

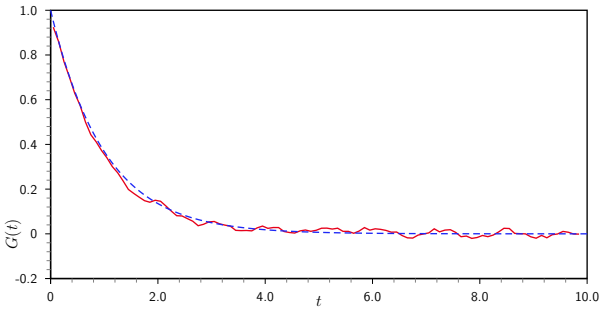

(c) $t_1 = 0.5$, $r = 16$, $d = 2$

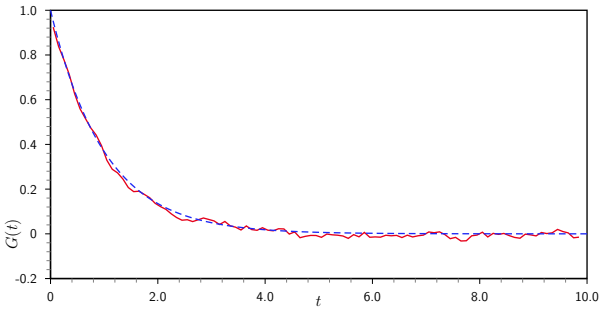

(d) $t_1 = 1$, $r = 18$, $d = 2$

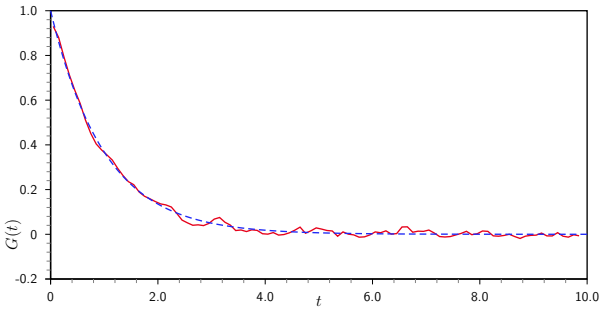

(e) $t_1 = 2$, $r = 20$, $d = 2$

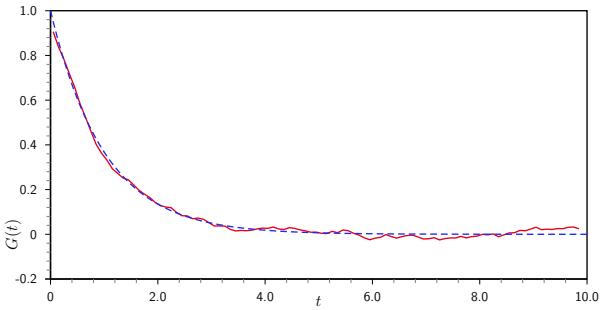

(f) $t_1 = 4$, $r = 24$, $d = 2$

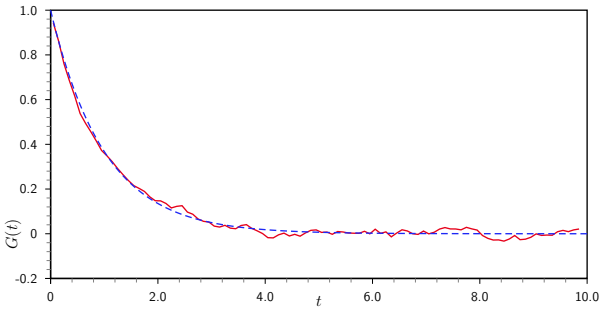

(g) $t_1 = 8$, $r = 24$, $d = 2$

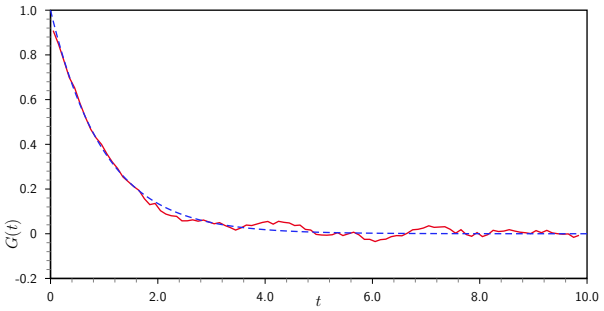

(h) $t_1 = 10$, $r = 26$, $d = 2$

Figure 6.1: Numerical solution: box function, Maxwell model ($\psi < 0$), (1%,5%) error, variable cut-off time.

t_1	Exact data	(1%,5%) error
0.01	$2.845\ 10^{1}$	$2.504\ 10^{2}$
0.1	$4.992\ 10^{3}$	$8.283\ 10^{12}$
0.5	$2.301\ 10^{4}$	$1.401\ 10^{10}$
1	$3.627\ 10^{5}$	$4.801\ 10^{17}$
2	$1.217\ 10^{5}$	$8.071\ 10^{11}$
4	$1.141\ 10^{5}$	$4.025\ 10^{14}$
8	$1.063\ 10^{5}$	$2.118\ 10^{40}$
10	$8.577\ 10^{4}$	$6.815\ 10^{43}$

Table 6.1: Condition numbers for A^R, box function applied torque, Maxwell model ($\psi < 0$).

rameter being the step-size, but may result in an unacceptably coarse grid and solution. Increasing the number of time-steps may result in better resolution of the solution, but causes greater numerical instability and has a detrimental effect on the conditioning of the matrix system which must be solved. As a compromise, the number of data points has been taken to be 10 per second in these examples.

6.1.3 Instrumental Setup

The effect of changing the instrumental parameters relating to the experimental setup may also have an effect on the quality of the data that may be obtained. The parameters which can typically be varied are:

1. inertia of the rotating instrument assembly (I), depending upon the material and dimensions of the interchangeable platen,
2. diameter of the platen (affects k and I), and
3. plate separation (affects k).

Note that the first two alterations require the experimental setup to be dismantled and reset, but the plate separation can be altered without affecting the course of the experiment. To investigate the effect of changing the instrumental parameters relative to the material parameters, a Maxwell fluid with $g = 1$ and $\lambda = 1$ is considered when subject to a box function applied torque with cut-off time $t_1 = 1$ and the parameter kI is varied such that the value of ψ as defined in Section 2.3.2 is either positive, zero or negative, respectively.

The condition numbers for the unregularized collocation discretization are shown in Table 6.2 for each of the three cases and for error levels of (0%,0%), (0.5%,1%) and (1%,5%) for the platen angular velocity and data function, respectively. Where exact data is concerned, the conditioning of the matrix system is improved when $\psi < 0$, or equivalently when the platen displacement exhibits oscillations rather than monotone behaviour, although the advantage is not considerable.

The solutions obtained using the two regularization methods described in Section 5.3 and Section 5.4 are plotted in Figure 6.2-Figure 6.7. For noise levels of 0.5% in the platen angular velocity and 1% in the data function, Figure 6.2 shows the solution for $\psi < 0$ for which the displacement has oscillations, Figure 6.4 shows the solution for $\psi = 0$ and Figure 6.6 the case where $\psi > 0$. In accordance with the numerical results in Chapter 5, in the absence of regularization the collocation method alone is inadequate to produce a stable solution. The future-polynomial method with $d = 0$, i.e. the future-constant method, requires a progressively larger amount of future information to obtain a stable solution for $\psi = 0$ and $\psi > 0$ and the solution near $t = 0$ is increasingly poorly reproduced. For $d = 1$, assuming a linear polynomial on the future interval, similar behaviour is seen with the least degree of regularization required for $\psi = 0$ and the solution near $t = 0$ becomes increasingly poor for $\psi = 0$ and $\psi > 0$. The best solution is obtained in all cases with the quadratic polynomial specified on the future interval ($d = 2$), although a larger amount of future information is required for $\psi = 0$ and $\psi > 0$. Similar behaviour is observed when the error levels are increased to 1% and 5% for the platen angular velocity and the data function, respectively. In all cases, reasonable solutions can be obtained if the regularization paramater r is chosen to be sufficiently large. Again, for $d = 0$ and $d = 1$, stable overall solutions can be obtained at the expense of accuracy near $t = 0$ for the cases $\psi = 0$ and $\psi > 0$.

Since the most stable solution occurs when the platen displacement exhibits oscillations upon application and removal of the applied torque in the form of a box function, it is desirable to choose the instrumental parameters such that oscillations occur. Choosing a material for the platen with a lower density will have the effect of decreasing the instrumental inertia, and increasing the platen diameter or decreasing the plate separation will result in a smaller value for the parameter k. The parallel plate geometry demonstrates a particular advantage here, since the plate separation can be varied without dismantling the apparatus as would be required with the cone-plate and concentric cylinder geometries.

	Exact data	(0.5%,1%) error	(1%,5%) error
$\psi > 0$	2.813 10^6	3.369 10^{43}	2.9678 10^{43}
$\psi = 0$	1.676 10^6	4.206 10^{44}	2.0801 10^{44}
$\psi < 0$	3.627 10^5	3.023 10^{34}	1.028 10^{43}

Table 6.2: Condition numbers for A^R, box function applied torque ($t_1 = 1$), Maxwell model, collocation.

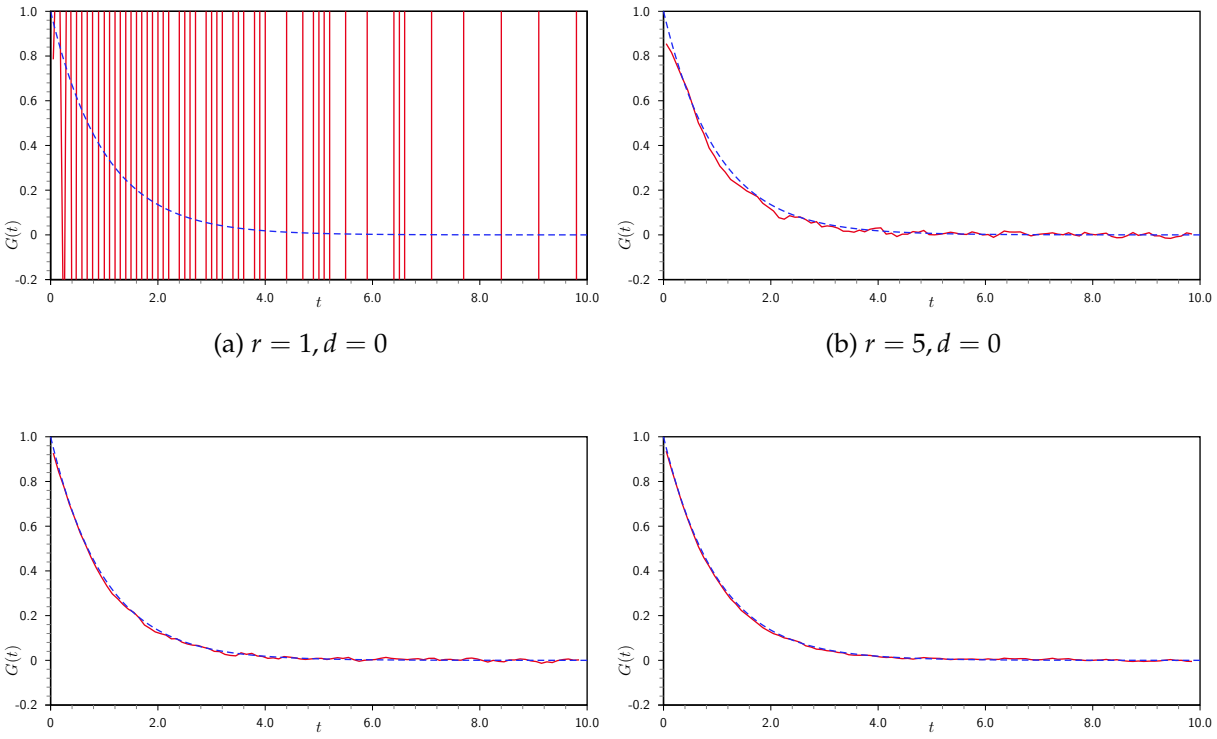

(a) $r = 1, d = 0$

(b) $r = 5, d = 0$

(c) $r = 11, d = 1$

(d) $r = 20, d = 2$

Figure 6.2: Numerical solution: box function, Maxwell model ($\psi < 0$), (0.5%,1%) error, future-polynomial regularization.

6.1.4 Data Processing

Subsequent to acquiring the experimental data for the torque and platen angular displacement, the scheme for obtaining the desired linear viscoelastic function must be decided upon. There are several options depending upon the nature of the applied torque which has been utilized and the characteristic material function which the experimenter wishes to obtain.

The first choice is Fourier Transform Mechanical Spectroscopy (FTMS), which has been discussed in detail in Section 1.1. In summary, the input and output signals are decomposed using a discrete Fourier transform into Fourier series, which allows the

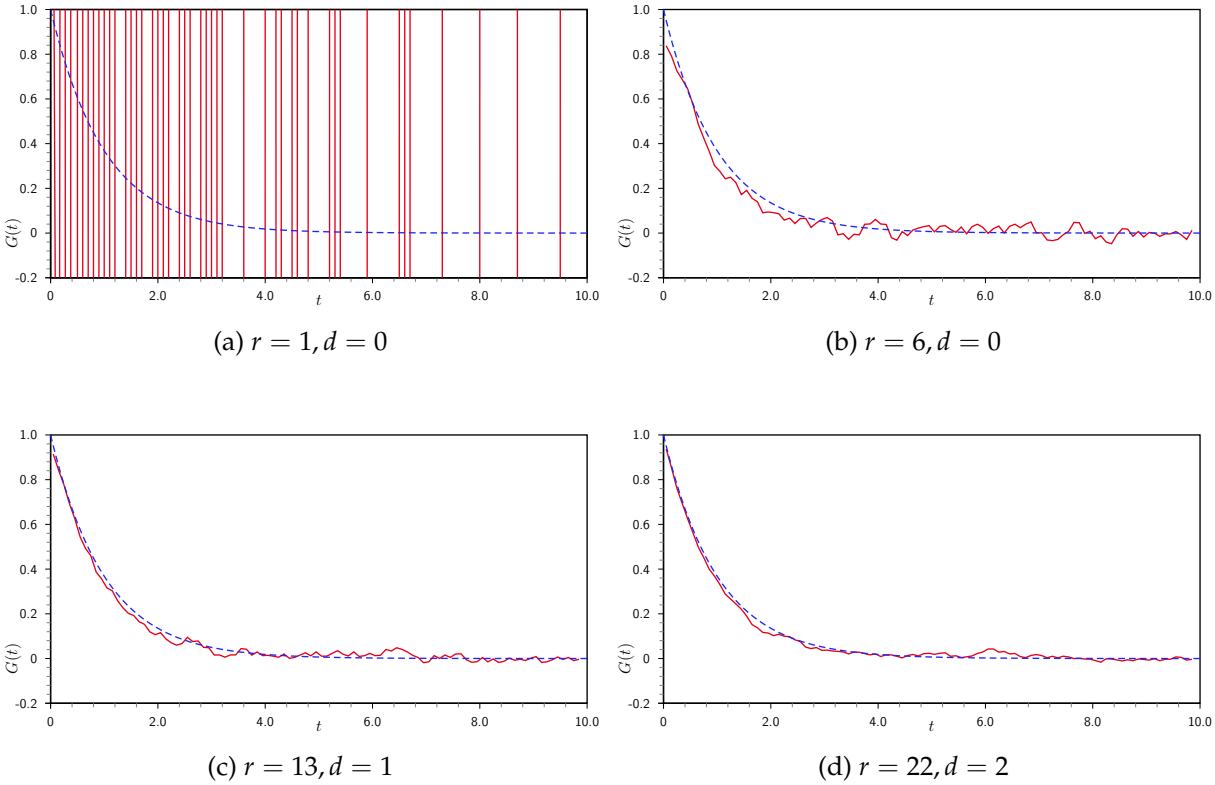

(a) $r = 1, d = 0$

(b) $r = 6, d = 0$

(c) $r = 13, d = 1$

(d) $r = 22, d = 2$

Figure 6.3: Numerical solution: box function, Maxwell model ($\psi < 0$), (1%,5%) error, future-polynomial regularization.

complex modulus to be obtained at each of the component frequencies as first used in [35]. However, strictly speaking this is only valid for periodic functions, since the equation from which the complex modulus is derived is based upon the assumption that a quasi-steady state has been reached. Where periodic functions are concerned, several cycles can be applied to allow the transient component to become negligible, however for non-periodic functions it is difficult to see how a steady state can be reached, since the period of such functions is effectively infinite. Nonetheless, this technique has used to produce reasonably accurate data for an applied torque in the form of a sinc function in [58]. A potential workaround for this would be to evaluate the Fourier transforms numerically in (2-35) to obtain the complex modulus accurately without the requirement for the existence of a steady state. The forward Fourier transform is well-posed, therefore stable discretization schemes can exist for obtaining the complex modulus by this method. The inversion of the integral transform is ill-posed, so regularization would be required to obtain the relaxation modulus via the complex modulus, however it would be unlikely that this method would be used in light of the extensive range of methods for converting the complex modulus to the relaxation modulus. An

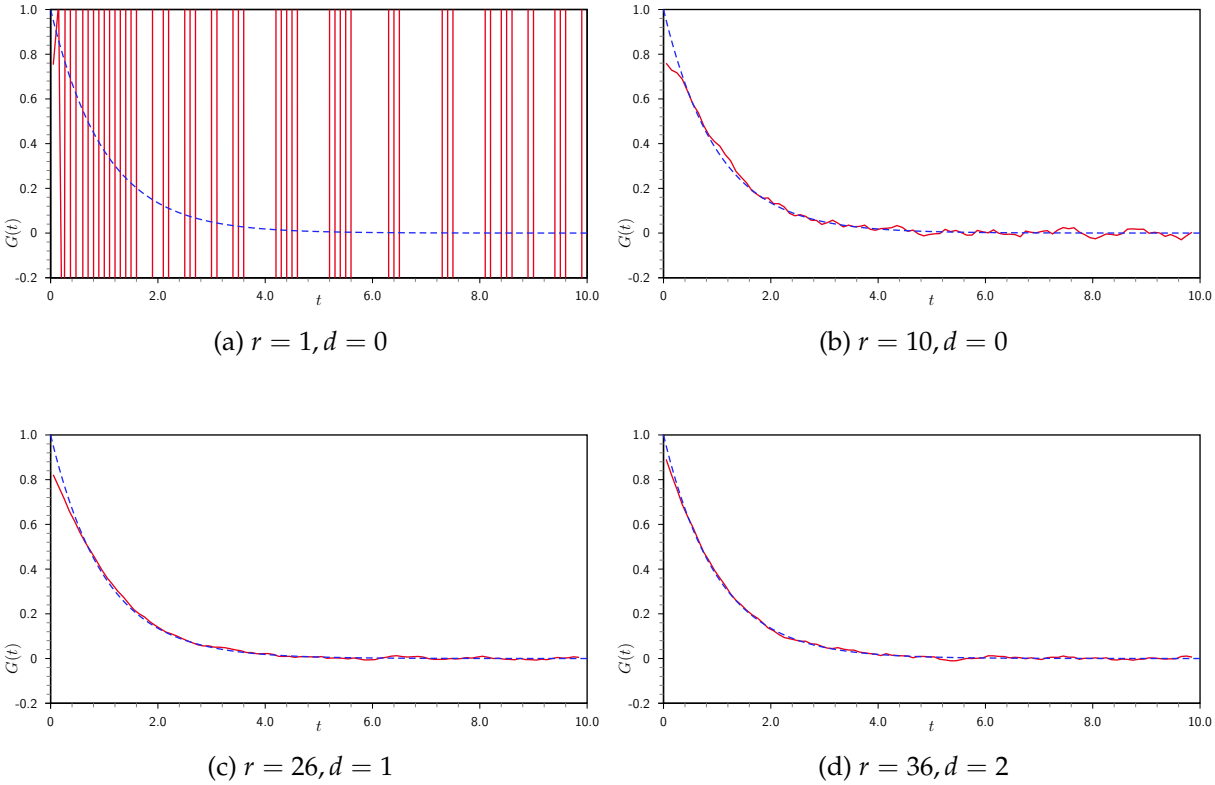

(a) $r = 1, d = 0$

(b) $r = 10, d = 0$

(c) $r = 26, d = 1$

(d) $r = 36, d = 2$

Figure 6.4: Numerical solution: box function, Maxwell model ($\psi = 0$), (0.5%,1%) error, future-polynomial regularization.

approach of this type was employed in [60] using Carson-Laplace transforms.

Alternatively, the Laplace transforms in (2-42) could be evaluated numerically, then inversion would be required to obtain the relaxation modulus. The forward transform is a well-posed problem and should present few problems, however the inversion of the Laplace transform is an ill-posed problem and a regularized inversion process will be required to obtain the relaxation modulus. Various regularization procedures may be found in the literature for the inverse Laplace transform and a Fortran program known as *Contin* [1] is available which has been used successfully for some rheological interconversion problems.

Possibly the most appropriate method for obtaining the relaxation modulus in this context is to solve the Volterra integral equation of the first kind directly. Since equations of this type are ill-posed, as discussed in Section 4.2, discretization alone is insufficient to obtain a stable solution in the presence of experimental noise. In Section 5.2 a selection of regularization procedures which are suitable for Volterra integral equations were described, the most suitable being the so-called local regularization meth-

[1] Contin: http://s-provencher.com/pages/contin.shtml

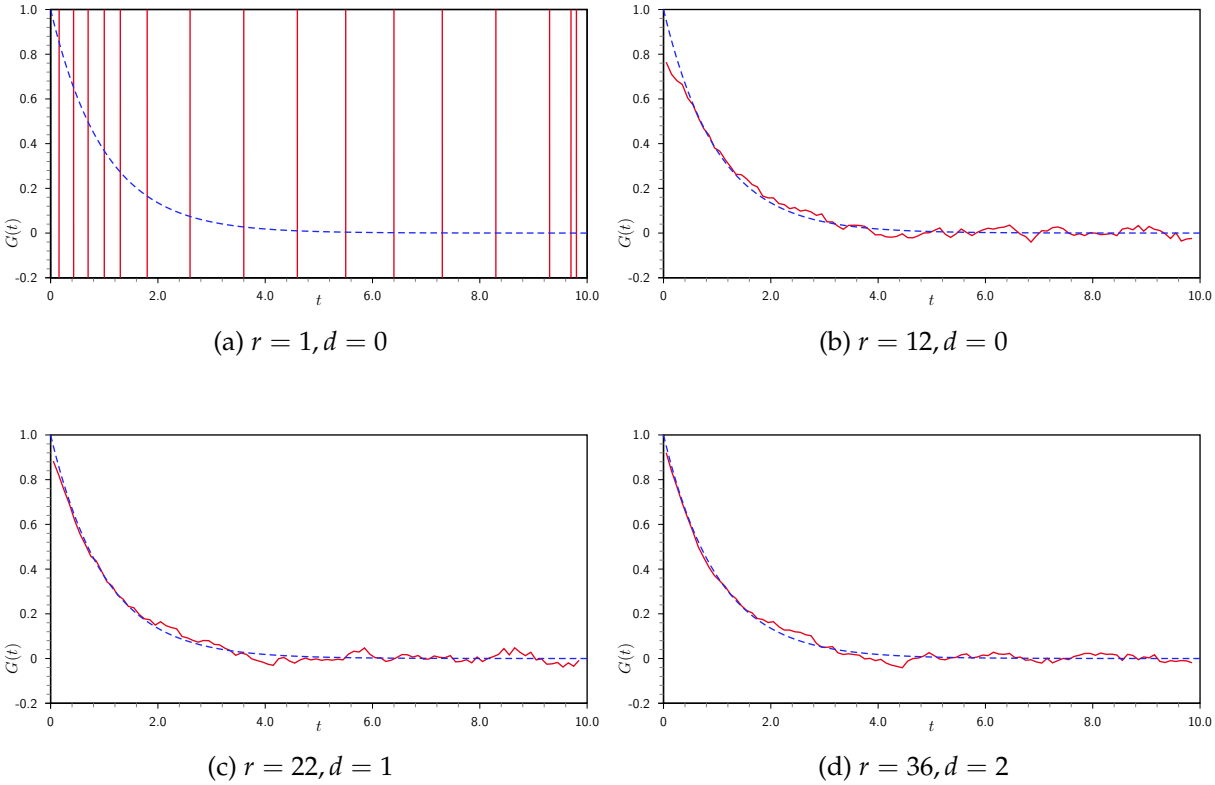

(a) $r = 1, d = 0$

(b) $r = 12, d = 0$

(c) $r = 22, d = 1$

(d) $r = 36, d = 2$

Figure 6.5: Numerical solution: box function, Maxwell model ($\psi = 0$), (1%,5%) error, future-polynomial regularization.

ods, which allow solution of the equation almost in real-time should it be required.

The examples chosen in this thesis are the future-constant predictor-corrector method of [47] and the more general future-polynomial regularization method found in [18]. Variations on this theme can be found in the literature using Tikhonov regularization locally, but these two methods have been chosen due to the simplicity of implementation and inexpensive computational demands which would imply their suitability for direct implementation into the firmware of a potential future rheometer. The methods were described in detail in Section 5.3 and numerical experiments performed to verify the efficacy of the methods for this problem. The best results are obtained using the future-polynomial method with a low degree polynomial representing the second regularization parameter d, typically $d = 2$ or $d = 3$ providing the best compromise between rigidity and smoothing of the solution. These values typically produce better resolution of the solution curve near $t = 0$ and hence a better estimate of $G(0)$, but require a greater amount of future information to produce the best results in general.

The length of the future interval used in the regularization process, represented by

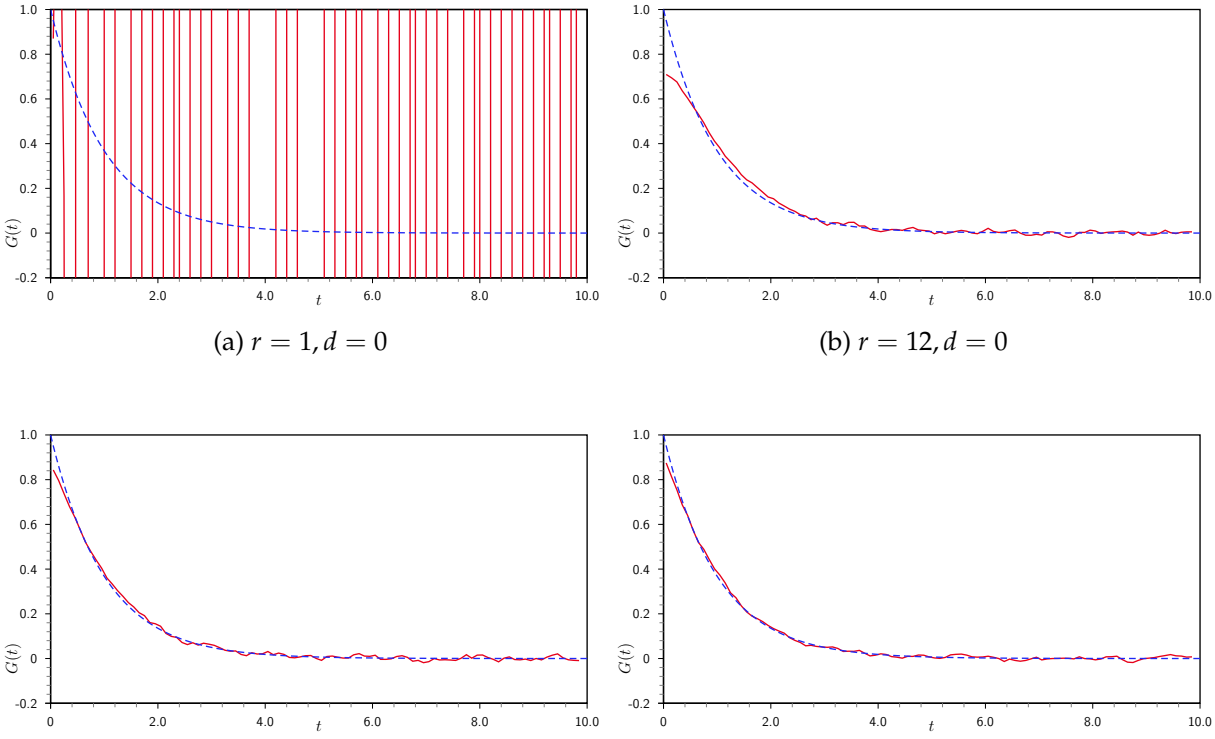

(a) $r = 1, d = 0$

(b) $r = 12, d = 0$

(c) $r = 22, d = 1$

(d) $r = 36, d = 2$

Figure 6.6: Numerical solution: box function, Maxwell model ($\psi > 0$), (0.5%,1%) error, future-polynomial regularization.

the parameter r, needs to be chosen carefully to obtain a balance between suppression of spurious oscillations in the solution and too much rigidity being imposed on the solution. Unfortunately, there is no theoretical means for selecting the optimal value for the regularization parameter, so various values need to be tried until the best value is reached by visual comparison. Ideally, this would be performed automatically by the rheometer software in near real-time, however a criterion for the selection of the optimal value for the regularization parameter would be required first.

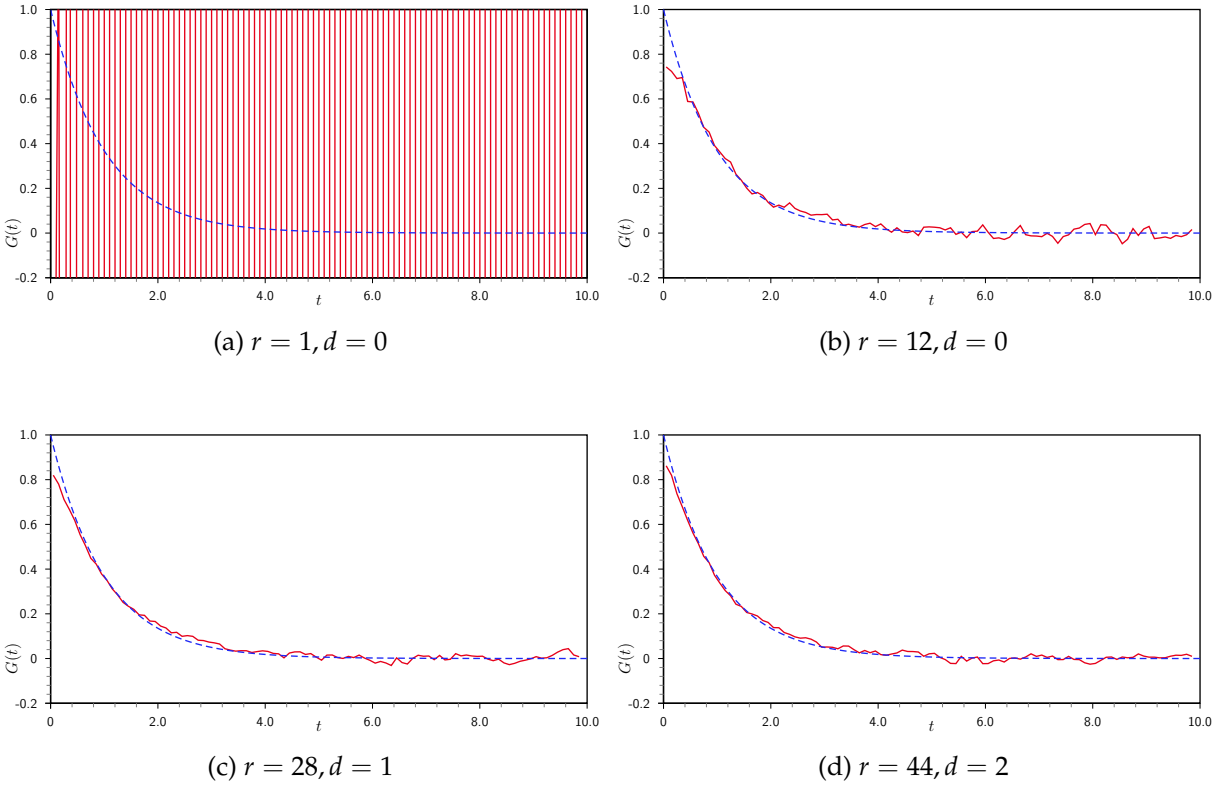

(a) $r = 1, d = 0$

(b) $r = 12, d = 0$

(c) $r = 28, d = 1$

(d) $r = 44, d = 2$

Figure 6.7: Numerical solution: box function, Maxwell model ($\psi < 0$), (1%,5%) error, future-polynomial regularization.

II. CONCLUSION

The main question addressed in this discourse is concerned with the best or 'optimal' choice of function for the applied torque in a controlled stress experiment to determine the linear viscoelastic properties of a material under investigation. A summary of the main results, achievements and limitations of the investigation are now provided, followed by a more in-depth discussion of the conclusions reached. The thesis is mainly concerned with a theoretical study of the equations which govern the behaviour of a stress-controlled rheometer when used to characterize a linear viscoelastic material. The salient feature of the problem is that when the equation is solved to obtain the relaxation modulus, it takes the form of a Volterra integral equation of the first kind, which is known to be ill-posed. The "optimal" applied torque is defined in a theoretical sense as the torque which minimizes the ill-posedness of the problem and thus allows the solution to be obtained in the most stable manner. The smoothing definition of [18] allows quantification of the degree of ill-posedness of the problem, whereby defining certain classes of functions for the applied torque which produce similar degrees of sta-

bility. Under this definition of optimality, the best choice for the applied torque would be a delta function, but since it is arguable whether an actual stress of this form can be reproduced experimentally, the best practical choice would be the box function. The second part of the thesis is concerned with the determination of the relaxation modulus using regularization methods to obtain a stable solution. Two Volterra-specific schemes are implemented - the future-constant predictor corrector method [47] and the future-polynomial version [50], which allow determination of the relaxation modulus almost in real-time and are demonstrated to be capable of obtaining a stable solution for the relaxation modulus even in the presence of noisy data for appropriate choice of the regularization parameter(s). The main advantage is the ability to determine the solution from a single test almost as soon as the data has been measured, with suitable experimental apparatus, and the requirement to wait for transient signals to decay and a steady-state to be attained as for oscillatory tests is no longer necessary.

The governing equations for an experiment carried out using a stress-controlled rheometer, or a strain-controlled rheometer - the same equation is applicable, are expressed most generally in the form of a first-order linear Volterra integro-differential equation of convolution type in the platen angular velocity, $\dot{\chi}(t)$, as given by (4-1). This relates the measured strain (or torque) to the applied torque (or strain) through the relaxation modulus $G(t)$, which fulfills the rôle of the kernel function within the integral equation. However, the function which is desired to be obtained from experiment is the relaxation modulus, thus a different approach is required to solve the equation to yield the required equation. It was noted in Chapter 4 that, due to the commutativity property of the convolution integral, the equation can be rearranged to produce the relaxation modulus as the solution, whereby changing the kernel function to be the platen angular velocity. As a result of this rearrangement, the governing equation takes the form of a Volterra integral equation of the first kind, which is known to be ill-posed in the presence of perturbed data, or even using exact data in extreme cases depending upon the nature of the kernel. Therefore, the solution process to obtain the relaxation modulus, which is an inverse problem, is considerably more problematic than solving the governing equation in its standard form; this would yield the strain or stress in terms of an already known relaxation modulus and is hence of little use for this problem.

Thus, from at least from a theoretical perspective, the optimal form for the applied torque in a controlled-stress experiment can be defined as that which minimizes the degree of ill-posedness of the problem in Volterra-1 form. Well-posedness in the sense

of Hadamard depends on the existence, uniqueness and stability of a solution, and since there exist proofs of the first two criteria, the difficulty lies with obtaining a stable solution in the presence of perturbed or noisy data. This indicates that when the data is perturbed slightly from the true value, the error in the solution may be arbitrarily large. In general, the *modus operandi* for dealing with Volterra integral equations of the first kind is to differentiate a sufficient number of times to transform the problem into a Volterra integral equation of the second kind, which is a well-posed problem and hence the solution depends continuously upon the data. The degree of ill-posedness of a Volterra integral equation of the first kind can be quantified using the definition of a ν-smoothing problem from [18], which essentially is a measure of the degree of differentiation required to convert the problem into one involving a Volterra integral equation of the second kind. If the n-th derivative of the kernel satisfies $K^{(}n)(t - t') = 0$ for $n \geq 0$, then further differentiation is required to obtain a Volterra integral equation of the second kind. Since differentiation is an ill-posed problem, the higher the order of differentiation necessary, the greater the degree of ill-posedness. Thus, the 1-smoothing problem, which corresponds to a step jump in the kernel $\dot{\chi}(t)$ at $t = 0$, is a class of functions for the applied torque which gives rise to the least degree of ill-posedness for the problem. The 2-smoothing problem, corresponding to a step jump in the derivative of the kernel, $\ddot{\chi}(t)$, represents the next least ill-posed class of functions, and so on and so forth. Under this definition, an optimal form for the applied torque would belong to the 1-smoothing class of functions.

It was noted in Section 3.1.1 that when the applied torque takes the form of the derivative of a delta function, the corresponding angular displacement possesses a step discontinuity at $t = 0$ and the resulting equation was shown in Chapter 4.1 to be a Volterra integral equation of the second kind. Hence, from a purely theoretical viewpoint, the optimal form for the applied torque would be the first derivative of the delta function, but since this is a distribution rather than a function and not reproducible physically it must be disallowed as a suitable form for the applied torque. However, in Section 3.1.1 it was demonstrated that a step discontinuity can exist in the first derivative of the platen angular displacement, provided the use of the delta function is allowed; although this also is a distribution, it is often used to represent an impulsive force in physical situations. This corresponds to the 1-smoothing problem for the Volterra-1 equation, for which the delta function as an applied torque is taken to be the canonical example. It was also shown in Section 3.1.1 that higher order derivatives of the angular platen displacement can possess a step discontinuity at $t = 0$ and

can be produced by physical forms for the applied torque which do not involve the use of distributions. The 2-smoothing case corresponds to a step discontinuity in the second derivative of the platen angular displacement at $t = 0$ and requires an applied torque which also has a step discontinuity at the same point in time, the canonical case being taken to be the Heaviside step function, or box function since any experiment must be of finite duration. The 3-smoothing case can be typified by an applied torque in the form of a slope or ramp function, which generates a step discontinuity in the third derivative of the angular platen displacement.

A wide variety of functions can be regarded as suitable for use as an applied torque in a controlled-stress experiment. In Chapter 2, a selection of functions were considered to represent some of the more common, and practical, of the functions as potential candidates. For each of the delta, box and ramp functions, which were taken to be canonical examples of the 1-smoothing to 3-smoothing problems along with the sinusoidal function, the response of a stress-controlled rheometer was simulated through the use of Laplace transform analysis, assuming the material has a known relaxation modulus representing the single or N-mode Maxwell model. Firstly, the delta function was considered as a representative of the class of 1-smoothing problems in Section 2.2. In the case of the Maxwell model, the response is dependent upon the relative values of the material parameters, λ and g, and the instrumental parameter kI. When the instrumental parameter is large relative to the material parameters, the displacement response takes the form of a monotone increasing function which tends to a constant value as t tends to infinity, whereas a relatively small instrumental parameter in comparison to the material parameters will yield an oscillatory response with a monotone decreasing exponential envelope, the exponent of which which can be expressed solely in terms of the relaxation time. This is essentially the free oscillation experiment described in [90, 97], where the attenuated oscillations were used to determine the complex modulus over an appropriate range of frequencies. The extension to a general N-mode Maxwell model results in much the same qualitative behaviour, with exponentially decaying oscillations unless the instrumental parameter is very large. The use of a delta function as an applied torque corresponds to a 1-smoothing problem using the definition of degree of ill-posedness above and is thus represents the optimal choice from a purely theoretical perspective.

An applied torque in the form of a step function, as considered in Section 2.3, results in a response which consists of a linear increase in angular displacement with a transient component superimposed. Since an experiment is of finite duration, the

function will necessarily be in the form of a box function; the torque cut-off can be coincident with the end of the measurement period T, or lie somewhere in the interval $[0, T]$. The transient component is essentially the displacement produced by a delta function to within a multiplicative constant and exhibits the same monotone or oscillatory behaviour in an analogous fashion depending upon the relative values of the instrumental and material parameters. If the cut-off time t_1 occurs before the experimental time T, then decaying or free oscillations are observed, which is essentially the output produced from a delta function located at $t = t_1$. The box function gives rise to a 2-smoothing problem and therefore represents the next best choice from a theoretical point of view after the delta function.

The slope (ramp) function, analyzed in Section 2.4, produces a platen displacement which increases quadratically in time with a transient function superimposed; as for the step function case the nature of this transient depends upon the relative values of the instrumental and material parameters. If the cut-off time t_1 occurs before the end of the experiment at T, free oscillations are observed in a similar fashion to the response to a delta function applied torque. The ramp function corresponds to a 3-smoothing problem and consequently would represent a poor choice of applied torque function. The response to an applied torque in the form of a sinusoidal function was also investigated in Section 2.5.1, but since this also corresponds to a 3-smoothing problem it would be an illogical choice for the applied torque function when performing experiments in the time domain, the considerable advantages of the steady-state assumption in the frequency domain being lost.

The stability analysis in Section 4.3 attempts to derive bounds on the error in the measured data which guarantees that a stable solution exists for the solution of the Volterra integral equation of the first kind in (4-15). The general form for the analysis is adapted from that used in [3], where bounds are derived for which stable interconversion can occur between the relaxation modulus and the creep compliance of a viscoelastic material. The interconversion equation is also a Volterra integral equation of the first kind, although with a fixed data function t rather than the myriad options which can exist for the data function in this problem. The approach taken here makes the assumption that the solution exists and considers the effect of regular perturbations in the measured data. The properties of the convolution integral norms and derivatives of the convolution integrals are then used to establish bounds upon the supremum of the perturbation in the solution for the relaxation modulus in terms of the suprema of the perturbations in the measured platen angular velocity $\dot{\chi}(t)$ and the data function

$f(t)$, which is calculated from the measured data and since it involves differentiation, will be subject to a greater degree of noise than the raw data alone.

The bounds on the maximum permissible error in the measured data, denoted by $\|\phi\|_\infty$ for the platen angular velocity, reflect the measure of ill-posedness under the smoothing definition in that the delta, box and ramp functions form a sequence of increasing ill-posedness. For the delta function, the perturbation in the measured angular velocity of the platen, $\phi(t)$, must satisfy the constraint that $\|\phi\|_1$ must be strictly less than a constant value which is proportional to the value kC_δ and the L_1-norm of the data function, i.e. the absolute integral of the error in the measured data must be sufficiently small. Similar conditions apply to the box function and other 2-smoothing problems, except that the restriction on $\|\phi\|_1$ is slightly tighter. For the 3-smoothing problem concerning the ramp function, the bounds on the supremum of the perturbation in the solution is much less tightly constrained, involving norms of the derivatives of the perturbations in the measured data. These may assume arbitrarily large values in the presence of noisy data and the result will be a large bound on the perturbation in the relaxation modulus solution, manifest in a highly oscillatory solution which may be arbitrarily far from the actual solution. It is also required that the L_1-norm of the derivative of the perturbation in the platen angular velocity $\|\phi\|_1$ satisfies a specified bound, which is unlikely in the presence of noisy data since perturbations in the data are not necessarily differentiable. These results reinforce the conclusion that the best choices for the applied torque function should be those corresponding to 1-smoothing or perhaps 2-smoothing problems such as the delta or box functions, with more ill-posed problems such as that arising from the use of the ramp function as an applied torque being much less desirable in terms of stability of the solution.

The second part of the investigation is concerned with solving the governing equation for the relaxation modulus in Volterra-1 form in real-time, or near real-time, so that the relaxation modulus can be obtained from a completely arbitrary applied torque almost as the strain data is acquired. The direct approach, without the use of any regularization method, is demonstrably inadequate except for the least ill-posed case and even then only with exact data, or at best with small noise levels. The 1-smoothing and 2-smoothing problems can be solved without regularization for exact data, but the 2-smoothing case becomes highly oscillatory in the presence of even small amounts of noise. The discretization method used here is the collocation method, using piecewise constant functions with collocation occurring at each of the grid-points. The collocation method is chosen owing to the simplicity of the implementation and also the

fact that it can easily be combined with regularization methods of predictor-corrector type which are implemented here. It is well known that the higher order quadrature methods such as the trapezoidal, Gregory and Newton-Cotes integration rules are numerically unstable for Volterra-1 problems [28] and therefore represent a poor choice for this problem.

Volterra integral equations of the first kind generally require the use of regularization to obtain a stable solution, as demonstrated in Section 5.3 for the solutions for the relaxation modulus resulting from applied torques in the form of the delta, box and ramp functions and using the collocation discretization method. The condition numbers of the matrix in the resulting linear system of equations generally increases considerably as the number of grid-points and the noise level increases, indicating that the matrix is close to singularity and ill-conditioned. Discretization alone has a regularizing effect, the regularization parameter being the step-size. For less ill-posed problems, increasing the step-size can often result in a stable solution, however as the degree of ill-posedness increases, this method becomes increasingly ineffective and sufficient stabilization may result in an unacceptably coarse grid. The 1-smoothing problem associated with the delta function applied torque can be regularized by this method even in the presence of moderately noisy data, but for the 2-smoothing box function applied torque a stable solution cannot be obtained for similar noise levels while maintaining a suitably fine grid. A more sophisticated regularization method is required to obtain a stable solution for the relaxation modulus from a stress-controlled experiment.

The range of regularization methods available for this problem was discussed in Section 5.2 and although Tikhonov regularization is considered the standard approach for many inverse problems, the most appropriate are those which preserve the causal property of the Volterra integral, i.e. the solution at any point in time t depends only upon the time which has already elapsed in $[0, t]$. This property allows the solution to be obtained in real-time or nearly so, rather than waiting for the data on the whole domain to be collated before processing can begin. The two regularization methods chosen as examples for this problem, the future-constant method [47] and the future-polynomial method [18], are examples of predictor-corrector regularization methods. These two were chosen for the reasons that firstly, the methods are of Volterra type and therefore preserve the causal nature of the Volterra integral equation such that the data at the current time depends only on the data already collected and consequently allow solution in near real-time. Secondly, the simplicity of the numerical implementation

allows fast and efficient data processing which could in theory be carried out by a suitably equipped rheometer.

The future-constant regularization method [47] as described in Section 5.3 obtains a stable solution at time $t \in [0, T]$ by holding the solution constant on a small future interval $[t, t + \Delta_r]$. The resulting equation under this assumption is a Volterra integral equation of the second kind, which is stable with respect to perturbations in the data. Once the solution has been obtained, i.e. the "predictor" step, the solution is discarded on the future interval to leave the solution at the time t by a "corrector" step. The regularization parameter is the length of the future interval r and controls the balance between data resolution and smoothing. The future-constant method was applied to the solution for the relaxation modulus using the delta, box and ramp functions for the applied torque in Section 5.3.1,Section 5.3.2 and Section 5.3.3, respectively, ranging from the use of exact data to high levels of noise in the simulated data. In all cases, the regularization method was found to result in a decrease in the condition number of the matrix arising from the discretization of the Volterra-1 equation, corresponding to an increase in stability of the solution and a less ill-conditioned matrix system of equations. It was noted that the higher the value for the condition number in the absence of regularization, the greater the reduction observed under the application of the future-constant method. The best results were obtained using the delta function applied torque, which is to be expected since the 1-smoothing problem represents the least ill-posed option, corresponding to the smallest value for the regularization parameter. However, reasonable results were shown to be obtainable even for the applied torque functions giving rise to the more ill-posed problems, provided a sufficiently large value for the regularization parameter is selected. One particular problem was noted with the use of this regularization method concerning the degree of smoothing attainable, particular for the more ill-posed cases. The regularization parameter must be chosen carefully to ensure a compromise between suppression of the spurious oscillations which arises from the ill-posedness of the problem and over-smoothing which results from excessive flattening of the curve when too large a value for the regularization parameter is chosen. The solution near $t = 0$ suffers in particular, although in general a larger value for the regularization parameters provides a better approximation for the flatter part of the solution curve at longer timescales.

The future-polynomial regularization method [18] is essentially a generalization of the future-constant method; instead of the solution being held constant on the small future interval, it is assumed to take the form of a polynomial of degree d on that

interval, giving rise to an extra regularization parameter which controls the degree of the polynomial utilized. A comparison was made in Section 5-42 between solutions obtained using simple collocation ($d = 0$), the future-constant method ($d = 1$) and the future-polynomial method with $d = 1$ and $d = 2$. It was demonstrated that better results are obtainable using the future-polynomial method with $d = 1$ and even more so with $d = 2$ than the future-constant method, although generally the higher the value for d, the longer the future interval that is required to obtain the optimal solution . The results are "better" in the sense that the solution near $t = 0$ suffers less from over-smoothing and hence flattening of the curve in this region. More than acceptable results were obtained using the future-polynomial method with $d = 2$ even in the most ill-posed case considered - the 3-smoothing ramp function.

Finally, the matters pertaining to the design of an experimental investigation were discussed in Section 6.1 using the results of the preceding chapters. Assuming the availability of a rheometer which is capable of applying a completely arbitrary torque chosen by the experimenter, discretized using a chosen sampling rate or time-step, the steps concerning the choice of applied torque and subsequent treatment of the acquired data were discussed. The fundamental choice of the optimal applied torque is defined using the smoothing definition of Definition 4.2.1 combined with the stability analysis in Section 4.3. The delta function would be the optimal choice for the applied torque, but due to the problems concerning experimental reproduction of such a function, the most appropriate function representing the next best choice would be the box function, although any applied torque corresponding to a 2-smoothing problem would share the same basic advantages. A further option where the box functions is concerned is the choice of the cut-off time, following which the torque becomes zero. The basic options are to choose the cut-off time to coincide with the experimental time, so that only forced platen displacements are measured, or at an intermediate time in $[0, T)$ whereby a mixture of forced and free platen displacements are observed. A simple empirical experiment using simulated data suggested that the most accurate and stable solution for the relaxation modulus occurs when the cut-off time is chosen such that free oscillations are permitted to occur before measurement ceases. A very short cut-off time provides good stability and is desirable in a theoretical sense, but when the diminutive platen displacements which result for much of the latter parts of the experiment are considered, it is clear that such measurements will be contaminated with significant noise. For materials with a very wide distribution of relaxation times it was suggested that it may be worthwhile to apply a sequence of box functions for

the torque, allowing the free oscillations to decay after each discrete box function.

A further consideration for the experimental setup was noted concerning the choice of the instrumental parameters such as the inertia of the rotating assembly, platen separation and platen radius. It was noted in Section 2.2.2 and later in that section that these parameters determine whether the platen displacement exhibits oscillations or a monotone increasing function. The experiments with simulated data in Section 6.1.3 suggest that the case where oscillations occur is more stable than the case where the platen displacement is monotone increasing, inferred from the relative condition numbers for the discretized system and the greater values for the regularization parameters required to obtain a stable solution using the future-constant and future-polynomial regularization methods.

6.2.1 Future Work

A number of areas of the research would benefit from further attention. First and foremost, an extensive experimental investigation of the theoretical techniques presented here would be worthwhile to refine the experimental procedure for obtaining the relaxation modulus using the results and techniques presented in this thesis. Only the theoretical framework has been investigated here, although initial experiments in [8] using the "Torque Table" software showed reasonable agreement between simulated and experimental results for the 2-mode Maxwell model representation of the A1 fluid. A lengthy and in-depth investigation would be required, the time for which was not available during the research period.

The potential use of adaptive torque profiles may be of some interest, should an optimal form be defined in terms of the material parameters. The feasibility of obtaining the relaxation modulus directly as the platen angular velocity was alluded to in Theorem 3.1.2, but a theoretical justification would be required to verify whether this is optimal. Such a result would require an iterative technique to obtain the desired output. Alternatively, since the solution can be obtained almost in real-time using the methods outlined here, the torque signal could be modified for the remainder of the experiment using the data already obtained up to the current time to improve the accuracy of the subsequent data.

The stability analysis in Section 4.3 was performed for the canonical cases within each ν-smoothing class of applied torque functions. It may be desirable to carry out the analysis for other functions within the 2-smoothing group of functions, should certain functions within the classification exhibit a slight advantage in terms of stability. A

particular example would be the sinc function, which is currently being considered as a candidate for the optimal choice of applied torque [58].

Enhancements to the governing equations would also provide a useful line of investigation. Primarily, the incorporation of fluid inertia into the analysis may provide greater insight into the stability of the solution, although it is only likely to prove significant for very low viscosity fluids or applied torques involving very rapid displacement gradients. A method for determination of the optimal value for the regularization parameter would also be desirable, to minimize the degree of human intervention involved in the solution process.

APPENDICES

APPENDIX A

Miscellaneous Identities

I. LAPLACE TRANSFORM IDENTITIES

Properties and identities for the Laplace transform which are made use of in the main text. Sources of information: [70, 88, 100, 87, 94].

The Laplace transform is defined by

$$\bar{f}(s) = \int_0^\infty f(t)\, \mathrm{e}^{-st}\, \mathrm{d}t \tag{A-1}$$

when the integral exists. The Laplace transform variable is in general complex; the Fourier transform can be obtained when the transform variable is pure imaginary.

1. **Differentiation**: The Laplace transform of the derivative of a function is obtained by

$$\mathscr{L}\left\{\frac{\mathrm{d}f}{\mathrm{d}t}\right\} = s\bar{f}(s) - f(0) \tag{A-2}$$

The latter term is required for functions which are discontinuous at $t = 0$, but the limit $\lim_{t\to 0} f(t) = f(0)$ exists. The second-order derivative is given by

$$\mathscr{L}\left\{\frac{\mathrm{d}^2 f}{\mathrm{d}t^2}\right\} = s^2\bar{f}(s) - sf(0) - f'(0) \tag{A-3}$$

and the general identity is

$$\mathscr{L}\left\{\frac{\mathrm{d}^n f}{\mathrm{d}t^n}\right\} = s^n\bar{f}(s) - \sum_{i=1}^{n-1} s^{n+i-1} f^{(i)}(0) \tag{A-4}$$

2. **Convolution**: Convolution in the time domain corresponds to multiplication in Laplace space. Two versions exist due to commutativity of the convolution integral which can be shown by a simple change of variable.

$$\mathscr{L}\left\{\int_0^t f(t-t')g(t')\,\mathrm{d}t'\right\} = \bar{f}(s)\bar{g}(s) \tag{A-5}$$

$$\mathscr{L}\left\{\int_0^t f(t')g(t-t')\,\mathrm{d}t'\right\} = \bar{f}(s)\bar{g}(s) \tag{A-6}$$

3. **Real integration**: The Laplace transform of the integral of a function on $[0, t]$ is determined by dividing the Laplace transform by the transform variable, s. Higher order integrals are obtained by successive division by the transform variable.

$$\mathscr{L}\left\{\int_0^t f(t)\,\mathrm{d}t\right\} = \frac{\bar{f}(s)}{s} \tag{A-7}$$

4. **Initial value theorem**: If the limit exists, the initial value theorem states that

$$\lim_{t\to 0} f(t) = \lim_{s\to\infty} \bar{f}(s). \tag{A-8}$$

5. **Final value theorem**: The final value theorem states that

$$\lim_{t\to\infty} f(t) = \lim_{s\to 0} \bar{f}(s) \tag{A-9}$$

if the limit exists.

6. **Shift theorems**: Translation of a function by an amount a in t-space corresponds to multiplication by e^{-as} in Laplace space. If $a \in \mathbb{R}$, then

$$\mathscr{L}\left\{f(t-a)H(t-a)\right\} = \bar{f}(s)\,\mathrm{e}^{-as} \tag{A-10}$$

and conversely, if the function is shifted in Laplace space, this corresponds in the time domain to

$$\bar{f}(s+a) = \mathscr{L}\left\{f(t)\,\mathrm{e}^{-at}\right\}. \tag{A-11}$$

A combination of a shift of amount a and multiplication by the Heaviside step function located at $t = b$ results in a more general expression In the case where $b \neq a$, then we have

$$\mathscr{L}\left\{f(t-a)H(t-b)\right\} = \mathrm{e}^{-as}\mathscr{L}\left\{f(t)H(t-(b-a))\right\}. \tag{A-12}$$

This is derived as follows

$$\begin{aligned}
\mathscr{L}\left\{f(t-a)H(t-b)\right\} &= \int_0^\infty f(t-a)\,\mathrm{e}^{-st}H(t-b)\,\mathrm{d}t \\
&= \int_b^\infty f(t-a)\,\mathrm{e}^{-st}\,\mathrm{d}t \\
&= \int_{b-a}^\infty f(u)\,\mathrm{e}^{-s(u+a)}\,\mathrm{d}t \\
&= \mathrm{e}^{-as}\int_0^\infty f(u)H(u-c)\,\mathrm{e}^{-us}\,\mathrm{d}u, \quad c = b-a \\
&= \mathrm{e}^{-as}\mathscr{L}\left\{f(t)H(t-c)\right\}
\end{aligned} \tag{A-13}$$

If $b = a$, this result reduces to (A-10), as expected.

7. **Periodicity theorem**: If a function $f_r(t)$ is repeated n times, where $f_r(t)$ is known as the *repeat* function, so that

$$f(t) = \sum_{j=0}^{n} f(t - jT)H(t - jT) \tag{A-14}$$

where T is the period, then the Laplace transform of $f(t)$ is

$$\bar{f}(s) = \bar{f}_r(s) \sum_{j=1}^{n} \mathrm{e}^{-nTs} \tag{A-15}$$

where

$$\bar{f}_r(s) = \int_0^T f(t)\,\mathrm{e}^{-st}\,\mathrm{d}t \tag{A-16}$$

If $n \to \infty$, then it can be shown that

$$\bar{f}(s) = \frac{\bar{f}_r(s)}{1 - \mathrm{e}^{-Ts}} \tag{A-17}$$

II. CONVOLUTION IDENTITIES

Identities used in the main text for the convolution integrals defined

$$f * g = \int_0^t f(t - t')g(t')\,\mathrm{d}t' = \int_0^t f(t')g(t') \tag{A-18}$$

and

$$f * g * h = \int_0^t f(t - t') \int_0^{t'} g(t' - t'')h(t'')\,\mathrm{d}t''\,\mathrm{d}t' \tag{A-19}$$

1. **Differentiation**: Differentiation of the convolution integral gives rise to the two forms

$$\begin{aligned} \frac{\mathrm{d}}{\mathrm{d}t}[f * g] &= f(0)g(t) + \dot{f} * g \\ &= g(0)f(t) + f * \dot{g} \end{aligned} \tag{A-20}$$

and for second-order differentiation

$$\frac{\mathrm{d}^2}{\mathrm{d}t^2}[f * g] = g(0)\frac{\mathrm{d}f}{\mathrm{d}t} + f(0)\frac{\mathrm{d}g}{\mathrm{d}t} + \dot{f} * \dot{g}. \tag{A-21}$$

The corresponding results for the triple convolution are

$$\frac{\mathrm{d}}{\mathrm{d}t}[f * g * h] = f(0)g * h + \dot{f} * g * h \tag{A-22}$$

and

$$\frac{\mathrm{d}^2}{\mathrm{d}t^2}[f * g * h] = f(0)g(0)h(t) + f(0)\dot{g} * h + g(0)\dot{f} * h + \dot{f} * \dot{g} * h \tag{A-23}$$

2. **Young's inequality**: Special case of Young's inequality for L_p norms [105]

$$\|f * g\|_r \leq \|f\|_p \|g\|_q \tag{A-24}$$

where

$$p^{-1} + q^{-1} = r^{-1} + 1 \tag{A-25}$$

Relatively loose bound, can be sharpened to

$$\|f * g\|_r \leq c_{p,q} \|f\|_p \|g\|_q \tag{A-26}$$

where the constant $c_{p,q} \leq 1$.
In the case where $p = 1$ and $q = \infty$, this gives rise to the identity

$$|f * g| \leq \beta \|f\|_1 \|g\|_\infty \tag{A-27}$$

where $0 < \beta \leq 1$, and for the triple convolution

$$|f * g * h| \leq \beta \|f\|_1 \|g\|_1 \|h\|_\infty. \tag{A-28}$$

APPENDIX B

Simulated Data

I. RELAXATION SPECTRUM

Bimodal log-normal relaxation spectrum [36] used in simulation.

Table B-1: Bimodal log-normal relaxation spectrum data.

i	g_i	λ_i	i	g_i	λ_i
1	0.0000947709	0.0010000000	51	0.0378212257	0.3351602651
2	0.0001483595	0.0011233240	52	0.0330278509	0.3764935807
3	0.0002291302	0.0012618569	53	0.0298559330	0.4229242874
4	0.0003491210	0.0014174742	54	0.0283173115	0.4750810162
5	0.0005248028	0.0015922828	55	0.0284162421	0.5336699231
6	0.0007782928	0.0017886495	56	0.0301524810	0.5994842503
7	0.0011387190	0.0020092330	57	0.0335210833	0.6734150658
8	0.0016436780	0.0022570197	58	0.0385089377	0.7564633276
9	0.0023406884	0.0025353645	59	0.0450884225	0.8497534359
10	0.0032884945	0.0028480359	60	0.0532089062	0.9545484567
11	0.0045580311	0.0031992671	61	0.0627870991	1.0722672220
12	0.0062328132	0.0035938137	62	0.0736974721	1.2045035400
13	0.0084084819	0.0040370173	63	0.0857640652	1.3530477750
14	0.0111912277	0.0045348785	64	0.0987549887	1.5199110830
15	0.0146948289	0.0050941380	65	0.1123807739	1.7073526470
16	0.0190361005	0.0057223677	66	0.1262974380	1.9179102620
17	0.0243286553	0.0064280731	67	0.1401147226	2.1544346900
18	0.0306750216	0.0072208090	68	0.1534094658	2.4201282650
19	0.0381573591	0.0081113083	69	0.1657435214	2.7185882430
20	0.0468272225	0.0091116276	70	0.1766851149	3.0538555090
21	0.0566950506	0.0102353102	71	0.1858320724	3.4304692860
22	0.0677202504	0.0114975700	72	0.1928350518	3.8535285940
23	0.0798028912	0.0129154967	73	0.1974187738	4.3287612810
24	0.0927780754	0.0145082878	74	0.1993993454	4.8626015800

Continued on next page

i	g_i	λ_i	i	g_i	λ_i
25	0.1064139984	0.0162975084	75	0.1986960638	5.4622772180
26	0.1204145148	0.0183073828	76	0.1953365731	6.1359072730
27	0.1344267216	0.0205651231	77	0.1894548624	6.8926121040
28	0.1480536384	0.0231012970	78	0.1812822686	7.7426368270
29	0.1608715738	0.0259502421	79	0.1711322969	8.6974900260
30	0.1724512508	0.0291505306	80	0.1593806289	9.7700995730
31	0.1823813006	0.0327454916	81	0.1464420824	10.9749876500
32	0.1902923707	0.0367837977	82	0.1327464752	12.3284673900
33	0.1958798997	0.0413201240	83	0.1187153308	13.8488637100
34	0.1989236150	0.0464158883	84	0.1047411418	15.5567614400
35	0.1993020284	0.0521400829	85	0.0911705289	17.4752840000
36	0.1970006197	0.0585702082	86	0.0782921669	19.6304065000
37	0.1921129690	0.0657933225	87	0.0663298195	22.0513074000
38	0.1848347566	0.0739072203	88	0.0554403520	24.7707635600
39	0.1754512214	0.0830217568	89	0.0457161661	27.8255940200
40	0.1643192730	0.0932603347	90	0.0371912079	31.2571585000
41	0.1518459123	0.1047615753	91	0.0298495251	35.1119173400
42	0.1384648964	0.1176811952	92	0.0236353057	39.4420605900
43	0.1246136406	0.1321941148	93	0.0184634001	44.3062145800
44	0.1107122018	0.1484968262	94	0.0142294723	49.7702356400
45	0.0971458605	0.1668100537	95	0.0108191357	55.9081018300
46	0.0842523478	0.1873817423	96	0.0081156442	62.8029144200
47	0.0723142410	0.2104904145	97	0.0060059275	70.5480231100
48	0.0615565005	0.2364489413	98	0.0043849418	79.2482898400
49	0.0521486380	0.2656087783	99	0.0031584517	89.0215085400
50	0.0442106055	0.2983647240	100	0.0022444570	100.0000000000

List of Symbols

Greek Letters

$\chi(t)$	Angular displacement of the rheometer platen
δ	Phase angle in small amplitude oscillatory shear
$\delta(t)$	Delta function
δ_{ik}	Kronecker delta: takes the value 0 for $i \neq k$ and unity for $i = k$
η	Viscosity
$\eta'(\omega)$	Dynamic viscosity
η_i	Viscosity of the i-th mode of the generalized Maxwell model, $i = 1, \ldots, N$
$\eta^*(\omega)$	Complex viscosity
$\varepsilon(t)$	Perturbation in the data function $f(t)$
$\gamma(t)$	Perturbation in the relaxation modulus $G(t)$
$\Omega(t)$	Angular velocity of rheometer platen, $\Omega(t) = \dot{\chi}(t)$
$\phi(t)$	Perturbation in the platen angular velocity $\Omega(t)$
ρ	Density
$\gamma(t)$	Strain, measure of displacement
γ_0	Strain amplitude
$\dot{\gamma}(t)$	Strain-rate or shear-rate
$\dot{\gamma}_e(t)$	Strain-rate of the elastic component (spring) of a spring-dashpot model representation
$\dot{\gamma}_v(t)$	Strain-rate of the viscous component (dashpot) of a spring-dashpot model representation

σ_0	Stress amplitude
$\sigma_e(t)$	Stress contribution of the elastic component (spring) of a spring-dashpot model representation
$\sigma_v(t)$	Stress contribution of the viscous component (dashpot) of a spring-dashpot model representation
$\sigma_{xy}(t)$	Shear stress
ω	Angular frequency, $[\text{rad } s^{-1}]$
λ_{exp}	Characteristic experimental time, see equation (1-22), page 21
λ_{mat}	Characteristic material time, see equation (1-22), page 21
λ	Relaxation time
λ_i	Relaxation time of the i-th mode of the generalized Maxwell model, $i = 1, \ldots, N$
τ	Retardation time
Ψ	Period of periodic applied torque
ψ	Discriminant term for Maxwell model, see equation (2-71), page 52

Roman Letters

a	Platen radius
$A^{(k)}$	Rivlin-Ericksen tensors, $k = 1, 2, \ldots$
$C(t)$	Applied torque on a stress controlled rheometer
$C_f(t)$	Torque exerted on the rheometer platen by the fluid
d	Damping coefficient of rheometer
D_e	Deborah number, see equation (1-22), page 21
g	Rigidity modulus of an elastic material
$G''(\omega)$	Loss modulus

$G'(\omega)$	Storage modulus
$G(t)$	Relaxation modulus, see equation (1-34), page 27
G_0	Glassy modulus, $\lim_{t\to 0} G(t)$
G_∞	Equilibrium modulus, $\lim_{t\to \infty} G(t)$
g_i	Elastic modulus of the i-th mode of the generalized Maxwell model, $i = 1, \ldots, N$
h	Platen separation
$H(\lambda)$	Relaxation spectrum (or distribution of relaxation times)
$H(t - t_0)$	The Heaviside step function located at $t = t_0$
I	Moment of inertia of rotating rheometer assembly
J	Spring compliance in a spring-dashpot model representation
$J''(\omega)$	Loss compliance
$J'(\omega)$	Storage compliance
$J(t)$	Creep compliance, see equation (1-37), page 28
J_0	Instantaneous or glassy compliance
J_∞	Equilibrium compliance
J_i	Compliance of the i-th mode of the generalized Kelvin-Voigt model
k	Instrumental parameter
$L(\tau)$	Retardation spectrum (or distribution of retardation times)
M	Number of modes in the generalized Kelvin-Voigt model
$M(t)$	Memory function
N	Number of elements in the generalized Maxwell model
$N_1(\dot{\gamma})$	First normal stress difference
$N_2(\dot{\gamma})$	Second normal stress difference

p	Isotropic pressure
s	Time lag, $s = t - t'$
T	Experimental time, $0 < T < \infty$
t	Present time
t'	Running time variable
T_{ik}	Extra-stress tensor (or $\boldsymbol{T}$)
$\boldsymbol{C}(\boldsymbol{x}, t, t')$	Cauchy-Green strain tensor
C_δ	Amplitude or 'area' of a delta-function applied torque
$\boldsymbol{D}$	Rate of strain tensor
d	Regularization parameter (polynomial degree)
$\boldsymbol{F}(\boldsymbol{x}, t, t')$	Deformation gradient tensor
$G^*(\omega)$	Complex modulus
$\boldsymbol{G}(\boldsymbol{x}, t, t')$	relative finite strain tensor
$\boldsymbol{I}$	Identity tensor
$J^*(\omega)$	Complex compliance
$\boldsymbol{L}$	Velocity gradient tensor
R	Number of grid-points in discretization
r	Regularization parameter (length of future interval)
s	Laplace transform variable
T	Experimental cut-off time
$\boldsymbol{T}$	Extra stress tensor

Operators

$\frac{\mathrm{D}}{\mathrm{D}t}$	Material derivative

$*$	Convolution integral on $[0, T]$
$\mathscr{F}$	Fourier transform operator
$\mathscr{L}$	Laplace transform operator
$\|\cdot\|_1$	L_1-norm, see equation (4-23), page 112
$\|\cdot\|_\infty$	L_∞-norm

Accents

$\dot{f}$	First derivative
$\ddot{f}$	Second derivative
$\hat{f}$	Fourier transform
$\bar{f}$	Laplace transform

Bibliography

[1] S. Ahn, U.J. Choi, and A.G. Ramm. A scheme for stable numerical differentiation. *Journal of Computational and Applied Maths*, 186:325–334, 2006.

[2] R.S. Anderssen, A.R. Davies, and F. de Hoog. On the Volterra integral equation relating creep and relaxation. Technical report, CMIS, March 2006.

[3] R.S. Anderssen, A.R. Davies, and F. de Hoog. On the sensitivity of interconversion between relaxation and creep. *Rheologica Acta*, 2007.

[4] C. Andrade, N. Franco, and S. McKee. Convergence of linear multistep methods for Volterra first kind integral equations with $k(t,t) \equiv 0$. *Computing*, 27:189–204, 1981.

[5] C. Andrade, N. Franco, and S. McKee. *The solution of Volterra integral equations of the first kind in the presence of large uncertainties*. Academic Press, 1982.

[6] G. Astarita and G. Marucci. *Principles of non-Newtonian Fluid Mechanics*. McGraw-Hill, 1974.

[7] C.T.H. Baker. A perspective on the numerical treatment of Volterra equations. *Journal of Computational and Applied Mathematics*, 125:217–249, 2000.

[8] D.M. Banaszek. Obtaining complex viscosity data from a continuous frequency sweep. Master's thesis, University of Wales, Aberystwyth, 2003.

[9] H.A. Barnes, J.F. Hutton, and K. Walters. *An Introduction to Rheology*. Elsevier, 1989.

[10] J.V. Beck, B. Blackwell, and J.C.R. St. Clair. *Inverse Heat Conduction*. Wiley-Interscience, 1985.

[11] B. Bernstein, E.A. Kearsley, and L.J. Zapas. A study of stress relaxation with finite strain. *Trans. Soc. Rheol.*, 7:391–410, 1963.

[12] D.M Binding and P.M. Phillips. Real-time determination of the gelling characteristics of time-dependent fluids. Technical report, 2007.

[13] R.B. Bird, R.L. Armstrong, and O. Hassager. *Dynamics of Polymeric Liquids*. Oxford University Press, 1986.

[14] D.R. Bland. *The theory of linear viscoelasticity*. Pergamon Press, 1960.

[15] L. Boltzmann. Zur theorie der elastischen nachwirkung. *Ann. Phys. Chem.*, 7: 624–654, 1876.

[16] H. Brunner and P.J. van der Houwen. *The numerical solution of Volterra equations*. CWI, 1986.

[17] A.L. Bughgeim. *Volterra Equations and Inverse Problems*. VSP, 1999.

[18] A.C. Cinzori and P.K. Lamm. Future polynomial regularization of ill-posed Volterra equations. *SIAM J. Numerical Analysis*, 37:949–979, 2000.

[19] B.D. Coleman and W. Noll. Foundations of linear viscoelasticity. *Rev. Mod. Phys.*, 33:239–249, 1961.

[20] A.A. Collyer and D.W. Clegg, editors. *Rheological Measurement*. Chapman & Hall, 1998.

[21] A.R. Davies and R.S. Anderssen. Sampling localization in determining the relaxation spectrum. *J. Non-Newtonian Fluid Mech.*, 73:163–179, 1997.

[22] J.M. Davies and T.E.R. Jones. Complex viscosity predictions for the S1 fluid using harmonic analysis on applied non-sinusoidal stress waveforms. *Journal of Non-Newtonian Fluid Mechanics*, 52:177–182, 1994.

[23] P.P.B. Eggermont. Collocation for Volterra integral equations of the first kind with iterated kernel. *SIAM J. Numer. Anal.*, 20:1032–1048, 1983.

[24] H.W. Engl and C.W. Groetsch, editors. *Inverse and Ill-Posed Problems*. Academic Press, 1987.

[25] H.W. Engl, M. Hanke, and A. Neubauer. *Regularization of Inverse Problems*. Kluwer, 1996.

[26] F. Fagnani and L. Pandolfi. A recursive algorithm for the approximate solution of Volterra integral equations of the first kind of convolution type. *Inverse Problems*, 19:23–47, 2003.

[27] J.D. Ferry. *Viscoelastic Properties of Polymers*. John Wiley & Sons, 1980.

[28] C.J. Gladwin and R. Jeltsch. Stability of quadrature rule methods for first kind Volterra integral equations. *Nordisk Tidskr. Informationsbehandling (BIT)*, 14:144–151, 1974.

[29] K. Golden and J.M. Davies. Complex viscosity data obtained from a continuous frequency sweep. In *Proc. 6th Euro. Conf. Rheology*, 2002.

[30] G.H. Golub and C.F. van Loan. *Matrix Computations*. John Hopkins, 1996.

[31] C.W. Groetsch. *The theory of Tikhonov regularization for Fredholm equations of the first kind*. Pitman, 1984.

[32] C.W. Groetsch. *Inverse Problems in the Mathematical Sciences*. Vieweg Verlag, 1993.

[33] B. Gross. *Theories of Viscoelasticity*. Hermann, 1953.

[34] J. Hadamard. Sur les problèmes aux dérivées partielles et leur signification physique. *Princeton University Bulletin*, 1902.

[35] E.E. Holly, S.K. Venketaraman, F. Chambon, and H.H. Winter. Fourier transform mechanical spectroscopy of viscoelastic materials with transient structure. *Journal of Non-Newtonian Fluid Mechanics*, 27:17–26, 1988.

[36] J. Honerkamp and J. Weese. Determination of the relaxation spectrum by a regularization method. *Macromolecules*, 22:4372–4377, 1989.

[37] R. Hooke. *Of Explaining the Power of Springing Bodies*. London, 1678.

[38] I.L. Hopkins and R.W. Hamming. On creep and relaxation. *Journal of Applied Physics*, 28:906–909, 1957.

[39] S.L. Huang. *Some Open Problems in Rheology*. PhD thesis, University of Wales, Aberystwyth, 2005.

[40] Ram P. Kanwal. *Linear integral equations*. Academic Press, 1971.

[41] Ram P. Kanwal. *Generalized Functions: Theory and Technique*. Academic Press, 1983.

[42] A. Kaye. Non-Newtonian flow in incompressible fluids. Technical Report 134, College of Aeronautics, Cranfield, U.K., 1963.

[43] W.F. Knoff and I.L. Hopkins. An improved numerical interconversion for creep compliance and relaxation modulus. *Journal of Applied Polymer Science*, 16:2963–2972, 1972.

[44] P.K. Lamm. Future-sequential regularization methods for ill-posed Volterra equations. *J. Math. Analysis Applic.*, 195:469–494, 1995.

[45] P.K. Lamm. On the local regularization of inverse problems of Volterra type. In *Proc. 1995 ASME Design Engineering Technical Conferences: Parameter Identification Symposium, Sept. 1995, Boston, MA*, 1995.

[46] P.K. Lamm. Approximation of ill-posed Volterra problems via predictor-corrector regularization methods. *SIAM J. Applied Math.*, 56:524–541, 1996.

[47] P.K. Lamm. Regularized inversion of finitely smoothing Volterra operators. *Inverse Problems*, 13:375–402, 1997.

[48] P.K. Lamm. *Inverse Problems in Geophysical Applications*, chapter Solution of ill-posed Volterra equations via variable-smoothing Tikhonov regularization, pages 92–108. SIAM, 1997.

[49] P.K. Lamm. *Theory and Practice of Control and Systems*, chapter Variable-smoothing regularization methods for inverse problems, pages 331–336. World Scientific, 1998.

[50] P.K. Lamm. *Surveys on Solution Methods for Inverse Problems*, chapter A survey of regularization methods for first-kind Volterra equations, pages 53–82. Springer, 2000.

[51] P.K. Lamm. Some recent developments and open problems in solution methods for mathematical inverse problems. In *Proceedings, XXIV National Congress of Applied and Computational Mathematics, Belo Hrizonte, Brazil, Sept. 2001*, 2001.

[52] P.K. Lamm. Some recent developments and open problems in solution methods for mathematical inverse problems. In *Proc. 6th Euro. Conf. Rheology*, 2002.

[53] P.K. Lamm. Variable-smoothing local regularization methods for first-kind integral equations. *Inverse Problems*, 19:195–216, 2003.

[54] P.K. Lamm. Full convergence of sequential local regularization methods for Volterra inverse problems. *Inverse Problems*, 21:785–803, 2005.

[55] P.K. Lamm and L. Eldén. Numerical solution of first-kind Volterra equations by sequential Tikhonov regularization. *SIAM Journal of Numerical Analysis*, 34: 1432–1450, 1997.

[56] P.K. Lamm and T.L. Scofield. Local regularization methods for the stabilization of linear ill-posed equations of Volterra type. *Numerical Functional Analysis and Optimization*, 22:913–940, 2001.

[57] M.M. Lavrent'ev, V.G. Romanov, and S.P. Shishatskii. *Ill-posed problems of mathematical physics and analysis*. American Mathematical Society, 1986.

[58] A.Y. Malkin. On the optimal form of a signal in Fourier Transform Mechanical Spectroscopy. *Rheologica Acta*, 43(1):1–5, 2004.

[59] A.Y. Malkin, V.P. Beghishev, and V.A. Mansurov. A method of non-harmonic oscillations for measuring dynamic characteristics of polymeric materials. *Vysokomol Soedin*, 26A:869–878, 1984.

[60] G. Marin, J. Peyrelasse, and Ph. Monge. A new method for evaluating the dynamic properties of polymers: time domain mechanical spectroscopy. *Rheologica Acta*, 22:476–481, 1983.

[61] J.C. Maxwell. On the dynamical theory of gases. *Philosophical Transactions of the Royal Society of London*, A157:49–88, 1867.

[62] D.W. Mead. Numerical interconversion of linear viscoelastic material functions. *Journal of Rheology*, 38:1769–1795, 1994.

[63] O.E. Meyer. *Pogg. Ann. Physik*, 151:108, 1874.

[64] Richard K. Miller. *Non-linear Volterra Integral Equations*. W.A. Benjamin, 1971.

[65] I. Newton. *Philosophiae Naturalis Principia Mathematica*. Cambridge University Press, 1934.

[66] A. Nikonov, A.R. Davies, and I. Emri. The determination of creep and relaxation functions from a single experiment. *Journal of Rheology*, 49:1193–1211, 2005.

[67] J.G. Oldroyd, D.J. Strawbridge, and B.A. Toms. A coaxial-cylinder elastoviscometer. *Proc. Phys. Soc., B*, 1951.

[68] R.G. Owens and T.N. Phillips. *Computational Rheology*. Imperial College Press, 2002.

[69] A.C. Pipkin. *Lectures on viscoelasticity theory*. Springer-Verlag, 2nd edition, 1986.

[70] H.A. Priestley. *Introduction to Complex Analysis*. Oxford University Press, 2nd edition, 2003.

[71] A. Ralston and P. Rabinowitz. *A First Course in Numerical Analysis*. McGraw-Hill, 2nd edition, 1978.

[72] A.G. Ramm and A. Galstian. On deconvolution methods. *International Journal of Engineering Science*, 41:31–43, 2003.

[73] A.G. Ramm and A.B. Smirnova. On stable numerical differentiation. *Mathematics of Computation*, 70(235):1131–1153, 2001.

[74] A.G. Ramm and A.B. Smirnova. Stable numerical differentiation: When is it possible? *SIAM*, 7(N1):47–61, 2005.

[75] A.G. Ramm and A.B. Smirnova. On deconvolution problems: numerical aspects. *Journal of Computational and Applied Mathematics*, 176:445–460, 2005.

[76] M. Reiner. The Deborah number. *Physics Today*, 17:62, 1964.

[77] M. Reiner. A mathematical theory of dilatency. *Am. J. Math.*, 67:1945, 350-362.

[78] W. Ring and J. Prix. Sequential predictor-corrector methods and their limitations. *Inverse Problems*, 16:619–633, 2000.

[79] R.S. Rivlin. The hydrodynamics of non-Newtonian fluids, part 1. *Proc. Roy. Soc.*, A193:260–281, 1948.

[80] R.S. Rivlin and J.L. Ericksen. Stress deformation relations for isotropic materials. *J. Rat. Mech. Anal.*, 4:323–425, 1955.

[81] R.S. Rivlin and K.N. Sawyers. non-linear continuum mechanics of viscoelastic fluids. *Ann. Rev. Fluid Mech.*, 3:117–146, 1971.

[82] R. Roscoe. Mechanical models for the representation of viscoelastic properties. *Brit. J. Appl. Phys*, 1:171–173, 1950.

[83] Walter Rudin. *Real and Complex Analysis*. McGraw-Hill, 1966.

[84] W.W. Schmaedecke. Approximate solutions for Volterra integral equations of the first kind. *J. Math Anal. App.*, 23:604–613, 1968.

[85] W.R. Schowalter. *Mechanics of Non-Newtonian Fluids*. Pergamon Press, 1978.

[86] F.R. Schwarzl. On the interconversion between viscoelastic material functions. *Pure Appl. Chem.*, 23:219–234, 1970.

[87] I.H. Sneddon. *The Use of Integral Transforms*. McGraw-Hill, 1972.

[88] Murray R. Spiegel. *Schaum's outline of theory and problems of Laplace transforms*. Schaum Publishing Co., 1965.

[89] G.G. Stokes. *Trans. Camb. Phil. Soc.*, 8:287, 1845.

[90] L.C.E. Struik. Free damped vibrations of linear viscoelastic materials. *Rheologica Acta*, 6:119–129, 1967.

[91] R.I. Tanner. *Engineering Rheology*. Oxford University Press, 2nd edition, 2000.

[92] A.Y. Teishev and A.Y. Malkin. On the relationship between relaxation and creep curves of polymers in the range of linear viscoelasticity. *Polym. Sci. USSR*, 32: 1669–1676, 1990.

[93] E.C. Titchmarsh. *The Theory of Functions*. Oxford University Press, 2nd edition, 1939.

[94] N.W. Tschoegl. *The Phenomenological Theory of Linear Viscoelastic Behaviour: An Introduction*. Springer-Verlag, 1989.

[95] P.P. Valko and J. Abate. Numerical laplace inversion in rheological characterization. *J. Non-Newtonian Fluid Mech.*, 116:395–406, 2004.

[96] K. Walters. *Rheometry*. Chapman & Halls, 1975.

[97] K. Walters and R.A. Kemp. On the use of a rheogoniometer - part iii. oscillatory shear between parallel plates. *Rheol. Acta*, 7:1, 1968.

[98] W. Weber. *Ann. Phys. Chem.*, 34:247, 1835.

[99] R.W. Whorlow. *Rheological techniques*. Ellis Horwood Ltd., 1980.

[100] D.V. Widder. *The Laplace Transform*. Princeton Univ. Press, 1941.

[101] E. Wiechert. *Ann. d. Phys. u. Chem.*, 50:546, 1893.

[102] Alan S. Wineman and K.R. Rajagopal. *Mechanical response of polymers: an introduction*. Cambridge University Press, 2000.

[103] G. M. Wing. *A Primer on Integral Equations of the First Kind*. SIAM, 1991.

[104] G. Winter, O. Kramer, and J.C. Dyer. An algorithm for fast determination of complex moduli. *J. Rheol.*, 38:1179–1193, 1994.

[105] W.H. Young. On the multiplication of successions of Fourier constants. *Proc. Roy. Soc. Lond. Series A*, 87:331–339, 1912.

[106] A.H. Zemanian. On the pole and zero locations of rational Laplace transformations of non-negative functions. *Proc. Amer. Math. Soc.*, 10(6):868–872, 1959.